Control for Robot Fingers with Nonholonomic Constraints

Dissertation

Akira NAKASHIMA

Department of Electronic and Mechanical Engineering
Graduate School of Engineering
Nagoya University
Nagoya, Japan

2005

Contents

Chapter 1

Introduction

1.1 Demands for Dexterity of End-Effectors

Since the industrial revolution, there has been an increasing demand for factory automation in industrial environments. Factory automation has contributed to improvements in product quality, manufacturing cost, work environment and labor shortage. To realize factory automation, robot manipulators have played an important role in recent decades. Especially, they have been introduced to product lines for simple specific tasks such as pick and place operation of same shaped objects. A traditional robot manipulator is composed of an arm and a simple gripper as an end-effector and the end-effector is designed on an ad hoc basis to perform specific tasks. Thus, they have produced good results in factory automation. However, such simple end-effector can grasp only a small class of objects and can not manipulate grasped objects due to the specific design.

On the other hand, in unstructured environments such as common places for human workers, medical fields and hazardous areas for human beings, there have been attempts of applications of robots. Robots in these environments require dexterous end-effectors However, as mentioned previously, the conventional grippers used in factory automation are not dexterous enough to perform more complicated tasks in unstructured environments. For instance, a gripper with a parallel jaw may break fragile objects such as glasses because it can not control forces to grasp the objects.

To sum up problems of simple grippers, they are lack of dexterity: they can only grasp a small class of objects; they can not manipulate grasped objects; they can not control forces to grasp objects. In addition to these problems, large motion of a robot arm may be needed for even small motion of grasped objects. Multi-fingered robot hands offer some solutions for robots to overcome the problems since they have the following abilities for dexterity: possibilities of grasp for various shaped objects, capabilities of manipulation of grasped objects and adjustments of forces to grasp objects. Moreover, since multi-fingered robot hands sometimes have some redundancies of the degrees of freedom, they can choose their configurations among possible configurations where objects can be grasped. Grasp and manipulation with these cooperative abilities is so-called *dexterous manipulation.*

Historically, multi-fingered robot hands are anthropomorphically motivated concept for dex-

terous manipulation as human action. The patterns of grasp of humans are pinching, encircling and immobilizing. Depending on the situation, humans manipulate grasped objects by using fingertips, palms or finger cushions and change the number of fingers grasping objects. To acquire the dexterity of human hands is an ultimate goal for multi-fingered robot hands.

In the research area of multi-fingered robot hands, the framework of dexterous manipulation is to determine the required actuator forces/torques which produce the desired motions of the objects and to accomplish the stability of grasping the objects. Although the fundamental theories for dexterous manipulation have been established, they have not satisfied the demands in the actual environments yet. Hence, more detailed analysis of multi-fingered robot hands grasping objects and more effective control schemes for dexterous manipulation are eagerly anticipated.

Dexterity in dexterous manipulation is described by abilities of fingers to provide specified actions to grasped objects. Basic abilities of dexterous manipulation are to restrain motions of an object and, to move the object from one configuration to another along a given trajectory. In addition, since the abilities of these concepts depend on the contact locations between fingers and grasped objects (e.g., see force-closure and manipulability in the following section), control of the contact locations is also important. In grasp and manipulation, the contact points can be *simultaneously* changed by utilizing the relative motions, such as rolling and/or sliding. Especially, the rolling contact is more beneficial to dexterous manipulation since the rolling contact is a well-known example of *nonholonomic* constraints. A notable characteristic of a system with nonholonomic constraints is that the system can be driven to a desired configuration using fewer inputs (forces/torques of actuators) than the degrees of the freedom of the system. However, since configurations of systems with contact constraints are composed of not only the generalized coordinates but also local coordinates of contact points, analysis of the systems is difficult. Hence, analysis of the systems has not been investigated enough. Thus, the simultaneous control of grasp/manipulation and contact points has not been established yet. Therefore, **In this thesis, we establish control schemes to realize *simultaneous control* of grasp/manipulation and contact points with *nonholonomy of rolling*.**

Studies concerned with the simultaneous control have been developed in the two different viewpoints: control of grasp and manipulation by multi-fingered robot hands and control of contact points for nonholonomic systems. In the following sections, studies concerned with these two viewpoints are summarized briefly in order to clarify the stand points of this thesis. Reflecting those studies, we show the purpose of this thesis in detail and the organization of this thesis.

1.2 Background on Multi-Fingered Robot Hands

Elemental technologies which are important to improve and develop dexterity of multi-fingered robot hands are the followings [1]:

1. *Mechanical designs of hands.*
   Hands are designed for tasks and are composed of fingers, the number of which are larger than or equal to two. Each finger has several degrees of freedom. Each finger is mainly actuated by electrical motors associated with the degrees of freedom.

2. *Sensor technology and information processing.*
   Sensors are attached to hands in order to gather information about hand links and interacted environments. Furthermore, gathered information is processed in order to extract other particular information.

3. *Control schemes.*
   Control schemes are to determine torques/forces of joints of fingers for desired tasks. They are mainly based on analysis of kinematics and dynamics of multi-fingered hands and grasped objects. On the other hand, there are those based on humanlike behaviors.

Issues to develop these terms have been studied by many researchers in decades. Our main interests in this thesis are related to the control schemes based on analysis of kinematics and dynamics of multi-fingered hands and grasped objects. In this section, the issues on this research area are summarized briefly. See Refs. [1, 2, 3, 4] for more details of the studies. The abilities of the dexterous manipulation are classified into *grasp robustness* and *manipulation dexterity* [2].

Grasp robustness

1) *Form-closure and **Force-closure**:* Form-closure and force-closure of grasps are instrumental in order to define grasp robustness. These concepts were introduced from the literature of the Mechanisms. Form-closure [5] is the ability of a hand to prevent motions of an object, where only unilateral and frictionless contact is considered. On the other hand, *force-closure* [6] is the ability of a hand to restrain the object despite whatever external disturbances by suitable frictional contact forces by the fingers. Since the force-closure has intuitive meaning and the ability to resist any external forces, this is a major ability of the dexterous manipulation.

2) *Power grasp:* Power grasp [7] is the action of a hand holding an object by using not only contacts of the fingertips but also those of the internal phalanges and the palm. Power grasp is equivalent to "enveloping grasp" [8] and "whole-arm manipulation" [9]. Power grasp causes hyperstatic contact forces, which are not provided by the fingers since the number of the degrees of freedom of the fingers are fewer than the number to forces at contacts. Hence, the hyperstatic contact forces can restrain the object against external forces without providing forces to the object by the fingers.

3) *Stability:* A further important property of grasps is stability. The term is used in the literature with two meanings of Lyapunov theory and Lagrange's. One refers to Lyapunov theory, and dictates that a grasp is asymptotically stable if its dynamics are that when the grasped object is displaced from the reference position, it will stay close to such position. One refers to Lagrange theory, and dictates that a configuration of a conservative system is stable if it corresponds to a strict local minimum of the potential energy. The second usage is prevalent in studies on stability of grasp (e.g., see Refs. [10, 11]).

Manipulation dexterity

1) ***Manipulability**:* The definition of *manipulability* is that for any object motion there exists the finger motion which satisfies the kinematic constraints of contacts. That is, the manipulability

means that a set of fingers can accommodate any motion of the object without losing contact. This ability of the dexterous manipulation was firstly introduced by Salisbury [12]. Since the manipulability has intuitive meaning and the ability to provide any desired object motion, this concept is a major ability of the dexterous manipulation.

2) *Regrasping and Finger gaiting:* Manipulation by regrasping or by finger gaiting is accomplished by detachment of contacts at some points and attachment of a new contact in a new different point. Manipulation by regrasping involves a sequence of alternate phases composed of grasping an object and releasing one. End-effectors as simple as on–off grippers can be often used in this effect (e.g., see Refs. [13, 14]). On the other hand, manipulation by finger gaiting involves the use of three or more fingers, one of which is repositioned on the object at a time while the other fingers are remained to manipulate the object locally (e.g., see Refs. [15, 16]).

3) *Sliding and **Rolling**:* A further degree of flexibility in manipulation is to introduce the movement of the contact points caused by sliding and rolling, which are actually often observed in manipulation of human hands. The analysis of manipulation in the presence of sliding and rolling has been pioneered by Montana [17] and Cai and Roth [18]. Manipulation by sliding are mainly classified into prediction of transition from fixed contact to sliding one (e.g., see Refs. [12, 19]) and into control of slippage motion (e.g., see Refs. [20, 14]). The details of manipulation by rolling are described in the following.

Manipulation by rolling

The manipulation by rolling has a great potential to enhance dexterity of manipulation since rolling contact is nonholonomic constraint. However, since configurations of systems with contact constraints are composed of not only the generalized coordinates but also local coordinates of contact points which depends on the generalized coordinates, analysis of the systems has not been investigated enough. Thus, the simultaneous control of grasp/manipulation and contact points has not been established yet. From this reason, the manipulation by rolling has been studied from different two viewpoints: control of grasp and manipulation of objects by multi-fingered robot hands with dynamic models and control of contact points for nonholonomic systems with simple kinematic models. In the following, studies on the dynamical models are stated, while studies of nonholonomic systems with the kinematic models are stated in the next section.

On the dynamical models, control of object motion and internal force by multi-fingered robot hand with rolling contact has been studied. Generally, the force-closure and the manipulability are assumed in the studies. Cole *et al.* [21] considered a three-fingered robot hand manipulating an object with rolling contact, where each finger has three degrees of freedom. They proposed a method to control the object motion and the internal force. Sarkar *et al.* [22] considered a two-fingered robot hand manipulating an object with the pure rolling contact, where each finger has six degrees of freedom. They proposed a method to control the object motion and the motion of a part of the contact points. However, in these studies, since the nonholonomy of the constraint has not been investigated enough and not been utilized, the control of all the contact points has not been achieved.

Summary

There exists many abilities of dexterous manipulation based on gasp robustness and manipulation dexterity. Among these abilities, the force-closure is very important and instrumental to the grasp robustness, since the force-closure is the ability to restrain the object despite whatever external disturbances Furthermore, the manipulability should be employed in order to accomplish arbitrary object motion. Therefore, *the manipulability and the force-closure are employed as a pair in this thesis.*

What abilities of the dexterous manipulation should be introduced in addition to the force-closure and the manipulability ? Operations of regrasping, finger gaiting and manipulation by sliding involve continuous dynamic systems and discrete-event systems, thus the whole systems can be interpreted as hybrid systems which are in part event-driven and in part time-driven [23]. These operations are called manipulation *at large*. On the other hand, *manipulation by rolling* is manipulation *at local* which means that there does not exist transition of contact condition in manipulation. The manipulation at large has a potential to realize more large classes of tasks. However, since these control problems are framed as hybrid systems, it is very difficult and hard to solve these problems. On the other hand, the reachable configuration of the manipulation by rolling can be as extensive as that of the manipulation at large due to the nonholonomy of rolling, even though the manipulation by rolling is local. However, since at present the analysis of the systems is not enough, there have been no control methods which can effectively utilize the nonholonomy of rolling. Therefore, ***it is essential to analyze systems with rolling contact in detail and to establish control methods which enables the utilization of nonholonomy of rolling.***

1.3 Background on Nonholonomic Systems

As stated in the last paragraph of the previous section, the rolling contact between two rigid bodies is a nonholonomic constraint. In this section, the properties of nonholonomic constraints and control schemes of systems with nonholonomic constraints are summarized briefly. See Refs. [6, 24, 25, 26, 27] for more details.

Properties of nonholonomic constraints

Consider a mechanical system whose configurations $\boldsymbol{q} \in \mathbb{R}^n$ evolve in a smooth n-dimensional manifold $\mathcal{M}$ with constraints restricting the motion of the system to a smooth m-dimensional manifold represented locally as a Pfaffian constraint, $\boldsymbol{A}(\boldsymbol{q})\dot{\boldsymbol{q}} = \boldsymbol{0}$, $\boldsymbol{A}(\boldsymbol{q}) \in \mathbb{R}^{m\times n}$. A system with the constraint as the Pfaffian constraint can be easily represented by $\dot{\boldsymbol{q}} = \boldsymbol{A}^{\perp}(\boldsymbol{q})\boldsymbol{v}$, $\boldsymbol{A}^{\perp}(\boldsymbol{q}) \in \mathbb{R}^{n\times(n-m)}$, $\boldsymbol{v} \in \mathbb{R}^{n-m}$, where the columns of $\boldsymbol{A}^{\perp}(\boldsymbol{q})$ form a basis for the annihilating distribution of $\boldsymbol{A}(\boldsymbol{q})$ and $\boldsymbol{v}$ is a vector of quasi-velocities taking values in $\mathbb{R}^{n-m}$. This system is so-called a *symmetric affine system*, a *driftless system* or a *kinematic model*. The vector $\boldsymbol{v}$ is interpreted as an input vector to the system. If the constraint is *maximally nonholonomic*, i.e., nonintegrable, the system is controllable. In the robotics literature, the system with maximally nonholonomic constraints is called nonholonomic systems. To sum up, "an n-dimensional nonholonomic system can be controlled to *any* configurations in n-dimensional manifold $\mathcal{M}$ by using $n-m$ inputs

which is fewer than n". This property is a typical contribution by the introduction of nonholonomic constraints.

Control of nonholonomic systems

In this paragraph, studies of control schemes of nonholonomic systems as symmetric affine systems are summarized briefly. It must be firstly mentioned that nonholonomic systems can not be asymptotically stabilized to a specified equilibrium of the closed loop by the continuous time-invariant static state-feedback. This fact was derived by Brockett [28]. Moreover, there exists no dynamic continuous time-invariant feedback controller which renders the closed loop locally asymptotically stable [29]. Furthermore, difficulty of control of nonholonomic systems depends on the structure of the controllability [26].

The control schemes of nonholonomic systems have been classified into feedback control and motion planning to overcome or avoid the difficulty due to so-called Brockett's theorem. As for the methods concerning feedback control, there are discontinuous feedback laws (e.g., see Ref. [30]), time-varying feedback laws (e.g., see Ref. [29]) and the control method based on the time-sate control form [31, 32]. As for the methods concerning motion planning, there exist differential geometric approaches [33], control parameterization approaches (e.g., see Ref. [34]) and geometric phase (holonomy) approaches [35]. The typical structure of nonholonomic systems is the chained form, which is a canonical control form. For the control of the chained form, there have been many fruits of research among a decade. As for the control methods concerning the forms which can not be transformed to the chained forms, the details are described in the following.

Control of two rigid bodies with rolling contact

Examples of the forms which can not be transformed to the chained forms are first-order systems [36] and second order systems [6]. Especially, control of the second order systems are more difficult [26]. A typical example of second order systems is the system of the rolling bodies with regular surface [17], which is represented by 5-dimensional contact coordinates and 2-inputs. As for the feedback control, there exits a feedback law based on the time-state control form where two bodies are assumed to a sphere and a plane [37]. However, this study can achieve only local stabilization to the origin since the control method is based on the linearized systems.

As for the motion planning, for a sphere and a plane, Bicchi *et al.* [38] proposed a control parameterization approach to solve a nonlinear many variable function of control parameters which is constructed by combining flows of the system from an initial to a target configuration. However, the convergence of the solution of the function is not guaranteed. On the other hand, there are several methods based on the geometric phase approaches. The methods utilize the property such that a closed path of quasi-velocities (input of the system) results in a change of the contact coordinates. Li *et al.* [39] proposed a path planning for a sphere on a plane by two types of closed paths. Bicchi *et al.* [40, 41] proposed a path planning for a object with a general surface and a plane by two types of closed paths. This is expanded to the case of polyhedra [42]. However, since these studies achieve the regulation of the contact coordinates by the sequential two methods using the two closed paths, the first method should be begun again if the regulated coordinates by the first are perturbed by disturbances in the process of the second

method. Harada *et al.* [43] proposed a path planning by using a set of multiple closed paths on the object surface for a system composed of a spherical object and a plane. Since the set of the closed paths consists of many pieces, the method is somewhat complex.

Summary

For the utilization of the nonholonomy of rolling in the dexterous manipulation, the geometric phase approaches have some great contributions: the approaches enable global steer to any configurations, the approaches can be easily interpreted intuitively, therefore it is easy to introduce the constraints on paths due to finger motions. However, the studies based on this approaches as mentioned previously have the weakness against disturbances and the complexity due to multi closed paths or many pieces. Therefore, ***it is essential to establish methods such that all of the contact coordinates can be regulated simultaneously by using a single specified closed path.***

1.4 Purpose of the Thesis

As mentioned previously in Section 1.1, the purpose of this thesis is to establish control methods to realize the simultaneous control of grasp/manipulation and contact points of an object by a multi-fingered robot hand with the nonholonomy of rolling. In this thesis, we use the word: the *simultaneous control* to mean control of grasp/manipulation and control of contact points of an object simultaneously with rolling contact. From the summaries of Sections 1.2 and 1.3, the key topics to realize the purpose are the followings:

(A) For a dynamical model composed of fingers and a grasped object, to establish control methods which can utilize the nonholonomy of rolling for control of contact points simultaneously with grasp and manipulation of the object. In this thesis, the number of the fingers will be restricted to two which is the minimum number.

(B) For a nonholonomic system of two rolling rigid bodies with pure rolling contact, to establish methods such that all of the contact coordinates can be regulated simultaneously by using a single specified closed path. In this thesis, the surfaces of the bodies will be restricted to a sphere and a plane.

The problems considered in this thesis are summarized as in the following sections **(I)–(IV)** from the viewpoints of **(A)** and **(B)**. It is easy to combine the methods for **(A)** and **(B)**, and the simultaneous control is achieved by the combination. The relationship between the sections **(I)–(IV)** is shown in Figure 1.1.

(I) Simultaneous Control by Two-fingered Robot Hand with Six Degrees of Freedom

The topics (A) and (B) are considered in this section.

Here, **we discuss the simultaneous control by a two-fingered robot hand, each finger of which has six degrees of freedom.** The contact motion between each finger and the object is assumed to be the pure rolling contact, and the surfaces of each finger and the object are assumed to be the regular surfaces. As for the control method to utilize the nonholonomy of rolling for

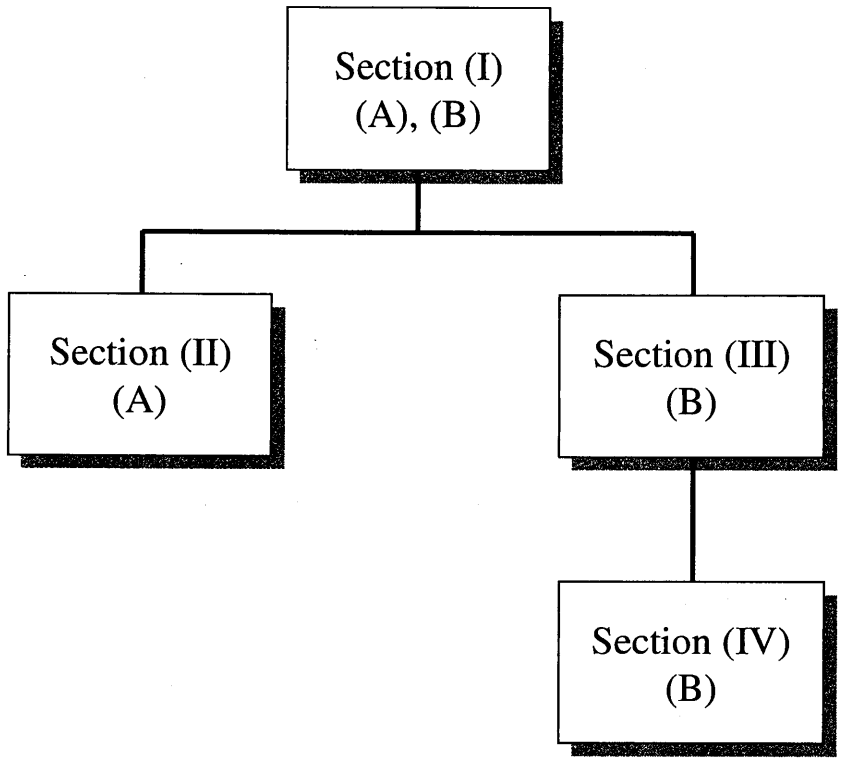

Figure 1.1 Relationship between the sections **(I)–(IV)**.

control of contact points, we first clarify the degree of freedom of the whole system by investigating the property of the motion constraint on the generalized coordinates, which can be associated with the constraint of the contact coordinates. Second, we propose a general formulation of a linearizing compensator for the internal force, the object motion and the rolling motion. Due to the linearization, the contact motion conforms to the kinematic model of two rolling bodies whose input is the rolling motion. As for the regulation algorithm, for the kinematic model of a sphere and a plane which correspond to a spherical finger and a cuboid object, we propose a method to regulate all the contact coordinates by iterative closed paths on the contact point of the sphere. The closed path is shaped as a trapezoid on the sphere parameterized by three variables. We call this closed path the *trapezoidal closed path*. The parameters is determined with respect to each interation. Furthermore, the convergence to arbitrary target points of the regulation method is guaranteed by proving that there always exist the parameters to reduce the euclidean norm of the distance to the target point. Since the method can be interpreted as a discrete-time feedback by regarding the start time of the iteration as the sampling instant, the method is expected to have robustness against disturbances.

(II) Simultaneous Control by Two-fingered Robot Hand with Constrained Degrees of Freedom

The topic (A) is considered in this section.

In the section **(I)**, we proposed a method can utilize the nonholonomy of rolling for control of contact points in the case that each finger has six degrees of freedom. However, more reasonable

control problem is the situation such that the number of the degrees of freedom (DOF) of each finger is less than six and the direction of the DOF is constrained. We say that the DOF of fingers are constrained.

Here, **for the simultaneous control, we propose a control method which can utilize the nonholonomy of rolling for control of contact points by a two-fingered robot hand with constrained DOF.** The contact motion between each finger and the object is assumed to be the pure rolling contact, and the surfaces of each finger and the object are assumed to be the regular surfaces. We first clarify the condition such that the position of the DOF of the whole system is maximum. This represents that arbitrary rolling motion can be generated by using finger and object motion. This is characterized by the number and the direction of the DOF of the fingers. Second, we propose a general formulation of a linearizing compensator for the internal force, the motion of a certain coordinates of the fingers and the object, and the rolling motion. For the construction of the linearizing compensator, the finger and object motion are decomposed into a component which causes the rolling motion and a component which does not cause the rolling motion. The second component correspond to a certain coordinates of the fingers and the object.

(III) Control of a Sphere Rolling on a Plane by Finite Iterative Closed Paths

The topic (B) is considered in this section.

In the section **(I)**, for the kinematic model of a sphere and a plane with pure rolling contact, we propose a method to regulate all the contact coordinates by iterating the trapezoidal closed path of the contact point on the sphere, which is characterized by the three parameters. However, in this method, the converge to arbitrary target points by infinite iteration is only guaranteed.

Here, **for the kinematic model of a sphere and a plane with pure rolling contact, we propose a regulation algorithm for the contact coordinates to converge to a target point by the finite iterative trapezoidal closed paths of the contact point on the sphere.** First, we show that, from the viewpoint of the norm minimization, one of the parameters can be determined independent of the other two parameters. Due to this determination, the control problem can be discussed on the two-dimensional space (plane) which characterizes the contact coordinates. Second, we prove that the reachable area of the closed path has two finite lines crossing at the origin which represents the contact coordinates at each iteration. Third, we propose a method for the contact coordinates to converge to a target point by the finite iterative shifts along the lines as mentioned earlier. At each iteration, since the proposed method requires solving only one variable equation, the solutions can be easily obtained by the bisection method.

(IV) Control of a Sphere Rolling on a Plane with Constrained Rolling Motion

The topic (B) is considered in this section.

In the section **(III)**, for the kinematic model of a sphere and a plane with pure rolling contact, we proposed a regulation algorithm for the contact coordinates to converge by the finite iterative trapezoidal closed paths on the sphere. In this method, it is utilized that the two finite lines exist in the reachable area of the closed path. However, since the lines are just a part of the reachable area, the method is somewhat conservative. Furthermore, since the rolling motion can not be constrained, it is difficult to apply these methods for control of contact points by multi-fingered robot hands.

Here, **for the kinematic model of a sphere and a plane with pure rolling contact, we discuss control of the contact coordinates by iteration of the trapezoidal closed path on the sphere with constrained rolling motion.** It is assumed that the parameter of the direction of the closed path is determined from the viewpoint of the norm minimization shown in **(III)**. Due to this determination, the control problem can be discussed on the two-dimensional space (plane) which characterizes the contact coordinates. First, in order to utilize the reachable area of the closed path at the maximum, we analyze the boundary of the reachable area of the closed path with constrained rolling motion in detail. Second, we propose a method for the contact coordinates to converge to a target point by the finite iterative shifts along the boundary as mentioned earlier. Since the proposed method can impose the limitation of the rolling motion, the method has the beneficial effect on the application to multi-fingered robot hands. Furthermore, similar to the section **(III)**, the parameters at each iteration can be easily calculated by the bisection method.

1.5 Organization of the Thesis

The detail organization of this thesis is as follows.

In Chapter 3, we discuss the simultaneous control by a two-fingered robot hand, each finger of which has six degrees of freedom. First, we clarify the degree of freedom of the whole system by investigating the property of the motion constraint on the generalized coordinates. Second, we propose a general formulation of a linearizing compensator for the internal force, the object motion and the rolling motion. Third, for the kinematic model of a sphere and a plane with pure rolling contact, we propose a method to regulate all the contact coordinates by iterating the trapezoidal closed path on the contact point on the sphere, which is characterized by three parameters. The convergence to arbitrary target points of the regulation method is guaranteed.

In Chapter 4, for the simultaneous control we propose a control method which can utilize the nonholonomy of rolling for control of contact points by a two-fingered robot hand with the constrained DOF. First, we clarify the condition such that arbitrary rolling motion can be generated from finger and object motion. This represents that the position of the DOF of the whole system is maximum number. Second, we propose a general formulation of a linearizing compensator for the internal force, the motion of the certain coordinates of the fingers and the object, and the rolling motion. For the construction of the linearizing compensator, the finger and object motion are decomposed into a component which causes the rolling motion and a component which does not cause the rolling motion.

In Chapter 5, for the kinematic model of a sphere and a plane with rolling contact, we propose a regulation algorithm for the contact coordinates to converge to a target point by the finite iterative trapezoidal closed paths of the contact point on the sphere. First, we show that, from the viewpoint of the norm minimization, one of the parameters can be determined independent of the other two parameters. Due to this determination, the control problem can be discussed on the two-dimensional space (plane) which characterizes the contact coordinates. Second, we prove that the reachable area of the closed path has two finite lines crossing at the origin which represents the contact coordinates at each iteration. Third, we propose a method for the contact

coordinates to converge to a target point by the finite iterative shifts along the lines as mentioned earlier.

In Chapter 6, for the kinematic model of a sphere and a plane with pure rolling contact, we discuss control of the contact coordinates by iteration of the trapezoidal closed path on the sphere with constrained rolling motion. First, in order to utilize the reachable area of the closed path at the maximum, we analyze the boundary of the reachable area of the closed path with constrained rolling motion in detail. Second, we propose a method for the contact coordinates to converge to a target point by the finite iterative shifts along the boundary as mentioned earlier.

Conclusions and further research are stated in Chapter 7.

The following notations are used in this thesis.

$\mathbb{R}^n$ is the n-dimensional Euclidean space.

$\boldsymbol{z} \in \mathbb{R}^n$ expresses a n-dimensional real vector.

$\boldsymbol{A} \in \mathbb{R}^{m \times n}$ means a $m \times n$ real matrix.

$\boldsymbol{I}_n$ is the n-dimensional unit matrix.

$\mathbf{0}_{m \times n}$ is the $m \times n$ zero matrix.

$\boldsymbol{A} > 0$ means a positive definite symmetric matrix.

$A := B$ means that A is defined by B.

$\boldsymbol{p}_1 /\!\!/ \boldsymbol{p}_2$ means that the vectors $\boldsymbol{p}_1$ and $\boldsymbol{p}_2$ are parallel each other.

The superscript $^{\mathrm{T}}$ stands for the transpose of a matrix.

The superscript $^{\wedge}$ stands for the skew-symmetric matrix equivalent to the vector product.

The superscript $^{+}$ stands for the pseudo inverse matrix of a matrix.

The superscript $^{-}$ stands for a generalized inverse matrix of a matrix.

Σ_A is the coordinate frame named A.

${}^A\boldsymbol{p}_B$ is the position vector of the origin of Σ_B from the origin of Σ_A expressed in Σ_A.

$\boldsymbol{R}_{AB}$ is the rotation matrix of Σ_B relative to Σ_A.

$\mathcal{R}(\boldsymbol{A})$ stands for the range of value of a matrix $\boldsymbol{A}$.

$\mathcal{N}(\boldsymbol{A})$ stands for the kernel (null space) of a matrix $\boldsymbol{A}$.

Chapter 2

Preliminaries

In this chapter, some preliminaries are described. the theoretical bases of multi-fingered robot hands and nonholonomic systems are summarized briefly. For more details, see Ref. [6].

2.1 Theoretical Basis of Multi-Fingered Robot Hands

In this section, kinematics and dynamics of fingers and an grasped object with contact constraints are summarized briefly.

2.1.1 Configuration and velocity

System configuration

In general, a configuration of a frame Σ_B relative to a frame Σ_A consists of the pair

$$g_{AB} = ({}^A\boldsymbol{p}_B, \boldsymbol{R}_{AB}) \in SE(3), \tag{2.1}$$

where ${}^A\boldsymbol{p}_B$ and $\boldsymbol{R}_{AB}$ are the position vector and the rotation matrix of Σ_B with respect to Σ_A respectively. $SE(3)$ is the *configuration space* of the system and the notation SE abbreviates *special Euclidean*. The precise definition are described in Appendix A.

Consider a finger i ($i = 1, 2, \cdots n$) and an object with a contact shown in Figure 2.1. The contact point between each finger and the object is single. Σ_B is the reference coordinate frame. Σ_{F_i} and Σ_O are the coordinate frames fixed to the ith finger and the object, respectively. The configurations of the finger i and the object are described by

$$g_{BF_i} = ({}^B\boldsymbol{p}_{F_i}, \boldsymbol{R}_{BF_i}) \in SE(3), \;\; g_{BO} = ({}^B\boldsymbol{p}_O, \boldsymbol{R}_{BO}) \in SE(3). \tag{2.2}$$

In this thesis, we use local parameterizations for g_{BF_i} and g_{BO}:

$$\boldsymbol{x}_{F_i} := \begin{bmatrix} {}^B\boldsymbol{p}_{F_i} \\ {}^B\boldsymbol{\phi}_{F_i} \end{bmatrix} \in \mathbb{R}^6, \;\; \boldsymbol{x}_O := \begin{bmatrix} {}^B\boldsymbol{p}_O \\ {}^B\boldsymbol{\phi}_O \end{bmatrix} \in \mathbb{R}^6, \tag{2.3}$$

where ${}^B\boldsymbol{\phi}_{F_i} \in \mathbb{R}^3$ and ${}^B\boldsymbol{\phi}_O \in \mathbb{R}^3$ are the local parameterizations of $\boldsymbol{R}_{BF_i} \in \mathbb{R}^{3\times3}$ and $\boldsymbol{R}_{BO} \in \mathbb{R}^{3\times3}$ respectively. Aggregating $\boldsymbol{\theta}_{F_i}$ for $i = 1, \cdots, n$, we will use $\boldsymbol{x}_F := [\, \boldsymbol{x}_{F_1}^{\mathrm{T}} \;\; \cdots \;\; \boldsymbol{x}_{F_n}^{\mathrm{T}} \,]^{\mathrm{T}} \in \mathbb{R}^{6n}$.

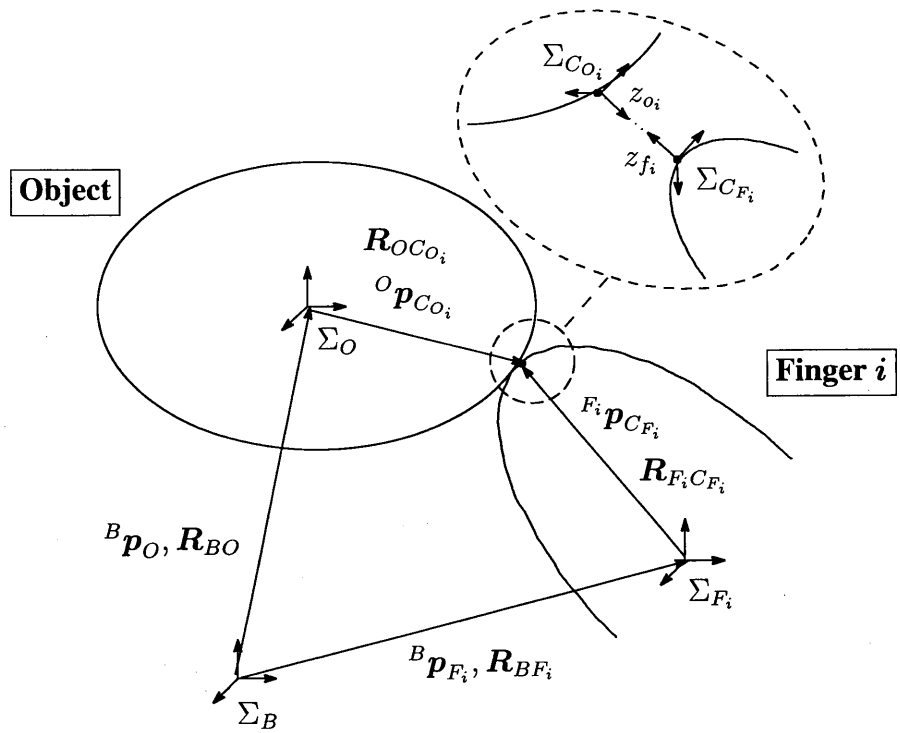

Figure 2.1 Coordinate frames for contact and object frames.

In a case where the number of the degrees of freedom of the ith finger is less than six and its direction is constrained, we use the generalized coordinates,

$$\boldsymbol{\theta}_{F_i} \in \mathbb{R}^{m_i}, \tag{2.4}$$

where m_i is the number of the independent degrees of freedom of the i finger. Aggregating $\boldsymbol{\theta}_{F_i}$ for $i = 1, \cdots, n$, we will use $\boldsymbol{\theta}_F := [\ \boldsymbol{\theta}_{F_1}^{\mathrm{T}} \ \cdots \ \boldsymbol{\theta}_{F_n}^{\mathrm{T}}\ ]^{\mathrm{T}} \in \mathbb{R}^m$, $m := m_1 + \cdots + m_n$. In the following, we consider the general case where the ith finger is constrained.

In the dashed area, $\Sigma_{C_{F_i}}$ and $\Sigma_{C_{O_i}}$ are the coordinate frames attached on the surfaces of the ith finger and the object with the origins at the ith contact point. The z_{f_i}- and z_{o_i}-axes of the frames are *outward* and *normal* to the surfaces of the ith finger and the object, respectively. To represent the contact location, the configurations of $\Sigma_{C_{F_i}}$ and $\Sigma_{C_{O_i}}$ are described by

$$g_{F_iC_{F_i}} = ({}^{F_i}\boldsymbol{p}_{C_{F_i}}, \boldsymbol{R}_{F_iC_{F_i}}) \in SE(3), \quad g_{OCo_i} = ({}^{O}\boldsymbol{p}_{Co_i}, \boldsymbol{R}_{OCo_i}) \in SE(3). \tag{2.5}$$

In addition, the following configuration describes the relative orientation with respect to the contact point:

$$g_{Co_iC_{F_i}} = ({}^{Co_i}\boldsymbol{p}_{C_{F_i}}, \boldsymbol{R}_{Co_iC_{F_i}}) \in SE(3), \tag{2.6}$$

where ${}^{Co_i}\boldsymbol{p}_{C_{F_i}} = 0$ since the origins of $\Sigma_{C_{F_i}}$ and $\Sigma_{C_{O_i}}$ coincide with each other.

In this thesis, to represent the contact configurations of (2.5) and (2.6), we use the *surface parameterizations*: the surfaces of each finger and the object are the regular surfaces, i.e., contact points on the surfaces of each finger and the object can be described by $\boldsymbol{c}(\boldsymbol{\alpha}) \in \mathbb{R}^3$, where $\boldsymbol{c}(\cdot) : \mathbb{R}^2 \mapsto \mathbb{R}^3$ is a local orthogonal chart and $\boldsymbol{\alpha} \in \mathbb{R}^2$ is a local coordinates. The details of the surface parameterizations are described in Appendix B. Figure 2.2 shows neighborhood of the

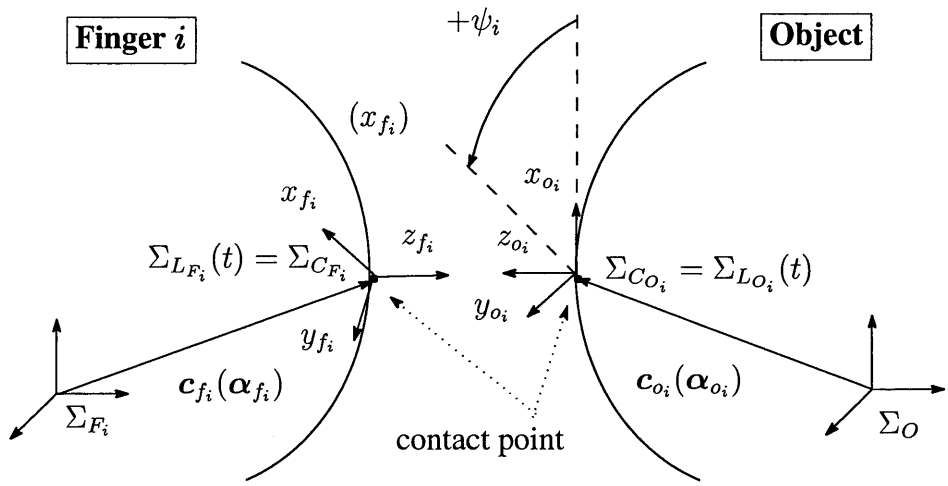

Figure 2.2 Contact coordinates of ith contact point.

ith contact point, where the ith finger and the object are depicted separately. Frames $\Sigma_{L_{F_i}}(t)$ and $\Sigma_{L_{O_i}}(t)$ are respectively the local frames fixed relative to Σ_{F_i} and Σ_O, which coincide at time t with $\Sigma_{C_{F_i}}$ and $\Sigma_{C_{O_i}}$. The contact configurations of (2.5) are described by

$$
{}^{F_i}\boldsymbol{p}_{C_{F_i}} = \boldsymbol{c}_{f_i}(\boldsymbol{\alpha}_{f_i}), \quad \boldsymbol{R}_{F_iC_{F_i}}(\boldsymbol{\alpha}_{f_i}) = \left[\frac{\boldsymbol{c}_{f_iu}}{\|\boldsymbol{c}_{f_iu}\|} \quad \frac{\boldsymbol{c}_{f_iv}}{\|\boldsymbol{c}_{f_iv}\|} \quad \frac{\boldsymbol{c}_{f_iu} \times \boldsymbol{c}_{f_iv}}{\|\boldsymbol{c}_{f_iu} \times \boldsymbol{c}_{f_iv}\|} \right] \tag{2.7}
$$

$$
{}^{O}\boldsymbol{p}_{C_{O_i}} = \boldsymbol{c}_{o_i}(\boldsymbol{\alpha}_{o_i}), \quad \boldsymbol{R}_{OC_{O_i}}(\boldsymbol{\alpha}_{o_i}) = \left[\frac{\boldsymbol{c}_{o_iu}}{\|\boldsymbol{c}_{o_iu}\|} \quad \frac{\boldsymbol{c}_{o_iv}}{\|\boldsymbol{c}_{o_iv}\|} \quad \frac{\boldsymbol{c}_{o_iu} \times \boldsymbol{c}_{o_iv}}{\|\boldsymbol{c}_{o_iu} \times \boldsymbol{c}_{o_iv}\|} \right], \tag{2.8}
$$

where $\boldsymbol{c}_{f_i}(\cdot), \boldsymbol{c}_{o_i}(\cdot) : \mathbb{R}^2 \mapsto \mathbb{R}^3$ are local orthogonal charts, $\boldsymbol{\alpha}_{f_i} \in \mathbb{R}^2$, $\boldsymbol{\alpha}_{o_i} \in \mathbb{R}^2$ are local coordinates and $\boldsymbol{c}_{f_iu}$ and $\boldsymbol{c}_{f_iv}$ are defined by $\boldsymbol{c}_{f_iu} := \partial \boldsymbol{c}_{f_i}/\partial u_{f_i}$ and $\boldsymbol{c}_{f_iv} := \partial \boldsymbol{c}_{f_i}/\partial v_{f_i}$, and terms $\boldsymbol{c}_{o_iu}$ and $\boldsymbol{c}_{o_iv}$ are defined by the similar way. In addition, let ψ_i be the angle between the x-axes of $\Sigma_{C_{F_i}}$ and $\Sigma_{C_{O_i}}$ as shown in Figure 2.2, then the contact configuration of (2.6) is described by only ψ_i such that

$$
\boldsymbol{R}_{C_{O_i}C_{F_i}} = \begin{bmatrix} \boldsymbol{R}_{\psi_i}(\psi_i) & 0_{2\times 1} \\ 0_{1\times 2} & -1 \end{bmatrix}, \quad \boldsymbol{R}_{\psi_i} := \begin{bmatrix} \cos\psi_i & -\sin\psi_i \\ -\sin\psi_i & -\cos\psi_i \end{bmatrix}, \tag{2.9}
$$

where $\boldsymbol{R}_{\psi_i} \in \mathbb{R}^{2\times 2}$ is the rotation matrix of the x- and y-axes of $\Sigma_{C_{F_i}}$ relative to the x- and y-axes of $\Sigma_{C_{O_i}}$. To sum up, the configuration of the ith contact point is completely described by

$$
\boldsymbol{\eta}_i := \begin{bmatrix} \boldsymbol{\alpha}_{f_i} \\ \boldsymbol{\alpha}_{o_i} \\ \psi_i \end{bmatrix} \in \mathbb{R}^5. \tag{2.10}
$$

This is called the *contact coordinates* for the contact point [17]. Aggregating $\boldsymbol{\eta}_i$ for $i = 1, \cdots, n$, we will use $\boldsymbol{\eta} := [\, \boldsymbol{\eta}_1^{\mathrm{T}} \ \cdots \ \boldsymbol{\eta}_n^{\mathrm{T}} \,]^{\mathrm{T}} \in \mathbb{R}^{5n}$.

Expression of velocity

To represent the motions of the finger i and the object, we use the translational and angular velocities:

$$\begin{bmatrix} {}^B\dot{\boldsymbol{p}}_{F_i} \\ {}^B\boldsymbol{\omega}_{F_i} \end{bmatrix} \in \mathbb{R}^6, \quad \begin{bmatrix} {}^B\dot{\boldsymbol{p}}_O \\ {}^B\boldsymbol{\omega}_O \end{bmatrix} \in \mathbb{R}^6, \tag{2.11}$$

where ${}^B\boldsymbol{\omega}_{F_i}$ and ${}^B\boldsymbol{\omega}_O$ are respectively angular velocities of Σ_{F_i} and Σ_O relative to Σ_B which are defined by

$${}^B\boldsymbol{\omega}_{F_i} := (\dot{\boldsymbol{R}}_{BF_i}\boldsymbol{R}_{BF_i})^\vee \in \mathbb{R}^3 \tag{2.12}$$

$${}^B\boldsymbol{\omega}_O := (\dot{\boldsymbol{R}}_{BO}\boldsymbol{R}_{BO})^\vee \in \mathbb{R}^3. \tag{2.13}$$

From (A.19), the operator $(\cdot)^\vee$ is the inverse operator of $(\cdot)^\wedge$ defined by

$$\boldsymbol{\omega}^\wedge := \begin{bmatrix} 0 & -\omega_3 & \omega_2 \\ \omega_3 & 0 & -\omega_1 \\ -\omega_2 & \omega_1 & 0 \end{bmatrix}, \tag{2.14}$$

which is the matrix equivalent to the vector product $\boldsymbol{\omega}\times$.

The relations between the velocities of the local parameterizations of (2.3) and the translational and angular velocities of (2.11) are given by

$$\begin{bmatrix} {}^B\dot{\boldsymbol{p}}_{F_i} \\ {}^B\boldsymbol{\omega}_{F_i} \end{bmatrix} = \boldsymbol{T}_{F_i}({}^B\boldsymbol{\phi}_{F_i})\dot{\boldsymbol{x}}_{F_i}, \quad \begin{bmatrix} {}^B\dot{\boldsymbol{p}}_O \\ {}^B\boldsymbol{\omega}_O \end{bmatrix} = \boldsymbol{T}_O({}^B\boldsymbol{\phi}_O)\dot{\boldsymbol{x}}_O, \tag{2.15}$$

where

$$\boldsymbol{T}_{F_i} := \begin{bmatrix} \boldsymbol{I}_3 & \boldsymbol{0}_{3\times3} \\ \boldsymbol{0}_{3\times3} & \boldsymbol{T}_{Fr_i}({}^B\boldsymbol{\phi}_{F_i}) \end{bmatrix}, \quad \boldsymbol{T}_O := \begin{bmatrix} \boldsymbol{I}_3 & \boldsymbol{0}_{3\times3} \\ \boldsymbol{0}_{3\times3} & \boldsymbol{T}_{Or}({}^B\boldsymbol{\phi}_O) \end{bmatrix} \tag{2.16}$$

and $\boldsymbol{T}_{Fr_i} \in \mathbb{R}^{3\times3}$ and $\boldsymbol{T}_{Or} \in \mathbb{R}^{3\times3}$ encode (2.12) and (2.12). In the case where the number of the degrees of freedom of the ith finger is less than six and its direction is constrained, we use the following relation:

$$\begin{bmatrix} {}^B\dot{\boldsymbol{p}}_{F_i} \\ {}^B\boldsymbol{\omega}_{F_i} \end{bmatrix} = \boldsymbol{J}_{F_i}(\boldsymbol{\theta}_{F_i})\dot{\boldsymbol{\theta}}_{F_i}, \tag{2.17}$$

where $\boldsymbol{J}_{F_i}(\boldsymbol{\theta}_{F_i}) \in \mathbb{R}^{6\times m_i}$ the Jacobian determined by the link mechanics of the ith finger.

2.1.2 Contact kinematics

Contact conditions

At the ith contact point, the following equations hold [44]:

$${}^B\boldsymbol{p}_{F_i} + \boldsymbol{R}_{BF_i}{}^{F_i}\boldsymbol{p}_{C_{F_i}} = {}^B\boldsymbol{p}_O + \boldsymbol{R}_{BO}{}^O\boldsymbol{p}_{C_{O_i}} \tag{2.18}$$

$$\boldsymbol{R}_{BF_i}\boldsymbol{R}_{F_iC_{F_i}} = \boldsymbol{R}_{BO}\boldsymbol{R}_{OC_{O_i}}\boldsymbol{R}_{C_{O_i}C_{F_i}}. \tag{2.19}$$

Eq. (2.18) requires that the position vectors of the contact frames $\Sigma_{C_{F_i}}$ and $\Sigma_{C_{O_i}}$ with respect to the reference frame Σ_B coincide with each other. Eq. (2.19) requires that the contact normals and the tangent planes at the origins of $\Sigma_{C_{F_i}}$ and $\Sigma_{C_{O_i}}$ coincide with each other. Note that the number of the essential independent equations of (2.19) are *three* since (2.19) is the relationship between the rotation matrices. Eqs. (2.18) and (2.19) relate the positions of the contact coordinates $\boldsymbol{\eta}_i$ to those of the generalized coordinates $(\boldsymbol{\theta}_{F_i}, \boldsymbol{x}_O)$.

Contact kinematics

To represent the contact motion, we use the body velocity $\boldsymbol{V}_{C_i} \in \mathbb{R}^6$, i.e., the velocity and angular velocity of $\Sigma_{L_{C_{F_i}}}$ relative to $\Sigma_{L_{C_{O_i}}}$ expressed in $\Sigma_{L_{C_{F_i}}}$, described by

$$\boldsymbol{V}_{C_i} = \begin{bmatrix} v_{Cx_i} \\ v_{Cy_i} \\ \hline v_{Cz_i} \\ \omega_{Cx_i} \\ \omega_{Cy_i} \\ \omega_{Cz_i} \end{bmatrix} := \boldsymbol{V}^b_{L_{O_i}L_{F_i}}. \tag{2.20}$$

Velocity $\boldsymbol{V}_{C_i}$ represents the *relative motion* between the ith finger and the object at ith contact point. The precise definition of the body velocity is shown in Appendix A.

Differentiating (2.18) and (2.19) with respect to time t leads to the motion of the contact coordinates $\dot{\boldsymbol{\eta}}_i$ as a function of the relative motion $\boldsymbol{V}_{C_i}$ [44, 17]:

$$\dot{\boldsymbol{\eta}}_i = \boldsymbol{H}_i(\boldsymbol{\eta}_i)\boldsymbol{V}_{C_i} \tag{2.21}$$

$$0 = v_{Cz_i}, \tag{2.22}$$

where

$$\boldsymbol{H}_i := \left[\begin{array}{cc|cc} -\boldsymbol{M}_{gf_i}^{-1}\boldsymbol{K}_{R_i}^{-1}\tilde{\boldsymbol{K}}_{go_i} & \boldsymbol{0}_{2\times1} & \boldsymbol{M}_{gf_i}^{-1}\boldsymbol{K}_{R_i}^{-1}\boldsymbol{E} & \boldsymbol{0}_{2\times1} \\ \boldsymbol{M}_{go_i}^{-1}\boldsymbol{R}_{\psi_i}\boldsymbol{K}_{R_i}^{-1}\boldsymbol{K}_{gf_i} & \boldsymbol{0}_{2\times1} & \boldsymbol{M}_{go_i}^{-1}\boldsymbol{R}_{\psi_i}\boldsymbol{K}_{R_i}^{-1}\boldsymbol{E} & \boldsymbol{0}_{2\times1} \\ \hline -\boldsymbol{T}_{gf_i}\boldsymbol{K}_{R_i}^{-1}\tilde{\boldsymbol{K}}_{go_i} & 0 & \boldsymbol{T}_{gf_i}\boldsymbol{K}_{R_i}^{-1}\boldsymbol{E} & 1 \\ +\boldsymbol{T}_{go_i}\boldsymbol{R}_{\psi_i}\boldsymbol{K}_{R_i}^{-1}\boldsymbol{K}_{gf_i} & & +\boldsymbol{T}_{go_i}\boldsymbol{R}_{\psi_i}\boldsymbol{K}_{R_i}^{-1}\boldsymbol{E} & \end{array}\right] \tag{2.23}$$

$$\boldsymbol{K}_{R_i} := \boldsymbol{K}_{gf_i} + \tilde{\boldsymbol{K}}_{go_i}, \tilde{\boldsymbol{K}}_{go_i} := \boldsymbol{R}_{\psi_i}\boldsymbol{K}_{go_i}\boldsymbol{R}_{\psi_i} \tag{2.24}$$

$$\boldsymbol{E} := \begin{bmatrix} 0 & -1 \\ 1 & 0 \end{bmatrix}, \boldsymbol{R}_{\psi_i} := \begin{bmatrix} \cos\psi_i & -\sin\psi_i \\ -\sin\psi_i & -\cos\psi_i \end{bmatrix}. \tag{2.25}$$

$\boldsymbol{M}_{gf_i}, \boldsymbol{M}_{go_i} \in \mathbb{R}^{2\times2}$, $\boldsymbol{K}_{gf_i}, \boldsymbol{K}_{go_i} \in \mathbb{R}^{2\times2}$ and $\boldsymbol{T}_{gf_i}, \boldsymbol{T}_{go_i} \in \mathbb{R}^{1\times2}$ are the *geometric parameters* described by using $\boldsymbol{c}_{f_i}$ and $\boldsymbol{c}_{o_i}$. $\boldsymbol{K}_{R_i} \in \mathbb{R}^{2\times2}$ is called the *relative curvature form*. $\boldsymbol{R}_{\psi_i} \in \mathbb{R}^{2\times2}$ is the rotation matrix of the x- and y-axes of $\Sigma_{C_{F_i}}$ relative to the x- and y-axes of $\Sigma_{C_{O_i}}$. In addition, $\boldsymbol{V}_{C_i}$ is given by

$$\boldsymbol{V}_{C_i} = \boldsymbol{D}_{J_{F_i}}(\boldsymbol{\theta}_{F_i}, \boldsymbol{\eta}_i)\dot{\boldsymbol{\theta}}_{F_i} - \boldsymbol{D}_{T_{O_i}}(\boldsymbol{x}_O, \boldsymbol{\eta}_i)\dot{\boldsymbol{x}}_O, \tag{2.26}$$

where

$$\boldsymbol{D}_{J_{F_i}} := \boldsymbol{D}_{F_i}\boldsymbol{J}_{F_i}(\boldsymbol{\theta}_{F_i}), \boldsymbol{D}_{T_{O_i}} := \boldsymbol{D}_{O_i}\boldsymbol{T}_O(\boldsymbol{x}_O), \tag{2.27}$$

$$\boldsymbol{D}_{F_i} := \begin{bmatrix} \boldsymbol{R}_{BC_{F_i}}^{\mathrm{T}} & -\boldsymbol{R}_{BC_{F_i}}^{\mathrm{T}}(\boldsymbol{R}_{BF_i}{}^{F_i}\boldsymbol{p}_{C_{F_i}})^\wedge \\ \boldsymbol{0}_{3\times3} & \boldsymbol{R}_{BC_{F_i}}^{\mathrm{T}} \end{bmatrix}, \tag{2.28}$$

$$\boldsymbol{D}_{O_i} := \begin{bmatrix} \boldsymbol{R}_{BC_{F_i}}^{\mathrm{T}} & -\boldsymbol{R}_{BC_{F_i}}^{\mathrm{T}}(\boldsymbol{R}_{BO}{}^{O}\boldsymbol{p}_{C_{O_i}})^\wedge \\ \boldsymbol{0}_{3\times3} & \boldsymbol{R}_{BC_{F_i}}^{\mathrm{T}} \end{bmatrix}. \tag{2.29}$$

$\boldsymbol{R}_{BC_{F_i}}$ is the rotation matrix of $\Sigma_{C_{F_i}}$ relative to Σ_B. Combining (2.26) and (2.21) leads to

$$\dot{\boldsymbol{\eta}}_i = \boldsymbol{H}_i(\boldsymbol{D}_{J_{F_i}}\dot{\boldsymbol{\theta}}_{F_i} - \boldsymbol{D}_{T_{O_i}}\dot{\boldsymbol{x}}_O). \tag{2.30}$$

Eq. (2.30) relates the velocities of the contact coordinates $\dot{\boldsymbol{\eta}}_i$ to those of the generalized coordinates $(\dot{\boldsymbol{\theta}}_{F_i}, \dot{\boldsymbol{x}}_O)$.

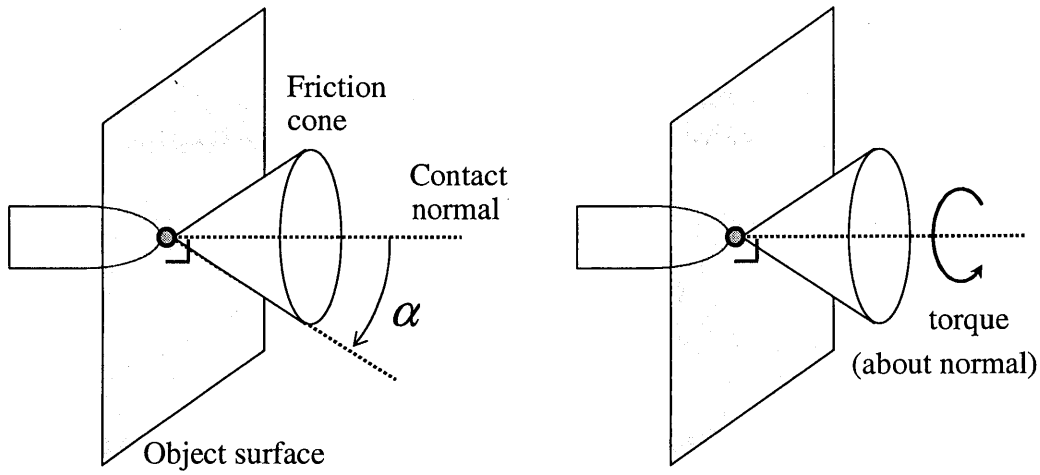

(a) Point contact with friction (b) Soft-finger contact

Figure 2.3 Geometric interpretation of the Coulomb friction model.

2.1.3 Grasp constraints

Contact models

For grasps in which we do wish to make use of frictional forces, we will use a simple model which is often referred to as the *Coulomb friction model.* The Coulomb friction model is an empirical model which asserts that the allowed tangential force is proportional to the applied normal force, and the constant of proportionality is a function of the materials which are in contact.

Typically, a finger will not be able to exert forces in every direction at a contact. We model a contact by using a *wrench basis* $\boldsymbol{B}_{C_i} \in \mathbb{R}^{6\times m_{c_i}}$ and a *friction cone* FC_i such that

$$\boldsymbol{F}_{C_i} = \boldsymbol{B}_{C_i}{}^{C}\boldsymbol{F}_{C_i} \in \mathbb{R}^6, \quad {}^{C}\boldsymbol{F}_{C_i} \in FC_i, \tag{2.31}$$

where $\boldsymbol{F}_{C_i} \in \mathbb{R}^6$ is the wrench applied by the contact at the origin of contact coordinate $\Sigma_{C_{F_i}}$ expressed in $\Sigma_{C_{F_i}}$ (Note that the wrench is the generalized force composed of linear and rotational components, and more details is shown in Appendix A). The dimension m_{c_i} of the wrench basis $\boldsymbol{B}_{C_i}$ indicates the number of independent forces that can be applied by the contact. Thus, ${}^{C}\boldsymbol{F}_{C_i} \in \mathbb{R}^{m_{c_i}}$ consists of the magnitudes of the independent forces at ith contact point. FC_i represents the set of forces which can be applied at the contact. We require that FC_i satisfy the following properties:

1. FC_i is a closed subset of $R^{m_{c_i}}$ with non-empty interior.

2. $\boldsymbol{f}_1, \boldsymbol{f}_2 \in FC_i \longrightarrow \alpha\boldsymbol{f}_1 + \beta\boldsymbol{f}_2 \in FC_i$ for $\alpha, \beta > 0$.

For a case where a contact is a *point contact with friction*, the wrench basis and the friction

cone are respectively described by

$$\boldsymbol{B}_{C_i} = \begin{bmatrix} 1 & 0 & 0 \\ 0 & 1 & 0 \\ 0 & 0 & 1 \\ 0 & 0 & 0 \\ 0 & 0 & 0 \\ 0 & 0 & 0 \end{bmatrix} \tag{2.32}$$

and

$$FC_i = \{\boldsymbol{f} \in \mathbb{R}^3 : \sqrt{f_1^2 + f_2^2} \leq \mu f_3,\ f_3 \geq 0\}, \tag{2.33}$$

where $\mu > 0$ is the (static) coefficient of friction. Eq. (2.33) can be represented geometrically as shown in (a) of Figure 2.3. The set of forces which can be applied at the contact must lie in the friction cone centered about the contact (surface) normal. The friction cone is characterized by the angle of the cone with respect to the normal given by

$$\alpha = \tan^{-1} \mu. \tag{2.34}$$

A more realistic contact model is the *soft-finger* contact. Here we allow not only forces to be applied in a friction cone about the contact normal, but also a torque about the normal, which is limited by a torsional friction coefficient. For the case, the wrench basis and the friction cone are respectively described by

$$\boldsymbol{B}_{C_i} = \begin{bmatrix} 1 & 0 & 0 & 0 \\ 0 & 1 & 0 & 0 \\ 0 & 0 & 1 & 0 \\ 0 & 0 & 0 & 0 \\ 0 & 0 & 0 & 0 \\ 0 & 0 & 0 & 1 \end{bmatrix} \tag{2.35}$$

and

$$FC_i = \{\boldsymbol{f} \in \mathbb{R}^4 : \sqrt{f_1^2 + f_2^2} \leq \mu f_3,\ f_3 \geq 0,\ |f_4| \geq \gamma f_3\}, \tag{2.36}$$

where $\gamma > 0$ is the coefficient of torsional friction. Eq. (2.36) can be represented geometrically as shown in (b) of Figure 2.3.

grasp constraints

In general, the directions in which motion is constrained are precisely the directions in which forces can be exerted by fingers at contacts as shown in Figure 2.4. Figure 2.4 shows a case where a contact model is a soft-finger contact. The left hand side (a) shows the directions by the contact and the right hand side (b) shows the directions constrained by the forces at the contact. Thus, the forces by the contact restrict the velocities of the finger and the object, i.e., the relative velocity $\boldsymbol{V}_{C_i}$ at the contact is zero. Hence, for a contact with a wrench basis $\boldsymbol{B}_{C_i} \in \mathbb{R}^{6 \times m_{c_i}}$, we require that

$$\boldsymbol{B}_{C_i}^{\mathrm{T}} \boldsymbol{V}_{C_i} = \boldsymbol{0}. \tag{2.37}$$

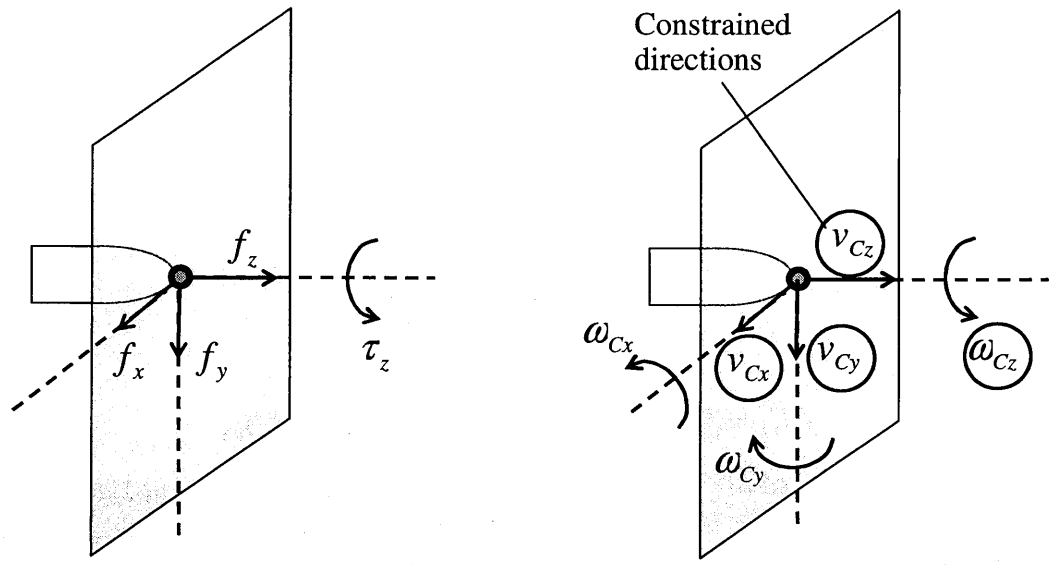

(a) Forces by a contact

(b) Directions constrained by forces at the contact of (a)

Figure 2.4 Constrained directions by forces at a contact: a case of a soft-finger contact.

Substituting (2.37) into (2.26) and aggregating the resultant equation for $i = 1, \cdots, n$, we get the *grasp constraint*:

$$\boldsymbol{A}_F(\boldsymbol{\theta}_F, \boldsymbol{\eta})\dot{\boldsymbol{\theta}}_F - \boldsymbol{A}_O(\boldsymbol{x}_O, \boldsymbol{\eta})\dot{\boldsymbol{x}}_O = 0, \tag{2.38}$$

where

$$\boldsymbol{A}_{F_i} := \begin{bmatrix} \boldsymbol{B}_{C_i}^{\mathrm{T}} \boldsymbol{D}_{J_{F_i}} & & \boldsymbol{0}_{m_{c_1} \times m_n} \\ & \ddots & \\ \boldsymbol{0}_{m_{c_n} \times m_1} & & \boldsymbol{B}_{C_n}^{\mathrm{T}} \boldsymbol{D}_{J_{F_n}} \end{bmatrix} \in \mathbb{R}^{m_c \times m} \tag{2.39}$$

$$\boldsymbol{A}_O := \begin{bmatrix} \boldsymbol{B}_{C_1}^{\mathrm{T}} \boldsymbol{D}_{T_{O_1}} \\ \vdots \\ \boldsymbol{B}_{C_n}^{\mathrm{T}} \boldsymbol{D}_{T_{O_n}} \end{bmatrix} \in \mathbb{R}^{m_c \times 6}, \tag{2.40}$$

where $m_c := m_{c_1} + \cdots + m_{c_n}$. Eq. (2.38) relates the velocities of the fingers to the velocity of the object.

The quantities $\boldsymbol{A}_F$, $\boldsymbol{A}_O$ and FC completely characterize the properties of the set of the fingers grasping the object. This motivate the following definition.

Definition 2.1 (Representation of a multi-fingered grasp).
A *multi-fingered grasp* is described by the Jacobians $\boldsymbol{A}_F : \mathbb{R}^m \mapsto \mathbb{R}^{m_c}$ and $\boldsymbol{A}_O : \mathbb{R}^6 \mapsto \mathbb{R}^{m_c}$, and the friction cone $FC \subset \mathbb{R}^{m_c}$ defined by

$$FC = FC_1 \times \cdots \times FC_n \subset \mathbb{R}^{m_c},$$

which satisfies the following properties:

1. FC_i is a closed subset of $R^{m_{c_i}}$ with non-empty interior.
2. $\boldsymbol{f}_1, \boldsymbol{f}_2 \in FC_i \longrightarrow \alpha \boldsymbol{f}_1 + \beta \boldsymbol{f}_2 \in FC_i$ for $\alpha, \beta > 0$.

Eq. (2.38) is also used in the force relationships. By equating the work done by the fingers, the object and the contacts, and using the grasp constraints, we get the following force relationships:

$$\boldsymbol{\tau}_F = \boldsymbol{A}_F^{\mathrm{T}C} \boldsymbol{F}_C \tag{2.41}$$

$${}^B\boldsymbol{F}_O = \boldsymbol{A}_O^{\mathrm{T}C} \boldsymbol{F}_C, \tag{2.42}$$

where ${}^C\boldsymbol{F}_C := [\, {}^C\boldsymbol{F}_{C_1}^{\mathrm{T}} \;\; \cdots \;\; {}^C\boldsymbol{F}_{C_{m_{c_n}}}^{\mathrm{T}} \,]^{\mathrm{T}} \in \mathbb{R}^{m_c}$ is the contact force, $\boldsymbol{\tau}_F \in \mathbb{R}^m$ is the vector composed of the resultant forces and/or torques produced by the contact force, and ${}^B\boldsymbol{F}_O \in \mathbb{R}^6$ is the object wrench which is produced by the contact force expressed in Σ_B.

2.1.4 Properties of grasp constraints

Here, we are in a position to study the mathematical properties of the grasp constraint in (2.38) and interpret them.

If a grasp can resist any wrench applied to the object, we say that such a grasp is *force-closure*. Formally, we make the following definition:

Definition 2.2 (Force-closure grasp).
A grasp is a *force-closure* grasp at a configuration $(\boldsymbol{x}_O, \boldsymbol{\eta})$ if given any external wrench ${}^B\boldsymbol{F}_e \in \mathbb{R}^6$ applied to the object, there exist contact forces $\boldsymbol{f}_C \in FC$ such that

$$\boldsymbol{A}_O^{\mathrm{T}C} \boldsymbol{F}_C = -{}^B\boldsymbol{F}_e.$$

A key feature of a force-closure grasp is the existence of *internal forces*. An internal force is a set of contact forces which result in no net force on the object. This motivates the following definition. Let int(FC) denote the interior of the friction cone.

Definition 2.3 (Internal forces).
If $\boldsymbol{F}_N \in \mathcal{N}(\boldsymbol{A}_O^{\mathrm{T}}) \cap FC$ at a configuration $(\boldsymbol{x}_O, \boldsymbol{\eta})$, then $\boldsymbol{F}_N$ is an *internal force*. If $\boldsymbol{F}_N \in \mathcal{N}(\boldsymbol{A}_O^{\mathrm{T}})$ and $\boldsymbol{F}_N \in \mathrm{int}(FC)$, then it is called a *strictly internal force*.

Internal forces can be used to insure that contact forces satisfy friction cone constraints. Note that an internal force is a set of contact forces, represented with respect to the wrench basis at each contact. The following proposition shows that the existence of a strictly internal force is a necessary condition for a grasp to be force-closure.

Proposition 2.1 (Necessity of internal forces).
A grasp is force-closure at a configuration $(\boldsymbol{x}_O, \boldsymbol{\eta})$ if and only if $\boldsymbol{A}_O^{\mathrm{T}}$ is surjective and there exists a vector of contact forces $\boldsymbol{F}_N \in \mathcal{N}(\boldsymbol{A}_O^{\mathrm{T}})$ such that $\boldsymbol{F}_N \in int(FC)$.

A fundamental property of a multi-fingered grasp is the ability of the robot fingers to accommodate an object motion. If a set of fingers can accommodate any motion of the object without losing contact, we say that such a grasp is *manipulable*:

Definition 2.4 (Manipulable grasp).
A multi-fingered grasp is *manipulable* at a configuration $(\boldsymbol{\theta}_F, \boldsymbol{x}_O, \boldsymbol{\eta})$ if for any object motion $\dot{\boldsymbol{x}}_O$ there exists $\dot{\boldsymbol{\theta}}_F$ which satisfies (2.38).

The following proposition follows from the definition.

Proposition 2.2 (Characterization of all manipulable grasp).
A grasp is manipulable at a configuration $(\boldsymbol{\theta}_F, \boldsymbol{x}_O, \boldsymbol{\eta})$ *if and only if*

$$\mathcal{R}(\boldsymbol{A}_O) \subset \mathcal{R}(\boldsymbol{A}_F).$$

It is important to distinguish between a force-closure grasp and a manipulable grasp. Force-closure requires only that the fingers can resist an external applied force, i.e., the opposing resistive force can be passive or structural. On the other hand, a manipulable grasp requires that the manipulator can actively accommodate all object motion directions while maintaining contact.

2.1.5 Dynamics with constraints

Pfaffian constraints

For a mechanical system whose configurations $\boldsymbol{q} \in \mathbb{R}^n$, we consider velocity constraints of the form

$$\boldsymbol{A}(\boldsymbol{q})\dot{\boldsymbol{q}} = \boldsymbol{0}, \tag{2.43}$$

where $\boldsymbol{A}(\boldsymbol{q}) \in \mathbb{R}^{k\times n}$ represents a set of k velocity constraints. A constraint of this form is called a *Pfaffian constraint.* The *constraint forces* by a set of Pfaffian constraint is described by the forces to insure that the system does not move in the directions given by the rows of the constraint matrix $\boldsymbol{A}(\boldsymbol{q})$. The constraint forces at a configuration $\boldsymbol{q}$ have the form

$$\boldsymbol{\Gamma} = \boldsymbol{A}^{\mathrm{T}}(\boldsymbol{q})\boldsymbol{\lambda}, \tag{2.44}$$

where $\boldsymbol{\lambda} \in \mathbb{R}^k$ is the vector of relative magnitudes of the constraint forces.

The constraint forces for a set of Pfaffian constraints prevent the motion of the system in directions which would violate the constraints. In order to include these forces in the dynamics, we must add one additional assumption about the nature of the constraints. Namely, we assume that the forces which are generated by the constraints do no work on the system, and hence conserve energy. This assumption is often referred to as *d'Alembert's principle.*

Lagrange's equations with constraints

Let $L(\boldsymbol{q}, \dot{\boldsymbol{q}})$ represent the Lagrangian for an unconstrained system. The constraints have the form of a Pfaffian form. Then, the equations of motion are formed by considering the constraint forces as an additional force which affects the motion of the system. Hence, the dynamics can be written in vector form as

$$\frac{d}{dt}\left(\frac{\partial L}{\partial \dot{\boldsymbol{q}}}\right) - \frac{\partial L}{\partial \boldsymbol{q}} + \boldsymbol{A}^{\mathrm{T}}(\boldsymbol{q})\boldsymbol{\lambda} - \boldsymbol{\Upsilon} = \boldsymbol{0}, \tag{2.45}$$

where $\boldsymbol{\Upsilon}$ represents nonconservative and externally applied forces. The scalars $\lambda_1, \cdots, \lambda_k$ are called *Lagrange multipliers.* and are determined by solving (2.43) and (2.45) for the $n + k$

variables $\boldsymbol{q}$ and $\boldsymbol{\lambda}$. They insure that no motion occurs in the constrained directions, and hence (2.43) holds for all time.

Consider the case where the Lagrangian has the form

$$L(\boldsymbol{q}, \dot{\boldsymbol{q}}) = \frac{1}{2}\dot{\boldsymbol{q}}^{\mathrm{T}}\boldsymbol{M}(\boldsymbol{q})\dot{\boldsymbol{q}} - V(\boldsymbol{q}), \tag{2.46}$$

where $\boldsymbol{M}(\boldsymbol{q}) \in \mathbb{R}^{n\times n}$ is the *inertia matrix* of the system and $V(\boldsymbol{q})$ is the *potential energy* due to the gravity. Substituting this Lagrangian into (2.45) leads to the following equations of motion with the constraints:

$$\boldsymbol{M}(\boldsymbol{q})\ddot{\boldsymbol{q}} + \boldsymbol{C}(\boldsymbol{q}, \dot{\boldsymbol{q}})\dot{\boldsymbol{q}} + \boldsymbol{N}(\boldsymbol{q}, \dot{\boldsymbol{q}}) = -\boldsymbol{A}^{\mathrm{T}}(\boldsymbol{q})\boldsymbol{\lambda} + \boldsymbol{\tau}, \tag{2.47}$$

where

$$\boldsymbol{C}(\boldsymbol{q}, \dot{\boldsymbol{q}}) := \dot{\boldsymbol{M}}(\boldsymbol{q}) - \frac{1}{2}\frac{\partial}{\partial \boldsymbol{q}}\left(\dot{\boldsymbol{q}}^{\mathrm{T}}\boldsymbol{M}(\boldsymbol{q})\right) \in \mathbb{R}^{n\times n} \tag{2.48}$$

is called the *Coriolis matrix*,

$$\boldsymbol{N}(\boldsymbol{q}, \dot{\boldsymbol{q}}) := \frac{\partial V(\boldsymbol{q})}{\partial \boldsymbol{q}} + \boldsymbol{\Upsilon} \in \mathbb{R}^{n} \tag{2.49}$$

includes nonconservative forces as well as potential forces, and $\boldsymbol{\tau} \in \mathbb{R}^n$ corresponds to the vector of external forces.

In the case where the Lagrangian has the form of (2.46), we can derive an explicit formula for the Lagrange multipliers. Differentiating the constraint equation (2.43) yields

$$\boldsymbol{A}(\boldsymbol{q})\ddot{\boldsymbol{q}} + \dot{\boldsymbol{A}}(\boldsymbol{q})\dot{\boldsymbol{q}} = \boldsymbol{0}.$$

Solving for $\ddot{\boldsymbol{q}}$ from (2.47) by using this equation, we get

$$\boldsymbol{\lambda} = (\boldsymbol{A}\boldsymbol{M}^{-1}\boldsymbol{A}^{\mathrm{T}})^{-1}\left(\boldsymbol{A}\boldsymbol{M}^{-1}(\boldsymbol{\tau} - \boldsymbol{C}\dot{\boldsymbol{q}} - \boldsymbol{N}) + \dot{\boldsymbol{A}}\dot{\boldsymbol{q}}\right).$$

By using this equation, the Lagrange multipliers can be computed as a function of the current state, $\boldsymbol{q}$ and $\dot{\boldsymbol{q}}$, and the applied forces $\boldsymbol{\tau}$.

Dynamics of fingers and a grasped object

Let the Lagrangian of the system composed of the fingers and the grasped object be

$$L(\boldsymbol{\theta}_F, \dot{\boldsymbol{\theta}}_F, \boldsymbol{x}_O, \dot{\boldsymbol{x}}_O) = \frac{1}{2}\dot{\boldsymbol{\theta}}_F^{\mathrm{T}}\boldsymbol{M}_F(\boldsymbol{\theta}_F)\dot{\boldsymbol{\theta}}_F + \frac{1}{2}\dot{\boldsymbol{x}}_O^{\mathrm{T}}\boldsymbol{M}_O(\boldsymbol{x}_O)\dot{\boldsymbol{x}}_O - V_F(\boldsymbol{\theta}_F) - V_O(\boldsymbol{x}_O), \tag{2.50}$$

where $\boldsymbol{M}_F(\boldsymbol{\theta}_F) \in \mathbb{R}^{m\times m}$ and $\boldsymbol{M}_O(\boldsymbol{x}_O) \in \mathbb{R}^{6\times 6}$ are the inertia matrices of the fingers and the object, and $V_F(\boldsymbol{\theta}_F)$ and $V_O(\boldsymbol{x}_O)$ are the potential energies due to the gravity of the fingers and the object. $\boldsymbol{M}_F$ and $\boldsymbol{M}_O$ are respectively defined by

$$\boldsymbol{M}_F := \begin{bmatrix} \boldsymbol{M}_{F_1} & & \boldsymbol{0}_{m_1\times m_n} \\ & \ddots & \\ \boldsymbol{0}_{m_n\times m_1} & & \boldsymbol{M}_{F_n} \end{bmatrix}, \tag{2.51}$$

where

$$\boldsymbol{M}_{F_i} := \boldsymbol{J}_{F_i}^{\mathrm{T}} \begin{bmatrix} m_{F_i}\boldsymbol{I}_3 & \boldsymbol{0}_{3\times3} \\ \boldsymbol{0}_{3\times3} & \boldsymbol{R}_{BF_i}\boldsymbol{\mathcal{I}}_{F_i}\boldsymbol{R}_{BF_i}^{\mathrm{T}} \end{bmatrix} \boldsymbol{J}_{F_i} \tag{2.52}$$

and

$$\boldsymbol{M}_O := \boldsymbol{T}_O^{\mathrm{T}} \begin{bmatrix} m_O\boldsymbol{I}_3 & \boldsymbol{0}_{3\times3} \\ \boldsymbol{0}_{3\times3} & \boldsymbol{R}_{BO}\boldsymbol{\mathcal{I}}_O\boldsymbol{R}_{BO}^{\mathrm{T}} \end{bmatrix} \boldsymbol{T}_O. \tag{2.53}$$

m_{F_i} and m_O are the mass of the ith finger and the mass of the object, and $\boldsymbol{\mathcal{I}}_{F_i} \in \mathbb{R}^{3\times3}$ and $\boldsymbol{\mathcal{I}}_O \in \mathbb{R}^{3\times3}$ are the moments of inertia tensors of the ith finger and the object. Let $\boldsymbol{q} = [\, \boldsymbol{\theta}_F^{\mathrm{T}} \;\; \boldsymbol{x}_O^{\mathrm{T}} \,]^{\mathrm{T}} \in \mathbb{R}^{m+6}$ be the generalized coordinates, and the constraint of the form (2.43) with $\boldsymbol{A} := [\, \boldsymbol{A}_F \;\; -\boldsymbol{A}_O \,] \in \mathbb{R}^{m_c\times(m+6)}$. Assume that there are no nonconservative forces on the system. Substituting the Lagrangian (2.50) into (2.45) leads to the following equations of motion with the constraints:

$$\boldsymbol{M}_F(\boldsymbol{\theta}_F)\ddot{\boldsymbol{\theta}}_F + \boldsymbol{C}_F(\boldsymbol{\theta}_F, \dot{\boldsymbol{\theta}}_F)\dot{\boldsymbol{\theta}}_F + \boldsymbol{N}_F(\boldsymbol{\theta}_F) = -\boldsymbol{A}_F^{\mathrm{T}}(\boldsymbol{\theta}_F, \boldsymbol{\eta})^C\boldsymbol{F}_C + \boldsymbol{\tau} \tag{2.54}$$

$$\boldsymbol{M}_O(\boldsymbol{x}_O)\ddot{\boldsymbol{x}}_O + \boldsymbol{C}_O(\boldsymbol{x}_O, \dot{\boldsymbol{x}}_O)\dot{\boldsymbol{x}}_O + \boldsymbol{N}_O(\boldsymbol{x}_O) = \boldsymbol{A}_O^{\mathrm{T}}(\boldsymbol{x}_O, \boldsymbol{\eta})^C\boldsymbol{F}_C, \tag{2.55}$$

where $\boldsymbol{C}_F \in \mathbb{R}^{m\times m}$ and $\boldsymbol{C}_O \in \mathbb{R}^{6\times6}$ are the Coriolis matrices and $\boldsymbol{N}_F \in \mathbb{R}^m$ and $\boldsymbol{N}_O \in \mathbb{R}^6$ are the potential forces due to the gravity respectively. Note that the contact force ${}^C\boldsymbol{F}_C$ plays the role of the Lagrange multipliers.

2.2 Theoretical Basis of Nonholonomic Systems

In this section, the properties of nonholonomic constraints and motion planning based on the geometric phase approaches [35] of nonholonomic systems are summarized briefly. See Refs. [6, 24, 25, 26, 27] for more details. In the following, nonlinear control theory and its technical terms are often used to explain these items. See Refs. [6, 45, 46] for more details.

2.2.1 Definition of nonholonomic constraints

Consider a mechanical system whose configurations $\boldsymbol{q} \in \mathbb{R}^n$ evolve in a smooth n-dimensional manifold $\mathcal{M}$. Constraints on the system are said to be *holonomic* if it restricts the motion of the system to a smooth m-dimensional manifold, which can be represented locally as a set of algebraic constraints on the configuration space as a vector-valued function,

$$\boldsymbol{h}(\boldsymbol{q}) = \boldsymbol{0}, \;\; \boldsymbol{h}(\boldsymbol{q}) \in \mathbb{R}^m. \tag{2.56}$$

The dimension of the manifold $\mathcal{M}' \subset \mathcal{M}$ on which the motion of the system evolves is $n - m$.

Next, consider constraints on the system to restrict the motion of the system to a smooth m-dimensional manifold, which can be represented locally as a Pfaffian constraint,

$$\boldsymbol{A}(\boldsymbol{q})\dot{\boldsymbol{q}} = \boldsymbol{0}, \;\; \boldsymbol{A}(\boldsymbol{q}) \in \mathbb{R}^{m\times n}. \tag{2.57}$$

A Pfaffian constraint of the form of (2.57) is *integrable* if there exist a vector-valued function $\boldsymbol{h} : \mathbb{R}^n \mapsto \mathbb{R}^m$ such that

$$\boldsymbol{h}(\boldsymbol{q}) = \boldsymbol{0} \iff \frac{\partial \boldsymbol{h}}{\partial \boldsymbol{q}}\dot{\boldsymbol{q}} = \boldsymbol{0}. \tag{2.58}$$

Thus, a Pfaffian constraint (2.57) is equivalent to a holonomic constraint of (2.56). Accordingly, a Pfaffian constraint (2.57) is said to be *nonholonomic* if it is not equivalent to a holonomic constraint as a vector-valued function.

2.2.2 Lie brackets and Frobenius's theorem

Some definitions and theorems in differential geometry are described for the latter discussion. Denote by $T_q\mathbb{R}^n$ the *tangent space* to $\mathbb{R}^n$ at a point $\boldsymbol{q} \in \mathbb{R}^n$. A *vector field* on $\mathbb{R}^n$ is a smooth map which assigns each point $\boldsymbol{q} \in \mathbb{R}^n$ to a tangent vector $\boldsymbol{g}(\boldsymbol{q}) \in T_q\mathbb{R}^n$.

Definition 2.5 (Lie brackets).
Given two vector fields $\boldsymbol{g}_1(\boldsymbol{q})$ and $\boldsymbol{g}_2(\boldsymbol{q})$, the *Lie bracket* of these two vectors is defined by

$$[\boldsymbol{g}_1, \boldsymbol{g}_2](\boldsymbol{q}) := \frac{\partial \boldsymbol{g}_2}{\partial \boldsymbol{q}} \boldsymbol{g}_1(\boldsymbol{q}) - \frac{\partial \boldsymbol{g}_1}{\partial \boldsymbol{q}} \boldsymbol{g}_2(\boldsymbol{q}) \subset T_q\mathbb{R}^n. \tag{2.59}$$

Definition 2.6 (Distribution).
Given a set of smooth vector fields $\boldsymbol{g}_1(\boldsymbol{q}), \cdots, \boldsymbol{g}_k(\boldsymbol{q})$, the *distribution* is defined by

$$\Delta_q = \text{span}\{\boldsymbol{g}_1(\boldsymbol{q}) \cdots \boldsymbol{g}_k(\boldsymbol{q})\}. \tag{2.60}$$

The distribution is said to be *regular* if the dimension of the subspace Δ_q does not vary with $\boldsymbol{q}$.

Definition 2.7 (Involutive distributions).
A distribution is *involutive* if for any two vector fields $\boldsymbol{f}, \boldsymbol{g} \in \Delta$ their Lie bracket $[\boldsymbol{f}, \boldsymbol{g}] \in \Delta$.

Definition 2.8 (Integrable distributions).
A distribution Δ is *integrable* if for any point $\boldsymbol{q} \in \mathbb{R}^n$ there exists a set of smooth functions $h_i : \mathbb{R}^n \mapsto \mathbb{R}$, $i = 1, \cdots, n-k$ such that the row vectors $\frac{\partial h_i}{\partial q}$ are linearly independent at $\boldsymbol{q}$, and for any $\boldsymbol{g} \in \Delta$

$$\frac{\partial h_i}{\partial \boldsymbol{q}} \boldsymbol{g}(\boldsymbol{q}) = 0, \quad i = 1, \cdots, n-k. \tag{2.61}$$

Furthermore, the hypersurfaces defined by the level sets

$$\{\boldsymbol{q} : h_1(\boldsymbol{q}) = c_1, \cdots, h_{n-k}(\boldsymbol{q}) = c_{n-k}\} \tag{2.62}$$

are called *integral manifolds* for the distribution.

Integral manifolds are related to involutive distributions by the following theorem [45, 46].

Theorem 2.1 (Frobenius's theorem).
A regular distribution is integrable if and only if it is involutive.

Thus, if Δ is an k-dimensional involutive distribution, then locally there exist $n-k$ functions $h_i : \mathbb{R}^n \mapsto \mathbb{R}$ such that integral manifolds of Δ are given by the level surfaces of $\boldsymbol{h} := [\, h_1 \ \cdots \ h_{n-k} \,]^{\mathrm{T}}$.

2.2.3 Nonlinear controllability

Some definitions and theorems in differential geometry and nonlinear control theory are described for the latter discussion. We consider the condition of integrable of a Pfaffian constraint of (2.57) based on Frobenius's theorem and controllability of a system with a nonholonomic constraint of the form as the Pfaffian constraint of (2.57).

A system with the constraint of (2.57) can easily be represented such that

$$\dot{\boldsymbol{q}} = \boldsymbol{A}^{\perp}(\boldsymbol{q})\boldsymbol{v}, \quad \boldsymbol{v} \in \mathbb{R}^{n-m}, \tag{2.63}$$

where the columns of

$$\boldsymbol{A}^{\perp}(\boldsymbol{q}) := \left[\boldsymbol{g}_1(\boldsymbol{q}) \quad \cdots \quad \boldsymbol{g}_{n-m}(\boldsymbol{q})\right] \in \mathbb{R}^{n\times(n-m)} \tag{2.64}$$

are a basis for the annihilating distribution of $\boldsymbol{A}(\boldsymbol{q})$ and $\boldsymbol{v}$ is a vector of quasi-velocities taking values in $\mathbb{R}^{n-m}$. Eq. (2.63) is called a *symmetry affine system* and a *kinematic model.* $\boldsymbol{v}$ is interpreted as the input to the system (2.63). Nonholonomy of the system (i.e., nonintegrability of (2.57)) can be checked through the contraposition of Frobenius's theorem, i.e., the distribution

$$\boldsymbol{\Delta} = \mathrm{span}\{\boldsymbol{g}_1(\boldsymbol{q}) \cdots \boldsymbol{g}_{n-m}(\boldsymbol{q})\} \tag{2.65}$$

is nonintegrable if and only if it is not involutive.

The controllability of system (2.63) can be checked by the *accessibility distribution* and *Chow's theorem.*

Definition 2.9 (Control Lie Algebra and accessibility distribution).
The *Control Lie Algebra* $\boldsymbol{\mathcal{L}}$ of a system of the form (2.63) is defined to be the span over the ring of smooth functions of elements of the form

$$[\boldsymbol{r}_k, [\boldsymbol{r}_{k-1}, [\cdots, [\boldsymbol{r}_2, \boldsymbol{r}_1]\cdots]]], \quad \boldsymbol{r}_i \in \{\boldsymbol{g}_1(\boldsymbol{q}), \cdots, \boldsymbol{g}_{n-m}(\boldsymbol{q})\}, \quad i \in \{1, \cdots, k\}, \quad k = 2, 3, \cdots. \tag{2.66}$$

The *accessibility distribution* is defined by

$$\overline{\boldsymbol{\Delta}} := \mathrm{span}\{\boldsymbol{f}(\boldsymbol{q}) : \boldsymbol{f} \in \boldsymbol{\mathcal{L}}\}. \tag{2.67}$$

Theorem 2.2 (Chow's theorem).
The control system (2.63) is locally controllable at $\boldsymbol{q} \in \mathbb{R}^n$ *if* $\overline{\boldsymbol{\Delta}}_q = T_q\mathbb{R}^n$.

If a system (2.63) is controllable, constraint (2.57) is so-called *maximally nonholonomic.* In robotics literature, the system with maximally nonholonomic constraints is called *nonholonomic systems.* To sum up, "an n-dimensional nonholonomic system can be controlled to *any* configurations in n-dimensional manifold $\mathcal{M}$ by using $n - m$ inputs which is fewer than n". This property is a typical contribution by the introduction of nonholonomic constraints.

2.2.4 Motion planning based on geometric phase approaches

In this subsection, motion planning based on *geometric phase approaches* is described briefly. Especially, we will concentrate on the motion of the contact coordinates for *pure rolling contact.*

Base vector and fiber vector

Here, we show a special form of a nonholonomic system of the form (2.63). Assume that the dimension of the distribution (2.65) is $m - n$. Then, there exist coordinate and input transformations and such that a system (2.63) is transformed to the form defined by

$$\frac{d}{dt}\begin{bmatrix}\boldsymbol{x}\\ \boldsymbol{\phi}\end{bmatrix} = \begin{bmatrix}\boldsymbol{I}_m\\ \hline \overline{\boldsymbol{g}}_1(\boldsymbol{x},\boldsymbol{\phi}) \quad \cdots \quad \overline{\boldsymbol{g}}_m(\boldsymbol{x},\boldsymbol{\phi})\end{bmatrix}\boldsymbol{u}, \tag{2.68}$$

where $\boldsymbol{x} \in \mathbb{R}^{m-n}$, $\boldsymbol{\phi} \in \mathbb{R}^m$ and $\overline{\boldsymbol{g}}_i : \mathbb{R}^n \mapsto \mathbb{R}^m$. $\boldsymbol{x}$ is referred to be the *base vector*, $\boldsymbol{\phi}$ is referred to be the *fiber vector*. This form is called a *strictly triangular form*. Strictly triangular forms have a contribution: the flow of the fiber vector fields and the geometric phases are obtained simply by subsequently integrating their components over time.

Geometric phases approaches to a spherical finger rolling on a plane

For simple notation, the subscript i is dropped. As described in Section 2.1.1, we parametrize the finger surface by $(\boldsymbol{c}_f, \boldsymbol{\alpha}_f)$, the object surface by $(\boldsymbol{c}_o, \boldsymbol{\alpha}_o)$, and the angle of the contact by ψ. Thus, configuration space is given by $\boldsymbol{\eta} = [\ \boldsymbol{\alpha}_f^{\mathrm{T}}\ \ \boldsymbol{\alpha}_o^{\mathrm{T}}\ \ \psi\ ]^{\mathrm{T}} \in \mathbb{R}^5$. Substituting the condition of pure rolling contact $v_{Cx} = v_{Cy} = v_{C_z} = \omega_{Cz} = 0$ into the kinematic equations of contact given by (2.21) yields the following constraint:

$$\boldsymbol{A}_\eta(\boldsymbol{\eta})\dot{\boldsymbol{\eta}} = \boldsymbol{0} \tag{2.69}$$

where

$$\boldsymbol{A}_\eta := \begin{bmatrix} -\boldsymbol{M}_{gf} & \boldsymbol{R}_\psi \boldsymbol{M}_{go} & 0 \\ -\boldsymbol{T}_{gf}\boldsymbol{M}_{gf} & -\boldsymbol{T}_{go}\boldsymbol{M}_{go} & 1 \end{bmatrix} \in \mathbb{R}^{3\times 5}. \tag{2.70}$$

A general solution of (2.69) with respect to $\dot{\boldsymbol{\eta}}$ is given by

$$\dot{\boldsymbol{\eta}} = \boldsymbol{A}_\eta^{\perp}(\boldsymbol{\eta})\boldsymbol{v}_\omega, \quad \boldsymbol{v}_\omega := [\ \omega_{Cx}\ \ \omega_{Cy}\ ]^{\mathrm{T}} \in \mathbb{R}^2, \tag{2.71}$$

where

$$\boldsymbol{A}_\eta^{\perp} := \begin{bmatrix} \boldsymbol{M}_{gf}^{-1}\boldsymbol{K}_R^{-1}\boldsymbol{E} \\ \boldsymbol{M}_{go}^{-1}\boldsymbol{R}_\psi\boldsymbol{K}_R^{-1}\boldsymbol{E} \\ \boldsymbol{T}_{gf}\boldsymbol{K}_R^{-1}\boldsymbol{E} \\ +\boldsymbol{T}_{go}\boldsymbol{R}_\psi\boldsymbol{K}_R^{-1}\boldsymbol{E} \end{bmatrix} \in \mathbb{R}^{5\times 2}. \tag{2.72}$$

Note that $\boldsymbol{A}_\eta\boldsymbol{A}_\eta^{\perp} = \boldsymbol{0}$ from (2.69) and (2.72). From (2.21), (2.23) and $v_{Cx} = v_{Cy} = v_{C_z} = \omega_{Cz} = 0$, we get

$$\boldsymbol{v}_\omega = -\boldsymbol{E}\boldsymbol{K}_R\boldsymbol{M}_{gf}\dot{\boldsymbol{\alpha}}_f. \tag{2.73}$$

Due to (2.73), (2.71) is transformed to

$$\dot{\boldsymbol{\eta}} = \begin{bmatrix} \boldsymbol{I}_2 \\ \boldsymbol{M}_{go}^{-1}\boldsymbol{R}_\psi\boldsymbol{M}_{gf} \\ (\boldsymbol{T}_{gf} + \boldsymbol{T}_{go}\boldsymbol{R}_\psi)\boldsymbol{M}_{gf} \end{bmatrix} \dot{\boldsymbol{\alpha}}_f = \begin{bmatrix} \boldsymbol{I}_2 \\ \boldsymbol{G}_\eta(\boldsymbol{\eta}) \end{bmatrix} \dot{\boldsymbol{\alpha}}_f. \tag{2.74}$$

Associated with the form (2.68), $\dot{\boldsymbol{\alpha}}_f$ is the base vector and $\widetilde{\boldsymbol{\eta}} = [\ \boldsymbol{\alpha}_o^{\mathrm{T}}\ \ \psi\ ]^{\mathrm{T}}$ is the fiber vector.

Suppose the base vector $\boldsymbol{\alpha}_f$ undergoes a cyclic motion $\boldsymbol{\alpha}_f(t)$, $0 \le t \le 1$, satisfying $\boldsymbol{\alpha}_f(0) = \boldsymbol{\alpha}_f(1)$. Then, the resulting change in the fiber vector $\widetilde{\boldsymbol{\eta}}$, $\widetilde{\boldsymbol{\eta}}(1) - \widetilde{\boldsymbol{\eta}}(0)$, can be written as a line integral along the path of the base vector:

$$\widetilde{\boldsymbol{\eta}}(1) - \widetilde{\boldsymbol{\eta}}(0) = \oint_\gamma \boldsymbol{G}(\boldsymbol{\eta})d\boldsymbol{\alpha}_f, \tag{2.75}$$

where $\gamma = \{\boldsymbol{\alpha}_f\ :\ 0 \le t \le 1\}$ is the base vector path. The value of this line integral is independent of any specific parametrization of the path and depends only the *geometry* of the

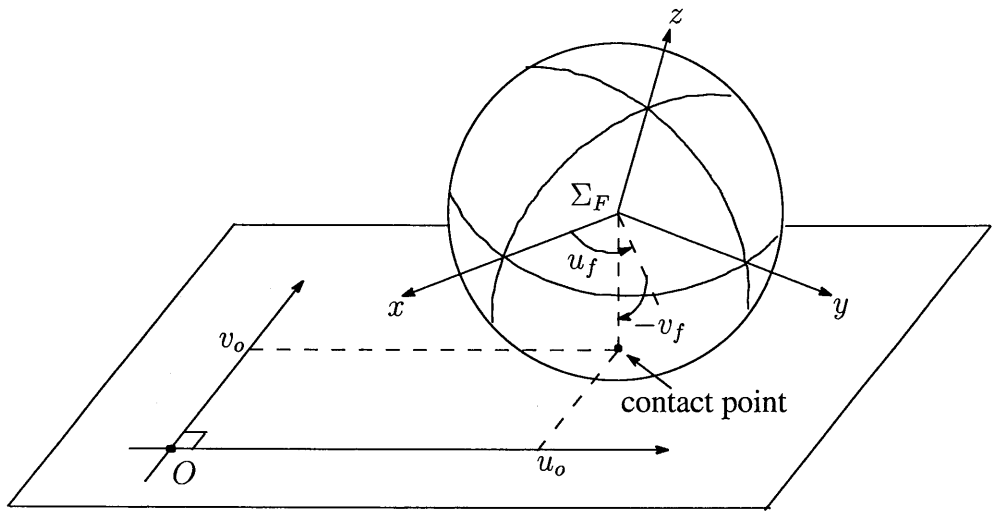

Figure 2.5 Spherical finger rolling on a plane.

path; hence, this value is referred to as the *geometric phase* or *holonomy*. Thus, the motion planning problem is reduced to finding an appropriate base space path which produces the desired geometric phase. Furthermore, by considering a parametrized finite dimensional family of base space paths, the problem can be reduced to a root-finding problem for the value of the parameters.

Let us restrict the surfaces of the finger and the object to a sphere and a plane as shown in Figure 2.5. The coordinate charts of the finger and the object are respectively described by

$$\boldsymbol{c}_f(\boldsymbol{\alpha}_f) = \begin{bmatrix} \rho \cos u_f \cos v_f \\ \rho \sin u_f \cos v_f \\ \rho \sin u_f \end{bmatrix}, \quad \boldsymbol{c}_o(\boldsymbol{\alpha}_o) = \begin{bmatrix} u_o \\ v_f \\ 0 \end{bmatrix}, \tag{2.76}$$

where ρ is the radius of the sphere. Then, the geometric parameters of the finger and the object are given by

$$\begin{aligned} \boldsymbol{K}_{go} &= \begin{bmatrix} 0 & 0 \\ 0 & 0 \end{bmatrix} \quad \boldsymbol{K}_{gf} = \begin{bmatrix} \frac{1}{\rho} & 0 \\ 0 & \frac{1}{\rho} \end{bmatrix} \\ \boldsymbol{M}_{go} &= \begin{bmatrix} 1 & 0 \\ 0 & 1 \end{bmatrix} \quad \boldsymbol{M}_{gf} = \begin{bmatrix} \rho \cos v_f & 0 \\ 0 & \rho \end{bmatrix} \\ \boldsymbol{T}_{go} &= [\,0 \;\; 0\,] \qquad \boldsymbol{T}_{gf} = [\,\tfrac{1}{\rho} \tan v_f \;\; 0\,]. \end{aligned} \tag{2.77}$$

Substituting these geometric parameters into (2.74) yields

$$\dot{\boldsymbol{\eta}} = \begin{bmatrix} \dot{\boldsymbol{\alpha}}_f \\ \dot{\boldsymbol{\alpha}}_o \\ \dot{\psi} \end{bmatrix} = \begin{bmatrix} 1 & 0 \\ 0 & 1 \\ \rho \cos v_f \cos \psi & -\rho \sin \psi \\ -\rho \cos v_f \sin \psi & -\rho \cos \psi \\ \sin v_f & 0 \end{bmatrix} \dot{\boldsymbol{\alpha}}_f. \tag{2.78}$$

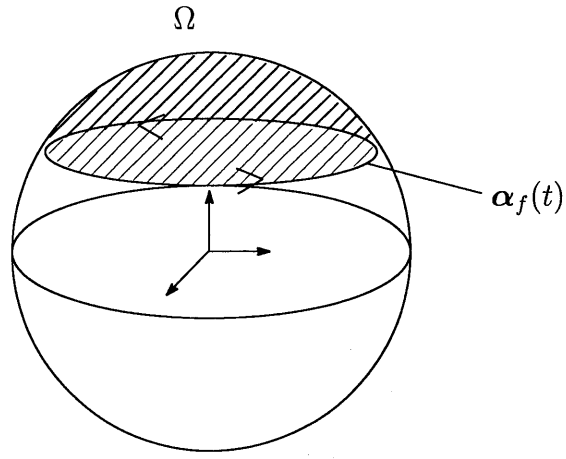

Figure 2.6 Geometric phase of a path in the sphere.

A nonholonomic system of a sphere and a plane with pure rolling contact has the following proposition:

Proposition 2.3.
A nonholonomic system of a sphere and a plane with pure rolling contact, i.e., (2.78) can not be put in the chained form [6]; it is not differentially flat [47]; it is not nilpotent [6].

The chained form, the properties the differentially flatness and nilpotent have some contributions to design control methods and many effective control methods based on the form and the properties have been proposed. However, these methods can not be applied to a system of a sphere and a plane with pure rolling contact. Thus, although a sphere rolling on a plane is a specified system, control of the system is a very challengeable problem.

Consider applying the geometric approaches to the system (2.78). Extracting the 5th row of (2.78) yields

$$\dot{\psi} = -\sin v_f \dot{u}_f. \tag{2.79}$$

Note that this equation is independent of the radius ρ of the sphere. Thus, the following theorem actually holds for spheres of arbitrary radius though stated for spheres of radius one.

Theorem 2.3 (Gauss-Bonnet theorem).
Let $\alpha_f : [0,1] \mapsto S_f$ be a closed path on the sphere of radius one which encloses a cap shaped region Ω as shown in Figure 2.6. Let $\Delta\psi$ be the change of the angle of contact as a result of rolling the sphere on the plane along the path given by $\alpha_f(\cdot)$. Then,

$$\Delta\psi = -Area\ of\ \Omega, \tag{2.80}$$

where the area of Ω is measured in the (curved) surface of the sphere of radius one.

$\Delta\psi$ is referred to as the geometric phase (holonomy) of the path $\alpha_f(\cdot)$. Furthermore, the following proposition specifies the motion of the object surface required to reposition the finger.

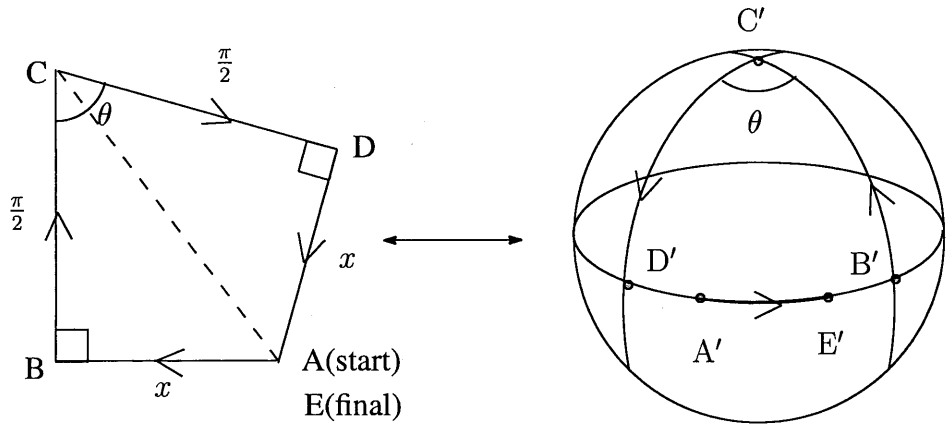

Figure 2.7 Closed path in the plane generates motion on the sphere.

Theorem 2.4 (Sphere rolling on a plane).
Let A' and E' be two points on the sphere which are a distance l apart on the sphere. Assume that $l < \frac{\pi}{2}$. Then, rolling the sphere on the plane along the closed curve $ABCDA$ shown in Figure 2.7 takes A' to E' provided the segments AB, DA are of length x and BC, CD are of length $\frac{\pi}{2}$, and x solves the equation

$$2\left(x - \tan^{-1}\frac{x}{\pi/2}\right) = l. \tag{2.81}$$

Chapter 3

Simultaneous Control by Two-fingered Robot Hand with Six Degrees of Freedom

In this chapter, we discuss the simultaneous control by a two-fingered robot hand, each finger of which has six degrees of freedom [48, 49, 50]. The contact motion between each finger and the object is assumed to be the pure rolling contact, and the surfaces of each finger and the object are assumed to be the regular surfaces. In Section 3.1, the modeling of the fingers and the object is summarized briefly.

Firstly, we consider the control method to utilize the nonholonomy of rolling for control of contact points. In Section 3.2, we clarify the degree of freedom of the whole system by investigating the property of the motion constraint on the generalized coordinates, which can be associated with the constraint of the contact coordinates. In Section 3.3 we propose a general formulation of a linearizing compensator for the internal force, the object motion and the rolling motion. Due to the linearization, the contact motion conforms to the kinematic model of two rolling bodies whose input is the rolling motion.

Secondly, we consider the regulation algorithm to control of the contact coordinates for the contact points. In Section 3.4, for the kinematic model of a sphere and a plane which correspond to a spherical finger and a cuboid object, we propose a method to regulate all the contact coordinates by iterative closed paths on the contact point of the sphere. The closed path is shaped as a trapezoid on the sphere parameterized by three variables. We call this closed path the *trapezoidal closed path*. The parameters is determined with respect to each interation. Furthermore, the convergence to arbitrary target points of the regulation method is guaranteed by proving that there always exist the parameters to reduce the euclidean norm of the distance to the target point. Since the method can be interpreted as a discrete-time feedback by regarding the start time of the iteration as the sampling instant, the method is expected to have robustness against disturbances. In Section 3.5, a numerical example is presented to show the effectiveness of the method.

3.1 Modeling

In this paper, we consider two fingertips grasping an object shown in Figure 3.1. The pair of two fingertips is a simplified model of a two-fingered robot hand, each of which has six degrees of freedom. The contact point between each finger and the object is single. In the following, the

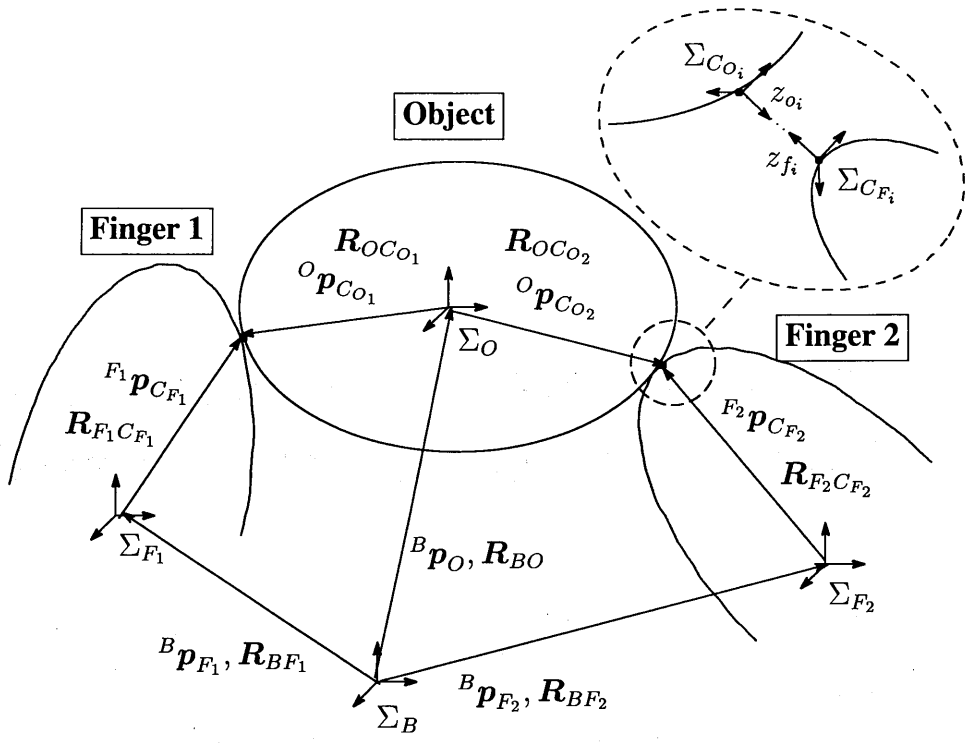

Figure 3.1 An object grasped by two finertips.

number of the fingers and the contact points is represented by $i = 1, 2$. Arguments of vectors and matrices are described explicitly only when they appear first time, and will be omitted in the sequel for notational simplicity. In this chapter, we make the following assumptions.

Assumption 3.1. The surfaces of each finger and the object are the regular surfaces [6]. Therefore, contact points on the surfaces of each finger and the object can be described by $\boldsymbol{c}(\boldsymbol{\alpha}) \in \mathbb{R}^3$, where $\boldsymbol{c}(\cdot) : \mathbb{R}^2 \mapsto \mathbb{R}^3$ is a local orthogonal chart and $\boldsymbol{\alpha} \in \mathbb{R}^2$ is a local coordinates.

Assumption 3.2. The frictional forces in the contact points follow the *Coulomb's law*. The contact force applied to the object by each finger is composed of translational forces and a moment about the contact normal.

Assumption 3.3. The constraint at each contact point is described by the pure rolling contact. The forces generated by the constraint do not work on the system (d'Alembert's principle).

The details of the system configuration, the kinematics and the dynamics of the fingers and the object are described in Chapter 2. Hence, they are summarized briefly in this section. Coordinate frames and configuration of the system are summarized in the following, as shown in Figure 3.1 and Figure 3.2.

(Definition of coordinate frames)

Σ_B Reference frame.

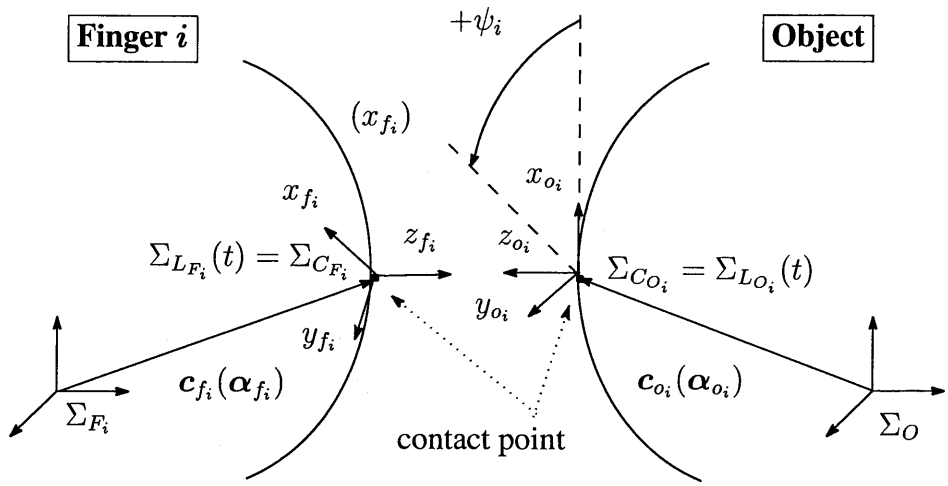

Figure 3.2 Contact coordinates of ith contact point.

Σ_{F_i}	Coordinate frame fixed to the ith finger.
Σ_O	Coordinates frame fixed to the object.
$\Sigma_{C_{F_i}}$	Contact frame attached on the surface of the ith finger with the origin at the ith contact point.
$\Sigma_{C_{O_i}}$	Contact frame attached on the surface of the object with the origin at the ith contact point.
$\Sigma_{C_{L_{F_i}}}$	Local frame fixed relative to Σ_{F_i} which coincides at time t with $\Sigma_{C_{F_i}}$.
$\Sigma_{C_{L_{O_i}}}$	Local frame fixed relative to Σ_O which coincides at time t with $\Sigma_{C_{O_i}}$.

(Variables of the system)

(Configuration of Fingers)

${}^B\boldsymbol{p}_{F_i} \in \mathbb{R}^3$	Position vector of Σ_{F_i} with respect to Σ_B.
$\boldsymbol{R}_{RF_i} \in \mathbb{R}^{3\times 3}$	Rotation matrix of Σ_{F_i} with respect to Σ_B.
${}^B\boldsymbol{\phi}_{F_i} \in \mathbb{R}^3$	Local parametrization of $\boldsymbol{R}_{RF_i}$.
$\boldsymbol{x}_{F_i} := [\ {}^B\boldsymbol{p}_{F_i}^{\mathrm{T}}\ {}^B\boldsymbol{\phi}_{F_i}^{\mathrm{T}}\ ]^{\mathrm{T}} \in \mathbb{R}^6$	Position and orientation of the ith finger.
$\boldsymbol{x}_F := [\ \boldsymbol{x}_{F_1}^{\mathrm{T}}\ \boldsymbol{x}_{F_2}^{\mathrm{T}}\ ]^{\mathrm{T}} \in \mathbb{R}^{12}$	Generalized coordinates of the fingers.

(Configuration of Object)

${}^B\boldsymbol{p}_O \in \mathbb{R}^3$	Position vector of Σ_O with respect to Σ_B.
$\boldsymbol{R}_{RO} \in \mathbb{R}^{3\times 3}$	Rotation matrix of Σ_O with respect to Σ_B.
${}^B\boldsymbol{\phi}_O \in \mathbb{R}^3$	Local parametrization of $\boldsymbol{R}_{RO}$.
$\boldsymbol{x}_O := [\ {}^B\boldsymbol{p}_O\ {}^B\boldsymbol{\phi}_O\ ]^{\mathrm{T}} \in \mathbb{R}^6$	Position and orientation of the object.

(Configuration of contacts)

${}^{F_i}\boldsymbol{p}_{C_{F_i}} \in \mathbb{R}^3$	Position vector of $\Sigma_{C_{F_i}}$ with respect to Σ_{F_i}.
$\boldsymbol{R}_{F_iC_{F_i}} \in \mathbb{R}^{3\times3}$	Rotation matrix of $\Sigma_{C_{F_i}}$ with respect to Σ_{F_i}.
${}^{O}\boldsymbol{p}_{C_{O_i}} \in \mathbb{R}^3$	Position vector of $\Sigma_{C_{O_i}}$ with respect to Σ_O.
$\boldsymbol{R}_{OC_{O_i}} \in \mathbb{R}^{3\times3}$	Rotation matrix of $\Sigma_{C_{O_i}}$ with respect to Σ_O.
$\boldsymbol{c}_{f_i}(\cdot) : \mathbb{R}^2 \mapsto \mathbb{R}^3$	Local orthogonal chart of the surface of the ith finger.
$\boldsymbol{c}_{o_i}(\cdot) : \mathbb{R}^2 \mapsto \mathbb{R}^3$	Local orthogonal chart of the surface of the object.
$\boldsymbol{\alpha}_{f_i} := [\ u_{f_i}\ \ v_{f_i}\ ]^{\mathrm{T}} \in \mathbb{R}^2$	Local coordinates on the surface of the ith finger.
$\boldsymbol{\alpha}_{o_i} := [\ u_{o_i}\ \ v_{o_i}\ ]^{\mathrm{T}} \in \mathbb{R}^2$	Local coordinates on the surface of the object.
$\psi_i \in \mathbb{R}^1$	Angle between the x- axes of $\Sigma_{C_{F_i}}$ and $\Sigma_{C_{O_i}}$.
$\boldsymbol{\eta}_i := [\ \boldsymbol{\alpha}_{f_i}^{\mathrm{T}}\ \ \boldsymbol{\alpha}_{o_i}^{\mathrm{T}}\ \ \psi_i]^{\mathrm{T}} \in \mathbb{R}^5$	Contact coordinates for the ith contact point.
$\boldsymbol{\eta} := [\ \boldsymbol{\eta}_1^{\mathrm{T}}\ \ \boldsymbol{\eta}_2^{\mathrm{T}}\ ]^{\mathrm{T}} \in \mathbb{R}^{10}$	Contact coordinates for the contact points.

(Forces)

${}^{C}\boldsymbol{F}_{C_i} \in \mathbb{R}^4$	Contact force at the i contact point.
${}^{C}\boldsymbol{F}_{C} := [\ {}^{C}\boldsymbol{F}_{C_1}^{\mathrm{T}}\ \ {}^{C}\boldsymbol{F}_{C_2}^{\mathrm{T}}\ ]^{\mathrm{T}} \in \mathbb{R}^8$	Contact force at the contact points.
$\boldsymbol{\tau}_i \in \mathbb{R}^6$	Input for the ith finger.
$\boldsymbol{\tau} := [\ \boldsymbol{\tau}_1^{\mathrm{T}}\ \ \boldsymbol{\tau}_2^{\mathrm{T}}\ ]^{\mathrm{T}} \in \mathbb{R}^{12}$	Input for the system.

Contact kinematics of the system are summarized in the following.

Let $\boldsymbol{V}_{C_i} := [\ v_{Cx_i}\ \ v_{Cy_i}\ \ v_{Cz_i}\ \ \omega_{Cx_i}\ \ \omega_{Cy_i}\ \ \omega_{Cz_i}\ ]^{\mathrm{T}} \in \mathbb{R}^6$ be the velocity of $\Sigma_{L_{F_i}}$ relative to $\Sigma_{L_{O_i}}$ seen from $\Sigma_{L_{F_i}}$. The motion of the contact coordinates $\dot{\boldsymbol{\eta}}_i$ as a function of the relative motion $\boldsymbol{V}_{C_i}$ is given by

$$\dot{\boldsymbol{\eta}}_i = \boldsymbol{H}_i(\boldsymbol{\eta}_i)\boldsymbol{V}_{C_i} \tag{3.1}$$

$$0 = v_{Cz_i}. \tag{3.2}$$

The precise definition of $\boldsymbol{H}_i \in \mathbb{R}^{5\times6}$ is given by (2.23). In addition, $\boldsymbol{V}_{C_i}$ is given by

$$\boldsymbol{V}_{C_i} = \boldsymbol{D}_{T_{F_i}}(\boldsymbol{x}_{F_i}, \boldsymbol{\eta}_i)\dot{\boldsymbol{x}}_{F_i} - \boldsymbol{D}_{T_{O_i}}(\boldsymbol{x}_O, \boldsymbol{\eta}_i)\dot{\boldsymbol{x}}_O, \tag{3.3}$$

where

$$\boldsymbol{D}_{T_{F_i}} := \boldsymbol{D}_{F_i}\boldsymbol{T}_{F_i}(\boldsymbol{x}_{F_i}), \boldsymbol{D}_{T_{O_i}} := \boldsymbol{D}_{O_i}\boldsymbol{T}_O(\boldsymbol{x}_O). \tag{3.4}$$

The precise definitions of $\boldsymbol{D}_{F_i} \in \mathbb{R}^{6\times6}$ and $\boldsymbol{D}_{O_i} \in \mathbb{R}^{6\times6}$ are given by (2.28) and (2.29). $\boldsymbol{T}_{F_i} \in \mathbb{R}^{6\times6}$ and $\boldsymbol{T}_O \in \mathbb{R}^{6\times6}$ are the transformation matrices from $[\ {}^{B}\dot{\boldsymbol{p}}_{F_i}^{\mathrm{T}}\ \ {}^{B}\dot{\boldsymbol{\phi}}_{F_i}^{\mathrm{T}}\ ]^{\mathrm{T}}$ to $[\ {}^{B}\dot{\boldsymbol{p}}_{F_i}^{\mathrm{T}}\ \ {}^{B}\boldsymbol{\omega}_{F_i}^{\mathrm{T}}\ ]^{\mathrm{T}}$ and the one from $[\ {}^{B}\dot{\boldsymbol{p}}_{O}^{\mathrm{T}}\ \ {}^{B}\dot{\boldsymbol{\phi}}_{O}^{\mathrm{T}}\ ]^{\mathrm{T}}$ to $[\ {}^{B}\dot{\boldsymbol{p}}_{O}^{\mathrm{T}}\ \ {}^{B}\boldsymbol{\omega}_{O}^{\mathrm{T}}\ ]^{\mathrm{T}}$ respectively. In this chapter, it is assumed that $\boldsymbol{T}_{F_i}$ and $\boldsymbol{T}_O$ are nonsingular respectively. Combining (3.3) and (3.1) leads to

$$\dot{\boldsymbol{\eta}}_i = \boldsymbol{H}_i(\boldsymbol{D}_{T_{F_i}}\dot{\boldsymbol{x}}_{F_i} - \boldsymbol{D}_{T_{O_i}}\dot{\boldsymbol{x}}_O). \tag{3.5}$$

Eq. (3.5) relates the velocities of contact coordinates $\dot{\boldsymbol{\eta}}_i$ to those of generalized coordinates $(\dot{\boldsymbol{x}}_{F_i}, \dot{\boldsymbol{x}}_O)$.

The motion constraint and the dynamics of the fingers/object are summarized in the following.

Motion Constraint

$$\boldsymbol{A}_F(\boldsymbol{x}_F, \boldsymbol{\eta})\dot{\boldsymbol{x}}_F - \boldsymbol{A}_O(\boldsymbol{x}_O, \boldsymbol{\eta})\dot{\boldsymbol{x}}_O = \boldsymbol{0}, \tag{3.6}$$

where

$$\boldsymbol{A}_F := \begin{bmatrix} \boldsymbol{B}_C^{\mathrm{T}}\boldsymbol{D}_{T_{F_1}} & \boldsymbol{0}_{4\times 6} \\ \boldsymbol{0}_{4\times 6} & \boldsymbol{B}_C^{\mathrm{T}}\boldsymbol{D}_{T_{F_2}} \end{bmatrix}, \boldsymbol{A}_O := \begin{bmatrix} \boldsymbol{B}_C^{\mathrm{T}}\boldsymbol{D}_{T_{O_1}} \\ \boldsymbol{B}_C^{\mathrm{T}}\boldsymbol{D}_{T_{O_2}} \end{bmatrix}, \boldsymbol{B}_C := \begin{bmatrix} \boldsymbol{I}_3 & \boldsymbol{0}_{3\times 1} \\ \boldsymbol{0}_{3\times 3} & \boldsymbol{e} \end{bmatrix}, \boldsymbol{e} := \begin{bmatrix} 0 \\ 0 \\ 1 \end{bmatrix} \tag{3.7}$$

Constraint on Contact Force

$${}^C\boldsymbol{F}_C \in FC, \tag{3.8}$$

where FC describes the set of the contact force which lies in the friction cone.

Equations of Motion

$$\boldsymbol{M}_F(\boldsymbol{x}_F)\ddot{\boldsymbol{x}}_F + \boldsymbol{C}_F(\boldsymbol{x}_F, \dot{\boldsymbol{x}}_F)\dot{\boldsymbol{x}}_F + \boldsymbol{N}_F(\boldsymbol{x}_F) = -\boldsymbol{A}_F^{\mathrm{T}}(\boldsymbol{x}_F, \boldsymbol{\eta}){}^C\boldsymbol{F}_C + \boldsymbol{T}_F^{\mathrm{T}}(\boldsymbol{x}_F)\boldsymbol{\tau} \tag{3.9}$$

$$\boldsymbol{M}_O(\boldsymbol{x}_O)\ddot{\boldsymbol{x}}_O + \boldsymbol{C}_O(\boldsymbol{x}_O, \dot{\boldsymbol{x}}_O)\dot{\boldsymbol{x}}_O + \boldsymbol{N}_O(\boldsymbol{x}_O) = \boldsymbol{A}_O^{\mathrm{T}}(\boldsymbol{x}_O, \boldsymbol{\eta}){}^C\boldsymbol{F}_C, \tag{3.10}$$

where $\boldsymbol{M}_F > 0 \in \mathbb{R}^{12\times 12}$, $\boldsymbol{M}_O > 0 \in \mathbb{R}^{6\times 6}$ are the generalized inertia matrices, $\boldsymbol{C}_F \in \mathbb{R}^{12\times 12}$, $\boldsymbol{C}_O \in \mathbb{R}^{6\times 6}$ are the Coriolis matrices, and $\boldsymbol{N}_F \in \mathbb{R}^{12}$, $\boldsymbol{N}_O \in \mathbb{R}^6$ are the gravity terms.

3.2 Properties of Motion Constraint

In this section, we clarify properties of motion constraint (3.6) on the generalized coordinates by associating with constraints on the contact coordinates. Consider the following conditions:

$$\boldsymbol{A}_{\eta_i}(\boldsymbol{\eta}_i)\dot{\boldsymbol{\eta}}_i = \boldsymbol{0} \qquad (i = 1, 2) \tag{3.11}$$

$$\boldsymbol{b}_C^{\mathrm{T}}(\boldsymbol{D}_{F_i}\dot{\boldsymbol{x}}_{F_i} - \boldsymbol{D}_{O_i}\dot{\boldsymbol{x}}_O) = 0 \quad (i = 1, 2), \tag{3.12}$$

where

$$\boldsymbol{A}_{\eta_i} := \begin{bmatrix} -\boldsymbol{M}_{gf_i} & \boldsymbol{R}_{\psi_i}\boldsymbol{M}_{go_i} & 0 \\ -\boldsymbol{T}_{gf_i}\boldsymbol{M}_{gf_i} & -\boldsymbol{T}_{go_i}\boldsymbol{M}_{go_i} & 1 \end{bmatrix} \in \mathbb{R}^{3\times 5} \tag{3.13}$$

$$\boldsymbol{b}_C := [\,0\ 0\ 1\ 0\ 0\ 0\,]^{\mathrm{T}}. \tag{3.14}$$

The following theorem holds.

Theorem 3.1.
(i) *Suppose (3.5) holds. Then, motion constraint (3.6) is equivalent to (3.11) and (3.12).*
(ii) *Suppose $\boldsymbol{K}_{R_i}$ defined by (2.24) is full rank and $\boldsymbol{c}_{f_i}$ is not the specular image [40] of $\boldsymbol{c}_{o_i}$. Then, the constraints on the contact coordinates (3.11) are the maximal nonholonomic constraints and constraints (3.12) on the generalized coordinates are the holonomic constraints.*

The definition of the specular image is stated in Appendix B.5. Roughly speaking, $\boldsymbol{c}_{f_i}$ being the specular image of $\boldsymbol{c}_{o_i}$ means that $\boldsymbol{c}_{f_i}$ is symmetrical to $\boldsymbol{c}_{o_i}$ with respect to the contact point.

Proof. **(i)** Equation (3.6) is represented as

$$\boldsymbol{B}_C^{\mathrm{T}}(\boldsymbol{D}_{F_i}\dot{\boldsymbol{x}}_{F_i} - \boldsymbol{D}_{O_i}\dot{\boldsymbol{x}}_O) = \boldsymbol{0}. \tag{3.15}$$

On the other hand, substituting (3.5) into (3.6) and combining the resultant equation with (3.12) lead to

$$\widetilde{\boldsymbol{B}}_C^{\mathrm{T}}(\boldsymbol{D}_{F_i}\dot{\boldsymbol{x}}_{F_i} - \boldsymbol{D}_{O_i}\dot{\boldsymbol{x}}_O) = 0, \quad \widetilde{\boldsymbol{B}}_C^{\mathrm{T}} := \begin{bmatrix} \boldsymbol{A}_{\eta_i}\boldsymbol{H}_i \\ \boldsymbol{b}_C^{\mathrm{T}} \end{bmatrix}. \tag{3.16}$$

Therefore, in order to clarify that Eqs. (3.15) and (3.16) are equivalent, it is enough to show that a nonsingular matrix $\boldsymbol{E}_4 \in \mathbb{R}^{4\times 4}$ exists such that $\boldsymbol{E}_4\widetilde{\boldsymbol{B}}_C^{\mathrm{T}} = \boldsymbol{B}_C^{\mathrm{T}}$. This is immediate since by using (3.13), (2.23), (2.24) and $\boldsymbol{R}_\psi = \boldsymbol{R}_\psi^{\mathrm{T}} = \boldsymbol{R}_\psi^{-1}$ we get

$$\widetilde{\boldsymbol{B}}_C^{\mathrm{T}} = \begin{bmatrix} 1 & 0 & 0 & 0 & 0 & 0 \\ 0 & 1 & 0 & 0 & 0 & 0 \\ 0 & 0 & 0 & 0 & 0 & 1 \\ 0 & 0 & 1 & 0 & 0 & 0 \end{bmatrix}. \tag{3.17}$$

(ii) Since $\boldsymbol{c}_{f_i}$ is not the specular image of $\boldsymbol{c}_{o_i}$, (4.12) are the maximal nonholonomic constraints [40]. From (2.28) and (2.29), note that (3.12) is rewritten as follows:

$$\boldsymbol{e}^{\mathrm{T}}\boldsymbol{R}_{BC_{F_i}}^{\mathrm{T}}\left[{}^B\dot{\boldsymbol{p}}_{F_i} - (\boldsymbol{R}_{BF_i}{}^{F_i}\boldsymbol{p}_{C_{F_i}})^{\wedge B}\boldsymbol{\omega}_{F_i} - \left({}^B\dot{\boldsymbol{p}}_O - (\boldsymbol{R}_{BO}{}^O\boldsymbol{p}_{C_{O_i}})^{\wedge B}\boldsymbol{\omega}_O\right)\right] = 0, \tag{3.18}$$

where $\boldsymbol{e} := [\,0\ 0\ 1\,]^{\mathrm{T}}$. Consider the constraint $h_{Cz_i}(\boldsymbol{x}_{F_i}, \boldsymbol{x}_O, \boldsymbol{\eta}_i) = 0$ where

$$h_{Cz_i} := \boldsymbol{e}^{\mathrm{T}}\boldsymbol{R}_{BC_{F_i}}^{\mathrm{T}}\left[{}^B\boldsymbol{p}_{F_i} + \boldsymbol{R}_{BF_i}{}^{F_i}\boldsymbol{p}_{C_{F_i}} - ({}^B\boldsymbol{p}_O + \boldsymbol{R}_{BO}{}^O\boldsymbol{p}_{C_{O_i}})\right]. \tag{3.19}$$

It is sufficient to show that the differential of (3.19) is equivalent to the left-hand of (3.18). Differentiating $h_{C_{z_i}} = 0$ with respect to time leads to

$$\begin{aligned}&\boldsymbol{e}^{\mathrm{T}}\dot{\boldsymbol{R}}_{BC_{F_i}}^{\mathrm{T}}\left[{}^B\boldsymbol{p}_{F_i} + \boldsymbol{R}_{BF_i}{}^{F_i}\boldsymbol{p}_{C_{F_i}} - ({}^B\boldsymbol{p}_O + \boldsymbol{R}_{BO}{}^O\boldsymbol{p}_{C_{O_i}})\right] \\ &+\boldsymbol{e}^{\mathrm{T}}\boldsymbol{R}_{BC_{F_i}}^{\mathrm{T}}\left[({}^B\dot{\boldsymbol{p}}_{F_i} + \dot{\boldsymbol{R}}_{BF_i}{}^{F_i}\boldsymbol{p}_{C_{F_i}} + \boldsymbol{R}_{BF_i}{}^{F_i}\dot{\boldsymbol{p}}_{C_{F_i}}) - ({}^B\dot{\boldsymbol{p}}_O + \dot{\boldsymbol{R}}_{BO}{}^O\boldsymbol{p}_{C_{O_i}} + \boldsymbol{R}_{BO}{}^O\dot{\boldsymbol{p}}_{C_{O_i}})\right] = 0.\end{aligned} \tag{3.20}$$

Substituting the contact condition (2.18) into (3.21) leads to

$$\boldsymbol{e}^{\mathrm{T}}\boldsymbol{R}_{BC_{F_i}}^{\mathrm{T}}\left[({}^B\dot{\boldsymbol{p}}_{F_i} + \dot{\boldsymbol{R}}_{BF_i}{}^{F_i}\boldsymbol{p}_{C_{F_i}} + \boldsymbol{R}_{BF_i}{}^{F_i}\dot{\boldsymbol{p}}_{C_{F_i}}) - ({}^B\dot{\boldsymbol{p}}_O + \dot{\boldsymbol{R}}_{BO}{}^O\boldsymbol{p}_{C_{O_i}} + \boldsymbol{R}_{BO}{}^O\dot{\boldsymbol{p}}_{C_{O_i}})\right] = 0. \tag{3.21}$$

Let us compute each term in the left hand side of (3.21) in the following. First, from the relationship between rotation matrices and rotation velocities such that $\dot{\boldsymbol{R}}\boldsymbol{R}^{\mathrm{T}} = \boldsymbol{\omega}^{\wedge}$ from (A.19), the terms $\dot{\boldsymbol{R}}_{BF_i}{}^{F}\boldsymbol{p}_{C_{F_i}}$ and $\dot{\boldsymbol{R}}_{BO}{}^{O}\boldsymbol{p}_{C_{O_i}}$ are transformed as follows:

$$\dot{\boldsymbol{R}}_{BF_i}{}^{F}\boldsymbol{p}_{C_{F_i}} = -(\boldsymbol{R}_{BF_i}{}^{F}\boldsymbol{p}_{C_{F_i}})^{\wedge_B}\boldsymbol{\omega}_{F_i}, \tag{3.22}$$

$$\dot{\boldsymbol{R}}_{BO}{}^{O}\boldsymbol{p}_{C_{O_i}} = -(\boldsymbol{R}_{BO}{}^{O}\boldsymbol{p}_{C_{O_i}})^{\wedge_B}\boldsymbol{\omega}_{O}. \tag{3.23}$$

Next, from the contact relationship with respect to the rotation matrices (2.19), $\boldsymbol{R}_{BF_i}{}^{F_i}\dot{\boldsymbol{p}}_{C_{F_i}}$ and $\boldsymbol{R}_{BO}{}^{O}\dot{\boldsymbol{p}}_{C_{O_i}}$ are given by

$$\boldsymbol{R}_{BF_i}{}^{F_i}\dot{\boldsymbol{p}}_{C_{F_i}} = \boldsymbol{R}_{BC_{F_i}}\boldsymbol{R}^{\mathrm{T}}_{F_iC_{F_i}}{}^{F_i}\dot{\boldsymbol{p}}_{C_{F_i}}, \tag{3.24}$$

$$\boldsymbol{R}_{BO}{}^{O}\dot{\boldsymbol{p}}_{C_{O_i}} = \boldsymbol{R}_{BC_{F_i}}\boldsymbol{R}^{\mathrm{T}}_{C_{O_i}C_{F_i}}\boldsymbol{R}^{\mathrm{T}}_{OC_{O_i}}{}^{F_i}\dot{\boldsymbol{p}}_{C_{O_i}}, \tag{3.25}$$

where $\boldsymbol{R}^{\mathrm{T}}_{F_iC_{F_i}}{}^{F_i}\dot{\boldsymbol{p}}_{C_{F_i}}$ and $\boldsymbol{R}^{\mathrm{T}}_{OC_{O_i}}{}^{O}\dot{\boldsymbol{p}}_{C_{O_i}}$ are the velocity of $\Sigma_{C_{F_i}}$ relative to Σ_{F_i} seen from $\Sigma_{C_{F_i}}$ and the velocity of $\Sigma_{C_{O_i}}$ relative to Σ_O seen from $\Sigma_{C_{O_i}}$ respectively. Therefore, from (B.8), these term are given by

$$\boldsymbol{R}^{\mathrm{T}}_{F_iC_{F_i}}{}^{F_i}\dot{\boldsymbol{p}}_{C_{F_i}} = \begin{bmatrix} \boldsymbol{M}_{gf_i}\dot{\boldsymbol{\alpha}}_{f_i} \\ 0 \end{bmatrix}, \quad \boldsymbol{R}^{\mathrm{T}}_{OC_{O_i}}{}^{O}\dot{\boldsymbol{p}}_{C_{O_i}} = \begin{bmatrix} \boldsymbol{M}_{go_i}\dot{\boldsymbol{\alpha}}_{o_i} \\ 0 \end{bmatrix}. \tag{3.26}$$

Finally, from the structure of $\boldsymbol{R}_{C_{O_i}C_{F_i}}$ of (2.9), $\boldsymbol{R}^{\mathrm{T}}_{C_{O_i}C_{F_i}}\boldsymbol{R}^{\mathrm{T}}_{OC_{O_i}}{}^{O}\dot{\boldsymbol{p}}_{C_{O_i}}$ is given by

$$\boldsymbol{R}^{\mathrm{T}}_{C_{O_i}C_{F_i}}\boldsymbol{R}^{\mathrm{T}}_{OC_{O_i}}{}^{O}\dot{\boldsymbol{p}}_{C_{O_i}} = \begin{bmatrix} \boldsymbol{R}_{\psi_i}\boldsymbol{M}_{go_i}\dot{\boldsymbol{\alpha}}_{o_i} \\ 0 \end{bmatrix}, \tag{3.27}$$

where $\boldsymbol{R}_{\psi} = \boldsymbol{R}^{\mathrm{T}}_{\psi} = \boldsymbol{R}^{-1}_{\psi}$ from (2.25). Substituting (3.22)–(3.27) into (3.21) leads to (3.18). Therefore, (3.18) is the holonomic constraint. □

Remark 3.1. From Theorem 3.1, the system has six nonholonomic constraints and two holonomic constraints. Since $\boldsymbol{x}_F \in \mathbb{R}^{12}$ and $\boldsymbol{x}_O \in \mathbb{R}^6$, the degrees of freedom of velocity $(\dot{\boldsymbol{x}}_F, \dot{\boldsymbol{x}}_O)$ is 10 and the degrees of freedom of position $(\boldsymbol{x}_F, \boldsymbol{x}_O)$ is 16.

3.3 Control Design

3.3.1 Control Objectives

The control objectives in this chapter are as follows:

(A) To make contact force ${}^{C}\boldsymbol{F}_C$ lie in the set of friction cone FC.

(B) To make object $\boldsymbol{x}_O \in \mathbb{R}^6$ follow a desired trajectory.

(C) To regulate contact coordinates $\boldsymbol{\eta} \in \mathbb{R}^{10}$ to a target point.

Control objective (A) represents that the fingers do not slip, and (B) and (C) represent the control of the object and the contact points. Note from Remark 3.1 that the system has the degrees of freedom which are necessary to realize the control objectives. To achieve these control objectives, we design a linearizing compensator for the object motion, the internal force and the rolling motion. Therefore, a desired trajectory and a target point in (B) and (C) can be chosen arbitrarily.

To design a linearizing compensator, we make the following assumptions:

Assumption 3.4.
(i) $\boldsymbol{A}_O^{\mathrm{T}} \in \mathbb{R}^{6\times 8}$ is full row rank.
(ii) There exists a internal force $\boldsymbol{F}_N \in \mathbb{R}^8$ such that $\boldsymbol{F}_N \in \mathcal{N}(\boldsymbol{A}_O^{\mathrm{T}})$ and $\boldsymbol{F}_N \in \mathrm{Int}(FC)$, where $\mathrm{Int}(FC)$ represents the interior of the friction cone and $\mathcal{N}(\boldsymbol{A}_O^{\mathrm{T}})$ represents the kernel of $\boldsymbol{A}_O^{\mathrm{T}}$.

Assumption 3.5. $\boldsymbol{A}_F \in \mathbb{R}^{8\times 12}$ is full row rank.

Assumption 3.4 and 3.5 correspond to the Force Closure and Manipulable [6] in the robotics literatures respectively. Generally, the conditions to guarantee these assumptions depend on the degrees of freedom of the fingers, the motion constraint, the number of elements of the contact force, the configuration of the contact points, etc. In our case, Assumption 4 can be satisfied by choosing the configuration of the contact points appropriately. Assumption 5 is always satisfied since $\boldsymbol{D}_{F_i}$ is nonsingular from (2.28).

3.3.2 Expression of Contact Force

Let ${}^B\boldsymbol{F}_O \in \mathbb{R}^6$ be

$$ {}^B\boldsymbol{F}_O := \boldsymbol{A}_O^{\mathrm{T}\,C}\boldsymbol{F}_C. \tag{3.28} $$

${}^B\boldsymbol{F}_O$ represents the resultant force applied to Σ_O by the contact force ${}^C\boldsymbol{F}_C \in \mathbb{R}^8$ (See (3.10)). From Assumption 3.4, a general solution of (3.28) with respect to ${}^C\boldsymbol{F}_C$ is given by

$$ {}^C\boldsymbol{F}_C = (\boldsymbol{A}_O^{\mathrm{T}})^{+B}\boldsymbol{F}_O + \boldsymbol{K}_{A_O^{\mathrm{T}}}(\boldsymbol{x}_O, \boldsymbol{\eta})\boldsymbol{f}_N, \tag{3.29} $$

where $(\cdot)^+$ denotes the pseudo inverse matrix and $\boldsymbol{K}_{A_O^{\mathrm{T}}} \in \mathbb{R}^{8\times 2}$ satisfies $\boldsymbol{A}_O^{\mathrm{T}}\boldsymbol{K}_{A_O^{\mathrm{T}}} = \boldsymbol{0}$ with $\mathrm{rank}(\boldsymbol{K}_{A_O^{\mathrm{T}}}) = 2$. In (3.29), $(\boldsymbol{A}_O^{\mathrm{T}})^{+B}\boldsymbol{F}_O$ represents the component of the contact force which produces the resultant force $\boldsymbol{F}_O$, and $\boldsymbol{K}_{A_O^{\mathrm{T}}}\boldsymbol{f}_N$ represents the internal force which causes no effect on the object motion, where $\boldsymbol{f}_N := [\, f_{N_1} \;\; f_{N_2} \,]^{\mathrm{T}} \in \mathbb{R}^2$ is its magnitude.

The expressions of $\boldsymbol{K}_{A_O^{\mathrm{T}}}$ have many possibilities. However, it is very important since the expressions of $\boldsymbol{K}_{A_O^{\mathrm{T}}}$ determine the physical meaning of $\boldsymbol{f}_N$. In this study, we propose the following $\boldsymbol{K}_{A_O^{\mathrm{T}}}$ which is effective to achieve the control objective (A):

$$ \boldsymbol{K}_{A_O^{\mathrm{T}}} := [\, \boldsymbol{k}_1 \;\; \boldsymbol{k}_2 \,] \tag{3.30} $$

$$ \boldsymbol{k}_1 := \begin{bmatrix} \boldsymbol{R}_{BC_{F_1}}^{\mathrm{T}}\,{}^B\boldsymbol{e}_{12} \\ 0 \\ \boldsymbol{R}_{BC_{F_2}}^{\mathrm{T}}\,{}^B\boldsymbol{e}_{21} \\ 0 \end{bmatrix}, \quad \boldsymbol{k}_2 := \begin{bmatrix} \boldsymbol{R}_{BC_{F_1}}^{\mathrm{T}}({}^B\boldsymbol{p}_{C_{O_{12}}}^{\wedge})^{+}\boldsymbol{\tau}_N \\ \dfrac{1}{({}^B\boldsymbol{p}_{C_{O_{12}}})^{\mathrm{T}\,B}\boldsymbol{e}_{1z}} \\ -\boldsymbol{R}_{BC_{F_2}}^{\mathrm{T}}({}^B\boldsymbol{p}_{C_{O_{12}}}^{\wedge})^{+}\boldsymbol{\tau}_N \\ \dfrac{-1}{({}^B\boldsymbol{p}_{C_{O_{12}}})^{\mathrm{T}\,B}\boldsymbol{e}_{2z}} \end{bmatrix}, \tag{3.31} $$

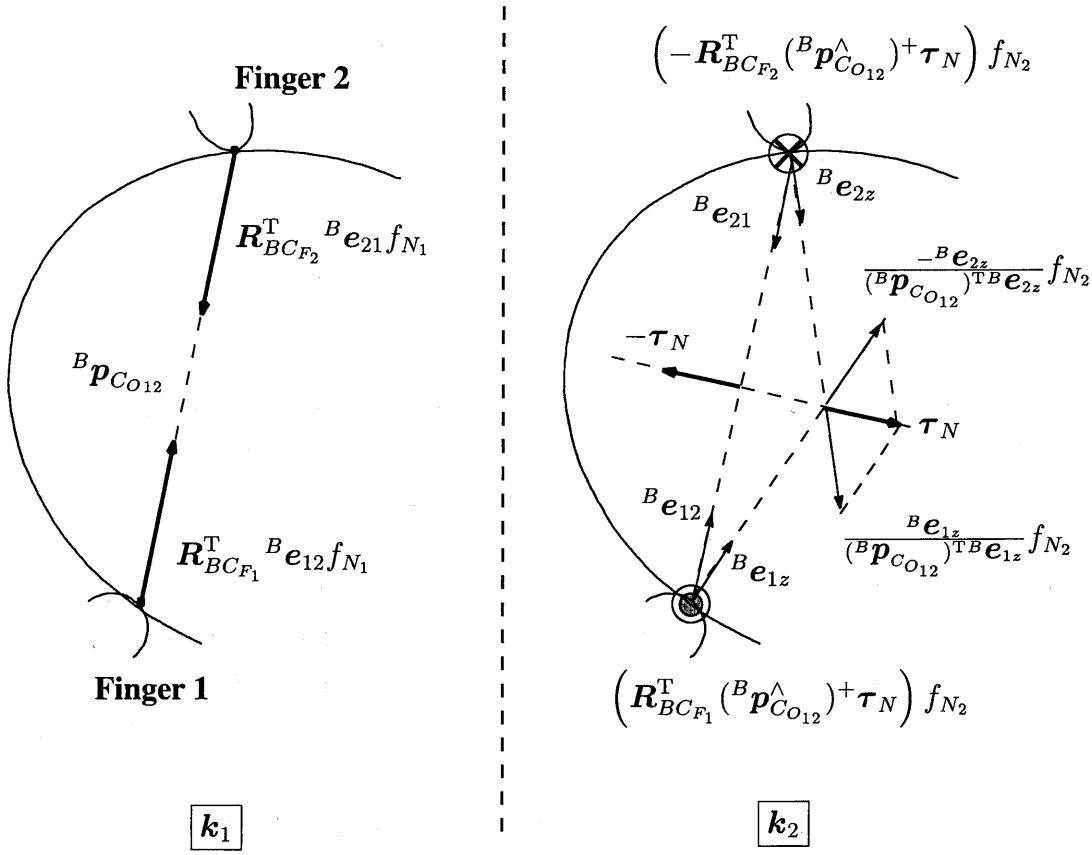

Figure 3.3 Internal forces.

where

$$\tau_N := \frac{{}^{B}e_{1z}}{({}^{B}p_{C_{O12}})^{\mathrm{T}}{}^{B}e_{1z}} + \frac{-{}^{B}e_{2z}}{({}^{B}p_{C_{O12}})^{\mathrm{T}}{}^{B}e_{2z}} \tag{3.32}$$

$${}^{B}p_{C_{O12}} := R_{BO}\,{}^{O}p_{C_{O_2}} - R_{BO}\,{}^{O}p_{C_{O_1}} \tag{3.33}$$

$${}^{B}e_{zi} := R_{BC_{F_i}}e, \quad e := [\,0\ 0\ 1\,]^{\mathrm{T}}. \tag{3.34}$$

The vector $e_{ij} \in \mathbb{R}^3$ $(i, j = 1, 2,\ i \neq j)$ is the unit vector directing from the contact point i to the contact point j ($e_{12} = -e_{21}$). The position vector ${}^{B}p_{C_{O12}}$ is the vector from the contact point 2 to the contact point 1 and $e_{iz} \in \mathbb{R}^3$ $(i = 1, 2)$ is the unit vector in direction of z_{f_i}-axis of $\Sigma_{C_{F_i}}$ (See Figure 3.3). The following lemma holds.

Lemma 3.1. *Consider $K_{A_O^{\mathrm{T}}}$ defined by (3.30)–(3.34). The following equations hold.*

$$\text{(i)}: \ A_O^{\mathrm{T}} K_{A_O^{\mathrm{T}}} = 0, \tag{3.35}$$

$$\text{(ii)}: \ k_1^{\mathrm{T}} k_2 = 0. \tag{3.36}$$

Proof. **(i)** From (2.29), (7.7) and (3.34), $\boldsymbol{A}_O^{\mathrm{T}}$ is rewritten as

$$\boldsymbol{A}_O^{\mathrm{T}} = \boldsymbol{T}_O^{\mathrm{T}} \begin{bmatrix} \boldsymbol{R}_{BC_{F_1}} & \boldsymbol{0}_{3\times 1} & \boldsymbol{R}_{BC_{F_2}} & \boldsymbol{0}_{3\times 1} \\ {}^B\boldsymbol{p}^{\wedge}_{C_{O_1}}\boldsymbol{R}_{BC_{F_1}} & {}^B\boldsymbol{e}_{1z} & {}^B\boldsymbol{p}^{\wedge}_{C_{O_2}}\boldsymbol{R}_{BC_{F_2}} & {}^B\boldsymbol{e}_{2z} \end{bmatrix}, \tag{3.37}$$

where ${}^B\boldsymbol{p}_{C_{O_i}} := \boldsymbol{R}_{BO}{}^O\boldsymbol{p}_{C_{O_i}}$. Firstly, from (3.31) and (3.37), noting that ${}^B\boldsymbol{p}^{\wedge}_{C_{O_{12}}}{}^B\boldsymbol{e}_{12} = \boldsymbol{0}$ from ${}^B\boldsymbol{e}_{12} /\!\!/ {}^B\boldsymbol{p}_{C_{O_{12}}}$ (See Figure 3.3), we get

$$\boldsymbol{A}_O^{\mathrm{T}}\boldsymbol{k}_1 = \boldsymbol{T}_O^{\mathrm{T}} \begin{bmatrix} \boldsymbol{0}_{3\times 1} \\ ({}^B\boldsymbol{p}^{\wedge}_{C_{O_1}} - {}^B\boldsymbol{p}^{\wedge}_{C_{O_2}}){}^B\boldsymbol{e}_{12} \end{bmatrix} = \boldsymbol{0}.$$

Secondly, from (3.31) and (3.37), we can easily confirm that the upper 3 elements of $\boldsymbol{A}_O^{\mathrm{T}}\boldsymbol{k}_2$ is zero. With $\boldsymbol{\tau}_N$ defined by (3.32), the lower 3 elements of $\boldsymbol{A}_O^{\mathrm{T}}\boldsymbol{k}_2$ result in

$$(\boldsymbol{I}_3 - {}^B\boldsymbol{p}^{\wedge}_{C_{O_{12}}}({}^B\boldsymbol{p}^{\wedge}_{C_{O_{12}}})^{+})\boldsymbol{\tau}_N. \tag{3.38}$$

Note that $\boldsymbol{\tau}_N$ and ${}^B\boldsymbol{p}_{C_{O_{12}}}$ are orthogonal to each other since $\boldsymbol{\tau}_N^{\mathrm{T}}{}^B\boldsymbol{p}_{C_{O_{12}}} = 0$ from (3.32). Hence, $\boldsymbol{\tau}_N$ can be represented as $\boldsymbol{\tau}_N = ({}^B\boldsymbol{p}^{\wedge}_{C_{O_{12}}})\boldsymbol{z}, \boldsymbol{z} \in \mathbb{R}^3$ because the column vectors of ${}^B\boldsymbol{p}^{\wedge}_{C_{O_{12}}}$ are orthogonal to ${}^B\boldsymbol{p}_{C_{O_{12}}}$. Substituting $\boldsymbol{\tau}_N = ({}^B\boldsymbol{p}^{\wedge}_{C_{O_{12}}})\boldsymbol{z}$ into (3.38) and utilizing the fact ${}^B\boldsymbol{p}^{\wedge}_{C_{O_{12}}}({}^B\boldsymbol{p}^{\wedge}_{C_{O_{12}}})^{+}{}^B\boldsymbol{p}^{\wedge}_{C_{O_{12}}} = {}^B\boldsymbol{p}^{\wedge}_{C_{O_{12}}}$, we can confirm that all elements of (3.38) are zero. Therefore, $\boldsymbol{A}_O^{\mathrm{T}}\boldsymbol{k}_2 = \boldsymbol{0}$.

(ii) Note that the pseudo inverse matrix $({}^B\boldsymbol{p}^{\wedge}_{C_{O_{12}}})^{+}$is given by $\frac{({}^B\boldsymbol{p}^{\wedge}_{C_{O_{12}}})^{\mathrm{T}}}{\|{}^B\boldsymbol{p}_{C_{O_{12}}}\|^2}$. Since $({}^B\boldsymbol{e}_{12} - {}^B\boldsymbol{e}_{21}) /\!\!/ {}^B\boldsymbol{p}_{C_{O_{12}}}$, we get

$$\boldsymbol{k}_1^{\mathrm{T}}\boldsymbol{k}_2 = \{{}^B\boldsymbol{p}^{\wedge}_{C_{O_{12}}}({}^B\boldsymbol{e}_{12} - {}^B\boldsymbol{e}_{21})\}^{\mathrm{T}}\frac{\boldsymbol{\tau}_N}{\|{}^B\boldsymbol{p}_{C_{O_{12}}}\|^2} = 0.$$

□

Remark 3.2. By using the expression of $\boldsymbol{K}_{A_O^{\mathrm{T}}}$ of (3.30), f_{N_1} represents the magnitude of the translational forces in the directions of ${}^B\boldsymbol{e}_{12}$ and ${}^B\boldsymbol{e}_{21}$ (See the left figure of Figure 3.3). On the other hand, f_{N_2} represents the magnitude of the moments about $\boldsymbol{\tau}_N$ and $-\boldsymbol{\tau}_N$. $\boldsymbol{\tau}_N$ is the moment produced by the moments about ${}^B\boldsymbol{e}_{1z}$ and ${}^B\boldsymbol{e}_{2z}$ and $-\boldsymbol{\tau}_N$ is the moment of a couple of the translational forces (See the right figure of Figure 3.3). From the observation of the friction cone of the soft-finger contact [6], we can directly achieve (A) by controlling f_{N_1} appropriately.

3.3.3 Expression of Finger Motion

From Assumption 3.5, a general solution of (3.6) with respect to $\dot{\boldsymbol{x}}_F$ is given by

$$\dot{\boldsymbol{x}}_F = \boldsymbol{A}_F^{-}\boldsymbol{A}_O\dot{\boldsymbol{x}}_O + \boldsymbol{K}_{A_F}(\boldsymbol{x}_F, \boldsymbol{\eta})\boldsymbol{v}_N, \tag{3.39}$$

where $\boldsymbol{A}_F^{-} \in \mathbb{R}^{12\times 8}$ is the reflective generalized inverse matrix of $\boldsymbol{A}_F$ satisfying $\boldsymbol{A}_F\boldsymbol{A}_F^{-} = \boldsymbol{I}_8$ and $\boldsymbol{K}_{A_F} \in \mathbb{R}^{12\times 4}$ satisfies $\boldsymbol{A}_F\boldsymbol{K}_{A_F} = \boldsymbol{0}$ with $\mathrm{rank}(\boldsymbol{K}_{A_F}) = 4$. In (3.39), $\boldsymbol{A}_F^{-}\boldsymbol{A}_O\dot{\boldsymbol{x}}_O$ represents the component of the finger motion which causes the object motion, and $\boldsymbol{K}_{A_F}\boldsymbol{v}_N$ represents the

internal motion which causes no effect on the object motion, where $\boldsymbol{v}_N = [\ \boldsymbol{v}_{N_1}^{\mathrm{T}}\ \ \boldsymbol{v}_{N_2}^{\mathrm{T}}\ ]^{\mathrm{T}} \in \mathbb{R}^4$, $\boldsymbol{v}_{N_i} \in \mathbb{R}^2$ is its magnitude.

The expressions of $\boldsymbol{A}_F^-$ and $\boldsymbol{K}_{A_F}\boldsymbol{v}_N$ have many possibilities. However, we consider the expressions of $\boldsymbol{A}_F^-$ and $\boldsymbol{K}_{A_F}\boldsymbol{v}_N$ which are effective to achieve the control objective (C). From Theorem 3.1, the motion of the contact coordinates $\boldsymbol{\eta}_i$ is restricted by the constraints (3.11). A general solution of (3.11) with respect to $\dot{\boldsymbol{\eta}}_i$ is given by

$$\dot{\boldsymbol{\eta}}_i = \boldsymbol{A}_{\eta_i}^{\perp}(\boldsymbol{\eta}_i)\boldsymbol{v}_{\omega_i},\ \ \boldsymbol{v}_{\omega_i} := [\ \omega_{Cx_i}\ \ \omega_{Cy_i}\ ]^{\mathrm{T}} \in \mathbb{R}^2, \tag{3.40}$$

where

$$\boldsymbol{A}_{\eta_i}^{\perp} := \begin{bmatrix} \boldsymbol{M}_{gf_i}^{-1}\boldsymbol{K}_{R_i}^{-1}\boldsymbol{E} \\ \hline \boldsymbol{M}_{go_i}^{-1}\boldsymbol{R}_{\psi_i}\boldsymbol{K}_{R_i}^{-1}\boldsymbol{E} \\ \hline \boldsymbol{T}_{gf_i}\boldsymbol{K}_{R_i}^{-1}\boldsymbol{E} \\ +\boldsymbol{T}_{go_i}\boldsymbol{R}_{\psi_i}\boldsymbol{K}_{R_i}^{-1}\boldsymbol{E} \end{bmatrix} \in \mathbb{R}^{5\times 2}. \tag{3.41}$$

Note that $\boldsymbol{A}_{\eta_i}\boldsymbol{A}_{\eta_i}^{\perp} = \boldsymbol{0}$ from (3.11) and (3.41). Since (3.11) are the maximal nonholonomic constraints from Theorem 3.1, $\boldsymbol{\eta}_i$ can be regulated by $\boldsymbol{v}_{\omega_i}$ in (3.40). Therefore, we consider choosing $\boldsymbol{A}_F^-$ and $\boldsymbol{K}_{A_F}$ such that $\boldsymbol{v}_{N_i} = \boldsymbol{v}_{\omega_i}$ holds. This can be achieved by the followings:

$$\boldsymbol{A}_F^- = \begin{bmatrix} \boldsymbol{A}_{F_1}^- \\ \boldsymbol{A}_{F_2}^- \end{bmatrix},\ \ \boldsymbol{K}_{A_F} = \begin{bmatrix} \boldsymbol{K}_{A_{F_1}} & \boldsymbol{0}_{6\times 2} \\ \boldsymbol{0}_{6\times 2} & \boldsymbol{K}_{A_{F_2}} \end{bmatrix}, \tag{3.42}$$

where

$$\boldsymbol{A}_{F_i}^- := \boldsymbol{D}_i + \boldsymbol{K}_{A_{F_i}}\bar{\boldsymbol{E}}_2^{\mathrm{T}}\boldsymbol{D}_{O_i}\boldsymbol{A}_O^+ \tag{3.43}$$

$$\boldsymbol{D}_1 := [\ \boldsymbol{D}_{F_1}^{-1}\boldsymbol{B}_C\ \ \boldsymbol{0}_{6\times 4}\ ],\ \boldsymbol{D}_2 := [\ \boldsymbol{0}_{6\times 4}\ \ \boldsymbol{D}_{F_2}^{-1}\boldsymbol{B}_C\ ] \tag{3.44}$$

$$\boldsymbol{K}_{A_{F_i}} := \boldsymbol{T}_{F_i}^{-1}\begin{bmatrix} (\boldsymbol{R}_{BF_i}{}^{F_i}\boldsymbol{p}_{C_{F_i}})^{\wedge}\boldsymbol{R}_{BC_{F_i}} \\ \boldsymbol{R}_{BC_{F_i}} \end{bmatrix}\boldsymbol{E}_2 \tag{3.45}$$

$$\bar{\boldsymbol{E}}_2 := \boldsymbol{0}_{2\times 3}\ \ \boldsymbol{E}_2^{\mathrm{T}}\ ]^{\mathrm{T}},\ \boldsymbol{E}_2 := [\ \boldsymbol{I}_2\ \ \boldsymbol{0}_{2\times 1}\ ]^{\mathrm{T}}. \tag{3.46}$$

The following lemma holds.

Lemma 3.2. *Consider the equation (3.39) and define $\boldsymbol{A}_F^-$ and $\boldsymbol{K}_{A_F}$ by (3.42). The following equations hold.*

$$\text{(i)}:\ \boldsymbol{A}_F\boldsymbol{K}_{A_F} = \boldsymbol{0}, \tag{3.47}$$

$$\text{(ii)}:\ \boldsymbol{v}_N = [\ \boldsymbol{v}_{\omega_1}^{\mathrm{T}}\ \ \boldsymbol{v}_{\omega_2}^{\mathrm{T}}\ ]^{\mathrm{T}}. \tag{3.48}$$

Proof. **(i)** Combining (2.28), (3.7), (3.42) and (3.45), we get (3.47) from direct calculation.

(ii) From (3.42), Eq. (3.39) is decomposed as $\dot{\boldsymbol{x}}_{F_i} = \boldsymbol{A}_{F_i}^-\boldsymbol{A}_O\dot{\boldsymbol{x}}_O + \boldsymbol{K}_{A_{F_i}}\boldsymbol{v}_{N_i}$. Substituting this equation into (3.3) and utilizing (3.43) and (3.7), we get

$$\boldsymbol{V}_{C_i} = (\boldsymbol{B}_C\boldsymbol{B}_C^{\mathrm{T}} + \boldsymbol{D}_{F_i}\boldsymbol{K}_{A_{F_i}}\bar{\boldsymbol{E}}_2^{\mathrm{T}} - \boldsymbol{I}_6)\boldsymbol{D}_{O_i}\dot{\boldsymbol{x}}_O + \boldsymbol{D}_{F_i}\boldsymbol{K}_{A_{F_i}}\boldsymbol{v}_{N_i}. \tag{3.49}$$

Note that $\boldsymbol{D}_{F_i}\boldsymbol{K}_{A_{F_i}} = \bar{\boldsymbol{E}}_2$ from $\boldsymbol{R}_{BC_{F_i}}^{\mathrm{T}}\boldsymbol{R}_{BC_{F_i}} = \boldsymbol{I}_3$, (3.7) and (3.45). Substituting $\boldsymbol{D}_{F_i}\boldsymbol{K}_{A_{F_i}} = \bar{\boldsymbol{E}}_2$ and $\boldsymbol{B}_C$ of (3.7) into (3.49), we get $\boldsymbol{V}_{C_i} = \bar{\boldsymbol{E}}_2\boldsymbol{v}_{N_i}$. This means $\boldsymbol{v}_{N_i} = [\ \omega_{Cx_i}\ \ \omega_{Cy_i}\ ]^{\mathrm{T}} = \boldsymbol{v}_{\omega_i}$ from the definition of $\boldsymbol{V}_{C_i}$. □

3.3.4 Linearizing Compensator

To achieve the control objectives (A), (B) and (C), we propose a linearizing compensator such that

$$\boldsymbol{\tau} = \boldsymbol{T}_F^{-\mathrm{T}} \left(\overline{\boldsymbol{M}} \begin{bmatrix} \boldsymbol{u}_O \\ \boldsymbol{u}_\omega \end{bmatrix} + \overline{\boldsymbol{C}} \begin{bmatrix} \dot{\boldsymbol{x}}_O \\ \boldsymbol{v}_\omega \end{bmatrix} + \overline{\boldsymbol{N}} + \boldsymbol{A}_F^{\mathrm{T}} \boldsymbol{K}_{A_O^{\mathrm{T}}} \boldsymbol{u}_{f_N} \right), \tag{3.50}$$

where

$$\begin{aligned} \overline{\boldsymbol{M}} &:= \left[\boldsymbol{M}_F \boldsymbol{A}_F^- \boldsymbol{A}_O + \boldsymbol{A}_F^{\mathrm{T}} (\boldsymbol{A}_O^{\mathrm{T}})^+ \boldsymbol{M}_O \;\; \boldsymbol{M}_F \boldsymbol{K}_{A_F} \right] \\ \overline{\boldsymbol{C}} &:= \left[\boldsymbol{M}_F \tfrac{d}{dt} (\boldsymbol{A}_F^- \boldsymbol{A}_O) + \boldsymbol{C}_F \boldsymbol{A}_F^- \boldsymbol{A}_O + \boldsymbol{A}_F^{\mathrm{T}} (\boldsymbol{A}_O^{\mathrm{T}})^+ \boldsymbol{C}_O \;\; \boldsymbol{M}_F \dot{\boldsymbol{K}}_{A_F} + \boldsymbol{C}_F \boldsymbol{K}_{A_F} \right] \\ \overline{\boldsymbol{N}} &:= \boldsymbol{N}_F + \boldsymbol{A}_F^{\mathrm{T}} (\boldsymbol{A}_O^{\mathrm{T}})^+ \boldsymbol{N}_O. \end{aligned} \tag{3.51}$$

In the controller (3.50), $\boldsymbol{u}_O \in \mathbb{R}^6$, $\boldsymbol{u}_\omega \in \mathbb{R}^4$ and $\boldsymbol{u}_{f_N} \in \mathbb{R}^2$ are the new inputs for $\boldsymbol{x}_O \in \mathbb{R}^6$, $\boldsymbol{v}_\omega \in \mathbb{R}^4$ and $\boldsymbol{f}_N \in \mathbb{R}^2$ respectively. The following theorem holds.

Theorem 3.2. *Consider the system (3.9) and (3.10) with the motion constraint (3.6). By the controller (3.50), the system is linearized as*

$$\ddot{\boldsymbol{x}}_O = \boldsymbol{u}_O, \;\; \dot{\boldsymbol{v}}_\omega = \boldsymbol{u}_\omega, \;\; \boldsymbol{f}_N = \boldsymbol{u}_{f_N}. \tag{3.52}$$

Proof. With the expressions of $\dot{\boldsymbol{x}}_F$, ${}^C\boldsymbol{F}_C$ and ${}^B\boldsymbol{F}_O$ described by (3.39), (3.29) and (3.28) respectively, (3.9) and (3.10) are transformed to

$$\overline{\boldsymbol{M}} \begin{bmatrix} \ddot{\boldsymbol{x}}_O \\ \dot{\boldsymbol{v}}_\omega \end{bmatrix} + \overline{\boldsymbol{C}} \begin{bmatrix} \dot{\boldsymbol{x}}_O \\ \boldsymbol{v}_\omega \end{bmatrix} + \bar{\boldsymbol{N}} + \boldsymbol{A}_F^{\mathrm{T}} \boldsymbol{K}_{A_O^{\mathrm{T}}} \boldsymbol{f}_N = \boldsymbol{T}_F^{\mathrm{T}} \boldsymbol{\tau}. \tag{3.53}$$

Substituting (3.50) into (3.53) leads to the closed loop system:

$$\overline{\boldsymbol{M}} \begin{bmatrix} \ddot{\boldsymbol{x}} - \boldsymbol{u}_O \\ \dot{\boldsymbol{v}}_\omega - \boldsymbol{u}_\omega \end{bmatrix} + \boldsymbol{A}_F^{\mathrm{T}} \boldsymbol{K}_{A_O^{\mathrm{T}}} (\boldsymbol{f}_N - \boldsymbol{u}_{f_N}) = \boldsymbol{0}. \tag{3.54}$$

Premultiplying (3.54) by $[\boldsymbol{A}_F^- \boldsymbol{A}_O \;\; \boldsymbol{K}_{A_F}]^{\mathrm{T}}$ and noting that (3.51), $\boldsymbol{A}_O^{\mathrm{T}} (\boldsymbol{A}_O^{\mathrm{T}})^+ = \boldsymbol{I}_6$, $\boldsymbol{A}_O^{\mathrm{T}} \boldsymbol{K}_{A_O^{\mathrm{T}}} = \boldsymbol{0}$, $\boldsymbol{A}_F \boldsymbol{A}_F^- = \boldsymbol{I}_8$ and $\boldsymbol{A}_F \boldsymbol{K}_{A_F} = \boldsymbol{0}$, we get the following equation:

$$\left[\tilde{\boldsymbol{A}}_O^{\mathrm{T}} \widetilde{\boldsymbol{M}}_F \tilde{\boldsymbol{A}}_O + \widetilde{\boldsymbol{M}}_O \right] \begin{bmatrix} \ddot{\boldsymbol{x}} - \boldsymbol{u}_O \\ \dot{\boldsymbol{v}}_\omega - \boldsymbol{u}_\omega \end{bmatrix} = \boldsymbol{0}, \tag{3.55}$$

where

$$\begin{aligned} \widetilde{\boldsymbol{M}}_F &:= [\, \boldsymbol{A}_F^- \;\; \boldsymbol{K}_{A_F} \,]^{\mathrm{T}} \boldsymbol{M}_F [\, \boldsymbol{A}_F^- \;\; \boldsymbol{K}_{A_F} \,] \\ \tilde{\boldsymbol{A}}_O &:= \begin{bmatrix} \boldsymbol{A}_O & \boldsymbol{0}_{8\times 4} \\ \boldsymbol{0}_{4\times 6} & \boldsymbol{I}_4 \end{bmatrix}, \;\; \widetilde{\boldsymbol{M}}_O := \begin{bmatrix} \boldsymbol{M}_O & \boldsymbol{0}_{6\times 4} \\ \boldsymbol{0}_{4\times 6} & \boldsymbol{0}_{4\times 4} \end{bmatrix}. \end{aligned}$$

From the definitions of $\boldsymbol{A}_F^-$ and $\boldsymbol{K}_{A_F}$, $[\, \boldsymbol{A}_F^- \;\; \boldsymbol{K}_{A_F} \,]$ is nonsingular. Therefore, $\widetilde{\boldsymbol{M}}_F$ is positive definite from $\boldsymbol{M}_F > 0$. $\tilde{\boldsymbol{A}}_O$ is full column rank because $\boldsymbol{A}_O$ is full column rank from

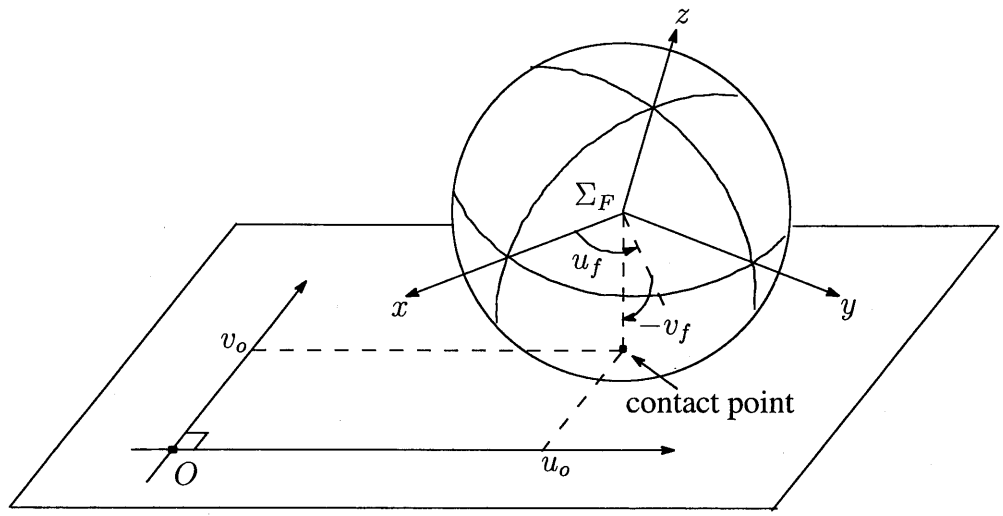

Figure 3.4 Spherical finger rolling on a plane.

Assumption 3.4 (i). From these facts, $\widetilde{\boldsymbol{A}}_O^{\mathrm{T}}\widetilde{\boldsymbol{M}}_F\widetilde{\boldsymbol{A}}_O$ is positive definite. Consequently, since $\left[\widetilde{\boldsymbol{A}}_O^{\mathrm{T}}\widetilde{\boldsymbol{M}}_F\widetilde{\boldsymbol{A}}_O + \widetilde{\boldsymbol{M}}_O\right]$ is nonsingular from $\boldsymbol{M}_O > 0$, we get $\ddot{\boldsymbol{x}}_O - \boldsymbol{u}_O = \boldsymbol{0}$, $\dot{\boldsymbol{v}}_\omega - \boldsymbol{u}_\omega = \boldsymbol{0}$. Substituting these results into (3.54) and premultiplying (3.54) by $\boldsymbol{K}_{A_O^{\mathrm{T}}}^{\mathrm{T}}(\boldsymbol{A}_F^-)^{\mathrm{T}}$, we get $\boldsymbol{K}_{A_O^{\mathrm{T}}}^{\mathrm{T}}\boldsymbol{K}_{A_O^{\mathrm{T}}}(\boldsymbol{f}_N - \boldsymbol{u}_{f_N}) = \boldsymbol{0}$. Since $\boldsymbol{K}_{A_O^{\mathrm{T}}}$ is full column rank, we get $\boldsymbol{f}_N - \boldsymbol{u}_{f_N} = \boldsymbol{0}$. □

Remark 3.3. From Theorem 4.2, the tracking control of $\boldsymbol{x}_O$, $\boldsymbol{v}_\omega$ and $\boldsymbol{f}_N$ can be easily realized by PD controller, for example. From Remark 3.2, the control objectives (A) and (B) are directly achieved by the tracking control of $\boldsymbol{x}_O$ and $\boldsymbol{f}_N$. The control objective (C) can be achieved by making the rolling velocity $\boldsymbol{v}_\omega$ follow appropriate trajectory.

3.4 Regulation of Contact Coordinates

In this section, to establish the regulation of the contact coordinates with the pure rolling contact, we consider as a first step the case where the shapes of each finger and the object are a sphere and a cuboid respectively. In this case, the kinematic model (3.40) is the sphere rolling on a plane of the cuboid shown in Figure 3.4. Since the configurations of the contact coordinates are the same for $i = 1, 2$, the subscript i is dropped in this section. The coordinates $\boldsymbol{\alpha}_f = [\, u_f \;\; v_f \,]^{\mathrm{T}} \in \mathbb{R}^2$ and $\boldsymbol{\alpha}_o = [\, u_o \;\; v_o \,]^{\mathrm{T}} \in \mathbb{R}^2$ are defined by the orthogonal coordinates and the spherical coordinates respectively. Due to (2.73), as in seen Subsection 2.2.4, (3.40) can be transformed to

$$\dot{\boldsymbol{\eta}} = \begin{bmatrix} \dot{\boldsymbol{\alpha}}_f \\ \dot{\boldsymbol{\alpha}}_o \\ \dot{\psi} \end{bmatrix} = \begin{bmatrix} 1 & 0 \\ 0 & 1 \\ \rho\cos v_f \cos\psi & -\rho\sin\psi \\ -\rho\cos v_f \sin\psi & -\rho\cos\psi \\ \sin v_f & 0 \end{bmatrix} \dot{\boldsymbol{\alpha}}_f, \tag{3.56}$$

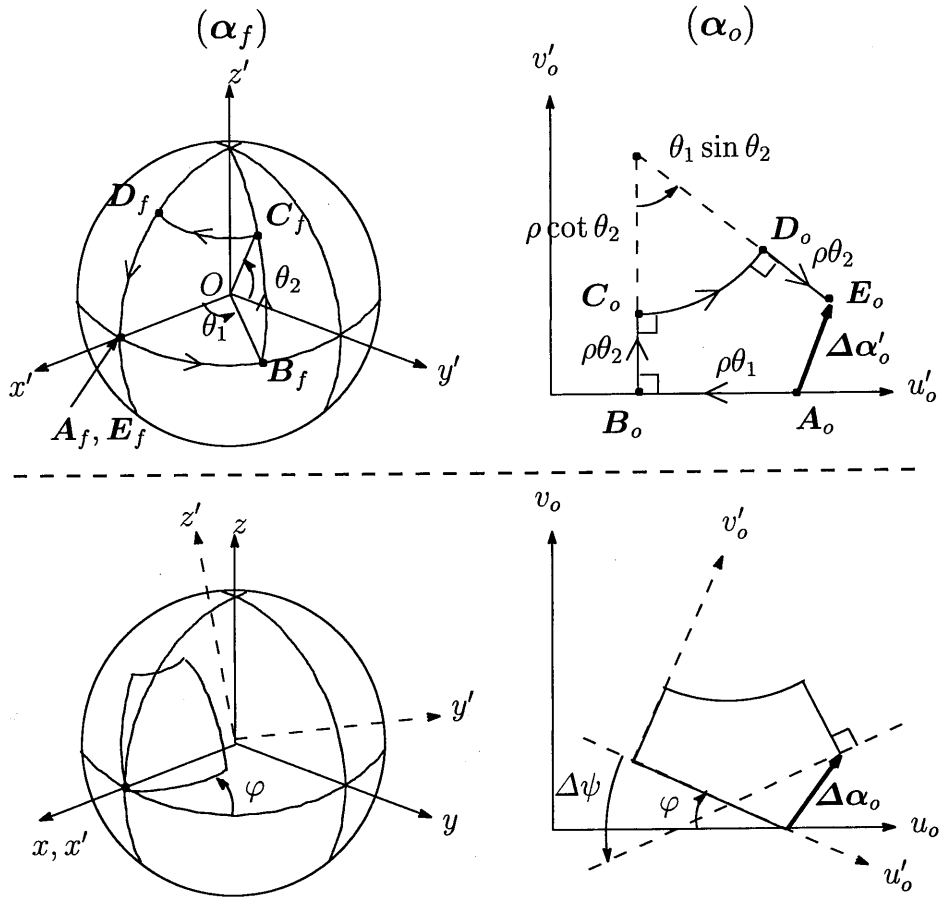

Figure 3.5 The proposed closed path on the sphere.

where ρ is the radius of the sphere.

For (3.56), we propose a method which regulates the contact coordinates $\boldsymbol{\eta} \in \mathbb{R}^5$ by iterating a single specified closed path of $\boldsymbol{\alpha}_f$. Without loss of generality, the target point is set to $\boldsymbol{\eta} = \mathbf{0}$. The scheme of the method is as follows:

Step 1: To regulate $\boldsymbol{\alpha}_f$ to $\boldsymbol{\alpha}_f = \mathbf{0}$.

Step 2: By iterating a single specified closed path of $\boldsymbol{\alpha}_f$, to regulate

$$\widetilde{\boldsymbol{\eta}} := [\ \boldsymbol{\alpha}_o^{\mathrm{T}}\ \ \psi\ ]^{\mathrm{T}} \in \mathbb{R}^3 \tag{3.57}$$

to $\widetilde{\boldsymbol{\eta}} = \mathbf{0}$. In the following in this chapter, the variable $\widetilde{\boldsymbol{\eta}}$ is called the control variable.

Figure 3.5 illustrates the proposed closed path and the incremental distances of $\boldsymbol{\alpha}_o$ and ψ by the closed path (initial condition: $\boldsymbol{\alpha}_f = \mathbf{0}$, $\psi = \pi$). In the upper of Figure 3.5, the left figure shows the closed path of $\boldsymbol{\alpha}_f$: $A_f \to B_f \to C_f \to D_f \to E_f(A_f)$ which is characterized by the parameters θ_1 and θ_2. In this thesis, we call this shaped closed path the *trapezoidal closed path*. The right figure shows the trajectory of $\boldsymbol{\alpha}_o$ generated by the closed path on the left hand side. The incremental distance is $\Delta\boldsymbol{\alpha}'_o$. In the lower of Figure 3.5, the left figure shows the proposed closed path of $\boldsymbol{\alpha}_f$. This is the path which is obtained by rotating the closed path in the upper figure through the parameter φ about x'-axis. The right figure shows the trajectory of $\boldsymbol{\alpha}_o$

generated by the closed path on the left hand side. Denote the incremental distances of $\boldsymbol{\alpha}_o$ and ψ $\boldsymbol{\Delta\alpha}_o$ and $\Delta\psi$ respectively. Define the incremental distance of $\widetilde{\boldsymbol{\eta}}$ by

$$\boldsymbol{\Delta\widetilde{\eta}} := [\ \boldsymbol{\Delta\alpha}_o^{\mathrm{T}}\ \ \Delta\psi\ ]^{\mathrm{T}} \in \mathbb{R}^3. \tag{3.58}$$

By integrating (3.56) along the closed path with the initial condition, the components of $\boldsymbol{\Delta\widetilde{\eta}}$ are given by

$$\boldsymbol{\Delta\alpha}_o(\theta_1, \theta_2, \varphi) = \boldsymbol{R}_\varphi(\varphi)\boldsymbol{\Delta\alpha}'_o(\theta_1, \theta_2), \tag{3.59}$$

$$\Delta\psi(\theta_1, \theta_2) = -\theta_1 \sin\theta_2, \tag{3.60}$$

where

$$\boldsymbol{R}_\varphi := \begin{bmatrix} \cos\varphi & \sin\varphi \\ -\sin\varphi & \cos\varphi \end{bmatrix} \tag{3.61}$$

$$\boldsymbol{\Delta\alpha}'_o := \begin{bmatrix} \Delta u'_o \\ \Delta v'_o \end{bmatrix} = \begin{bmatrix} -\rho\theta_1 + \rho(\cot\theta_2 + \theta_2)\sin(\theta_1 \sin\theta_2) \\ \rho(\cot\theta_2 + \theta_2)(1 - \cos(\theta_1 \sin\theta_2)) \end{bmatrix}. \tag{3.62}$$

Note that the range of θ_1, θ_2 and φ are

$$-\pi < \theta_1 < \pi, -\frac{\pi}{2} < \theta_2 < \frac{\pi}{2}, -\pi < \varphi < \pi \tag{3.63}$$

As for the incremental distance $\widetilde{\boldsymbol{\eta}}$, the following lemma holds.

Lemma 3.3. *$\boldsymbol{\Delta\alpha}'_o$, $\Delta\psi$ defined by (3.60), (3.62) have the following properties.*
(i) *$\boldsymbol{\Delta\alpha}'_o$, $\Delta\psi$ are continuous with respect to θ_1, θ_2.*
(ii) *The following equivalent conditions hold:*

$$\|\boldsymbol{\Delta\alpha}'_o\| = 0 \Longleftrightarrow \theta_1 = 0 \text{ or } \theta_2 = 0, \tag{3.64}$$

$$\Delta\psi = 0 \Longleftrightarrow \theta_1 = 0 \text{ or } \theta_2 = 0. \tag{3.65}$$

Proof. **(i)** From (3.60) and (3.62), it is evident that $\boldsymbol{\Delta\alpha}'_o$ and $\Delta\psi$ are continuous relative to θ_1 and θ_2 except $\theta_2 = 0$, since $\boldsymbol{\Delta\alpha}'_o$ and $\Delta\psi$ are composed of sums and products of sin, cos and cot. Hence, we investigate the limit value at $\theta_2 \to 0$ of $\boldsymbol{\Delta\alpha}'_o = [\ \Delta u'_o\ \ \Delta v'_o\ ]^{\mathrm{T}}$ because $\Delta u'_o$ and $\Delta v'_o$ involve $\cot\theta_2 = \frac{\cos\theta_2}{\sin\theta_2}$.

Calculating $\lim_{\theta_2 \to 0} \Delta u'_o$ leads to

$$\lim_{\theta_2 \to 0} \Delta u'_o = -\rho\theta_1 + \lim_{\theta_2 \to 0} \rho \frac{\cos\theta_2 \sin(\theta_1 \sin\theta_2)}{\sin\theta_2}. \tag{3.66}$$

Applying l'Hospital's theorem to the second term of the right hand side of (3.66), we get

$$\lim_{\theta_2 \to 0} \rho \frac{-\sin\theta_2 \sin(\theta_1 \sin\theta_2) + \theta_1 \cos^2\theta_2 \cos(\theta_1 \sin\theta_2)}{\cos\theta_2} = \rho\theta_1. \tag{3.67}$$

Therefore, substituting (3.67) into (3.66) leads to

$$\lim_{\theta_2 \to 0} \Delta u'_o = 0. \tag{3.68}$$

Furthermore, calculating $\lim_{\theta_2 \to 0} \Delta v'_o$ by l'Hospital's theorem similarly, we get

$$\lim_{\theta_2 \to 0} \Delta v'_o = 0. \tag{3.69}$$

Therefore, $\boldsymbol{\Delta\alpha}'_o$ is continuous at $\theta_2 = 0$.

(ii) It is evident from (3.60) that (3.65) holds. On the other hand, it is evident from (3.62) and (3.68) that the necessity of (3.64) holds. Next, consider the sufficiency of (3.64). From (3.62), the condition equivalent to $\Delta v'_o = 0$ is

$$\cot\theta_2 + \theta_2 = 0 \ \text{ or } \ 1 - \cos(\theta_1 \sin\theta_2) = 0. \tag{3.70}$$

However, since $\cot\theta_2 + \theta_2 \neq 0$ from $-\frac{\pi}{2} < \theta_2 < \frac{\pi}{2}$, $\Delta v'_o = 0$ holds if and only if $\theta_1 = 0$ or $\theta_2 = 0$ holds from the second term of (3.70). □

From **Lemma 3.3**, since $\boldsymbol{R}_\varphi$ is a rotation matrix, $\boldsymbol{\Delta\widetilde{\eta}} = [\ (\boldsymbol{R}_\varphi \boldsymbol{\Delta\alpha}'_o)^{\mathrm{T}} \ \ \Delta\psi\ ]^{\mathrm{T}}$ can not span $[*\ \ *\ \ 0]^{\mathrm{T}}$, $[0\ \ 0\ \ *]^{\mathrm{T}}$. However, the following theorem guarantees that the control variables $\widetilde{\boldsymbol{\eta}}$ converges to the target point by interation of the closed paths.

Theorem 3.3. *Consider $\widetilde{\boldsymbol{\eta}} \in \mathbb{R}^3$ defined by (3.57) and $\boldsymbol{\Delta\widetilde{\eta}} \in \mathbb{R}^3$ defined by (3.58)–(3.62). For any $\widetilde{\boldsymbol{\eta}}$, there always exist parameters θ_1, θ_2 and φ of the closed path satisfying*

$$\|\widetilde{\boldsymbol{\eta}} + \boldsymbol{\Delta\widetilde{\eta}}\| < \|\widetilde{\boldsymbol{\eta}}\|. \tag{3.71}$$

Proof. Since $\boldsymbol{\Delta\widetilde{\eta}} = [\ (\boldsymbol{R}_\varphi \boldsymbol{\Delta\alpha}'_o)^{\mathrm{T}} \ \ \Delta\psi\ ]^{\mathrm{T}}$,

$$\begin{aligned} \|\widetilde{\boldsymbol{\eta}} + \boldsymbol{\Delta\widetilde{\eta}}\|^2 - \|\widetilde{\boldsymbol{\eta}}\|^2 &= 2\widetilde{\boldsymbol{\eta}}^{\mathrm{T}} \boldsymbol{\Delta\widetilde{\eta}} + \boldsymbol{\Delta\widetilde{\eta}}^{\mathrm{T}} \boldsymbol{\Delta\widetilde{\eta}} \\ &= [\ 2(\boldsymbol{R}_\varphi^{\mathrm{T}} \boldsymbol{\alpha}_o) + \boldsymbol{\Delta\alpha}'_o\ ]^{\mathrm{T}} \boldsymbol{\Delta\alpha}'_o + (2\psi + \Delta\psi)\Delta\psi, \end{aligned} \tag{3.72}$$

where $\boldsymbol{R}_\varphi^{\mathrm{T}} \boldsymbol{R}_\varphi = \boldsymbol{I}_2$ is utilized from (3.61). Since $\boldsymbol{R}_\varphi$ is a rotation matrix, there always exists φ which satisfies

$$\boldsymbol{R}_\varphi^{\mathrm{T}} \boldsymbol{\alpha}_o = -\|\boldsymbol{\alpha}_o\| \frac{\boldsymbol{\Delta\alpha}'_o}{\|\boldsymbol{\Delta\alpha}'_o\|}. \tag{3.73}$$

Therefore, substituting (3.73) into (3.72) leads to

$$^{\forall}\boldsymbol{\alpha}_o, {}^{\forall}\psi, \ {}^{\exists}\theta_1, {}^{\exists}\theta_2 \ \text{s.t.} \ \left(-2\frac{\|\boldsymbol{\alpha}_o\|}{\|\boldsymbol{\Delta\alpha}'_o\|} + 1\right) \|\boldsymbol{\Delta\alpha}'_o\|^2 + (2\psi + \Delta\psi)\Delta\psi < 0. \tag{3.74}$$

The proof is divided into the following three cases.

1) $\boxed{\|\boldsymbol{\alpha}_o\| \neq 0, \psi \neq 0}$: In this case, Eq. (3.74) holds if the following inequalities hold:

$$-2\frac{\|\boldsymbol{\alpha}_o\|}{\|\Delta\boldsymbol{\alpha}'_o\|} + 1 < 0, \tag{3.75}$$

$$(2\psi + \Delta\psi)\Delta\psi < 0. \tag{3.76}$$

Eq. (3.75) holds if $\|\Delta\boldsymbol{\alpha}'_o\|$ is sufficiently smaller than $\|\boldsymbol{\alpha}_o\|$. On the other hand, Eq. (3.76) holds if $|\Delta\psi|$ is sufficiently smaller than $|2\psi|$ and the sign of $\Delta\psi$ differ from the sign of ψ. From Lemma 3.3, there exist $\theta_1, \theta_2 \ll 1$ such that $\|\Delta\boldsymbol{\alpha}'_o\|$ and $|\Delta\psi|$ are sufficiently as small as the described above. Furthermore, from (3.62) and (3.60), since $\|\Delta\boldsymbol{\alpha}'_o\|$ is a even function of (θ_1, θ_2) and $\Delta\psi$ is a odd function of (θ_1, θ_2), there exist θ_1 and θ_2 in the above $\theta_1, \theta_2 \ll 1$ such that the sign of $\Delta\psi$ differ from the sign of ψ. Therefore (3.74) holds.

2) $\boxed{\|\boldsymbol{\alpha}_o\| \neq 0, \psi = 0}$: In this case, Eq. (3.74) is transformed to

$$\left(1 + \frac{\Delta\psi^2}{\|\Delta\boldsymbol{\alpha}'_o\|^2} - 2\frac{\|\boldsymbol{\alpha}_o\|}{\|\Delta\boldsymbol{\alpha}'_o\|}\right)\|\Delta\boldsymbol{\alpha}'_o\|^2 < 0. \tag{3.77}$$

The ratio of the plus term to the minus term in the brackets of (3.77) is given by

$$\left(1 + \frac{\Delta\psi^2}{\|\Delta\boldsymbol{\alpha}'_o\|^2}\right) \Big/ 2\frac{\|\boldsymbol{\alpha}_o\|}{\|\Delta\boldsymbol{\alpha}'_o\|} = \frac{\|\Delta\boldsymbol{\alpha}'_o\| + \dfrac{\Delta\psi^2}{\|\Delta\boldsymbol{\alpha}'_o\|}}{2\|\boldsymbol{\alpha}_o\|}. \tag{3.78}$$

From Lemma 3.3(ii), (3.60) and (3.62), the limit value of (3.78) with respect to $\theta_1 \to 0$ is given by

$$\lim_{\theta_1 \to 0} \frac{\|\Delta\boldsymbol{\alpha}'_o\| + \dfrac{\Delta\psi^2}{\|\Delta\boldsymbol{\alpha}'_o\|}}{2\|\boldsymbol{\alpha}_o\|} = \lim_{\theta_1 \to 0} \frac{1}{2\|\boldsymbol{\alpha}_o\|}\frac{\Delta\psi^2}{\|\Delta\boldsymbol{\alpha}'_o\|} = \frac{1}{2\|\boldsymbol{\alpha}_o\|}\lim_{\theta_1 \to 0} \frac{\sin^2\theta_2}{\sqrt{\left(\dfrac{\Delta u'_o}{\theta_1^2}\right)^2 + \left(\dfrac{\Delta v'_o}{\theta_1^2}\right)^2}}. \tag{3.79}$$

Calculation of the first term on the denominator by l'Hospital's theorem leads to

$$\lim_{\theta_1 \to 0} \frac{\Delta u'_o}{\theta_1^2} = \lim_{\theta_1 \to 0} \rho \frac{-1 + (\cot\theta_2 + \theta_2)\sin\theta_2 \cos(\theta_1 \sin\theta_2)}{2\theta_1} = \infty.$$

Therefore, since the value of (3.79) is zero irrespective of θ_2, there exists sufficient small θ_1 such that Eq. (3.77) holds.

3) $\boxed{\|\boldsymbol{\alpha}_o\| = 0, \psi \neq 0}$: In this case, Eq. (3.74) is transformed to

$$\left(\frac{\|\Delta\boldsymbol{\alpha}'_o\|^2}{\Delta\psi} + \Delta\psi + 2\psi\right)\Delta\psi < 0. \tag{3.80}$$

Eq. (3.80) holds if the following inequalities hold:

$$\left|\frac{\|\Delta\boldsymbol{\alpha}'_o\|^2}{\Delta\psi} + \Delta\psi\right| < |2\psi|, \tag{3.81}$$

$$\psi\Delta\psi < 0. \tag{3.82}$$

Eq. (3.81) holds if the left term is smaller than $|2\psi|$. On the other hand, Eq. (3.82) holds if the sign of $\Delta\psi$ differ from the sign of ψ. From (3.62) and (3.60), calculation of $\|\Delta\boldsymbol{\alpha}_o'\|^2/\Delta\psi$ leads to

$$\frac{\|\Delta\boldsymbol{\alpha}_o'\|^2}{\Delta\psi} = \rho\frac{\theta_1 - 2(\cot\theta_2+\theta_2)\sin(\theta_1\sin\theta_2) + 2(\cot\theta_2+\theta_2)^2\dfrac{1-\cos(\theta_1\sin\theta_2)}{\theta_1}}{-\sin\theta_2}. \tag{3.83}$$

The limit value of (3.83) with respect to $\theta_1 \to 0$ is given by

$$\lim_{\theta_1\to 0}\frac{\|\Delta\boldsymbol{\alpha}_o'\|^2}{\Delta\psi} = \rho\frac{2(\cot\theta_2+\theta_2)^2}{-\sin\theta_2}\lim_{\theta_1\to 0}\frac{1-\cos(\theta_1\sin\theta_2)}{\theta_1}. \tag{3.84}$$

By l'Hospital's theorem, the last term of (3.84) is

$$\lim_{\theta_1\to 0}\frac{1-\cos(\theta_1\sin\theta_2)}{\theta_1} = 0.$$

Therefore, in the case $\theta_2 \neq 0$, $\lim_{\theta_1\to 0}\|\Delta\boldsymbol{\alpha}_o'\|^2/\Delta\psi = 0$ holds. Therefore, from Lemma 3.3, there exist $\theta_1, \theta_2 \ll 1$ such that (3.81) holds. Furthermore, from (3.62) and (3.60), since $\|\Delta\boldsymbol{\alpha}_o'\|$ is a even function of (θ_1, θ_2) and $\Delta\psi$ is a odd function of (θ_1, θ_2), there exist θ_1 and θ_2 in the above $\theta_1, \theta_2 \ll 1$ such that the sign of $\Delta\psi$ differ from the sign of ψ, i. e. Eq. (3.82) holds. Therefore, Eq. (3.80) holds. □

Taking Theorem 3.3 into account, we propose a method to determine the parameters to regulate $\widetilde{\boldsymbol{\eta}}$ by solving the following equation:

$$(\theta_1[k], \theta_2[k], \varphi[k]) = \underset{\theta_1[k],\theta_2[k],\varphi[k]}{\arg\min}\ \|\widetilde{\boldsymbol{\eta}}[k] + \Delta\widetilde{\boldsymbol{\eta}}[k]\|, \tag{3.85}$$

where k is the number of the iterations.

Remark 3.4. Note that the parameters $\theta_1[k]$, $\theta_2[k]$ and $\varphi[k]$ can be obtained only from $\widetilde{\boldsymbol{\eta}}[k]$ which is the sates at the start time of kth number of iterations. Therefore, the method can be interpreted as a discrete-time feedback by regarding the start time of the iteration as the sampling instant. Therefore, the method is expected to have robustness against disturbances.

3.5 Numerical Example

In a numerical example, each finger is a sphere of a radius 1.0×10^{-2}[m] and mass $1.0[\times10^{-2}$kg]. The object is a cube of length 0.10[m] and mass $5.0[\times10^{-2}$kg]. Figure 3.6 shows the overview of the configuration of the simulation. The initial states are

$$\begin{aligned}
\boldsymbol{x}_O &= [\,[0\ \ 0\ \ 0.15][\mathrm{m}]\ [0\ \ 0\ \ 0][\mathrm{rad}]\,]^{\mathrm{T}},\\
\boldsymbol{\eta}_1 &= [\,[0.50\ \ 1.0][\mathrm{rad}]\ [1.0\ \ 1.0][\times10^{-2}\mathrm{m}]\ \frac{\pi}{6}[\mathrm{rad}]\,]^{\mathrm{T}},\\
\boldsymbol{\eta}_2 &= [\,[0.50\ \ 1.0][\mathrm{rad}]\ [-1.0\ \ 1.0][\times10^{-2}\mathrm{m}]\ \frac{\pi}{3}[\mathrm{rad}]\,].
\end{aligned}$$

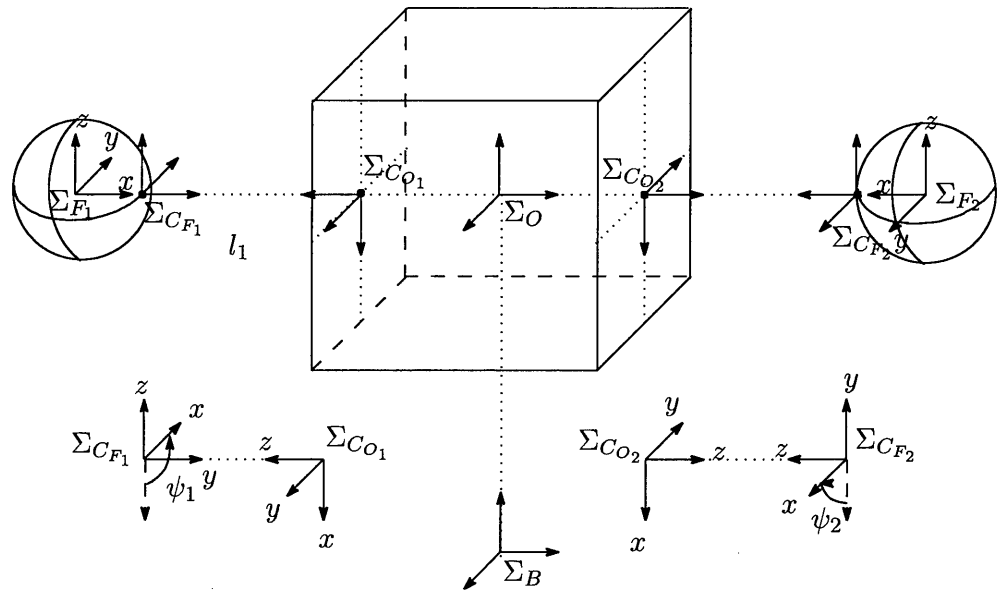

Figure 3.6 Overview of the configuration of the simulation.

The target points are

$$\boldsymbol{x}_O = \boldsymbol{x}_O = [\,[0\ \ 0.050\ \ 0.20][\mathrm{m}]\ [0\ \ 0\ \ \frac{\pi}{2}][\mathrm{rad}]\,]^{\mathrm{T}},$$
$$\boldsymbol{\eta}_1 = [\,[0\ \ 0][\mathrm{rad}]\ [0\ \ 0][\times 10^{-2}\mathrm{m}]\ 0[\mathrm{rad}]\,]^{\mathrm{T}},$$
$$\boldsymbol{\eta}_2 = [\,[0\ \ 0][\mathrm{rad}]\ [0\ \ 0][\times 10^{-2}\mathrm{m}]\ 0[\mathrm{rad}]\,]^{\mathrm{T}}.$$

The desired trajectory of $\boldsymbol{f}_N$ is determined as the method shown in Appendix C for the contact force to lie in the friction corn.

Figure 3.7 shows the time responses of $\boldsymbol{x}_O$, $\boldsymbol{\alpha}_{f_1}$, $\boldsymbol{\alpha}_{f_2}$ and f_{N_1} by the linearizing compensator. The broken lines are the desired trajectories and the solid lines are the controlled trajectories. The both lines coincide with each other. Figure 3.8 shows the motion of $\boldsymbol{\alpha}_{o_i}$ and ψ_i on the plane of $\boldsymbol{\alpha}_o = [\,u_{o_i}\ \ v_{o_i}\,]^{\mathrm{T}}$ $(i = 1, 2)$. In the figure, the numbers in the parenthesis of step 2 represent the number of the iterations of the closed path, and the circles represent the start positions of the closed paths. The arrows represent ψ_i. The coordinates $\boldsymbol{\alpha}_{o_i}$ and ψ_i are shifted to the target points respectively after two number of iterations.

3.6 Summary

In this chapter, we discussed the simultaneous control by a two-fingered robot hand, each finger of which had six degrees of freedom. The contact motion between each finger and the object was assumed to be the pure rolling contact, and the surfaces of each finger and the object were assumed to be the regular surfaces. As for the control method to utilize the nonholonomy of rolling for control of contact points, we first clarified the degree of freedom of the whole system. Second, we proposed the general formulation of the linearizing compensator for the internal force, the object motion and the rolling motion. Due to the linearization, the contact motion

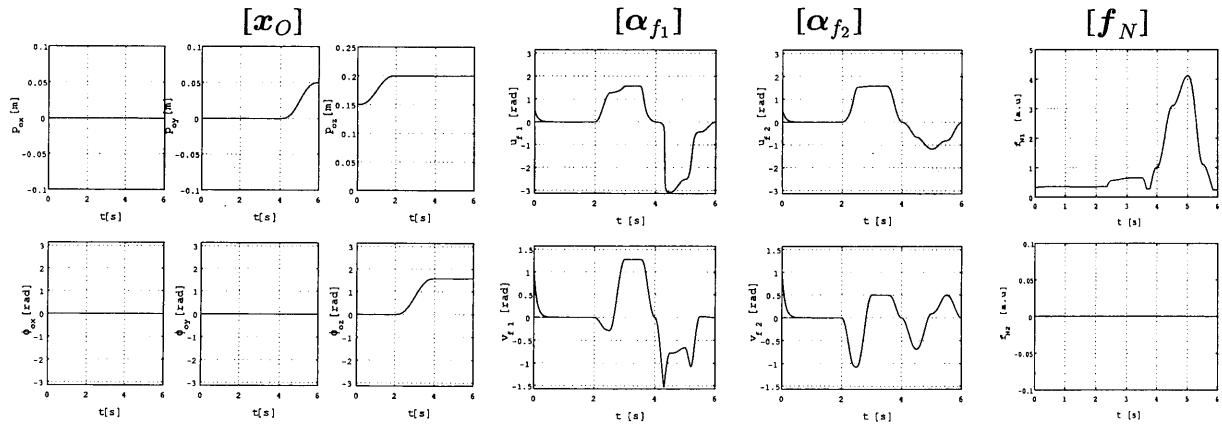

Figure 3.7 Time responses of the linearized variables.

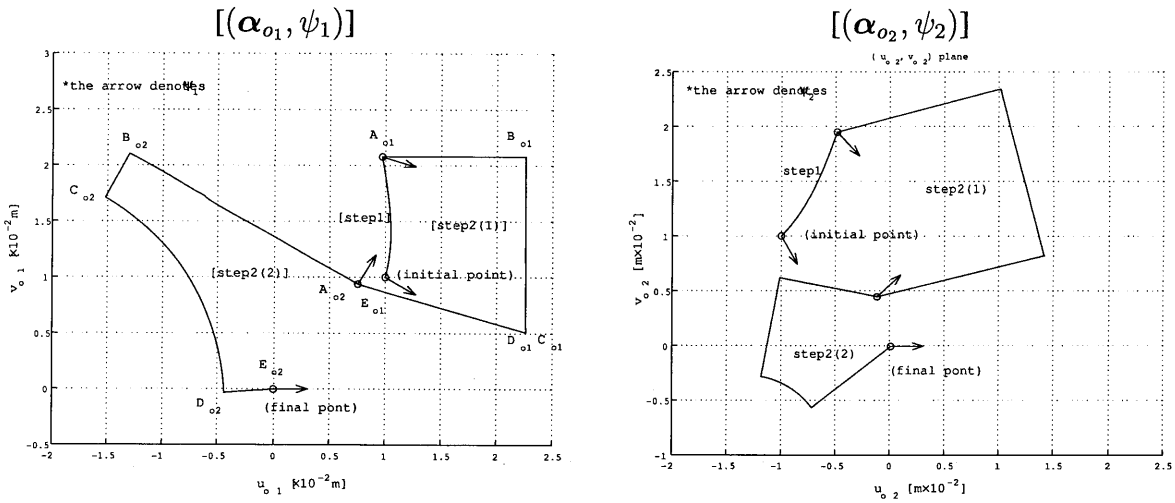

Figure 3.8 The motion of α_{o_i} and ψ_i on the plane of α_{o_i} $(i = 1, 2)$.

conforms to the kinematic model of two rolling bodies whose input is the rolling motion of the linearized variables. As for the regulation algorithm, for the kinematic model of a sphere and a plane with pure rolling contact, we proposed the method to regulate all the contact coordinates by iterative closed paths on the contact point of the sphere. The closed path was shaped as a trapezoid on the sphere parameterized by three variables, which was called the *trapezoidal closed path*. The parameters was determined with respect to each interation. The convergence to arbitrary target points of the regulation method was guaranteed.

Chapter 4

Simultaneous Control by Two-fingered Robot Hand with Constrained Degrees of Freedom

In Chapter 3, we discussed the simultaneous control by a two-fingered robot hand, each of which has six degrees of freedom. In this method, the decoupling of the object motion and the rolling motion can be achieved by the linearization. However, if the degrees of freedom (DOF) of each finger is less than six, the object motion and the rolling motion surely interfere with each other. Therefore, the control problem become more difficult than that of Chapter 3. Furthermore, it need be guaranteed that arbitrary rolling motion can be generated by using finger and object motion.

In this chapter, for the simultaneous control, we propose a control method which can utilize the nonholonomy of rolling for control of contact points by a two-fingered robot hand with constrained DOF [51, 52, 53, 54]. The contact motion between each finger and the object is assumed to be the pure rolling contact, and the surfaces of each finger and the object are assumed to be the regular surfaces. In Section 4.1, the modeling of the fingers and the object is summarized briefly. In Section 4.2, we clarify the condition such that the position of the DOF of the whole system is maximum. This represents that arbitrary rolling motion can be generated by using finger and object motion. This is characterized by the number and the direction of the DOF of the fingers. In Section 4.3, we propose a general formulation of a linearizing compensator for the internal force, the motion of a certain coordinates of the fingers and the object, and the rolling motion. For the construction of the linearizing compensator, the finger and object motion are decomposed into a component which causes the rolling motion and a component which does not cause the rolling motion. The second component correspond to a certain coordinates of the fingers and the object. In Section 4.4, a numerical example shows the effectiveness of the method.

4.1 Modeling

In this paper, we consider two fingertips grasping an object shown in Figure 4.1. The pair of two fingertips is a simplified model of a two-fingered robot hand, each finger of which has m_i DOF ($0 \leq m_i \leq 6$). The contact point between each finger and the object is single. In the following,

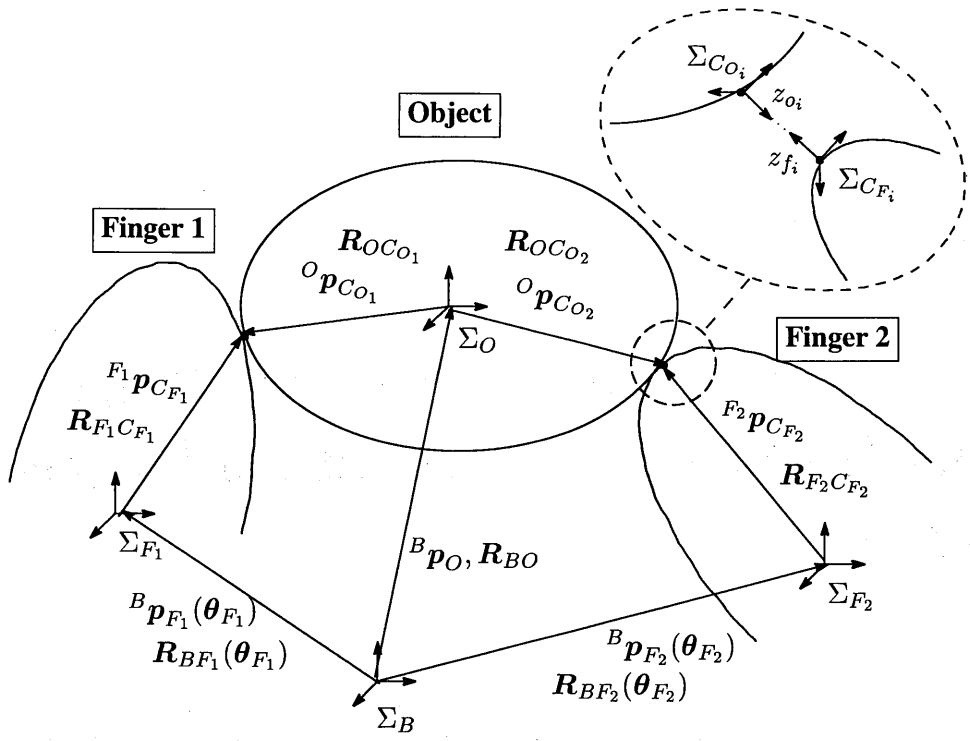

Figure 4.1 An object grasped by two fingertips with constrained DOF.

the number of the fingers and the contact points is described by $i = 1, 2$. For notational simplicity, arguments of vectors and matrices are described explicitly only when they appear first time, and will be omitted in the following discussion. In this chapter, we make the following assumptions.

Assumption 4.1. The surfaces of each finger and the object are the regular surfaces [6]. Therefore, contact points on the surfaces of each finger and the object can be described by $\boldsymbol{c}(\boldsymbol{\alpha}) \in \mathbb{R}^3$, where $\boldsymbol{c}(\cdot) : \mathbb{R}^2 \mapsto \mathbb{R}^3$ is a local orthogonal chart and $\boldsymbol{\alpha} \in \mathbb{R}^2$ is a local coordinates.

Assumption 4.2. The frictional forces at the contact points follow the *Coulomb's law*. The contact force applied to the object by each finger is composed of translational forces and a moment about the contact normal.

Assumption 4.3. The constraint at each contact point is described by the pure rolling contact. The forces generated by the constraint do not work on the system (*d'Alembert's principle*).

The details of the system configuration, the kinematics and the dynamics of the fingers and the object are described in Chapter 2. Hence, they are summarized briefly in this section. Coordinate frames and configuration of the system are summarized in the following, as shown in Figure 4.1 and Figure 4.2.

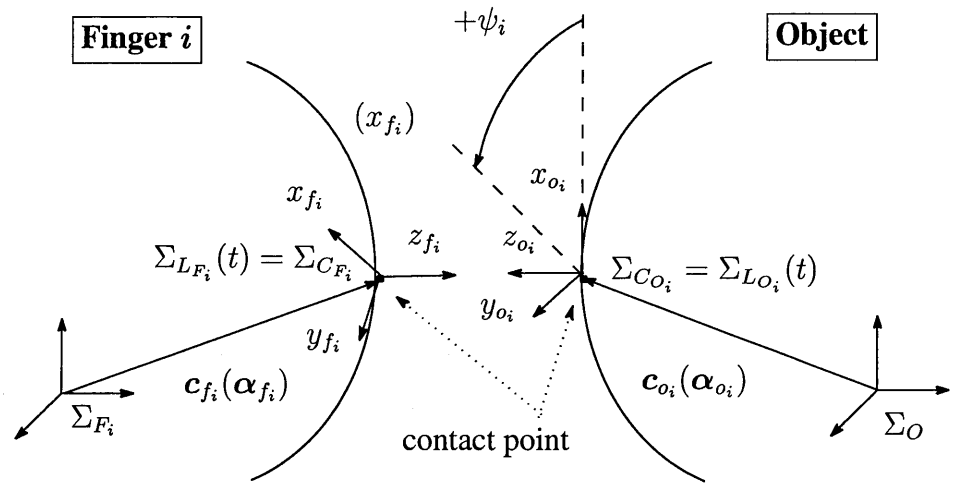

Figure 4.2 Contact coordinates of ith contact point.

(Definition of coordinate frames)

Σ_B	Reference frame.
Σ_{F_i}	Coordinate frame fixed to the ith finger.
Σ_O	Coordinates frame fixed to the object.
$\Sigma_{C_{F_i}}$	Contact frame attached on the surface of the ith finger with the origin at the ith contact point.
$\Sigma_{C_{O_i}}$	Contact frame attached on the surface of the object with the origin at the ith contact point.
$\Sigma_{C_{L_{F_i}}}$	Local frame fixed relative to Σ_{F_i} which coincides at time t with $\Sigma_{C_{F_i}}$.
$\Sigma_{C_{L_{O_i}}}$	Local frame fixed relative to Σ_O which coincides at time t with $\Sigma_{C_{O_i}}$.

(Variables of the system)

(Configuration of Fingers)

${}^B\boldsymbol{p}_{F_i}(\boldsymbol{\theta}_{F_i}) \in \mathbb{R}^3$	Position vector of Σ_{F_i} with respect to Σ_B.
$\boldsymbol{R}_{RF_i}(\boldsymbol{\theta}_{F_i}) \in \mathbb{R}^{3\times 3}$	Rotation matrix of Σ_{F_i} with respect to Σ_B.
$\boldsymbol{\theta}_{F_i} \in \mathbb{R}^{m_i}$	Generalized coordinates of the ith finger ($0 \leq m_i \leq 6$).
$\boldsymbol{\theta}_F := [\, \boldsymbol{\theta}_{F_1}^{\mathrm{T}} \;\; \boldsymbol{\theta}_{F_2}^{\mathrm{T}} \,]^{\mathrm{T}} \in \mathbb{R}^m$	Generalized coordinates of the fingers ($m := m_1 + m_2$).

(Configuration of Object)

${}^B\boldsymbol{p}_O \in \mathbb{R}^3$	Position vector of Σ_O with respect to Σ_B.
$\boldsymbol{R}_{RO} \in \mathbb{R}^{3\times 3}$	Rotation matrix of Σ_O with respect to Σ_B.

${}^{B}\boldsymbol{\phi}_O \in \mathbb{R}^3$	Local parametrization of $\boldsymbol{R}_{RO}$.
$\boldsymbol{x}_O := [\ {}^{B}\boldsymbol{p}_O\ \ {}^{B}\boldsymbol{\phi}_O\ ]^{\mathrm{T}} \in \mathbb{R}^6$	Position and orientation of the object.
(Configuration of contacts)	
${}^{F_i}\boldsymbol{p}_{C_{F_i}} \in \mathbb{R}^3$	Position vector of $\Sigma_{C_{F_i}}$ with respect to Σ_{F_i}.
$\boldsymbol{R}_{F_iC_{F_i}} \in \mathbb{R}^{3\times3}$	Rotation matrix of $\Sigma_{C_{F_i}}$ with respect to Σ_{F_i}.
${}^{O}\boldsymbol{p}_{C_{O_i}} \in \mathbb{R}^3$	Position vector of $\Sigma_{C_{O_i}}$ with respect to Σ_O.
$\boldsymbol{R}_{OC_{O_i}} \in \mathbb{R}^{3\times3}$	Rotation matrix of $\Sigma_{C_{O_i}}$ with respect to Σ_O.
$\boldsymbol{c}_{f_i}(\cdot) : \mathbb{R}^2 \mapsto \mathbb{R}^3$	Local orthogonal chart of the surface of the ith finger.
$\boldsymbol{c}_{o_i}(\cdot) : \mathbb{R}^2 \mapsto \mathbb{R}^3$	Local orthogonal chart of the surface of the object.
$\boldsymbol{\alpha}_{f_i} := [\ u_{f_i}\ \ v_{f_i}\ ]^{\mathrm{T}} \in \mathbb{R}^2$	Local coordinates on the surface of the ith finger.
$\boldsymbol{\alpha}_{o_i} := [\ u_{o_i}\ \ v_{o_i}\ ]^{\mathrm{T}} \in \mathbb{R}^2$	Local coordinates on the surface of the object.
$\psi_i \in \mathbb{R}^1$	Angle between the x- axes of $\Sigma_{C_{F_i}}$ and $\Sigma_{C_{O_i}}$.
$\boldsymbol{\eta}_i := [\ \boldsymbol{\alpha}_{f_i}^{\mathrm{T}}\ \ \boldsymbol{\alpha}_{o_i}^{\mathrm{T}}\ \ \psi_i]^{\mathrm{T}} \in \mathbb{R}^5$	Contact coordinates for the ith contact point.
$\boldsymbol{\eta} := [\ \boldsymbol{\eta}_1^{\mathrm{T}}\ \ \boldsymbol{\eta}_2^{\mathrm{T}}\ ]^{\mathrm{T}} \in \mathbb{R}^{10}$	Contact coordinates for the contact points.
(Forces)	
${}^{C}\boldsymbol{F}_{C_i} \in \mathbb{R}^4$	Contact force at the i contact point.
${}^{C}\boldsymbol{F}_{C} := [\ {}^{C}\boldsymbol{F}_{C_1}^{\mathrm{T}}\ \ {}^{C}\boldsymbol{F}_{C_2}^{\mathrm{T}}\ ]^{\mathrm{T}} \in \mathbb{R}^8$	Contact force at the contact points.
$\boldsymbol{\tau}_i \in \mathbb{R}^{m_i}$	Input for the ith finger.
$\boldsymbol{\tau} := [\ \boldsymbol{\tau}_1^{\mathrm{T}}\ \ \boldsymbol{\tau}_2^{\mathrm{T}}\ ]^{\mathrm{T}} \in \mathbb{R}^m$	Input for the system.

Contact kinematics of the system are summarized in the following.

Let $\boldsymbol{V}_{C_i} := [\ v_{Cx_i}\ \ v_{Cy_i}\ \ v_{Cz_i}\ \ \omega_{Cx_i}\ \ \omega_{Cy_i}\ \ \omega_{Cz_i}\ ]^{\mathrm{T}} \in \mathbb{R}^6$ be the velocity of $\Sigma_{L_{F_i}}$ relative to $\Sigma_{L_{O_i}}$ seen from $\Sigma_{L_{F_i}}$. The motion of the contact coordinates $\dot{\boldsymbol{\eta}}_i$ as a function of the relative motion $\boldsymbol{V}_{C_i}$ is given by

$$\dot{\boldsymbol{\eta}}_i = \boldsymbol{H}_i(\boldsymbol{\eta}_i)\boldsymbol{V}_{C_i} \tag{4.1}$$

$$0 = v_{Cz_i}. \tag{4.2}$$

The precise definition of $\boldsymbol{H}_i \in \mathbb{R}^{5\times6}$ is given by (2.23). In addition, $\boldsymbol{V}_{C_i}$ is given by

$$\boldsymbol{V}_{C_i} = \boldsymbol{D}_{J_{F_i}}(\boldsymbol{\theta}_{F_i}, \boldsymbol{\eta}_i)\dot{\boldsymbol{\theta}}_{F_i} - \boldsymbol{D}_{T_{O_i}}(\boldsymbol{x}_O, \boldsymbol{\eta}_i)\dot{\boldsymbol{x}}_O, \tag{4.3}$$

where

$$\boldsymbol{D}_{T_{F_i}} := \boldsymbol{D}_{F_i}\boldsymbol{J}_{F_i}(\boldsymbol{\theta}_{F_i}), \boldsymbol{D}_{T_{O_i}} := \boldsymbol{D}_{O_i}\boldsymbol{T}_O(\boldsymbol{x}_O). \tag{4.4}$$

The precise definitions of $\boldsymbol{D}_{F_i} \in \mathbb{R}^{6\times6}$ and $\boldsymbol{D}_{O_i} \in \mathbb{R}^{6\times6}$ are given by (2.28) and (2.29). $\boldsymbol{J}_{F_i}(\boldsymbol{\theta}_{F_i}) \in \mathbb{R}^{6\times m_i}$ is the transformation matrix from $\dot{\boldsymbol{\theta}}_{F_i}$ to $[\ {}^{B}\dot{\boldsymbol{p}}_{F_i}^{\mathrm{T}}\ \ {}^{B}\boldsymbol{\omega}_{F_i}^{\mathrm{T}}\ ]^{\mathrm{T}}$. defined by

$$\begin{bmatrix} {}^{B}\dot{\boldsymbol{p}}_{F_i} \\ {}^{B}\boldsymbol{\omega}_{F_i} \end{bmatrix} = \boldsymbol{J}_{F_i}\dot{\boldsymbol{\theta}}_{F_i}, \tag{4.5}$$

and $\boldsymbol{T}_O \in \mathbb{R}^{6\times 6}$ is the transformation matrix from $[\ {}^B\dot{\boldsymbol{p}}_O^{\mathrm{T}}\ \ {}^B\dot{\boldsymbol{\phi}}_O^{\mathrm{T}}\ ]^{\mathrm{T}}$ to $[\ {}^B\dot{\boldsymbol{p}}_O^{\mathrm{T}}\ \ {}^B\boldsymbol{\omega}_O^{\mathrm{T}}\ ]^{\mathrm{T}}$. In this chapter, it is assumed that $\boldsymbol{J}_{F_i}$ and $\boldsymbol{T}_O$ are full column rank and nonsingular respectively. Note that $\boldsymbol{J}_{F_i}$ is determined by the link mechanics of the ith finger. Combining (4.3) and (4.1) leads to

$$\dot{\boldsymbol{\eta}}_i = \boldsymbol{H}_i(\boldsymbol{D}_{T_{F_i}}\dot{\boldsymbol{x}}_{F_i} - \boldsymbol{D}_{T_{O_i}}\dot{\boldsymbol{x}}_O). \tag{4.6}$$

Eq. (4.6) relates the velocities of the contact coordinates $\dot{\boldsymbol{\eta}}_i$ to those of the generalized coordinates $(\dot{\boldsymbol{\theta}}_{F_i}, \dot{\boldsymbol{x}}_O)$.

The motion constraint and the dynamics of the fingers/object are summarized in the following.

Motion Constraint

$$\boldsymbol{A}_F(\boldsymbol{\theta}_F, \boldsymbol{\eta})\dot{\boldsymbol{\theta}}_F - \boldsymbol{A}_O(\boldsymbol{x}_O, \boldsymbol{\eta})\dot{\boldsymbol{x}}_O = \boldsymbol{0}, \tag{4.7}$$

where

$$\boldsymbol{A}_F := \begin{bmatrix} \boldsymbol{B}_C^{\mathrm{T}}\boldsymbol{D}_{J_{F_1}} & \boldsymbol{0}_{4\times m_2} \\ \boldsymbol{0}_{4\times m_1} & \boldsymbol{B}_C^{\mathrm{T}}\boldsymbol{D}_{J_{F_2}} \end{bmatrix},\ \boldsymbol{A}_O := \begin{bmatrix} \boldsymbol{B}_C^{\mathrm{T}}\boldsymbol{D}_{T_{O_1}} \\ \boldsymbol{B}_C^{\mathrm{T}}\boldsymbol{D}_{T_{O_2}} \end{bmatrix}, \boldsymbol{B}_C := \begin{bmatrix} \boldsymbol{I}_3 & \boldsymbol{0}_{3\times 1} \\ \boldsymbol{0}_{3\times 3} & \boldsymbol{e} \end{bmatrix}, \boldsymbol{e} := \begin{bmatrix} 0 \\ 0 \\ 1 \end{bmatrix} \tag{4.8}$$

Constraint on Contact Force

$${}^C\boldsymbol{F}_C \in FC, \tag{4.9}$$

where FC describes the set of the contact force which lies in the friction cone [6].

Equations of Motion

$$\boldsymbol{M}_F(\boldsymbol{\theta}_F)\ddot{\boldsymbol{\theta}}_F + \boldsymbol{C}_F(\boldsymbol{\theta}_F, \dot{\boldsymbol{\theta}}_F)\dot{\boldsymbol{\theta}}_F + \boldsymbol{N}_F(\boldsymbol{\theta}_F) = -\boldsymbol{A}_F^{\mathrm{T}}(\boldsymbol{\theta}_F, \boldsymbol{\eta})^C\boldsymbol{F}_C + \boldsymbol{\tau} \tag{4.10}$$

$$\boldsymbol{M}_O(\boldsymbol{x}_O)\ddot{\boldsymbol{x}}_O + \boldsymbol{C}_O(\boldsymbol{x}_O, \dot{\boldsymbol{x}}_O)\dot{\boldsymbol{x}}_O + \boldsymbol{N}_O(\boldsymbol{x}_O) = \boldsymbol{A}_O^{\mathrm{T}}(\boldsymbol{x}_O, \boldsymbol{\eta})^C\boldsymbol{F}_C, \tag{4.11}$$

where $\boldsymbol{M}_F > 0 \in \mathbb{R}^{m\times m}$, $\boldsymbol{M}_O > 0 \in \mathbb{R}^{6\times 6}$ are the generalized inertia matrices, $\boldsymbol{C}_F \in \mathbb{R}^{m\times m}$, $\boldsymbol{C}_O \in \mathbb{R}^{6\times 6}$ are the Coriolis matrices, and $\boldsymbol{N}_F \in \mathbb{R}^m$, $\boldsymbol{N}_O \in \mathbb{R}^6$ are the gravity terms.

4.2 Analysis of Degrees of Freedom of System

4.2.1 Condition to generate rolling motion

In this subsection, we clarify the DOF of the velocity and the position of the system.

Firstly, since the motion constraint (4.7) consists of 8 constraint equations of the velocity, the DOF of the velocity of the system is $(m-2)$.

Secondly, consider the DOF of the position. From Theorem 3.1, the motion constraint (4.7) is equivalent to the following conditions:

$$\boldsymbol{A}_{\eta_i}(\boldsymbol{\eta}_i)\dot{\boldsymbol{\eta}}_i = \boldsymbol{0} \qquad (i = 1, 2) \tag{4.12}$$

$$\boldsymbol{b}_C^{\mathrm{T}}(\boldsymbol{D}_{F_i}\dot{\boldsymbol{x}}_{F_i} - \boldsymbol{D}_{O_i}\dot{\boldsymbol{x}}_O) = 0 \quad (i = 1, 2), \tag{4.13}$$

where

$$\boldsymbol{A}_{\eta_i} := \begin{bmatrix} -\boldsymbol{M}_{gf_i} & \boldsymbol{R}_{\psi_i}\boldsymbol{M}_{go_i} & 0 \\ -\boldsymbol{T}_{gf_i}\boldsymbol{M}_{gf_i} & -\boldsymbol{T}_{go_i}\boldsymbol{M}_{go_i} & 1 \end{bmatrix} \in \mathbb{R}^{3\times 5} \tag{4.14}$$

$$\boldsymbol{b}_C := [\,0\ 0\ 1\ 0\ 0\ 0\,]^{\mathrm{T}}. \tag{4.15}$$

A general solution of the constraints (4.12) with respect to $\dot{\boldsymbol{\eta}}_i$ is given by

$$\dot{\boldsymbol{\eta}}_i = \boldsymbol{A}_{\eta_i}^{\perp}(\boldsymbol{\eta}_i)\boldsymbol{v}_{\omega_i},\quad \boldsymbol{v}_{\omega_i} := [\,\omega_{Cx_i}\ \ \omega_{Cy_i}\,]^{\mathrm{T}} \in \mathbb{R}^2, \tag{4.16}$$

where

$$\boldsymbol{A}_{\eta_i}^{\perp} := \begin{bmatrix} \boldsymbol{M}_{gf_i}^{-1}\boldsymbol{K}_{R_i}^{-1}\boldsymbol{E} \\ \hline \boldsymbol{M}_{go_i}^{-1}\boldsymbol{R}_{\psi_i}\boldsymbol{K}_{R_i}^{-1}\boldsymbol{E} \\ \hline \boldsymbol{T}_{gf_i}\boldsymbol{K}_{R_i}^{-1}\boldsymbol{E} \\ +\boldsymbol{T}_{go_i}\boldsymbol{R}_{\psi_i}\boldsymbol{K}_{R_i}^{-1}\boldsymbol{E} \end{bmatrix} \in \mathbb{R}^{5\times 2}. \tag{4.17}$$

Note that $\boldsymbol{A}_{\eta_i}\boldsymbol{A}_{\eta_i}^{\perp} = 0$ from (4.12) and (4.17). Since (4.12) are the maximal nonholonomic constraints from Theorem 3.1, $\boldsymbol{\eta}_i$ can be regulated by $\boldsymbol{v}_{\omega_i}$ in (4.16). Therefore, the DOF of the position depends on whether the rolling velocity $\boldsymbol{\omega}_C := [\,\boldsymbol{\omega}_{C_1}^{\mathrm{T}}\ \ \boldsymbol{\omega}_{C_2}^{\mathrm{T}}\,]^{\mathrm{T}} \in \mathbb{R}^4$ can be generated from the $(m-2)$ DOF of the velocity or not. The following theorem holds.

Theorem 4.1. *The relation between $(\dot{\boldsymbol{\theta}}_F, \dot{\boldsymbol{x}}_O)$ and $\boldsymbol{\omega}_C$ is given by*

$$\boldsymbol{\mathcal{A}}(\boldsymbol{\theta}_F, \boldsymbol{x}_O, \boldsymbol{\eta}) \begin{bmatrix} \dot{\boldsymbol{\theta}}_F \\ \dot{\boldsymbol{x}}_O \end{bmatrix} = \overline{\boldsymbol{A}}_{\omega_C}\boldsymbol{\omega}_C, \tag{4.18}$$

where

$$\boldsymbol{\mathcal{A}}(\boldsymbol{\theta}_F, \boldsymbol{x}_O, \boldsymbol{\eta}) := [\,\overline{\boldsymbol{A}}_F\ \ -\overline{\boldsymbol{A}}_O\,] \in \mathbb{R}^{12\times(m+6)}, \tag{4.19}$$

$$\overline{\boldsymbol{A}}_F := \begin{bmatrix} \overline{\boldsymbol{B}}_C^{\mathrm{T}}\boldsymbol{D}_{J_{F_1}} & 0_{6\times m_2} \\ 0_{6\times m_1} & \overline{\boldsymbol{B}}_C^{\mathrm{T}}\boldsymbol{D}_{J_{F_2}} \end{bmatrix},\quad \overline{\boldsymbol{A}}_O := \begin{bmatrix} \overline{\boldsymbol{B}}_C^{\mathrm{T}}\boldsymbol{D}_{T_{O_1}} \\ \overline{\boldsymbol{B}}_C^{\mathrm{T}}\boldsymbol{D}_{T_{O_2}} \end{bmatrix}, \tag{4.20}$$

$$\overline{\boldsymbol{A}}_{\omega_C} := \begin{bmatrix} \overline{\boldsymbol{B}}_C^{\mathrm{T}}\boldsymbol{K}_{B_C^{\mathrm{T}}} & 0_{6\times 2} \\ 0_{6\times 2} & \overline{\boldsymbol{B}}_C^{\mathrm{T}}\boldsymbol{K}_{B_C^{\mathrm{T}}} \end{bmatrix} \in \mathbb{R}^{12\times 4}, \tag{4.21}$$

$$\overline{\boldsymbol{B}}_C := [\,\boldsymbol{B}_C\ \ \boldsymbol{K}_{B_C^{\mathrm{T}}}\,] \in \mathbb{R}^{6\times 6},\quad \boldsymbol{K}_{B_C^{\mathrm{T}}} := [\,0_{2\times 3}\ \ \boldsymbol{I}_2\ \ 0_{2\times 1}\,]^{\mathrm{T}}. \tag{4.22}$$

Furthermore, $\boldsymbol{\omega}_C$ is generated from $\dot{\boldsymbol{\theta}}_F$, $\dot{\boldsymbol{x}}_O$ iff $\boldsymbol{\mathcal{A}}$ of (4.19) is full row rank.

Proof. From the definition $\boldsymbol{\omega}_{C_i} := [\,\omega_{Cx_i}\ \ \omega_{Cy_i}\,]^{\mathrm{T}}$,

$$\boldsymbol{\omega}_{C_i} = \boldsymbol{K}_{B_C^{\mathrm{T}}}^{\mathrm{T}}\boldsymbol{V}_{C_i}. \tag{4.23}$$

Therefore, substituting (4.3) into (4.23), $\boldsymbol{\omega}_{C_i}$ is expressed by $\dot{\boldsymbol{\theta}}_{F_i}$ and $\dot{\boldsymbol{x}}_O$ as

$$\boldsymbol{\omega}_{C_i} = \boldsymbol{K}_{B_C^{\mathrm{T}}}^{\mathrm{T}} \boldsymbol{D}_{J_{F_i}} \dot{\boldsymbol{\theta}}_{F_i} - \boldsymbol{K}_{B_C^{\mathrm{T}}}^{\mathrm{T}} \boldsymbol{D}_{T_{O_i}} \dot{\boldsymbol{x}}_O. \tag{4.24}$$

Combining (4.24) and (4.7), we get (4.18). For the proof of the latter part, notice that (4.18) can be interpreted as the simultaneous linear equations with respect to $[\dot{\boldsymbol{\theta}}_F^{\mathrm{T}} \ \dot{\boldsymbol{x}}_O^{\mathrm{T}}]^{\mathrm{T}}$. Since $\overline{\boldsymbol{B}}_C^{\mathrm{T}} \boldsymbol{K}_{B_C^{\mathrm{T}}} = [\boldsymbol{0}_{2\times 4} \ \boldsymbol{I}_2]^{\mathrm{T}}$ from (4.22) and (4.23), $\overline{\boldsymbol{A}}_{\omega_C}$ of (4.21) is full column rank. Therefore, (4.18) can be solved with respect to $[\dot{\boldsymbol{\theta}}_F^{\mathrm{T}} \ \dot{\boldsymbol{x}}_O^{\mathrm{T}}]^{\mathrm{T}}$ for the arbitrary $\boldsymbol{\omega}_C$ iff $\boldsymbol{\mathcal{A}} \in \mathbb{R}^{12\times(m+6)}$ of (4.18) is full row rank. This fact proves the claim. □

From Theorem 4.1, $\boldsymbol{\omega}_C \in \mathbb{R}^4$ can be generated from the $(m-2)$ DOF of the velocity iff the number of the DOF of the fingers m is greater than or equal to 6 and $\boldsymbol{\mathcal{A}}$ is full row rank. In that case, the contact coordinates $\boldsymbol{\eta} \in \mathbb{R}^{10}$ can be regulated by $\boldsymbol{\omega}_C$ from (4.16). Combining the rest of the DOF of the velocity except $\boldsymbol{\omega}_C$, the DOF of the position is $10 + (m-6) = (m+4)$.

Remark 4.1. Since $\boldsymbol{\mathcal{A}}$ of (4.19) depends on $\boldsymbol{J}_{F_i}$ determined by the link mechanics of the fingers, $\boldsymbol{D}_{F_i}$ of (2.28) and $\boldsymbol{D}_{O_i}$ of (2.29) determined by contact location, it is difficult to describe the general condition of whether $\boldsymbol{\mathcal{A}}$ is full row rank or not. However, since the structure of $\boldsymbol{\mathcal{A}}$ is

$$\boldsymbol{\mathcal{A}} = \begin{bmatrix} \overline{\boldsymbol{B}}_C^{\mathrm{T}} & \boldsymbol{0}_{6\times 6} \\ \boldsymbol{0}_{6\times 6} & \overline{\boldsymbol{B}}_C^{\mathrm{T}} \end{bmatrix} \begin{bmatrix} \boldsymbol{D}_{J_{F_1}} & \boldsymbol{0}_{6\times m_2} & -\boldsymbol{D}_{T_{O_1}} \\ \boldsymbol{0}_{6\times m_1} & \boldsymbol{D}_{J_{F_2}} & -\boldsymbol{D}_{T_{O_2}} \end{bmatrix}, \tag{4.25}$$

the upper six row of $\boldsymbol{\mathcal{A}}$ and the lower six row of $\boldsymbol{\mathcal{A}}$ are full row rank respectively. From this fact, it is expected that $\boldsymbol{\mathcal{A}}$ is full row rank in many practical situations.

4.2.2 Examples of finger link mechanics

Here, we consider some specific finger link mechanics such that $\overline{\boldsymbol{\mathcal{A}}}$ is full row rank. From (4.3) and (4.25), note that it is equivalent to the independency of all components of the relative motion $\boldsymbol{V}_{C_i} \in \mathbb{R}^6$ $(i = 1, 2)$.

Firstly, consider the finger link mechanics as shown in (a) of Figure 4.3. Each finger is a sphere and the object is the cube. The number of the DOF of each finger is four and the directions of its DOF are the rotations with respect to x-, y- and z-axes and translational direction of z-axis of Σ_B. The structure of $\boldsymbol{J}_{F_i} \in \mathbb{R}^{6\times 4}$ is determined as follows:

$$\boldsymbol{J}_{F_i}(\boldsymbol{\theta}_{F_i}) = \left[\begin{array}{ccc|c} 0 & 0 & 0 & 0 \\ 0 & 0 & 0 & 0 \\ 0 & 0 & 0 & 1 \\ \hline \multicolumn{3}{c|}{\boldsymbol{J}_{F_i\omega}(\boldsymbol{\theta}_{F_i})} & \boldsymbol{0}_{3\times 1} \end{array}\right], \tag{4.26}$$

where

$$\boldsymbol{J}_{F_i\omega} := \begin{bmatrix} \cos\theta_{F_{i3}} \cos\theta_{F_{i2}} & -\sin\theta_{F_{i3}} & 0 \\ \sin\theta_{F_{i3}} \cos\theta_{F_{i2}} & \cos\theta_{F_{i3}} & 0 \\ -\sin\theta_{F_{i2}} & 0 & 1 \end{bmatrix}. \tag{4.27}$$

Consider nonsingular and nonsingular configurations as shown in of Figure 4.4. For simplicity, the orientation of the object is set to ${}^B\boldsymbol{\phi}_O = [\ {}^B\phi_{Ox} \ \ 0 \ \ 0\ ]^{\mathrm{T}}$. In Figure 4.4, case (a-1) is the

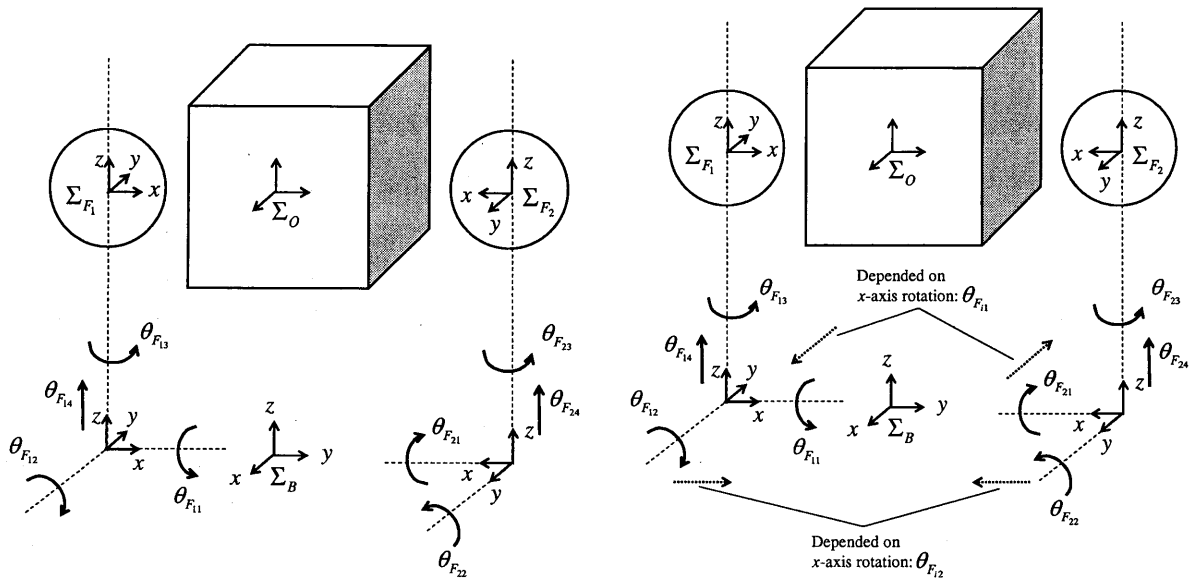

(a) Finger link having no depended directions. (b) Finger link having depended directions.

Figure 4.3 Link mechanics of the fingers.

situation such that ${}^B\phi_{Ox} \neq 0$ and case (a-2) is the situation such that ${}^B\phi_{Ox} = 0$. The fingers have no degrees of the freedom with respect to the directions of x- and y- axes of Σ_B. However, in case (a-1), since the translational velocity of the z- axis of Σ_B and the tangential velocity generated by the rotation about the y- axis are *independent* of each other, each finger can generate the translations with respect to arbitrary directions in (y, z) plane of Σ_B. Therefore, for example, the fingers can generate the contact force with the direction of the internal force, i.e. a pair of pushing forces each other.

On the other hand, in case (a-2), since the translational velocity of the z- axis of Σ_B and the tangential velocity generated by the rotation about the y- axis are *dependent* on each other, each finger can not generate the translations with respect to arbitrary directions in (y, z) plane of Σ_B, i.e., the fingers can not control the internal force. To sum up, the link mechanics of (4.26) is a type such that the rank of $\overline{\boldsymbol{A}}$ is *not* full row rank at a *singular point*, e.g., ${}^B\phi_{Ox} = 0$.

To avoid this singular point, for instance, we consider the finger link mechanics as shown in (b) of Figure 4.3. The number of the DOF of each finger is four and the directions of its DOF are the rotations with respect to x-, y- and z-axes and translational direction of z-axis of Σ_B, where the translational directions of x- and y- axes *depend* on the rotations of y- and x- axes respectively. The structure of $\boldsymbol{J}_{F_i} \in \mathbb{R}^{6\times 4}$ is determined as follows:

$$\boldsymbol{J}_{F_i}(\boldsymbol{\theta}_{F_i}) = \left[\begin{array}{cccc|c} 0 & 1 & 0 & & 0 \\ -1 & 0 & 0 & & 0 \\ 0 & 0 & 0 & & 1 \\ \hline \multicolumn{4}{c|}{\boldsymbol{J}_{F_i\omega}(\boldsymbol{\theta}_{F_i})} & \boldsymbol{0}_{3\times 1} \end{array}\right], \tag{4.28}$$

where $\boldsymbol{J}_{F_i\omega}$ is the same of (4.27). Since this mechanics have the translation with the direction of the x- axis, it is evident that each finger can not generate the translations with respect to arbitrary directions in (y, z) plane of Σ_B in the situation such as case (a-2).

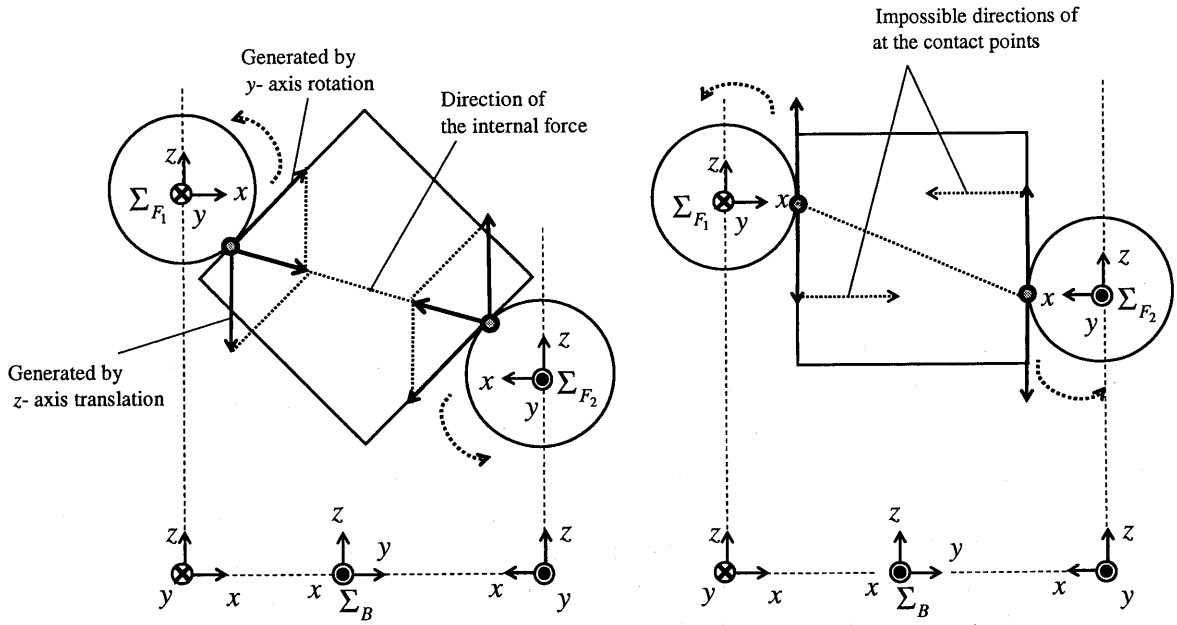

(a-1): Nonsingular configuration. (a-2): Singular configuration.

Figure 4.4 Nonsingular and singular configurations of case (a).

4.3 Control Design

In this section, we consider a control design to achieve the control of the $(m + 4)$ DOF of the position of the system.

4.3.1 Control Objectives

Consider the following control objectives:

(A) To make the contact force ${}^C\boldsymbol{F}_C$ lie in the set of friction cone FC.

(B) To make the rolling velocity $\boldsymbol{\omega}_C \in \mathbb{R}^4$ follow a desired trajectory.

(C) To make the fingers and object motion $\boldsymbol{v}_N \in \mathbb{R}^{(m-6)}$ follow a desired trajectory, where $\boldsymbol{v}_N$ causes no effect on the rolling velocity $\boldsymbol{\omega}_C$.

Control objective (A) represents that the fingers do not slip, and (B) and (C) represent the control of the $(m - 2)$ DOF of the velocity of the system. To achieve these control objectives, we design a linearizing compensator for the rolling velocity, the finger and object motion and the internal force. Therefore, a desired trajectory and a target point in (B) and (C) can be chosen arbitrarily. Since contact coordinates $\boldsymbol{\eta} \in \mathbb{R}^{10}$ can be regulated by making $\boldsymbol{\omega}_C$ follow appropriate trajectory as mentioned previously, all of the $(m+4)$ DOF of the position of the system is controlled. These $(m + 4)$ control variables $(\boldsymbol{\eta}, \boldsymbol{v}_N)$ can be associated with the others of the $(m + 16)$ variables $(\boldsymbol{\theta}_F, \boldsymbol{x}_O, \boldsymbol{\eta})$ since we have 12 equations from (2.18) and (2.19) (Note that (2.19) gives only 3 equations because it relates the 2 rotation matrices). Therefore, the control of the other variables can be realized.

To realize the control objectives, we make the following assumptions:

Assumption 4.4.
(i) $\boldsymbol{A}_O^{\mathrm{T}} \in \mathbb{R}^{6\times 8}$ is full row rank.
(ii) There exists an internal force $\boldsymbol{F}_N \in \mathbb{R}^8$ such that $\boldsymbol{F}_N \in \mathcal{N}(\boldsymbol{A}_O^{\mathrm{T}})$ and $\boldsymbol{F}_N \in \mathrm{Int}(FC)$.

Assumption 4.5.
(i) $\boldsymbol{A}_F^{\mathrm{T}} \in \mathbb{R}^{m\times 8}$ is maximal full rank.
(ii) $\mathcal{N}(\boldsymbol{A}_O^{\mathrm{T}}) \subset \mathcal{R}((\boldsymbol{A}_F^{\mathrm{T}})^+)$.

Assumption 4.6. $\boldsymbol{\mathcal{A}}$ is full row rank.

$\mathrm{Int}(FC)$ represents the interior of the friction cone, $\mathcal{N}(\cdot)$ represents the kernel, $\mathcal{R}(\cdot)$ represents the range of value and $(\cdot)^+$ represents the pseudo inverse matrix. Assumption 4.4 corresponds to the Force Closure [6] in the robotics literatures. Assumption 4.5 guarantees that the internal force can be generated by the inputs to the fingers $\boldsymbol{\tau}$. Assumption 4.6 guarantees that $\boldsymbol{\omega}$ can be generated by the $(m-2)$ DOF of the velocity. Generally, the conditions to guarantee these assumptions depend on the link mechanics of the fingers, the motion constraint, the number of elements of the contact force, the contact location, etc. In our case, Assumption 4 can be satisfied by choosing the contact location appropriately. Assumption 5 and 6 can be satisfied by choosing the link mechanics of the fingers and the contact location appropriately.

4.3.2 Expression of Contact Force

In this subsection, we give an explicit relationship between the contact force and the internal force, which is effective to achieve the control objective (A). The given expression is same expression as that shown in Chapter 3. However, For the readability of this chapter, the expression is summarized briefly.

Let ${}^B\boldsymbol{F}_O \in \mathbb{R}^6$ be

$$ {}^B\boldsymbol{F}_O := \boldsymbol{A}_O^{\mathrm{T}C}\boldsymbol{F}_C. \tag{4.29}$$

${}^B\boldsymbol{F}_O$ represents the resultant force applied to Σ_O by the contact force ${}^C\boldsymbol{F}_C \in \mathbb{R}^8$ (See (4.11)). From Assumption 4.4, a general solution of (4.29) with respect to ${}^C\boldsymbol{F}_C$ is given by

$$ {}^C\boldsymbol{F}_C = (\boldsymbol{A}_O^{\mathrm{T}})^{+B}\boldsymbol{F}_O + \boldsymbol{K}_{A_O^{\mathrm{T}}}(\boldsymbol{x}_O, \boldsymbol{\eta})\boldsymbol{f}_N, \tag{4.30}$$

where $(\cdot)^+$ denotes the pseudo inverse matrix and $\boldsymbol{K}_{A_O^{\mathrm{T}}} \in \mathbb{R}^{8\times 2}$ satisfies $\boldsymbol{A}_O^{\mathrm{T}}\boldsymbol{K}_{A_O^{\mathrm{T}}} = \boldsymbol{0}$ with $\mathrm{rank}(\boldsymbol{K}_{A_O^{\mathrm{T}}}) = 2$. In (4.30), $(\boldsymbol{A}_O^{\mathrm{T}})^{+B}\boldsymbol{F}_O$ represents the component of the contact force which produces the resultant force $\boldsymbol{F}_O$, and $\boldsymbol{K}_{A_O^{\mathrm{T}}}\boldsymbol{f}_N$ represents the internal force which causes no effect on the object motion, where $\boldsymbol{f}_N := [\, f_{N_1} \;\; f_{N_2} \,]^{\mathrm{T}} \in \mathbb{R}^2$ is its magnitude.

From Lemma 3.1 in Chapter 3, the expression of the internal force is given by

$$ \boldsymbol{K}_{A_O^{\mathrm{T}}} := [\, \boldsymbol{k}_1 \;\; \boldsymbol{k}_2 \,] \tag{4.31}$$

$$ \boldsymbol{k}_1 := \begin{bmatrix} \boldsymbol{R}_{BC_{F_1}}^{\mathrm{T}}\,{}^B\boldsymbol{e}_{12} \\ 0 \\ \boldsymbol{R}_{BC_{F_2}}^{\mathrm{T}}\,{}^B\boldsymbol{e}_{21} \\ 0 \end{bmatrix}, \quad \boldsymbol{k}_2 := \begin{bmatrix} \boldsymbol{R}_{BC_{F_1}}^{\mathrm{T}}({}^B\boldsymbol{p}_{C_{O_{12}}}^{\wedge})^+\boldsymbol{\tau}_N \\ \dfrac{1}{({}^B\boldsymbol{p}_{C_{O_{12}}})^{\mathrm{T}B}\boldsymbol{e}_{1z}} \\ -\boldsymbol{R}_{BC_{F_2}}^{\mathrm{T}}({}^B\boldsymbol{p}_{C_{O_{12}}}^{\wedge})^+\boldsymbol{\tau}_N \\ \dfrac{-1}{({}^B\boldsymbol{p}_{C_{O_{12}}})^{\mathrm{T}B}\boldsymbol{e}_{2z}} \end{bmatrix}, \tag{4.32}$$

where

$$\boldsymbol{\tau}_N := \frac{{}^B\boldsymbol{e}_{1z}}{({}^B\boldsymbol{p}_{C_{O_{12}}})^{\mathrm{T}}{}^B\boldsymbol{e}_{1z}} + \frac{-{}^B\boldsymbol{e}_{2z}}{({}^B\boldsymbol{p}_{C_{O_{12}}})^{\mathrm{T}}{}^B\boldsymbol{e}_{2z}} \tag{4.33}$$

$${}^B\boldsymbol{p}_{C_{O_{12}}} := \boldsymbol{R}_{BO}{}^O\boldsymbol{p}_{C_{O_2}} - \boldsymbol{R}_{BO}{}^O\boldsymbol{p}_{C_{O_1}} \tag{4.34}$$

$${}^B\boldsymbol{e}_{zi} := \boldsymbol{R}_{BC_{F_i}}\boldsymbol{e}, \quad \boldsymbol{e} := [\,0\ 0\ 1\,]^{\mathrm{T}}. \tag{4.35}$$

The vector $\boldsymbol{e}_{ij} \in \mathbb{R}^3$ $(i, j = 1, 2,\ i \neq j)$ is the unit vector directing from the contact point i to the contact point j $(\boldsymbol{e}_{12} = -\boldsymbol{e}_{21})$. The position vector ${}^B\boldsymbol{p}_{C_{O_{12}}}$ is the vector from the contact point 2 to the contact point 1 and $\boldsymbol{e}_{iz} \in \mathbb{R}^3$ $(i = 1, 2)$ is the unit vector in direction of z_{f_i}-axis of $\Sigma_{C_{F_i}}$ (See Figure 3.3). This expression satisfies the following equations:

$$\boldsymbol{A}_O^{\mathrm{T}}\boldsymbol{K}_{A_O^{\mathrm{T}}} = \boldsymbol{0}, \tag{4.36}$$

$$\boldsymbol{k}_1^{\mathrm{T}}\boldsymbol{k}_2 = 0. \tag{4.37}$$

By using the expression of $\boldsymbol{K}_{A_O^{\mathrm{T}}}$ of (4.31), f_{N_1} represents the magnitude of the translational forces in the directions of ${}^B\boldsymbol{e}_{12}$ and ${}^B\boldsymbol{e}_{21}$ (See the left figure of Figure 3.3). On the other hand, f_{N_2} represents the magnitude of the moments about $\boldsymbol{\tau}_N$ and $-\boldsymbol{\tau}_N$. $\boldsymbol{\tau}_N$ is the moment produced by the moments about ${}^B\boldsymbol{e}_{1z}$ and ${}^B\boldsymbol{e}_{2z}$ and $-\boldsymbol{\tau}_N$ is the moment of a couple of the translational forces (See the right figure of Figure 3.3). From the observation of the friction cone of the soft-finger contact [6], we can directly achieve (A) by controlling f_{N_1} appropriately.

4.3.3 Expression of Finger and Object Motion

From Assumption 4.6, a general solution of (4.18) with respect to $[\,\dot{\boldsymbol{\theta}}_F^{\mathrm{T}}\ \ \dot{\boldsymbol{x}}_O^{\mathrm{T}}\,]^{\mathrm{T}}$ is given by

$$\begin{bmatrix} \dot{\boldsymbol{\theta}}_F \\ \dot{\boldsymbol{x}}_O \end{bmatrix} = \boldsymbol{\mathcal{A}}^- \overline{\boldsymbol{A}}_{\omega_C}\boldsymbol{\omega}_C + \boldsymbol{K}_{\mathcal{A}}(\boldsymbol{\theta}_F, \boldsymbol{x}_O, \boldsymbol{\eta})\boldsymbol{v}_N, \tag{4.38}$$

where $\boldsymbol{\mathcal{A}}^- \in \mathbb{R}^{(m+6)\times 12}$ is the reflective generalized inverse matrix of $\boldsymbol{\mathcal{A}}$ satisfying $\boldsymbol{\mathcal{A}}\boldsymbol{\mathcal{A}}^- = \boldsymbol{I}_{12}$ and $\boldsymbol{K}_{\mathcal{A}} \in \mathbb{R}^{(m+6)\times(m-6)}$ satisfies $\boldsymbol{\mathcal{A}}\boldsymbol{K}_{\mathcal{A}} = \boldsymbol{0}$ with $\mathrm{rank}(\boldsymbol{K}_{\mathcal{A}}) = m + 6$. In (4.38), $\boldsymbol{\mathcal{A}}^-\overline{\boldsymbol{A}}_{\omega_C}\boldsymbol{\omega}_C$ represents the component of the finger and object motion which causes the rolling velocity, and $\boldsymbol{K}_{\mathcal{A}}\boldsymbol{v}_N$ represents the finger and object motion which causes no effect on the rolling velocity, where $\boldsymbol{v}_N$ is its magnitude.

The expressions of $\boldsymbol{\mathcal{A}}^-$ and $\boldsymbol{K}_{\mathcal{A}}\boldsymbol{v}_N$ have many possibilities. However, we consider the expressions of $\boldsymbol{\mathcal{A}}^-$ and $\boldsymbol{K}_{\mathcal{A}}\boldsymbol{v}_N$ which are effective to achieve the control objective (B) and (C) as follows:

$$\boldsymbol{\mathcal{A}}^- := \boldsymbol{\mathcal{A}}^+ - \boldsymbol{K}_{\mathcal{A}}\boldsymbol{T}_{\mathcal{A}}^{\mathrm{T}}\boldsymbol{\mathcal{A}}^+ \tag{4.39}$$

$$\boldsymbol{K}_{\mathcal{A}} := \overline{\boldsymbol{\mathcal{A}}}^{-1}\begin{bmatrix} \boldsymbol{0}_{12\times(m-6)} \\ \boldsymbol{I}_{(m-6)} \end{bmatrix}, \tag{4.40}$$

where

$$\overline{\boldsymbol{\mathcal{A}}} := \begin{bmatrix} \boldsymbol{\mathcal{A}} \\ \boldsymbol{T}_{\mathcal{A}}^{\mathrm{T}} \end{bmatrix}, \boldsymbol{T}_{\mathcal{A}} := [\boldsymbol{T}_{\theta_F}^{\mathrm{T}}\ \ \boldsymbol{T}_{x_O}^{\mathrm{T}}\,]^{\mathrm{T}}. \tag{4.41}$$

$\boldsymbol{T}_{\theta_F} \in \mathbb{R}^{m\times(m-6)}$ and $\boldsymbol{T}_{x_O} \in \mathbb{R}^{6\times(m-6)}$ are arbitrary matrices to make $\overline{\boldsymbol{\mathcal{A}}}$ of (4.41) nonsingular. These $\boldsymbol{\mathcal{A}}^-$ and $\boldsymbol{K}_{\mathcal{A}}$ satisfy the following lemma.

Lemma 4.1. *Consider $\boldsymbol{\mathcal{A}}^-$ and $\boldsymbol{K}_{\mathcal{A}}$ defined by (4.39)–(4.41). Suppose that $\boldsymbol{T}_{\mathcal{A}}$ is chosen to make $\overline{\boldsymbol{\mathcal{A}}}$ of (4.41) nonsingular. The following equations hold.*

$$\text{(i)} : \boldsymbol{\mathcal{A}}\boldsymbol{K}_{\mathcal{A}} = \boldsymbol{0} \tag{4.42}$$

$$\text{(ii)} : \boldsymbol{v}_N = \boldsymbol{T}_{\theta_F}^{\mathrm{T}}\dot{\boldsymbol{\theta}}_F + \boldsymbol{T}_{x_O}^{\mathrm{T}}\dot{\boldsymbol{x}}_O \tag{4.43}$$

Proof. **(i)** Noting that $\boldsymbol{\mathcal{A}} = \left[\, \boldsymbol{I}_{12} \;\; \boldsymbol{0}_{12\times(m-6)} \,\right]\overline{\boldsymbol{\mathcal{A}}}$ from (4.41), we get

$$\boldsymbol{\mathcal{A}}\boldsymbol{K}_{\mathcal{A}} = \left[\, \boldsymbol{I}_{12} \;\; \boldsymbol{0}_{12\times(m-6)} \,\right] \begin{bmatrix} \boldsymbol{0}_{12\times(m-6)} \\ \boldsymbol{I}_{(m-6)} \end{bmatrix} = \boldsymbol{0}.$$

(ii) Premultiplying (4.38) by $\overline{\boldsymbol{\mathcal{A}}}$ and noting (4.39)–(4.41) and $\boldsymbol{\mathcal{A}}\boldsymbol{\mathcal{A}}^+ = \boldsymbol{I}_{12}$, the result is obtained as:

$$\begin{aligned}
\begin{bmatrix} \boldsymbol{\mathcal{A}} \\ \boldsymbol{T}_{\mathcal{A}}^{\mathrm{T}} \end{bmatrix} \begin{bmatrix} \dot{\boldsymbol{\theta}}_F \\ \dot{\boldsymbol{x}}_O \end{bmatrix} &= \overline{\boldsymbol{\mathcal{A}}}\boldsymbol{\mathcal{A}}^-\overline{\boldsymbol{A}}_{\omega_C}\boldsymbol{\omega}_C + \begin{bmatrix} \boldsymbol{0}_{12\times(m-6)} \\ \boldsymbol{I}_{(m-6)} \end{bmatrix} \boldsymbol{v}_N \\
&= \left\{ \begin{bmatrix} \boldsymbol{\mathcal{A}} \\ \boldsymbol{T}_{\mathcal{A}}^{\mathrm{T}} \end{bmatrix} \boldsymbol{\mathcal{A}}^+ - \begin{bmatrix} \boldsymbol{0}_{12\times(m-6)} \\ \boldsymbol{I}_{(m-6)} \end{bmatrix} \boldsymbol{T}_{\mathcal{A}}^{\mathrm{T}}\boldsymbol{\mathcal{A}}^+ \right\} \overline{\boldsymbol{A}}_{\omega_C}\boldsymbol{\omega}_C + \begin{bmatrix} \boldsymbol{0}_{12\times(m-6)} \\ \boldsymbol{I}_{(m-6)} \end{bmatrix} \boldsymbol{v}_N \\
&= \begin{bmatrix} \boldsymbol{I}_{12} \\ \boldsymbol{0}_{(m-6)\times 12} \end{bmatrix} \overline{\boldsymbol{A}}_{\omega_C}\boldsymbol{\omega}_C + \begin{bmatrix} \boldsymbol{0}_{12\times(m-6)} \\ \boldsymbol{I}_{(m-6)} \end{bmatrix} \boldsymbol{v}_N.
\end{aligned} \tag{4.44}$$

It is evident from the structure of (4.44) that the upper 12 column of (4.44) is (4.18) and the lower of $(m-6)$ of (4.44) is (4.43). □

Remark 4.2. Notice that $\boldsymbol{T}_{\theta_F}$ and $\boldsymbol{T}_{x_O}$ can be chosen arbitrarily under the condition such that $\overline{\boldsymbol{\mathcal{A}}}$ in nonsingular. If we choose by choosing $\boldsymbol{T}_{\theta_F}$ and $\boldsymbol{T}_{x_O}$ as constant matrices, for example, it follows that

$$\int_{t_0}^{t} \boldsymbol{v}_N(t)dt = \int_{t_0}^{t} \left\{ \boldsymbol{T}_{\theta_F}^{\mathrm{T}}\dot{\boldsymbol{\theta}}_F(t) + \boldsymbol{T}_{x_O}^{\mathrm{T}}\dot{\boldsymbol{x}}_O(t) \right\} dt = \boldsymbol{x}_N(t) - \boldsymbol{x}_N(t_0), \tag{4.45}$$

where

$$\boldsymbol{x}_N := \boldsymbol{T}_{\theta_F}^{\mathrm{T}}\boldsymbol{\theta}_F + \boldsymbol{T}_{x_O}^{\mathrm{T}}\boldsymbol{x}_O \in \mathbb{R}^{(m-6)} \tag{4.46}$$

and t_0 is the initial time. Due to (4.45), $\boldsymbol{x}_N$ in calculated from the generalized coordinates $\boldsymbol{\theta}_F$ and $\boldsymbol{x}_O$ by multiplication with constant matrices $\boldsymbol{T}_{\theta_F}^{\mathrm{T}}$ and $\boldsymbol{T}_{x_O}^{\mathrm{T}}$. Therefore, control of the generalized coordinates and the contact coordinates can be achieved in directly by the control of $\boldsymbol{x}_N$.

4.3.4 Linearizing Compensator

In this subsection, we propose a linearizing compensator for $\boldsymbol{\omega}_C \in \mathbb{R}^4$, $\boldsymbol{v}_N \in \mathbb{R}^{m-6}$ and $\boldsymbol{f}_N \in \mathbb{R}^2$. A controller for the linearized system which achieves the control objectives (A), (B) and (C) can be easily designed from the linear control theory. The linearizing compensator is given by

$$\boldsymbol{\tau} = \widehat{\boldsymbol{M}} \begin{bmatrix} \boldsymbol{u}_{\omega_C} \\ \boldsymbol{u}_{v_N} \end{bmatrix} + \widehat{\boldsymbol{C}} \begin{bmatrix} \boldsymbol{\omega}_C \\ \boldsymbol{v}_N \end{bmatrix} + \overline{\boldsymbol{N}} + \boldsymbol{A}_F^{\mathrm{T}} \boldsymbol{K}_{A_O^{\mathrm{T}}} \boldsymbol{u}_{f_N}, \tag{4.47}$$

where

$$\widehat{\boldsymbol{M}} := \overline{\boldsymbol{M}} \boldsymbol{S} \tag{4.48}$$

$$\widehat{\boldsymbol{C}} := \overline{\boldsymbol{M}} \dot{\boldsymbol{S}} + \overline{\boldsymbol{C}} \boldsymbol{S}$$

$$\overline{\boldsymbol{M}} := \begin{bmatrix} \boldsymbol{M}_F & \boldsymbol{A}_F^{\mathrm{T}} (\boldsymbol{A}_O^{\mathrm{T}})^{+} \boldsymbol{M}_O \end{bmatrix} \tag{4.49}$$

$$\overline{\boldsymbol{C}} := \begin{bmatrix} \boldsymbol{C}_F & \boldsymbol{A}_F^{\mathrm{T}} (\boldsymbol{A}_O^{\mathrm{T}})^{+} \boldsymbol{C}_O \end{bmatrix}$$

$$\overline{\boldsymbol{N}} := \boldsymbol{N}_F + \boldsymbol{A}_F^{\mathrm{T}} (\boldsymbol{A}_O^{\mathrm{T}})^{+} \boldsymbol{N}_O$$

$$\boldsymbol{S} = \begin{bmatrix} \boldsymbol{S}_F \\ \boldsymbol{S}_O \end{bmatrix} := \begin{bmatrix} \boldsymbol{\mathcal{A}}^{-} \overline{\boldsymbol{A}}_{\omega_C} & \boldsymbol{K}_{\mathcal{A}} \end{bmatrix} \tag{4.50}$$

($\boldsymbol{S}_F \in \mathbb{R}^{m \times (m-2)}$, $\boldsymbol{S}_O \in \mathbb{R}^{6 \times (m-2)}$). $\boldsymbol{u}_{\omega_C} \in \mathbb{R}^4$, $\boldsymbol{u}_{v_N} \in \mathbb{R}^{(m-6)}$ and $\boldsymbol{u}_{f_N} \in \mathbb{R}^2$ are the new inputs for $\boldsymbol{\omega}_C$, $\boldsymbol{v}_N$ and $\boldsymbol{f}_N$ respectively. The following theorem holds.

Theorem 4.2. *Consider the system (4.10) and (4.11) with the motion constraint (4.7). By the controller (4.47), the system is linearized as*

$$\dot{\boldsymbol{\omega}}_C = \boldsymbol{u}_{\omega_C}, \quad \dot{\boldsymbol{v}}_N = \boldsymbol{u}_{v_N}, \quad \boldsymbol{f}_N = \boldsymbol{u}_{f_N}. \tag{4.51}$$

Proof. With the expressions of ${}^C\boldsymbol{F}_C$ and ${}^B\boldsymbol{F}_O$ described by (4.30) and (4.29) respectively, (4.10) and (4.11) are transformed to

$$\overline{\boldsymbol{M}} \begin{bmatrix} \ddot{\boldsymbol{\theta}}_F \\ \ddot{\boldsymbol{x}}_O \end{bmatrix} + \overline{\boldsymbol{C}} \begin{bmatrix} \dot{\boldsymbol{\theta}}_F \\ \dot{\boldsymbol{x}}_O \end{bmatrix} + \overline{\boldsymbol{N}} + \boldsymbol{A}_F^{\mathrm{T}} \boldsymbol{K}_{A_O^{\mathrm{T}}} \boldsymbol{f}_N = \boldsymbol{\tau}. \tag{4.52}$$

Furthermore, with $\boldsymbol{S}$ defined in (4.50), the expression of $[\ \dot{\boldsymbol{\theta}}_F^{\mathrm{T}} \ \ \dot{\boldsymbol{x}}_O^{\mathrm{T}}\ ]$ described by (4.38) is expressed as

$$\begin{bmatrix} \dot{\boldsymbol{\theta}}_F \\ \dot{\boldsymbol{x}}_O \end{bmatrix} = \boldsymbol{S} \begin{bmatrix} \boldsymbol{\omega}_C \\ \boldsymbol{v}_N \end{bmatrix}. \tag{4.53}$$

Note that $\boldsymbol{S}$ is full column rank since $\boldsymbol{\mathcal{A}}^{-}$ and $\boldsymbol{K}_{\mathcal{A}}$ are full column rank from Assumption 4.6 and $\overline{\boldsymbol{A}}_{\omega_C}$ is full column rank. With (4.53), (4.52) is transformed to

$$\widehat{\boldsymbol{M}} \begin{bmatrix} \dot{\boldsymbol{\omega}}_C \\ \dot{\boldsymbol{v}}_N \end{bmatrix} + \widehat{\boldsymbol{C}} \begin{bmatrix} \boldsymbol{\omega}_C \\ \boldsymbol{v}_N \end{bmatrix} + \overline{\boldsymbol{N}} + \boldsymbol{A}_F^{\mathrm{T}} \boldsymbol{K}_{A_O^{\mathrm{T}}} \boldsymbol{u}_{f_N} = \boldsymbol{\tau}. \tag{4.54}$$

Substituting (4.47) into (4.54) leads to the following closed loop system:

$$\widehat{M}\begin{bmatrix}\dot{\omega}_C - u_{\omega_C}\\ \dot{v}_N - u_{v_N}\end{bmatrix} + A_F^{\mathrm{T}} K_{A_O^{\mathrm{T}}}(f_N - u_{f_N}) = 0. \tag{4.55}$$

Noting that (4.53) is the solution of and the motion constraint (4.7) since (4.53) is the solution of (4.18) where (4.7) is contained, we get the following equation by substituting (4.53) into (4.7):

$$A_F S_F = A_O S_O. \tag{4.56}$$

Premultiplying (4.55) by S_F^{T} and noting that (4.48), (4.49), $S_F^{\mathrm{T}} A_F^{\mathrm{T}} = S_O^{\mathrm{T}} A_O^{\mathrm{T}}$ from (4.56), $A_O^{\mathrm{T}}(A_O^{\mathrm{T}})^+ = I_6$ and $A_O^{\mathrm{T}} K_{A_O^{\mathrm{T}}} = 0$, we get the following equation:

$$\begin{bmatrix} S_F^{\mathrm{T}} & S_O^{\mathrm{T}}\end{bmatrix}\begin{bmatrix} M_F & 0_{m\times 6}\\ 0_{6\times m} & M_O\end{bmatrix}\begin{bmatrix} S_F\\ S_O\end{bmatrix}\begin{bmatrix}\dot{\omega}_C - u_{\omega_C}\\ \dot{v}_N - u_{v_N}\end{bmatrix} = 0. \tag{4.57}$$

Since the coefficient matrix of the above equation is nonsingular from $M_F > 0$ and $M_O > 0$, we get $\dot{\omega}_C - u_{\omega_C} = 0$ and $\dot{v}_N - u_{v_N} = 0$. Next, substituting these results into (4.55), we get $A_F^{\mathrm{T}} K_{A_O^{\mathrm{T}}}(f_N - u_{f_N}) = 0$. Note that the following equation holds [55]:

$$\dim(\mathcal{R}(A_F^{\mathrm{T}} K_{A_O^{\mathrm{T}}})) + \dim(\mathcal{N}(A_F^{\mathrm{T}}) \cap \mathcal{R}(K_{A_O^{\mathrm{T}}})) = \dim(\mathcal{R}(K_{A_O^{\mathrm{T}}})), \tag{4.58}$$

where $\dim(\cdot)$ describe the dimension and $\dim(\mathcal{R}(\cdot)) = \mathrm{rank}(\cdot)$. Since $\mathcal{N}(A_O^{\mathrm{T}}) \subset \mathcal{R}((A_F^{\mathrm{T}})^+)$ from Assumption 4.5 (ii) and $\mathbb{R}^m = \mathcal{R}((A_F^{\mathrm{T}})^+) \oplus \mathcal{N}(A_F^{\mathrm{T}})$, $\mathcal{N}(A_F^{\mathrm{T}}) \cap \mathcal{N}(A_O^{\mathrm{T}}) = \emptyset$ holds ($\emptyset$ is the empty set). Therefore, since $\dim(\mathcal{N}(A_F^{\mathrm{T}}) \cap \mathcal{R}(K_{A_O^{\mathrm{T}}})) = 0$ from $\mathcal{R}(K_{A_O^{\mathrm{T}}}) = \mathcal{N}(A_O^{\mathrm{T}})$, $\dim(\mathcal{R}(A_F^{\mathrm{T}} K_{A_O^{\mathrm{T}}})) = \dim(\mathcal{R}(K_{A_O^{\mathrm{T}}})) = 2$ from (4.58). Since $A_F^{\mathrm{T}} K_{A_O^{\mathrm{T}}} \in \mathbb{R}^{m\times 2}$ is full column rank, we get $f_N - u_{f_N} = 0$. □

4.4 Numerical Example

In a numerical example, each finger is a semisphere of a radius 2.0×10^{-2}[m] whose mass $1.0[\times 10^{-2}$kg]. The object is a cube of length 0.10[m] and mass $5.0[\times 10^{-2}$kg]. The overview of the configuration of the simulation is shown in the left hand side of Figure 4.5. The number of the DOF of each finger is four and the directions of its DOF are the rotations with respect to x-, y- and z-axes and translational direction of z-axis of Σ_B shown in the right hand side of Figure 4.5. The structure of $J_{F_i} \in \mathbb{R}^{6\times 4}$ is given by (4.26). T_{θ_F} and T_{x_O} of (4.41) are chosen as:

$$T_{\theta_F} = 0_{8\times 2},\ T_{x_O} = \begin{bmatrix} 0 & 0 & 1 & 0 & 0 & 0\\ 0 & 0 & 0 & 0 & 0 & 1\end{bmatrix}^{\mathrm{T}}. \tag{4.59}$$

Then, the states of the fingers and the object which causes no effect on the rolling contact is

$$x_N = [\, p_{Oz}\ \ \phi_{Oz}\,]^{\mathrm{T}}, \tag{4.60}$$

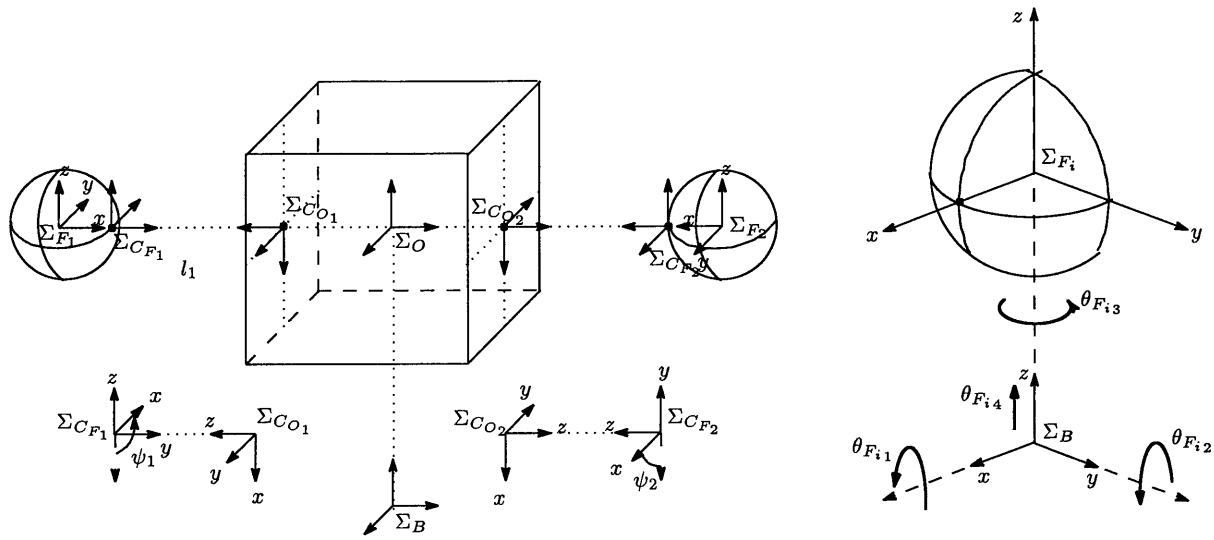

Figure 4.5 Overview of the configuration of the simulation.

where $\boldsymbol{x}_O = [p_{Ox}\ p_{Oy}\ p_{Oz}\ \phi_{Ox}\ \phi_{Oy}\ \phi_{Oz}]^{\mathrm{T}}$. The initial states are

$$\begin{aligned}
\boldsymbol{x}_N &= [\ 0.10[\mathrm{m}]\ \ 0[\mathrm{rad}]\ ]^{\mathrm{T}},\\
\boldsymbol{\eta}_1 &= [\ [\ \tfrac{\pi}{6}\ \ -\tfrac{\pi}{4}\ ][\mathrm{rad}]\ \ [\ 0\ \ 0\ ][\times 10^{-2}\mathrm{m}]\ \ 0[\mathrm{rad}]\ ]^{\mathrm{T}},\\
\boldsymbol{\eta}_2 &= [\ [\ \tfrac{\pi}{6}\ \ \tfrac{\pi}{4}\ ][\mathrm{rad}]\ \ [\ 0\ \ 0\ ][\times 10^{-2}\mathrm{m}]\ \ 0[\mathrm{rad}]\ ]^{\mathrm{T}}.
\end{aligned}$$

The target points are

$$\begin{aligned}
\boldsymbol{x}_N &= [\ 0.15[\mathrm{m}]\ \ \frac{\pi}{3}[\mathrm{rad}]\ ]^{\mathrm{T}},\\
\boldsymbol{\eta}_1 &= [\ [\ 0\ \ 0\ ][\mathrm{rad}]\ \ [\ 1.0\ \ 2.0\ ][\times 10^{-2}\mathrm{m}]\ \ \tfrac{\pi}{6}[\mathrm{rad}]\ ]^{\mathrm{T}},\\
\boldsymbol{\eta}_2 &= [\ [\ 0\ \ 0\ ][\mathrm{rad}]\ \ [\ 2.0\ \ -1.0\ ][\times 10^{-2}\mathrm{m}]\ \ -\frac{\pi}{6}[\mathrm{rad}]\ ]^{\mathrm{T}}.
\end{aligned}$$

The desired trajectory of $\boldsymbol{f}_N$ is determined as the method shown in Appendix C for the contact force to lie in the friction corn. The regulation of $\boldsymbol{\eta}$ can be achieved by the iteration of the closed path of $\boldsymbol{\alpha}_{f_1}$ and $\boldsymbol{\alpha}_{f_2}$, where the rolling velocity $\boldsymbol{\omega}_C$ is transposed to $\dot{\boldsymbol{\alpha}}_{f_1}$ and $\dot{\boldsymbol{\alpha}}_{f_2}$ as shown in Chapter 3. The parameters of the closed path are determined by the method described in Chapter 6, which considers the case where the rolling motion is constrained. In this numerical example, the rolling motion is restricted to the area on the semisphere.

Figure 4.6 shows the time responses of $\boldsymbol{\alpha}_{f_1}$, $\boldsymbol{\alpha}_{f_2}$, $\boldsymbol{v}_N$ and f_N by the linearizing compensator. The broken lines are the desired trajectories and the solid lines are the controlled trajectories. The both lines coincide with each other. The trajectories of $\boldsymbol{\alpha}_{f_1}$ and $\boldsymbol{\alpha}_{f_2}$ are the closed paths in the time interval 2–4[s] and 4–6[s]. The trajectories of $\boldsymbol{\alpha}_{f_1}$ and $\boldsymbol{\alpha}_{f_2}$ lie in the interval between each two heavy lines, which represent the boundaries of $\boldsymbol{\alpha}_{f_1}$ and $\boldsymbol{\alpha}_{f_2}$ due to the fingers of semispheres. Figure 4.7 shows the motion of $\boldsymbol{\alpha}_{o_i}$ and ψ_i on the plane of $\boldsymbol{\alpha}_o = [\ u_{o_i}\ \ v_{o_i}\ ]^{\mathrm{T}}$ $(i = 1, 2)$. The arrows represent ψ_i. The coordinates $\boldsymbol{\alpha}_{o_i}$ and ψ_i are shifted to the target points respectively after two number of iterations.

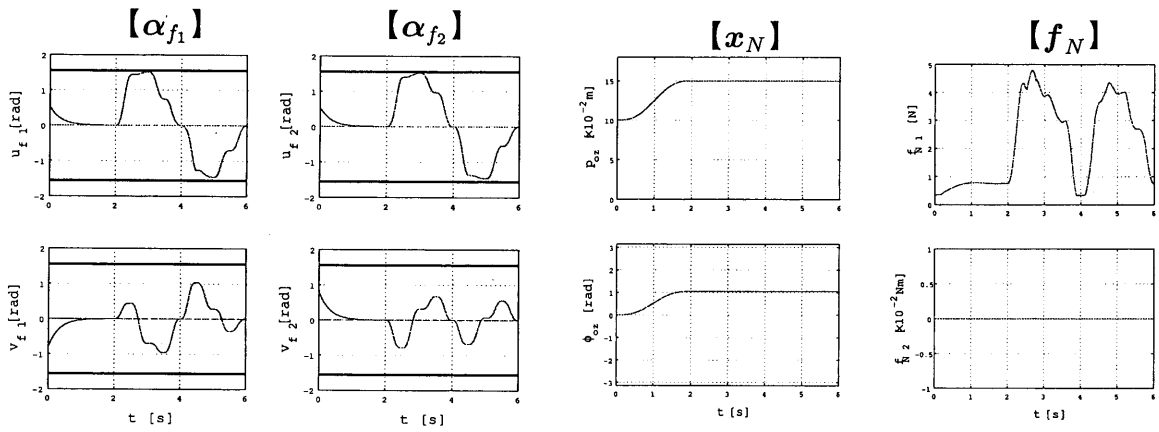

Figure 4.6 Tracking of the linearized variables.

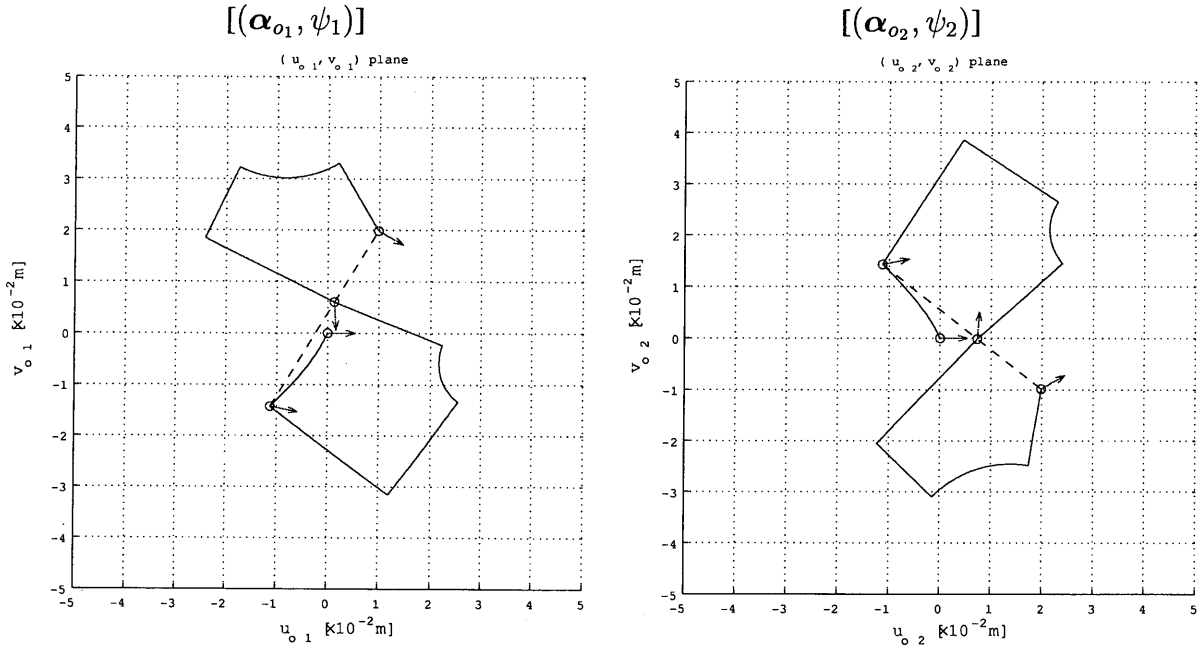

Figure 4.7 The motion of α_{o_i} and ψ_i on the plane of α_{o_i} $(i = 1, 2)$.

4.5 Summary

In this chapter, for the simultaneous control we proposed the control method which could utilize the nonholonomy of rolling for control of contact points by a two-fingered robot hand with the constrained DOF. First, we clarified the condition such that arbitrary rolling motion can be generated from finger and object motion. This represents that the position of the DOF of the whole system is maximum number. Second, we propose the general formulation of the linearizing compensator for the internal force, the motion of the certain coordinates of the fingers and the object, and the rolling motion. For the construction of the linearizing compensator, the finger and object motion were decomposed into a component which caused the rolling motion and a component which did not cause the rolling motion.

Chapter 5

Control of a Sphere Rolling on a Plane by Finite Iterative Closed Paths

In Chapter 3, for the nonholonomic system composed of a sphere and a plane with pure rolling contact, we proposed the trapezoidal closed path on the sphere characterized by three parameters in order to regulate all the contact coordinates by the iterative closed paths. Furthermore, we proved that there always existed the parameters to reduce the euclidean norm of the distance to the target point. However, it guarantees only the converge to arbitrary target points by infinite iteration.

In this chapter, for the kinematic model of a sphere and a plane with pure rolling contact, we propose a regulation algorithm for the contact coordinates to converge to a target point by finite iterative trapezoidal closed paths of the contact point on the sphere. [56, 57]. In Section 5.1, the control problem is summarized briefly. In Section 5.2, we firstly show that, from the viewpoint of the norm minimization, one of the parameters can be determined independent of the other two parameters. Due to this determination, the control problem can be discussed on the two-dimensional space (plane) which characterizes the contact coordinates. We secondly prove that the reachable area of the closed path has two finite lines crossing at the origin which represents the contact coordinates at each iteration. In Section 5.3, we propose a method for the contact coordinates to converge to a target point by the finite iterative shifts along the lines as mentioned earlier. At each iteration, since the proposed method requires solving only one variable equation, the solutions can be easily obtained by the bisection method. In Section 5.4, a numerical example is shown to prove the effectiveness of the proposed method.

5.1 Control Problem

In this section, system configuration and the closed path shown in Chapter 3 are mentioned for the readability of this chapter.

Figure 5.1 shows a spherical finger rolling on a plane of a object. Σ_F is the coordinate frame fixed at the center of the sphere and Σ_O is the coordinate frame at an appropriate point on the plane. The position vectors of the contact point with respect to Σ_F and Σ_O are expressed by $\boldsymbol{c}(\boldsymbol{\alpha}_f) \in \mathbb{R}^3$ and $\boldsymbol{c}(\boldsymbol{\alpha}_o) \in \mathbb{R}^3$, where $\boldsymbol{\alpha}_f \in \mathbb{R}^2$ and $\boldsymbol{\alpha}_o \in \mathbb{R}^2$ are the spherical coordinates and the orthogonal coordinates respectively. The figure on the upper left in Figure 5.1 is the zoom of the

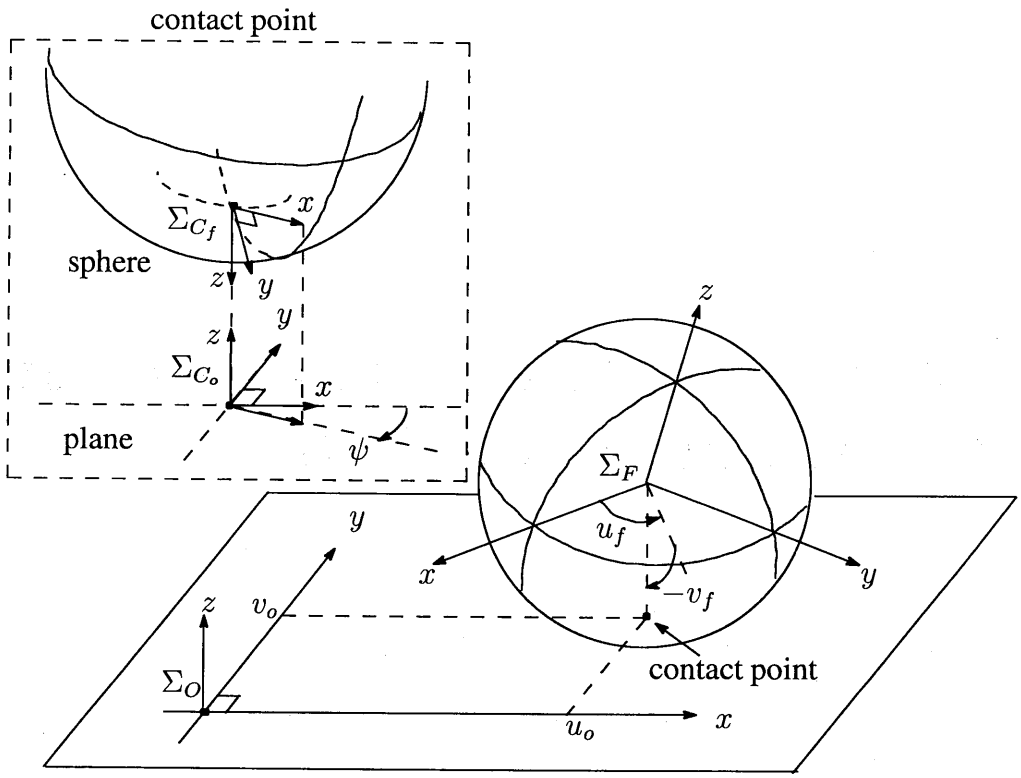

Figure 5.1 A sphere rolling on a plane

neighborhood of the contact point where the contact point is depicted separately for explanations. Σ_{C_f} is the orthogonal coordinate frame at the contact point on the sphere (u_f, v_f), each axis of which is defined by $\partial \boldsymbol{c}_f/\partial u_f$, $\partial \boldsymbol{c}_f/\partial v_f$ and $(\partial \boldsymbol{c}_f/\partial u_f) \times (\partial \boldsymbol{c}_f/\partial v_f)$ respectively. Σ_{C_o} is the orthogonal coordinate frame defined by the similar way. Let $\psi \in \mathbb{R}$ be the angle between x-axes of Σ_{C_f} and Σ_{C_o}. Therefore, the configuration of the system is expressed by the contact coordinates:

$$\boldsymbol{\eta} := [\, \boldsymbol{\alpha}_f^{\mathrm{T}} \;\; \boldsymbol{\alpha}_o^{\mathrm{T}} \;\; \psi \,]^{\mathrm{T}} \in \mathbb{R}^5. \tag{5.1}$$

In this chapter, a type of the rolling contact is assumed to be the pure rolling contact [6]. For the explanation of the pure rolling contact, the relative velocity of Σ_{C_f} relative to Σ_{C_o} seen from Σ_{C_f} is defined by $V_C := [\, v_{Cx} \;\; v_{Cy} \;\; v_{Cz} \;\; \omega_{Cx} \;\; \omega_{Cy} \;\; \omega_{Cz} \,]^{\mathrm{T}} \in \mathbb{R}^6$. The definition of the pure rolling contact is $v_{Cx} = v_{Cy} = v_{Cz} = \omega_{Cz} = 0$, which represents no sliding and no stationary steering. Then, the relationship between $\dot{\boldsymbol{\eta}}$ and $\dot{\boldsymbol{\alpha}}_f$ is as follows [6, 17]:

$$\begin{bmatrix} \dot{\boldsymbol{\alpha}}_f \\ \dot{\boldsymbol{\alpha}}_o \\ \dot{\psi} \end{bmatrix} = \begin{bmatrix} 1 & 0 \\ 0 & 1 \\ \rho \cos v_f \cos \psi & -\rho \sin \psi \\ -\rho \cos v_f \sin \psi & -\rho \cos \psi \\ \sin v_f & 0 \end{bmatrix} \dot{\boldsymbol{\alpha}}_f, \tag{5.2}$$

where ρ is the radius of the sphere. This is the kinematic model where $\dot{\boldsymbol{\alpha}}_f$ is the input.

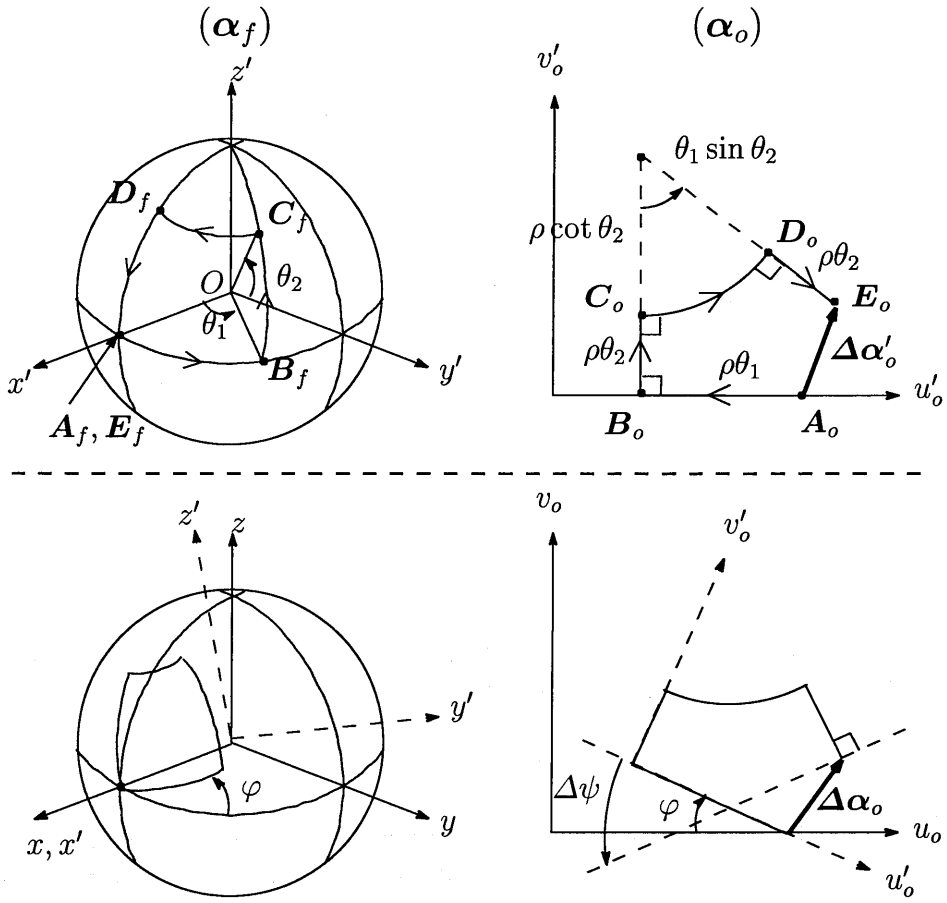

Figure 5.2 The proposed closed path on the sphere.

For simplicity, the target point is assumed to be the origin of $\boldsymbol{\eta}$ and $\dot{\boldsymbol{\alpha}}_f$ is assumed to be able to controlled directly. Hence, the initial state of the contact point on the sphere $\boldsymbol{\alpha}_f$ is assumed to be the origin. Consequently, the control problem is reduced to be the regulation of the others of the contact coordinates

$$\widetilde{\boldsymbol{\eta}} := [\, \boldsymbol{\alpha}_o^{\mathrm{T}} \;\; \psi \,]^{\mathrm{T}} \in \mathbb{R}^3 \tag{5.3}$$

to the origin by the iterative closed paths on the sphere. In the following, $\widetilde{\boldsymbol{\eta}}$ is called the control variable.

The trapezoidal closed path on the sphere for the regulation is shown in Figure 5.2. Figure 5.2 illustrates the proposed closed path and the incremental distances of $\boldsymbol{\alpha}_o$ and ψ by the closed path (initial condition: $\boldsymbol{\alpha}_f = \mathbf{0}$, $\psi = \pi$). In the upper of Figure 5.2, the left figure shows the closed path along the path $\boldsymbol{\alpha}_f$: $A_f \to B_f \to C_f \to D_f \to E_f(A_f)$ which is characterized by the parameters θ_1 and θ_2. The right figure shows the trajectory of $\boldsymbol{\alpha}_o$ generated by the closed path on the left hand side. The incremental distance is $\Delta\boldsymbol{\alpha}'_o$. In the lower of Figure 5.2, the left figure shows the proposed closed path of $\boldsymbol{\alpha}_f$. This is the path which is obtained by rotating the closed path in the upper figure through the parameter φ about x'-axis. The right figure shows the trajectory of $\boldsymbol{\alpha}_o$ generated by the closed path on the left hand side. Denote the incremental distances of $\boldsymbol{\alpha}_o$ and ψ $\Delta\boldsymbol{\alpha}_o$ and $\Delta\psi$ respectively. Define the incremental distance of $\widetilde{\boldsymbol{\eta}}$ by

$$\Delta\widetilde{\boldsymbol{\eta}} := [\, \Delta\boldsymbol{\alpha}_o^{\mathrm{T}} \;\; \Delta\psi \,]^{\mathrm{T}} \in \mathbb{R}^3. \tag{5.4}$$

By integrating (5.2) along the closed path with the initial condition, the components of $\Delta\tilde{\boldsymbol{\eta}}$ are given by

$$\Delta\boldsymbol{\alpha}_o(\theta_1, \theta_2, \varphi) = \boldsymbol{R}_\varphi(\varphi)\Delta\boldsymbol{\alpha}'_o(\theta_1, \theta_2) \tag{5.5}$$

$$\Delta\psi(\theta_1, \theta_2) = -\theta_1 \sin\theta_2, \tag{5.6}$$

where

$$\boldsymbol{R}_\varphi := \begin{bmatrix} \cos\varphi & \sin\varphi \\ -\sin\varphi & \cos\varphi \end{bmatrix} \tag{5.7}$$

$$\Delta\boldsymbol{\alpha}'_o = \begin{bmatrix} -\rho\theta_1 + \rho(\cot\theta_2 + \theta_2)\sin(\theta_1 \sin\theta_2) \\ \rho(\cot\theta_2 + \theta_2)(1 - \cos(\theta_1 \sin\theta_2)) \end{bmatrix}. \tag{5.8}$$

Note that the range of θ_1, θ_2 and φ are

$$-\pi < \theta_1 < \pi, \quad -\frac{\pi}{2} < \theta_2 < \frac{\pi}{2}, \quad -\pi < \varphi < \pi. \tag{5.9}$$

In order to realize a desire shift of the control variable by the closed path, it is necessary to obtain the parameters by solving the following nonlinear equation

$$\Delta\tilde{\boldsymbol{\eta}}(\theta_1, \theta_2, \varphi) = \Delta\tilde{\boldsymbol{\eta}}_d, \tag{5.10}$$

where $\Delta\tilde{\boldsymbol{\eta}}(\theta_1, \theta_2, \varphi)$ is composed of (5.4)–(5.8) and $\Delta\tilde{\boldsymbol{\eta}}_d$ is the incremental distance for the desire shift of the control variable. This is seen as the numerical calculation problem and Newton method is usually used for solving (5.10). However, there is a possibility such that the solution of (5.10) is trapped in local minimums. Furthermore, since there exist the parameters such that the Jacobian matrix of $\Delta\tilde{\boldsymbol{\eta}}$ used in Newton method is singular (for example, $\theta_1 = 0$ or $\theta_2 = 0$ from Lemma 3.3 (ii)), Newton method is no appropriate for solving (5.10). Therefore, it is necessary to investigate the properties of $\Delta\tilde{\boldsymbol{\eta}}$ and to propose a method utilizing the properties except Newton method.

In the following sections, we propose a regulation algorithm for $\tilde{\boldsymbol{\eta}}$ to converge to the origin by finite iterative closed paths. The fundamental idea is composed of the following items:

(1) To determine the parameter φ from the viewpoint of the norm minimization independent of the other two parameters. Due to this determination, the control problem can be discussed on the two-dimensional space (plane) which characterizes the control variables $\tilde{\boldsymbol{\eta}}$.

(2) In the plane, to prove that the reachable area of the closed path includes two finite lines crossed at the origin of the point, which represents the sate of the control variables $\tilde{\boldsymbol{\eta}}$ at each iteration.

(3) To propose the method for $\tilde{\boldsymbol{\eta}}$ to converge to the origin by the finite iterative shifts along the two lines. The parameters at each iteration can be calculated by the bisection method.

The details of the algorithm are shown in Section 5.3. Note that the convergence is guaranteed by appropriate iteration since arbitrary points on a plane can be represented by linear combinations with two independent vectors characterized by the finite lines.

5.2 Properties of the Incremental Distances

Lemmas and a theorem for the regulation algorithm are shown in this section. For reachability of this chapter, Lemma 3.3 is inserted again.

For the incremental distance $\Delta\tilde{\boldsymbol{\eta}}$, the following lemma holds.

Lemma 3.3. $\Delta\boldsymbol{\alpha}'_o$, $\Delta\psi$ defined by (5.6), (5.8) has the following properties.
(i) $\Delta\boldsymbol{\alpha}'_o$, $\Delta\psi$ is continuous with respect to θ_1, θ_2.
(ii) The following equivalent conditions hold.

$$\|\Delta\boldsymbol{\alpha}'_o\| = 0 \Longleftrightarrow \theta_1 = 0 \text{ or } \theta_2 = 0 \tag{5.11}$$

$$\Delta\psi = 0 \Longleftrightarrow \theta_1 = 0 \text{ or } \theta_2 = 0 \tag{5.12}$$

As for the parameter φ which represents the start direction of the closed path, the following lemma holds.

Lemma 5.1. *Consider $\tilde{\boldsymbol{\eta}}$ and $\Delta\tilde{\boldsymbol{\eta}}$ defined by (5.3) and (5.4). Then, the parameter φ to minimize $\|\tilde{\boldsymbol{\eta}} + \Delta\tilde{\boldsymbol{\eta}}\|$ satisfies the following equation:*

$$\boldsymbol{R}_\varphi \frac{\Delta\boldsymbol{\alpha}'_o}{\|\Delta\boldsymbol{\alpha}'_o\|} = -\frac{\boldsymbol{\alpha}_o}{\|\boldsymbol{\alpha}_o\|}. \tag{5.13}$$

Proof. From (5.4) and (5.5) with $\Delta\tilde{\boldsymbol{\eta}} = [\ (\boldsymbol{R}_\varphi\Delta\boldsymbol{\alpha}'_o)^{\mathrm{T}}\ \ \Delta\psi\ ]^{\mathrm{T}}$,

$$\|\tilde{\boldsymbol{\eta}} + \Delta\tilde{\boldsymbol{\eta}}\|^2 = \|\boldsymbol{\alpha}_o\|^2 + \psi^2 + \underbrace{2\boldsymbol{\alpha}_o^{\mathrm{T}}(\boldsymbol{R}_\varphi\Delta\boldsymbol{\alpha}'_o)}_{A} + 2\psi\Delta\psi + \|\Delta\boldsymbol{\alpha}'_o\|^2 + \Delta\psi^2, \tag{5.14}$$

where $\boldsymbol{R}_\varphi^{\mathrm{T}}\boldsymbol{R}_\varphi = \boldsymbol{I}_2$ from (5.7). In the right hand side of (5.14), note that only the term A which is the inner product between $\boldsymbol{\alpha}_o$ and $\boldsymbol{R}_\varphi\Delta\boldsymbol{\alpha}'_o$ depends on φ. Therefore, the term A is minimized with respect to φ when the angle made by $\boldsymbol{\alpha}_o$ and $\boldsymbol{R}_\varphi\Delta\boldsymbol{\alpha}'_o$ is π, i.e. φ satisfies (5.13). □

Consider the interpretation of Lemma 5.1 form a geometric view point. From (5.4) and (5.5), the incremental distance $\Delta\tilde{\boldsymbol{\eta}}$ is rewritten as

$$\Delta\tilde{\boldsymbol{\eta}} = \begin{bmatrix} \boldsymbol{R}_\varphi\Delta\boldsymbol{\alpha}'_o \\ \Delta\psi \end{bmatrix} = \begin{bmatrix} \|\Delta\boldsymbol{\alpha}'_o\| \left(\boldsymbol{R}_\varphi \dfrac{\Delta\boldsymbol{\alpha}'_o}{\|\Delta\boldsymbol{\alpha}'_o\|}\right) \\ \Delta\psi \end{bmatrix}. \tag{5.15}$$

This structure of (5.15) is illustrated in the left hand of Figure 5.3. In the left hand of Figure 5.3, the point P represents the point of $\tilde{\boldsymbol{\eta}} = [\ \boldsymbol{\alpha}_o^{\mathrm{T}}\ \ \psi\ ]^{\mathrm{T}} = [\ u_o\ \ v_o\ \ \psi\ ]^{\mathrm{T}}$ in the space of $\tilde{\boldsymbol{\eta}}$ and the reachable area of the closed path on the plane $(\|\Delta\boldsymbol{\alpha}'_o\|, \Delta\psi)$ at P with the origin is represented by the shaded area. We call this area the reachable area Ω. Observing the structure of (5.15) leads to the fact that the reachable area of $\Delta\tilde{\boldsymbol{\eta}}$ is obtained by rotating the area Ω through φ about $\Delta\psi$-axis. Therefore, the geometric interpretation of (5.13) is that the parameter φ is determined

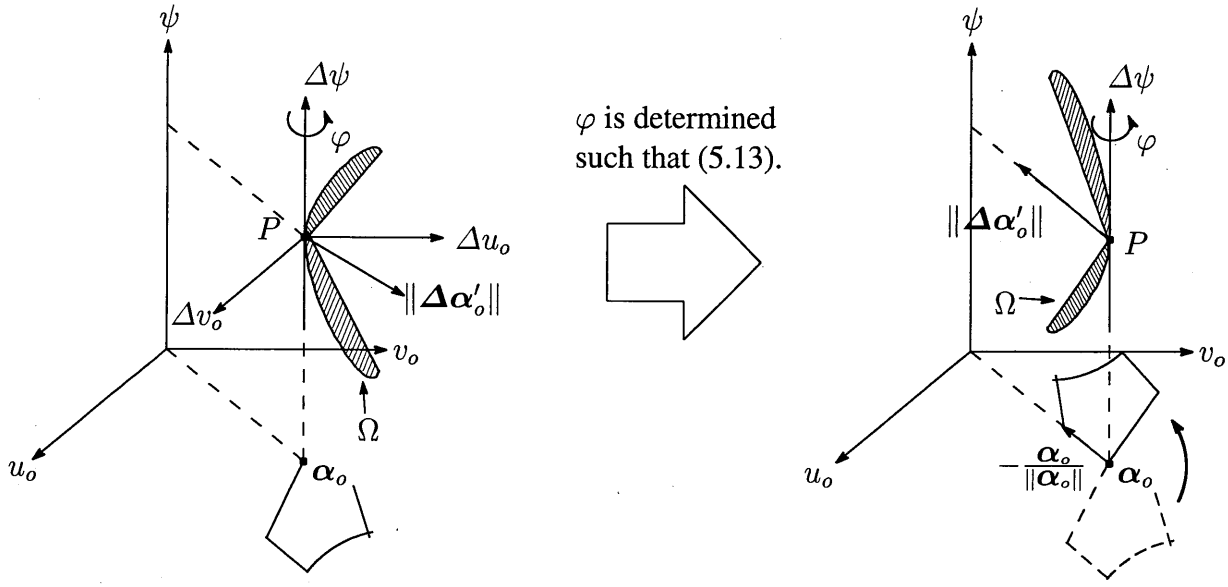

Figure 5.3 The interpretation of Lemma 5.1 form a geometric view point.

such that the direction of Ω defined by $\|\Delta\boldsymbol{\alpha}'_o\|$ -axis coincides $-\frac{\boldsymbol{\alpha}_o}{\|\boldsymbol{\alpha}_o\|}$ as seen in the right hand of Figure 5.3. By using φ satisfying (5.13), $\|\widetilde{\boldsymbol{\eta}} + \Delta\widetilde{\boldsymbol{\eta}}\|$ is written as

$$\|\widetilde{\boldsymbol{\eta}} + \Delta\widetilde{\boldsymbol{\eta}}\| = \left\| \begin{bmatrix} (\|\boldsymbol{\alpha}_o\| - \|\Delta\boldsymbol{\alpha}'_o\|) \dfrac{\boldsymbol{\alpha}_o}{\|\boldsymbol{\alpha}_o\|} \\ \psi + \Delta\psi \end{bmatrix} \right\| = \sqrt{(\|\boldsymbol{\alpha}_o\| - \|\Delta\boldsymbol{\alpha}'_o\|)^2 + (\psi + \Delta\psi)^2}. \quad (5.16)$$

Consequently, the determination problem of $(\theta_1, \theta_2, \varphi)$ for the convergence of $\|\widetilde{\boldsymbol{\eta}} + \Delta\widetilde{\boldsymbol{\eta}}\|$ is reduced to that of (θ_1, θ_2) since $\|\Delta\boldsymbol{\alpha}'_o\|$ and $\Delta\psi$ are functions of θ_1 and θ_2.

Figure 5.4 shows the concept for $\widetilde{\boldsymbol{\eta}}$ to converge to the target point by using the reachable area Ω. The areas surrounded by dashed lines are the reachable areas Ω at each iteration. As in Figure 5.4, $\widetilde{\boldsymbol{\eta}}$ can converges to the target point by shifting to points on the reachable areas Ω iteratively. To do so, precise analysis of the reachable area Ω is necessary. In the following, the properties of the reachable area Ω at the plane $(\|\Delta\boldsymbol{\alpha}'_o\|, \Delta\psi)$ are investigated.

As for the reachable area Ω, the following lemma holds.

Lemma 5.2. *Consider the reachable area Ω at the plane $(\|\Delta\boldsymbol{\alpha}'_o\|, \Delta\psi)$ given by (5.6) and (5.8). Then, Ω is symmetry with respect to the $\|\Delta\boldsymbol{\alpha}'_o\|$-axis.*

Proof. The values of $\Delta\psi$ and $\Delta\boldsymbol{\alpha}'_o$ at $(\widehat{\theta}_1, \widehat{\theta}_2)$ are set to $\Delta\psi = \Delta\widehat{\psi}$ and $\Delta\boldsymbol{\alpha}'_o = [\ \Delta\widehat{u}'_o\ \ \Delta\widehat{v}'_o\ ]^{\mathrm{T}}$ respectively. From (5.6), $\Delta\psi = -\Delta\widehat{\psi}$ is equivalent to the case such that $(\theta_1, \theta_2) = (-\widehat{\theta}_1, \widehat{\theta}_2)$ or $(\widehat{\theta}_1, -\widehat{\theta}_2)$. Then, from (5.8), since the values of $\Delta\boldsymbol{\alpha}'_o$ are

$$\Delta\boldsymbol{\alpha}'_o(-\widehat{\theta}_1, \widehat{\theta}_2) = \begin{bmatrix} -\Delta\widehat{u}'_o \\ \Delta\widehat{v}'_o \end{bmatrix}, \quad \Delta\boldsymbol{\alpha}'_o(\widehat{\theta}_1, -\widehat{\theta}_2) = \begin{bmatrix} \Delta\widehat{u}'_o \\ -\Delta\widehat{v}'_o \end{bmatrix},$$

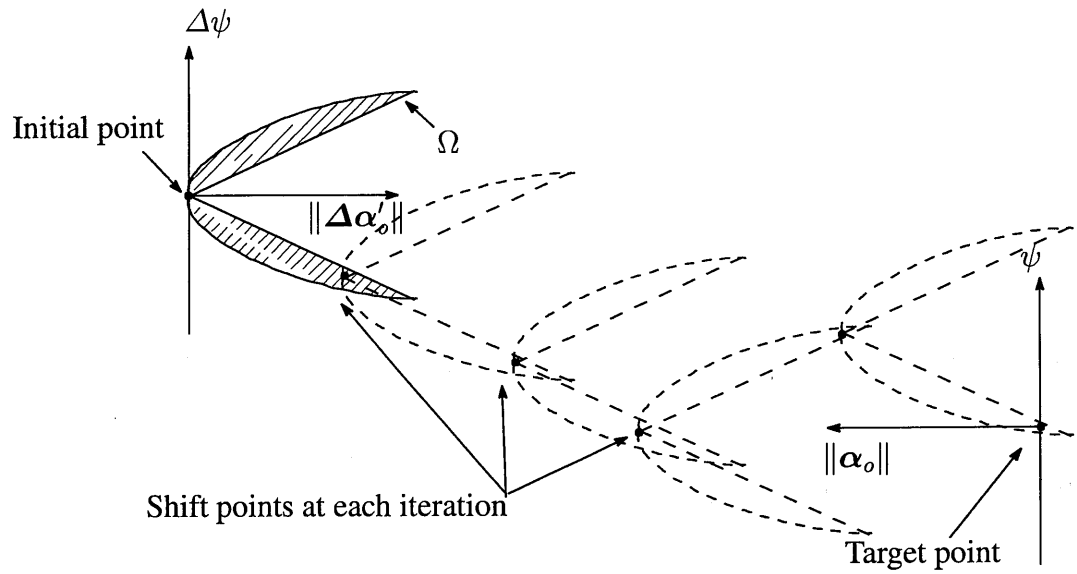

Figure 5.4 Concept for $\widetilde{\boldsymbol{\eta}}$ to converge to the target point.

the following equation holds:

$$\|\Delta\boldsymbol{\alpha}'_o(\widehat{\theta}_1, \widehat{\theta}_2)\| = \|\Delta\boldsymbol{\alpha}'_o(-\widehat{\theta}_1, \widehat{\theta}_2)\| = \|\Delta\boldsymbol{\alpha}'_o(\widehat{\theta}_1, -\widehat{\theta}_2)\|. \tag{5.17}$$

Therefore, since $\|\Delta\boldsymbol{\alpha}'_o\|$ is invariant at $(\widehat{\theta}_1, \widehat{\theta}_2)$ such that $\Delta\psi = \Delta\widehat{\psi}$ and $\Delta\psi = -\Delta\widehat{\psi}$, Ω is symmetry with respect to the $\|\Delta\boldsymbol{\alpha}'_o\|$-axis. □

Furthermore, the following theorem holds as for the reachable area Ω.

Theorem 5.1. *Consider $\Delta\boldsymbol{\alpha}'_o$ and $\Delta\psi$ defined by (5.6) and (5.8). Then, for arbitrary ε such that*

$$-\frac{\pi}{2} < \varepsilon < \frac{\pi}{2}, \tag{5.18}$$

there exist θ_1 and θ_2 such that the following equation holds.

$$\Delta\psi = \varepsilon, \ \|\Delta\boldsymbol{\alpha}'_o\| = \rho|\varepsilon|. \tag{5.19}$$

Proof. Since it is evident from Lemma 3.3(ii) that Theorem 5.1 holds when $\varepsilon = 0$, $\varepsilon \neq 0$ is assumed in the following.

First, consider the first term of (5.19). Since $\Delta\psi = -\theta_1 \sin\theta_2$ from (5.6) and the ranges $-\pi < \theta_1 < \pi$ and $-\frac{\pi}{2} < \theta_2 < \frac{\pi}{2}$ from (5.9), there exist θ_1 and θ_2 to satisfy $\Delta\psi = -\theta_1 \sin\theta_2 = \varepsilon$.

Second, consider the second term of (5.19) with the condition $\Delta\psi = \varepsilon$. In order to make the proof easy, the variable θ_1 of $\|\Delta\boldsymbol{\alpha}'_o(\theta_1, \theta_2)\|$ is transformed to ε by the condition $\Delta\psi = -\theta_1 \sin\theta_2 = \varepsilon$. The condition is transformed to

$$\theta_1 = -\frac{\varepsilon}{\sin\theta_2}. \tag{5.20}$$

Substituting (5.20) into the domain $-\pi < \theta_1 < \pi$ and solving the resultant inequality with respect to θ_2 lead to the range of θ_2 to guarantee the existence of the transformation from θ_1 to ε:

$$\begin{cases} -\frac{\pi}{2} < \theta_2 < \sin^{-1}(-\frac{\varepsilon}{\pi}) \text{ or } \sin^{-1}(\frac{\varepsilon}{\pi}) < \theta_2 < \frac{\pi}{2} \ (\varepsilon > 0), \\ -\frac{\pi}{2} < \theta_2 < \sin^{-1}(\frac{\varepsilon}{\pi}) \text{ or } \sin^{-1}(-\frac{\varepsilon}{\pi}) < \theta_2 < \frac{\pi}{2} \ (\varepsilon < 0). \end{cases} \tag{5.21}$$

By substituting (5.20) into $\|\boldsymbol{\Delta\alpha}'_o(\theta_1, \theta_2)\|^2$, $\|\boldsymbol{\Delta\alpha}'_o\|^2$ is transformed to the following function of θ_2 and ε:

$$\|\boldsymbol{\Delta\alpha}'_o(\varepsilon, \theta_2)\|^2 = \rho^2 \frac{\varepsilon^2 - 2(\cos\theta_2 + \theta_2 \sin\theta_2)\varepsilon \sin\varepsilon + 2(\cos\theta_2 + \theta_2 \sin\theta_2)^2(1 - \cos\varepsilon)}{\sin^2\theta_2}, \tag{5.22}$$

where $\|\boldsymbol{\Delta\alpha}'_o(-\frac{\varepsilon}{\sin\theta_2}, \theta_2)\|$ $(= \|\boldsymbol{\Delta\alpha}'_o(\theta_1, \theta_2)\|)$ is rewritten as $\|\boldsymbol{\Delta\alpha}'_o(\varepsilon, \theta_2)\|$ for simplicity. In this function, the ranges of ε and θ_2 are (5.18) and (5.21) respectively. The function (5.22) is continuous with respect to ε and θ_2 since ε $(= -\theta_1 \sin\theta_2)$ is continuous with respect to θ_1 and θ_2 and $\boldsymbol{\Delta\alpha}'_o(\theta_1, \theta_2)$ is continuous with respect to θ_1 and θ_2 from Lemma 3.3 (i). Since $\|\boldsymbol{\Delta\alpha}'_o\|$ is symmetry with respect to the ε $(= \Delta\psi)$-axis from Lemma 5.2 and $\|\boldsymbol{\Delta\alpha}'_o(\varepsilon, \theta_2)\| = \|\boldsymbol{\Delta\alpha}'_o(\varepsilon, -\theta_2)\|$ holds from (5.22), only the case such that $\varepsilon > 0$ and $\theta_2 > 0$ is considered in the following. In order to prove that there exists θ_2 to satisfy the following equation

$$\|\boldsymbol{\Delta\alpha}'_o(\varepsilon, \theta_2)\|^2 = (\rho\varepsilon)^2 \tag{5.23}$$

with the condition (5.21) and (5.18), we prove that there exist θ_{2L} and θ_{2U} to satisfy the following inequality

$$\|\boldsymbol{\Delta\alpha}'_o(\varepsilon, \theta_{2L})\|^2 \leq (\rho\varepsilon)^2 \leq \|\boldsymbol{\Delta\alpha}'_o(\varepsilon, \theta_{2U})\|^2 \tag{5.24}$$

for arbitrary $0 < \varepsilon < \frac{\pi}{2}$ from the intermediate-value theorem. Specifying the values of θ_{2L} and θ_{2U} to the upper bound and the lower bound of the domain (5.21) of θ_2 leads to the following equations:

$$\lim_{\theta_{2L} \to \frac{\pi}{2}} \|\boldsymbol{\Delta\alpha}'_o(\varepsilon, \theta_{2L})\|^2 = \rho^2 \left\{ \varepsilon^2 - \pi\varepsilon \sin\varepsilon + \frac{\pi^2}{2}(1 - \cos\varepsilon) \right\},$$

$$\lim_{\theta_{2U} \to \sin^{-1}\frac{\varepsilon}{\pi}} \|\boldsymbol{\Delta\alpha}'_o(\varepsilon, \theta_{2U})\|^2 = \rho^2 \left\{ \pi^2 - \frac{2\pi^2}{\varepsilon} \sin\varepsilon\Theta + \frac{2\pi^2}{\varepsilon^2}(1 - \cos\varepsilon)\Theta^2 \right\},$$

where $\Theta := (\cos\theta_2 + \theta_2 \sin\theta_2)|_{\theta_2 = \sin^{-1}(\frac{\varepsilon}{\pi})}$. From these equations and (5.24), we prove the following inequalities in the condition $0 < \varepsilon < \frac{\pi}{2}$:

$$\varepsilon^2 - \pi\varepsilon \sin\varepsilon + \frac{\pi^2}{2}(1 - \cos\varepsilon) < \varepsilon^2, \tag{5.25}$$

$$\pi^2 - \frac{2\pi^2}{\varepsilon} \sin\varepsilon\Theta + \frac{2\pi^2}{\varepsilon^2}(1 - \cos\varepsilon)\Theta^2 > \varepsilon^2. \tag{5.26}$$

1) $\boxed{\|\boldsymbol{\Delta\alpha}'_o(\varepsilon, \theta_{2L})\|^2 \leq (\rho\varepsilon)^2\text{: (5.25)}}$

Eq. (5.25) is rewritten as

$$\frac{\pi^2}{2}(1 - f(\varepsilon)) < 0, \tag{5.27}$$

where

$$f(\varepsilon) := \cos\varepsilon + \frac{2}{\pi}\varepsilon\sin\varepsilon. \tag{5.28}$$

The differential of $f(\varepsilon)$ with respect to ε is given by

$$f'(\varepsilon) = \left(\frac{2}{\pi} - 1\right)\sin\varepsilon + \frac{2}{\pi}\varepsilon\cos\varepsilon, \tag{5.29}$$

where $f' := \frac{df}{d\varepsilon}$. In the following of this proof, the description $(\cdot)'$ stands for the differential with respect to ε. Setting $f'(\varepsilon) = 0$ leads to

$$\frac{2}{\pi - 2}\varepsilon = \tan\varepsilon. \tag{5.30}$$

Since the functions $\frac{2}{\pi-2}\varepsilon$ and $\tan\varepsilon$ are monotone increasing functions and the values of its differentials at $\theta_2 = 0, \frac{\pi}{2}$ are

$$\left(\frac{2}{\pi - 2}\varepsilon\right)'\Big|_{\theta_2=0,\frac{\pi}{2}} = \frac{2}{\pi - 2} > 1, \quad \begin{cases} (\tan\varepsilon)'|_{\varepsilon=0} = 1 \\ \lim\limits_{\varepsilon\to\frac{\pi}{2}}(\tan\varepsilon)' = \infty \end{cases},$$

there exists one ε^* such that $f'(\varepsilon^*) = 0$ in the domain $0 < \varepsilon < \frac{\pi}{2}$. Furthermore, by calculating the values of $f'(\varepsilon)$ and $f(\varepsilon)$ at $\theta_2 = 0, \frac{\pi}{2}$ from (5.28) and (5.29), the increase and decrease chart of $f(\varepsilon)$ is given by

ε	0	$\cdots$	ε^*	$\cdots$	$\frac{\pi}{2}$
f'	0	+	0	−	$\frac{2}{\pi} - 1$
f	1	↗	$f(\varepsilon^*)$	↘	1

Therefore,

$$f(\varepsilon) > 1, \quad 0 < \varepsilon < \frac{\pi}{2}.$$

It follows that (5.25) holds from (5.27).

2) $\boxed{(\rho\varepsilon)^2 \le \|\Delta\boldsymbol{\alpha}'_o\|^2(\varepsilon, \theta_{2U})}$: (5.26)

By making the completing square with respect to Θ in the left term of (5.26), (5.26) is rewritten as

$$\begin{aligned} &\frac{\pi^2}{\varepsilon^2} - \frac{2\pi^2}{\varepsilon^3}\sin\varepsilon\Theta + \frac{2\pi^2}{\varepsilon^4}(1 - \cos\varepsilon)\Theta^2 \\ &= \frac{2\pi^2}{\varepsilon^4}(1 - \cos\varepsilon)\left\{\Theta - \frac{\varepsilon\sin\varepsilon}{2(1 - \cos\varepsilon)}\right\}^2 + \frac{\pi^2}{\varepsilon^2}\left\{1 - \frac{\sin^2\varepsilon}{2(1 - \cos\varepsilon)}\right\} \\ &\ge g(\varepsilon) > 1, \end{aligned} \tag{5.31}$$

where

$$g(\varepsilon) := \frac{\pi^2}{\varepsilon^2}\left\{1 - \frac{\sin^2\varepsilon}{2(1 - \cos\varepsilon)}\right\}. \tag{5.32}$$

The differential of $g(\varepsilon)$ with respect to ε is given by

$$\begin{aligned} g'(\varepsilon) &= -2\frac{\pi^2}{\varepsilon^3}\left\{1 - \frac{\sin^2\varepsilon}{2(1-\cos\varepsilon)}\right\} - \frac{\pi^2}{\varepsilon^2}\frac{\sin\varepsilon(2\cos\varepsilon - 2\cos^2\varepsilon - \sin^2\varepsilon)}{2(1-\cos\varepsilon)^2} \\ &= \frac{\pi^2}{\varepsilon^2}\left\{\frac{1}{\varepsilon}\left(-2 + \frac{\sin^2\varepsilon}{1-\cos\varepsilon}\right) - \frac{\sin\varepsilon(2\cos\varepsilon - \cos^2\varepsilon - 1)}{2(1-\cos\varepsilon)^2}\right\} \\ &= \frac{\pi^2}{\varepsilon^2}\left\{\frac{1}{\varepsilon}\left(\frac{-2 + 2\cos\varepsilon + 1 - \cos^2\varepsilon}{1-\cos\varepsilon}\right) + \frac{1}{2}\sin\varepsilon\right\} \\ &= \frac{\pi^2}{\varepsilon^2}\left(-\frac{1-\cos\varepsilon}{\varepsilon} + \frac{1}{2}\sin\varepsilon\right). \end{aligned} \tag{5.33}$$

Setting $g'(\varepsilon) = 0$ leads to

$$\frac{\varepsilon}{2} = \frac{(1-\cos\varepsilon)}{\sin\varepsilon} = \frac{2\sin^2\frac{\varepsilon}{2}}{2\sin\frac{\varepsilon}{2}\cos\frac{\varepsilon}{2}} = \tan\frac{\varepsilon}{2}. \tag{5.34}$$

Since the functions $\frac{1}{2}\varepsilon$ and $\tan\frac{\varepsilon}{2}$ are monotone increasing functions and the values of its differentials at $\theta_2 = 0, \frac{\pi}{2}$ are

$$\left(\frac{1}{2}\varepsilon\right)'\Big|_{\varepsilon=0,\frac{\pi}{2}} = \frac{1}{2}, \quad \begin{cases} \left(\tan\frac{\varepsilon}{2}\right)'|_{\varepsilon=0} = \frac{1}{2} \\ \lim\limits_{\varepsilon\to\frac{\pi}{2}}\left(\tan\frac{\varepsilon}{2}\right)' = \infty \end{cases},$$

there does not exist ε such that $g'(\varepsilon) = 0$ in the domain $0 < \varepsilon < \frac{\pi}{2}$. Furthermore, since $g'(\frac{\pi}{2}) = 4\left(-\frac{2}{\pi} + \frac{1}{2}\right) < 0$ from (5.33), $g(\varepsilon)$ is monotone decreasing function. Therefore, the following inequality holds from (5.32):

$$g(\varepsilon) > g\left(\frac{\pi}{2}\right) = 2.$$

It follows that(5.26) holds from (5.31). □

Eq. (5.19) of Theorem 5.1 shows that there exist two finite lines into the reachable area Ω on the plane $(\|\Delta\boldsymbol{\alpha}'_o\|, \Delta\psi)$ as illustrated in Figure 5.5. Therefore, the control variable $\tilde{\boldsymbol{\eta}}$ can converge to the target point by the finite iterative shifts along the finite two lines.

Remark 5.1. The solution of (5.19) for given $-\frac{\pi}{2} < \varepsilon < \frac{\pi}{2}$ is equal to the solution of (5.20) and (5.23) with (5.22). Since θ_1 can be easily given by (5.20) if θ_2 is given, it is only necessary to obtain the numerical solution of (5.23) with (5.22) such that

$$\frac{\varepsilon^2 - 2(\cos\theta_2 + \theta_2\sin\theta_2)\varepsilon\sin\varepsilon + 2(\cos\theta_2 + \theta_2\sin\theta_2)^2(1-\cos\varepsilon)}{\sin^2\theta_2} = \varepsilon^2. \tag{5.35}$$

Eq. (5.35) is a nonlinear function of θ_2 for which the existence of its solution is guaranteed by Theorem 5.1. Furthermore, since the difference between the both sides of (5.35) has positive and negative values at $\theta_2 = \theta_{2L}$ and $\theta_2 = \theta_{2U}$ respectively, the numerical solution of (5.35) can be easily obtained by the bisection method.

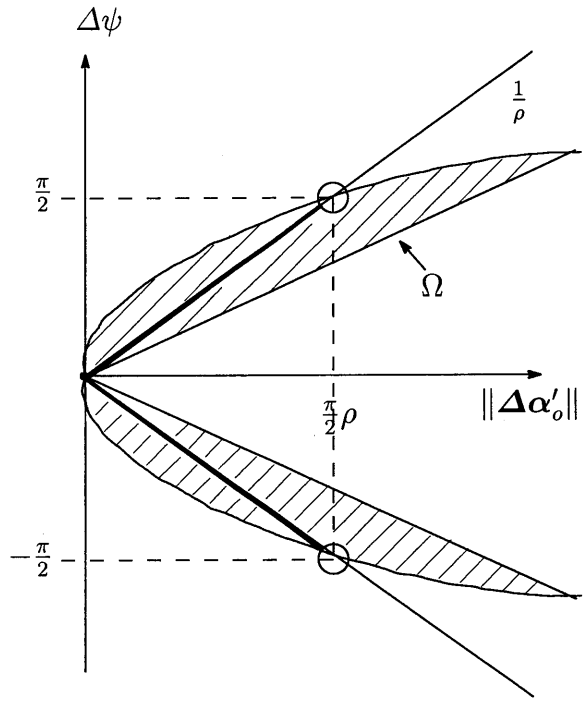

Figure 5.5 Two finite lines in the reachable area Ω.

5.3 Algorithm for Determination of Parameters

In this section, we propose a regulation algorithm for the control variable $\widetilde{\boldsymbol{\eta}}$ to converge to the origin by the finite iterative shifts along the two lines in Figure 5.5.

For discussions concerned with the method, the area surrounded with solid lines on the plane $(\|\Delta\boldsymbol{\alpha}'_o\|, \Delta\psi)$ shown in Figure 5.6 is introduced. In this chapter, we call this area Ω^2. In Figure 5.6, the negative range with respect to the $\|\Delta\boldsymbol{\alpha}'_o\|$-axis is depicted for simplicity of explanation. This negative range can be given by transforming φ of (5.13) into $\varphi + \pi$. The heavy solid lines represent the reachable area by one iteration. The oblique coordinate system (X, Y) is composed of the X-axis with the gradient $\frac{1}{\rho}$ and the Y-axis with the gradient $-\frac{1}{\rho}$. The length l is the maximum distance by one iteration, which is given by

$$l := \left(\frac{\pi}{2}\sqrt{\rho^2+1}\right)c, \quad 0 < c < 1. \tag{5.36}$$

The origin O represents the initial point of $(\|\boldsymbol{\alpha}_o\|, \psi)$ and the point A is the target point. For simplicity of description, in the following, the coordinates $\|\Delta\boldsymbol{\alpha}'_o\|$ and $\Delta\psi$ is represented by x and y respectively and the plane $(\|\Delta\boldsymbol{\alpha}'_o\|, \Delta\psi)$ is called the plane (x, y).

First, consider the case where there exists the target point A in the area Ω^2 as shown in Figure 5.6. By the two iteration: the shift from O to O' along X-axis at first time and the shift from O' to A along Y'-axis parallel to Y-axis at second time, $(\|\boldsymbol{\alpha}_o\|, \psi)$ can converge to the target point A. Therefore, the area Ω^2 represents the reachable area by two iteration of the closed paths.

Second, consider the case where the target point A is outside of the area Ω^2 as shown in Figure 5.7. In Figure 5.7, the distance between dashed lines of the oblique coordinate system

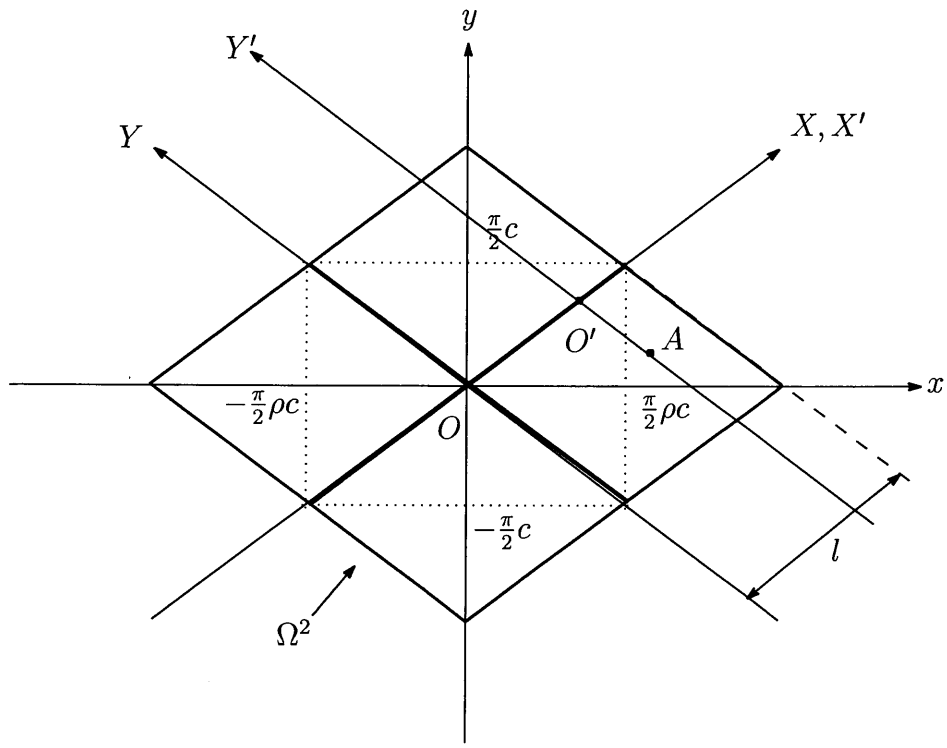

Figure 5.6 Reachable area Ω^2 by the iteration of two closed paths.

(X, Y) are normalized by l. The origin O of (x, y) represents the initial point and the point A is the target point which is the origin of the plane $(\|\boldsymbol{\alpha}_o\|, \psi)$. The method for the control variable to converge to the target point is composed of the following two sections:

(i) To involve the target point A in the reachable area Ω^2 by the iteration of shifts between intersection points of dashed lines. The number of the iterations is finite since each shift has the finite length l.

(ii) To converge the control variable on the target point A by two iteration as mentioned previous paragraph. Then, the number of the iterations N is given by

$$N = \text{int}(|X[0]|) + \text{int}(|Y[0]|) + 2, \tag{5.37}$$

where $(X[0], Y[0])$ is the coordinate of the target point A represented in the oblique coordinate system (X, Y) and $\text{int}(\cdot)$ represents integral parts of its arguments. The term $\text{int}(|X[0]|) + \text{int}(|Y[0]|)$ in the right hand of (5.37) is the minimum number for the target point A to be involved in the reachable area Ω^2 since $P(\text{int}(|X[0]|), \text{int}(|Y[0]|))$ is the nearest point from the initial point O among the corners of the area surrounded by dashed lines which involves the target point A.

Summarizing the discussion in the previous section, we show the algorithm to determine the parameters $(\theta_1, \theta_2, \varphi)$ in the following. The variable k is the number of the iterations of the closed paths and $(x[k], y[k])$ is the target point represented in the orthogonal coordinate system (x, y) at kth interation.

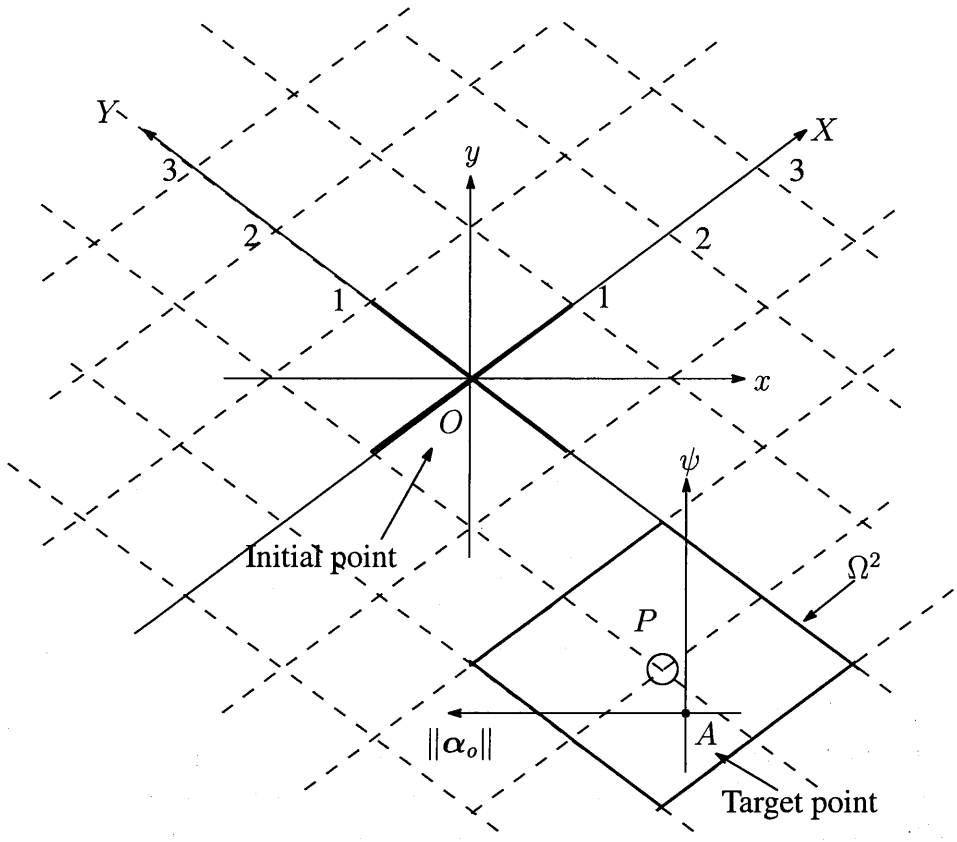

Figure 5.7 Scheme for the initial point to converge to the target point.

Algorithm for Determination of Parameters of the Closed Path

1) To transform the target point $(x[k], y[k])$ to the target point $(X[k], Y[k])$ on the oblique coordinate system (X, Y) as follows:

$$\begin{bmatrix} X[k] \\ Y[k] \end{bmatrix} = \boldsymbol{T} \begin{bmatrix} x[k] \\ y[k] \end{bmatrix}, \quad \boldsymbol{T} := \frac{1}{\pi} \begin{bmatrix} \frac{1}{\rho} & 1 \\ -\frac{1}{\rho} & 1 \end{bmatrix}. \tag{5.38}$$

2) With the target point $(X[k], Y[k])$, to calculate the target point at kth interation $(X_d[k], Y_d[k])$ by the following equation:

$$\begin{bmatrix} X_d[k] \\ Y_d[k] \end{bmatrix} = \begin{cases} \begin{bmatrix} \operatorname{sgn}(X[k]) \min(c, |X[k]|) \\ 0 \end{bmatrix} & (|X[k]| \geq |Y[k]|) \\ \begin{bmatrix} 0 \\ \operatorname{sgn}(Y[k]) \min(c, |Y[k]|) \end{bmatrix} & (|X[k]| < |Y[k]|) \end{cases} \tag{5.39}$$

3) To transform the target point $(X_d[k], Y_d[k])$ to the target point $(x_d[k], y_d[k])$ on the orthogonal system (x, y). Furthermore, with the obtained target point $(x_d[k], y_d[k])$, to determine the kth

parameters $\theta_1[k]$ and $\theta_2[k]$ by solving the following equations:

$$\theta_1[k] = -\frac{y_d[k]}{\sin(\theta_2[k])}, \tag{5.40}$$

$$\frac{\left\{\begin{array}{r} y_d[k]^2 - 2(\cos\theta_2[k] + \theta_2[k]\sin\theta_2[k])y_d[k]\sin y_d[k] \\ +2(\cos\theta_2[k] + \theta_2[k]\sin\theta_2[k])^2(1-\cos y_d[k]) \end{array}\right\}}{\sin^2\theta_2[k]} = x_d[k]^2, \tag{5.41}$$

where

$$\begin{bmatrix} x_d[k] \\ y_d[k] \end{bmatrix} := \boldsymbol{T}^{-1}\begin{bmatrix} X_d[k] \\ Y_d[k] \end{bmatrix}. \tag{5.42}$$

4) To determine $\varphi[k]$ by solving the following equation with the obtained parameters $(\theta_1[k], \theta_2[k])$:

$$\boldsymbol{R}_\varphi(\varphi[k])\frac{\boldsymbol{\Delta\alpha}_o'(\theta_1[k],\theta_2[k])}{\|\boldsymbol{\Delta\alpha}_o'(\theta_1[k],\theta_2[k])\|} = -\frac{\boldsymbol{\alpha}_o[k]}{\|\boldsymbol{\alpha}_o[k]\|}. \tag{5.43}$$

In the step 2), (5.39) chooses the direction of the X-axis or the Y-axis such that the control variable approximates to the target point. When the target point is outside of Ω^2, the terms $\mathrm{sgn}(X_d[k])\min(c, |X_d[k]|)$ and $\mathrm{sgn}(Y_d[k])\min(c, |Y_d[k]|)$ select the shift with the length c. On the other hand, when the target point is inside of Ω^2, the terms select the shift with the length $|X_d[k]|$ or $|Y_d[k]|$ for the control variable at kth iteration to converge to the target point by two interation as in Figure 5.6. Eqs. (5.40), (5.41) and (5.43) correspond to (6.15), (5.35) and (5.13) respectively. These equations except (5.41) can be solved analytically. As for (5.41), the numerical solution can be easily calculated by the bisection method as mentioned in Remark 5.1.

Remark 5.2. Note that the parameters $\theta_1[k]$, $\theta_2[k]$ and $\varphi[k]$ can be obtained only from $\widetilde{\boldsymbol{\eta}}[k]$ which is the sates at the start time of kth number of iterations. Therefore, the method can be interpreted as a discrete-time feedback by regarding the start time of the iteration as the sampling instant. Therefore, the method is expected to have robustness against disturbances.

5.4 Numerical Example

In this section, the effectiveness of the algorithm proposed in the previous section is evaluated by a numerical example. The radius of the sphere is $\rho = 1$[m]. The initial states are $\boldsymbol{\alpha}_f = [\,0\ \ 0\,]^{\mathrm{T}}$[rad] and $\boldsymbol{\alpha}_o = [\,3\ \ 3.5\,]^{\mathrm{T}}$[m], $\psi = \frac{\pi}{2}$[rad]. The maximum length of the shift by the closed path on the plane $(\|\boldsymbol{\Delta\alpha}_o'\|, \Delta\psi)$ is $c = 0.7$. In this case, the number of the iterations of the closed paths for the control variable to converge is $N = 5$ from (5.37).

Figures 5.8 and 5.9 show the simulation result. Figure 5.8 shows the shifts of $\boldsymbol{\alpha}_o$ on the plane $\boldsymbol{\alpha}_o$, where the kth circle represents the position of $\boldsymbol{\alpha}_o[k]$ and the kth arrow represent the angle of $\psi[k]$. Figure 5.9 shows the shifts on the plane (x, y) i.e. $(\|\boldsymbol{\Delta\alpha}_o'\|, \Delta\psi)$, where the kth circle represents the position $(\|\boldsymbol{\Delta\alpha}_o'[k]\|, \Delta\psi[k])$ by the kth closed path, the oblique lines represent

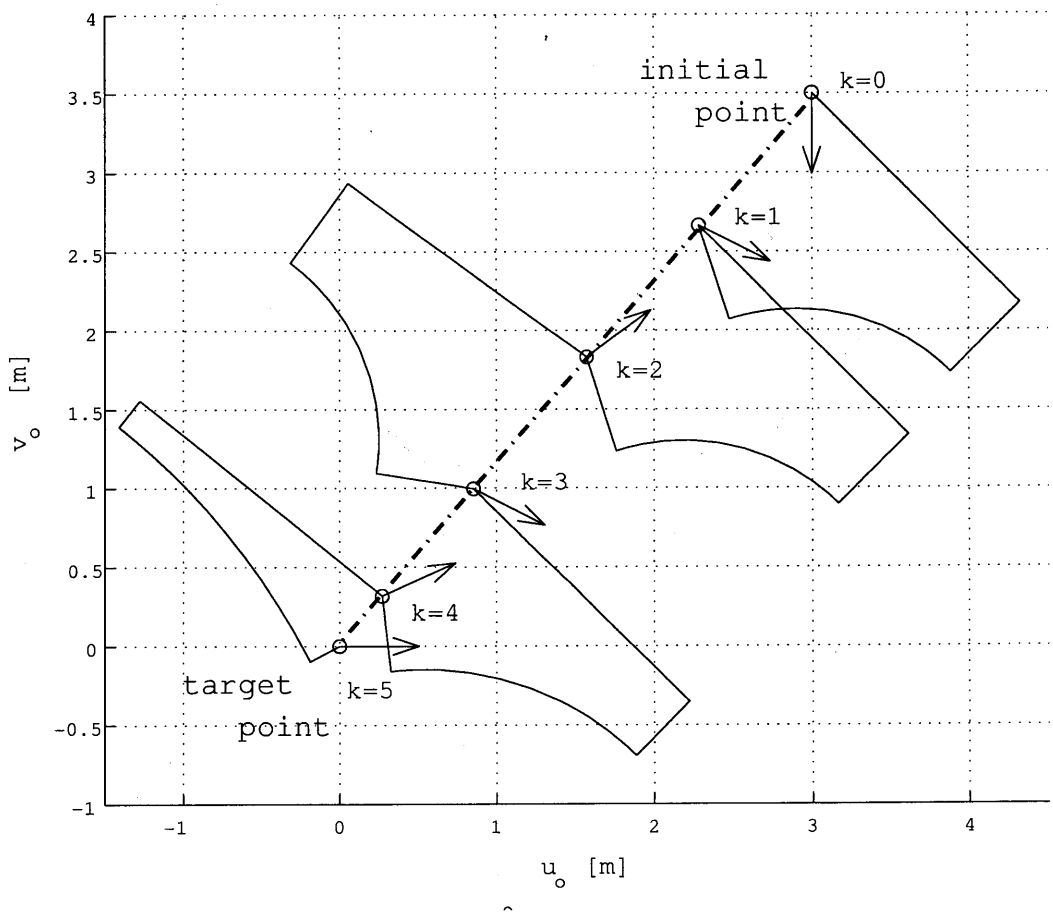

Figure 5.8 Shifts of $\boldsymbol{\alpha}_o$ and ψ on $\boldsymbol{\alpha}_o$ plane.

the oblique coordinate system (X, Y) and the area surrounded by the heavy solid lines is the reachable area Ω^2. In Figure 5.8, $\boldsymbol{\alpha}_o$ and ψ have converged on the target point simultaneously by five number of the iterations. Furthermore, there exist the circles o on the dash dotted line from the initial point to the target point. This corresponds to the fact that the direction of the shift of $\boldsymbol{\alpha}_o$ is determined by φ satisfying (5.13) (See Figure 5.3). In Figure 5.9, the distances of the shifts of $k = 1, 2, 3$ are maximum length and the target point is involved into the reachable area Ω^2 at 3rd point. Next, those of $k = 4, 5$ are adjusted for the control variable to converge to the target point. These transitions show the effectiveness of the algorithm.

5.5 Summary

In this chapter, for the kinematic model of a sphere and a plane with rolling contact, we proposed the regulation algorithm for the contact coordinates to converge to a target point by the finite iterative trapezoidal closed paths of the contact point on the sphere. First, we showed that, from the viewpoint of the norm minimization, one of the parameters could be determined independent of the other two parameters. Due to this determination, the control problem was discussed on the

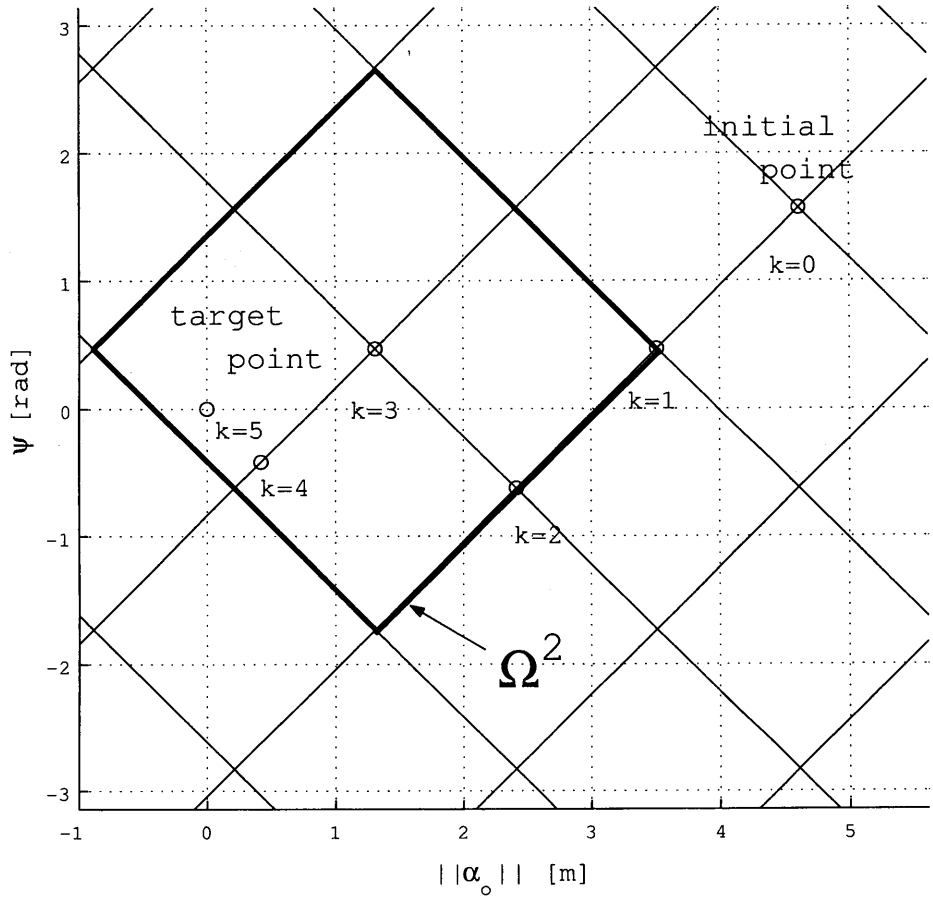

Figure 5.9 Shift of $(\|\boldsymbol{\alpha}_o\|, \psi)$ on $(\|\boldsymbol{\Delta\alpha}'_o\|, \Delta\psi)$ plane.

two-dimensional space (plane) which characterizes the contact coordinates. Second, we proved that the reachable area of the closed path had two finite lines crossing at the origin which represented the contact coordinates at each iteration. Third, we proposed the method for the contact coordinates to converge to a target point by the finite iterative shifts along the lines as mentioned earlier.

Chapter 6

Control of a Sphere Rolling on a Plane with Constrained Rolling Motion

In Chapter 5, for the nonholonomic system composed of a sphere and a plane with pure rolling contact, we proposed the regulation algorithm for the contact coordinates to converge by the finite iterative trapezoidal closed paths on the sphere. In this method, It was utilized that there existed the two finite lines in the reachable area of the closed path. However, since the lines is just parts of the reachable area, the method is somewhat conservative. Furthermore, since in the control problem of Chapters 3 and 5 the rolling motion is not constrained, it is difficult to apply these methods to control of contact points by multi-fingered robot hands.

In this chapter, we discuss the control of the contact coordinates by the iterative trapezoidal closed paths on the sphere with constrained rolling motion [58, 59]. In Section 6.1, the control problem is summarized briefly. It is assumed that the parameter of the direction of the closed path is determined from the viewpoint of the norm minimization shown in Chapter 5. Due to this determination, the control problem can be discussed on the two-dimensional space (plane) which characterizes the contact coordinates. In Section 6.2, in order to utilize the reachable area of the closed path at the maximum, we analyze the boundary of the reachable area of the closed path with constrained rolling motion in detail. In Section 6.3, we propose a method for the contact coordinates to converge to a target point by the finite iterative shifts along the boundary as mentioned earlier. Since the proposed method can impose the limitation of the rolling motion, the method has the beneficial effect on the application to multi-fingered robot hands. Furthermore, similar to Chapter 5, the parameters at each iteration can be easily calculated by the bisection method. In Section 6.4, a numerical example where the rolling motion is restricted to the area on the semisphere shows the effectiveness of the proposed method.

6.1 Control Problem

In this section, we describe the control problem in which the constrained rolling motion is considered. For the readability of this chapter, system configuration and the closed path shown in Chapter 5 are summarized briefly.

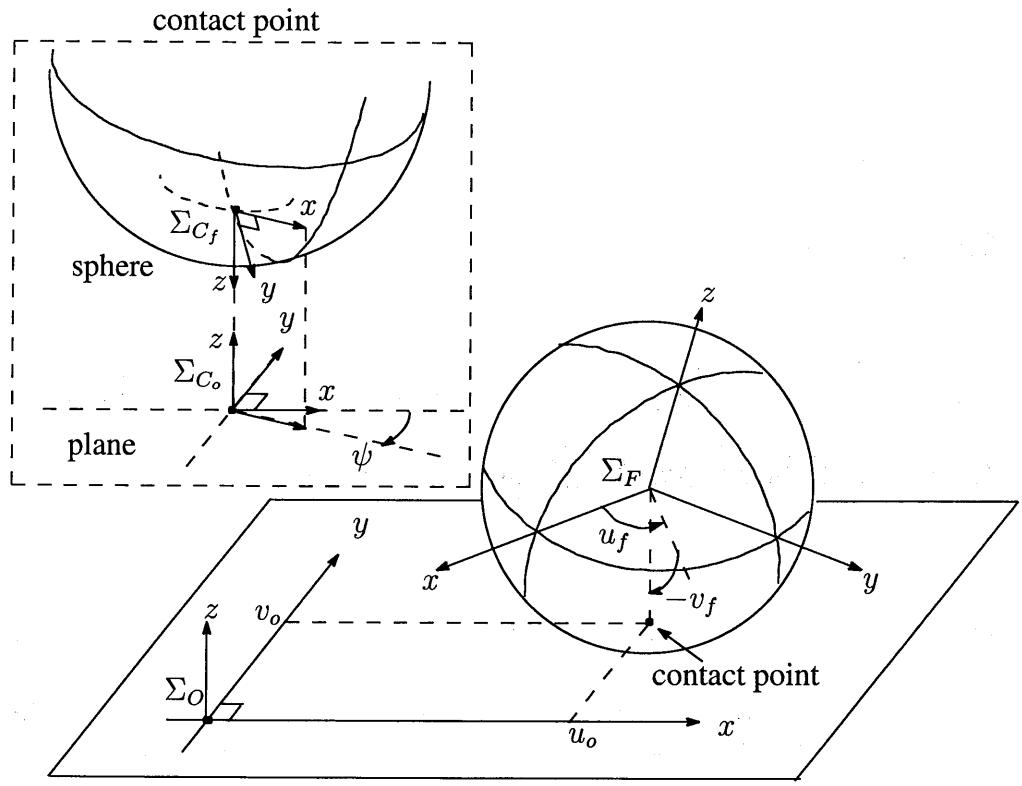

Figure 6.1 A sphere rolling on a plane

Figure 6.1 shows a spherical finger rolling on a plane of a object by fingers. The configuration of the system is expressed by the contact coordinates:

$$\eta := [\, \alpha_f^{\mathrm{T}} \;\; \alpha_o^{\mathrm{T}} \;\; \psi \,]^{\mathrm{T}} \in \mathbb{R}^5, \tag{6.1}$$

where $\alpha_f \in \mathbb{R}^2$, $\alpha_o \in \mathbb{R}^2$ and $\psi \in \mathbb{R}$ are and the spherical coordinates, the orthogonal coordinates and the angle between x- axes of Σ_{C_f} and Σ_{C_o} as in Figure 6.1 respectively. The system with the pure rolling contact is as follows [6, 17]:

$$\begin{bmatrix} \dot{\alpha}_f \\ \dot{\alpha}_o \\ \dot{\psi} \end{bmatrix} = \begin{bmatrix} 1 & 0 \\ 0 & 1 \\ \rho \cos v_f \cos\psi & -\rho \sin\psi \\ -\rho \cos v_f \sin\psi & -\rho \cos\psi \\ \sin v_f & 0 \end{bmatrix} \dot{\alpha}_f, \tag{6.2}$$

where ρ is the radius of the sphere. This is the kinematic model where $\dot{\alpha}_f$ is the input. For simplicity, the target point is assumed to the origin of η and $\dot{\alpha}_f$ is assumed to be able to controlled directly. Hence, the initial state of the contact point on the sphere α_f is assumed to be the origin. Consequently, the control problem is the regulation of the others of the contact coordinates

$$\tilde{\eta} := [\, \alpha_o^{\mathrm{T}} \;\; \psi \,]^{\mathrm{T}} \in \mathbb{R}^3 \tag{6.3}$$

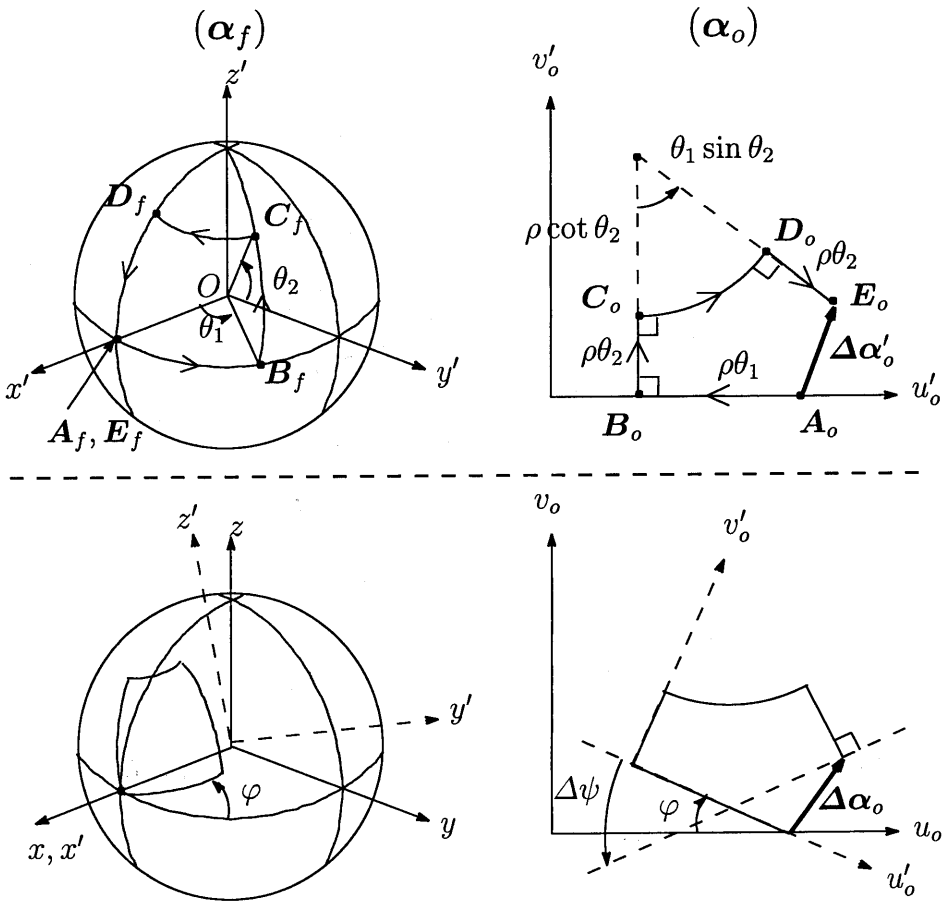

Figure 6.2 The proposed closed path on the sphere.

to the origin by the iterative closed paths on the sphere. In the following, $\widetilde{\boldsymbol{\eta}}$ is called the control variable.

The trapezoidal closed path on the sphere for the regulation is shown in Figure 6.2. In Figure 6.2, the left hand side shows the closed path and the right hand side shows incremental distances $\boldsymbol{\alpha}_o$ and ψ, i.e., $\boldsymbol{\Delta\alpha}_o$ and $\Delta\psi$. Define the incremental distance of $\widetilde{\boldsymbol{\eta}}$ by

$$\boldsymbol{\Delta}\widetilde{\boldsymbol{\eta}} := [\ \boldsymbol{\Delta\alpha}_o^{\mathrm{T}}\ \ \Delta\psi\ ]^{\mathrm{T}} \in \mathbb{R}^3. \tag{6.4}$$

By integrating (6.2) along the closed path, the components of $\boldsymbol{\Delta}\widetilde{\boldsymbol{\eta}}$ are given by

$$\boldsymbol{\Delta\alpha}_o(\theta_1, \theta_2, \varphi) = \boldsymbol{R}_\varphi(\varphi)\boldsymbol{\Delta\alpha}'_o(\theta_1, \theta_2) \tag{6.5}$$

$$\Delta\psi(\theta_1, \theta_2) = -\theta_1 \sin\theta_2, \tag{6.6}$$

where

$$\boldsymbol{R}_\varphi := \begin{bmatrix} \cos\varphi & \sin\varphi \\ -\sin\varphi & \cos\varphi \end{bmatrix} \tag{6.7}$$

$$\boldsymbol{\Delta\alpha}'_o = \begin{bmatrix} -\rho\theta_1 + \rho(\cot\theta_2 + \theta_2)\sin(\theta_1 \sin\theta_2) \\ \rho(\cot\theta_2 + \theta_2)(1 - \cos(\theta_1 \sin\theta_2)) \end{bmatrix}. \tag{6.8}$$

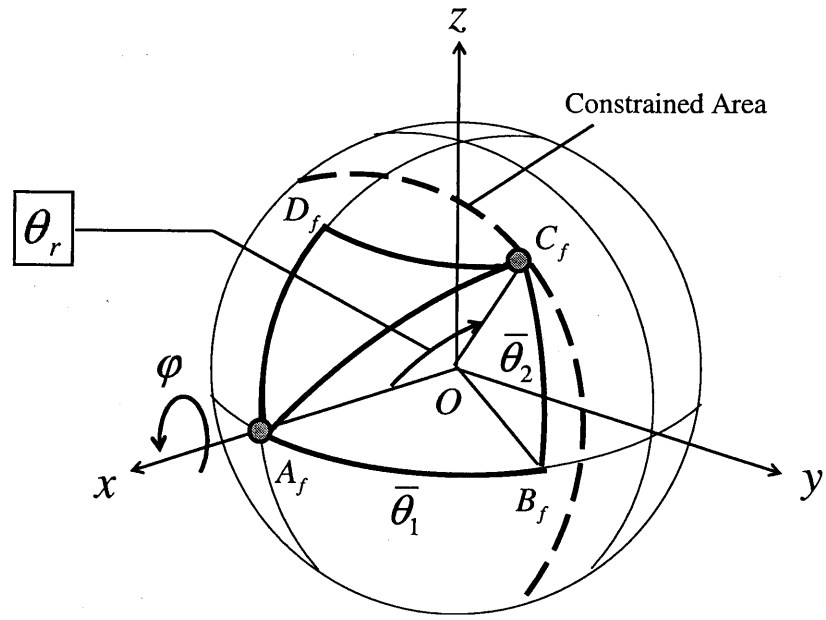

Figure 6.3 Constrained area on the surface of the sphere.

In this chapter, the constrained rolling motion is considered. Therefore, the range of θ_1, θ_2 and φ are defined by

$$|\theta_1| \leq \bar{\theta}_1, \ |\theta_2| \leq \bar{\theta}_2, \ |\varphi| \leq \pi, \tag{6.9}$$

where

$$0 < \bar{\theta}_1 < \pi, \ 0 < \bar{\theta}_2 < \frac{\pi}{2}. \tag{6.10}$$

Note that the start direction of the closed path φ is not constrained. This means that the rolling motion can be generated in arbitrary directions at the start position of the closed path A_f. This assumption holds from the study results of Chapter 4.

Remark 6.1. In order to apply the method proposed in this chapter to control of contact points by multi-fingered robot hands, it is necessary to obtain the area on the sphere by the constrained rolling motion. When the parameters are constrained as in (6.9) and (6.10), the constrained area on the sphere is shown in Figure 6.3. In Figure 6.3, the constrained area on the sphere is shown as the circled area surrounded by the dashed line, which is depicted by rotating the point C_f through 2π about x- axis. This circled area is characterized by the angle $\theta_r := \angle A_f O C_f$. It follows that the boundaries of $\boldsymbol{\alpha}_f := [\ u_f \ \ v_f\ ]^{\mathrm{T}}$ are

$$|u_f| \leq \theta_r, \ |v_f| \leq \theta_r, \tag{6.11}$$

where

$$\theta_r = \cos^{-1}(\cos\bar{\theta}_1 \cos\bar{\theta}_2). \tag{6.12}$$

This θ_r is given by applying Law of cosines to the triangle $\triangle A_f O C_f$.

In the following sections, we propose a regulation algorithm for $\tilde{\boldsymbol{\eta}}$ to converge to the origin by finite iterative closed paths with constrained rolling motion. As similar ways in Chapter 5, the fundamental idea is composed of the following items:

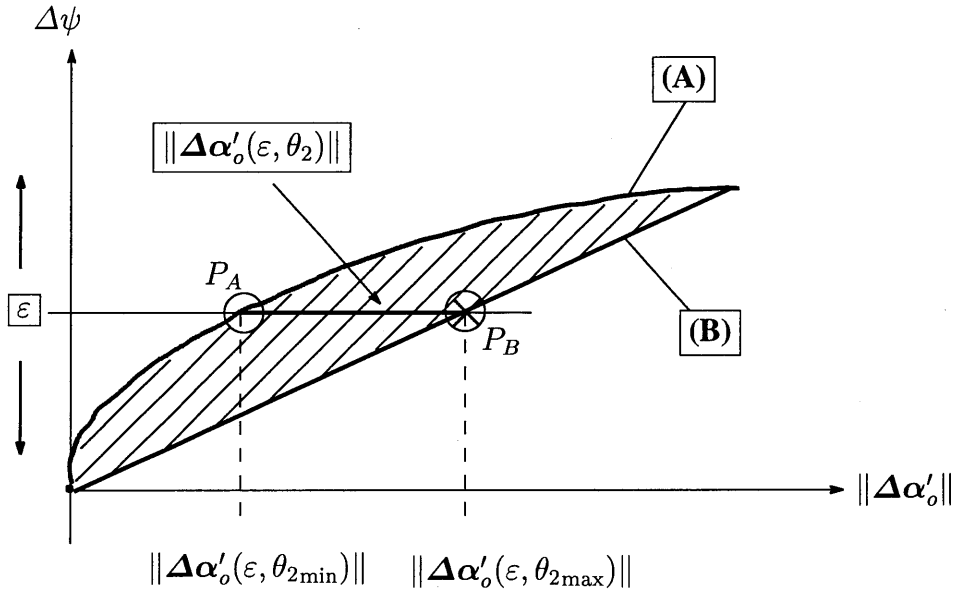

Figure 6.4 Concept of estimation of the reachable area on the plane $(\|\Delta\boldsymbol{\alpha}'_o\|, \Delta\psi)$.

(1) To determine the parameter φ such that Lemma 5.1 as Figure 5.3 in Chapter 5. Due to this determination, the control problem can be discussed on the two-dimensional space (plane) which characterizes the contact coordinates. To be more precise, as in Figure 5.4, the control problem is to converge the control variable $(\|\boldsymbol{\alpha}_o\|, \psi)$ on the origin by iterative shifts on the reachable area Ω represented on the plane $(\|\Delta\boldsymbol{\alpha}'_o\|, \Delta\psi)$.

(2) To estimate the boundary of the reachable area Ω. The transformation from θ_1 to ε is utilized as in Chapter 5.

(3) To propose the method for $(\|\boldsymbol{\alpha}_o\|, \psi)$ to converge to the origin by the finite iterative shifts along the boundary. The parameters at each iteration can be calculated by the bisection method .

Since the item **(1)** is the same as Chapter 5, the description of this item is omitted. See Section 5.2 for the details of the terms **(1)**. The details of the terms **(2)** and **(3)** are shown in Sections 6.2 and 6.3 respectively.

6.2 Evaluation of Boundary of Reachable Area

In this section, we evaluate the boundary of the reachable area of the closed path. For the estimation, the fundamental properties of the reachable area as mentioned in Section 5.2 are used. See Section 5.2 for the details of the properties.

The idea of this section is summarized briefly by Figure 6.4. In Figure 6.4, the shaded area is the reachable area Ω on the plane $(\|\Delta\boldsymbol{\alpha}'_o\|, \Delta\psi)$, where the part such that $\Delta\psi \geq 0$ of Ω is depicted because the reachable area is symmetry with respect to $\|\Delta\boldsymbol{\alpha}'_o\|$- axis from Lemma 5.2. The boundary of the reachable area is composed of the boundaries **(A)** and **(B)**, which is represented by the heavy lines **(A)** and **(B)** as in Figure 6.4. The line parallel to $\|\Delta\boldsymbol{\alpha}'_o\|$- axis represents the line by $\Delta\psi(\theta_1, \theta_2) = \varepsilon$ and the segment depicted by the heavy line represents the product

set of $\Delta\psi(\theta_1, \theta_2) = \varepsilon$ and the reachable area Ω, i.e. $\|\Delta\boldsymbol{\alpha}'_o(\varepsilon, \theta_2)\|$ as mentioned in Section 5.2. Then, the points on the boundary **(A)** corresponds to the points $P_A(\|\Delta\boldsymbol{\alpha}'_o\|, \varepsilon)$ when $\|\Delta\boldsymbol{\alpha}'_o\|$ is minimum and the points on the boundary **(B)** corresponds to the points $P_B(\|\Delta\boldsymbol{\alpha}'_o\|, \varepsilon)$ when $\|\Delta\boldsymbol{\alpha}'_o\|$ is maximum. Therefore, in the following, we investigate the minimum and maximum of $\|\Delta\boldsymbol{\alpha}'_o(\varepsilon, \theta_2)\|$.

For the preliminary of the estimation, from (6.6) and (6.9), the variable θ_1 of $\|\Delta\boldsymbol{\alpha}'_o(\theta_1, \theta_2)\|$ is transformed to ε by the condition

$$\Delta\psi(\theta_1, \theta_2) = -\theta_1 \sin\theta_2 = \varepsilon, \tag{6.13}$$

where

$$|\varepsilon| \leq \bar{\varepsilon}, \quad \bar{\varepsilon} := \bar{\theta}_1 \sin\bar{\theta}_2. \tag{6.14}$$

The condition (6.13) is transformed to

$$\theta_1 = -\frac{\varepsilon}{\sin\theta_2}. \tag{6.15}$$

Substituting (6.15) into the domain (6.9) and solving the resultant inequality with respect to θ_2 lead to the range of θ_2 to guarantee the transformation from θ_1 to ε:

$$-\bar{\theta}_2 \leq \theta_2 \leq \sin^{-1}\left(-\frac{|\varepsilon|}{\bar{\theta}_1}\right) \quad \text{or} \quad \sin^{-1}\left(\frac{|\varepsilon|}{\bar{\theta}_1}\right) \leq \theta_2 \leq \bar{\theta}_2. \tag{6.16}$$

By substituting (6.15) into $\|\Delta\boldsymbol{\alpha}'_o(\theta_1, \theta_2)\|^2$ of (6.8), $\|\Delta\boldsymbol{\alpha}'_o\|^2$ is transformed to the following function of θ_2 and ε:

$$\|\Delta\boldsymbol{\alpha}'_o(\varepsilon, \theta_2)\|^2 = \rho^2 \frac{\varepsilon^2 - 2\Theta(\theta_2)\varepsilon\sin\varepsilon + 2\Theta(\theta_2)^2(1-\cos\varepsilon)}{\sin^2\theta_2}, \tag{6.17}$$

where

$$\Theta(\theta_2) := \cos\theta_2 + \theta_2 \sin\theta_2. \tag{6.18}$$

Note that $\|\Delta\boldsymbol{\alpha}'_o(-\frac{\varepsilon}{\sin\theta_2}, \theta_2)\|$ $(= \|\Delta\boldsymbol{\alpha}'_o(\theta_1, \theta_2)\|)$ is rewritten as $\|\Delta\boldsymbol{\alpha}'_o(\varepsilon, \theta_2)\|$ for simple description. The function (6.17) is continuous with respect to ε and θ_2 since ε $(= -\theta_1 \sin\theta_2)$ is continuous with respect to θ_1 and θ_2 and $\Delta\boldsymbol{\alpha}'_o(\theta_1, \theta_2)$ is continuous with respect to θ_1 and θ_2 from Lemma 3.3 (i). Since $\|\Delta\boldsymbol{\alpha}'_o\|$ is symmetry with respect to the ε $(= \Delta\psi)$-axis from Lemma 5.2 and $\|\Delta\boldsymbol{\alpha}'_o(\varepsilon, \theta_2)\| = \|\Delta\boldsymbol{\alpha}'_o(\varepsilon, -\theta_2)\|$ holds from (6.17), only the case such that $\varepsilon > 0$ and $\theta_2 > 0$ is considered in the following.

Consider investigating the property of $\|\Delta\boldsymbol{\alpha}'_o(\varepsilon, \theta_2)\|$ with respect to θ_2 in the ranges $0 < \theta_2 < \frac{\pi}{2}$ and $0 < \varepsilon < \pi$ from (6.9) and (6.14). Then the following theorem holds.

Theorem 6.1. *Suppose that $\|\Delta\boldsymbol{\alpha}'_o(\varepsilon, \theta_2)\|^2$ is the function of θ_2, ε is the parameter of the function and the ranges of θ_2 and ε are $0 < \theta_2 < \frac{\pi}{2}$, $0 < \varepsilon < \pi$. Then, the following properties hold.*

(i) *$\varepsilon < \frac{\pi}{2}$: The function has only a minimum value with respect to θ_2.*
(ii) *$\varepsilon \geq \frac{\pi}{2}$: The function is a monotone decreasing function with respect to θ_2.*

Proof. Partial differentiation of (6.17) with respect to θ_2 is given by

$$\frac{\partial}{\partial\theta_2}\|\Delta\boldsymbol{\alpha}_o'(\varepsilon,\theta_2)\|^2 = 2\rho^2\frac{\begin{array}{l}\{-\theta_2\cos\theta_2\varepsilon\sin\varepsilon + 2\theta_2\cos\theta_2\Theta(1-\cos\varepsilon)\}\sin\theta_2 \\ \quad -\cos\theta_2\{\varepsilon^2 - 2\Theta\varepsilon\sin\varepsilon + 2\Theta^2(1-\cos\varepsilon)\}\end{array}}{\sin^3\theta_2}$$

$$= \frac{2\rho^2\cos\theta_2}{\sin^3\theta_2}f(\varepsilon,\theta_2), \tag{6.19}$$

where

$$f(\varepsilon,\theta_2) := \varepsilon\sin\varepsilon\Theta_1(\theta_2) - 2(1-\cos\varepsilon)\Theta_2(\theta_2) - \varepsilon^2, \tag{6.20}$$

$$\begin{cases}\Theta_1(\theta_2) := 2\cos\theta_2 + \theta_2\sin\theta_2 \\ \Theta_2(\theta_2) := \cos\theta_2(\cos\theta_2 + \theta_2\sin\theta_2)\end{cases}. \tag{6.21}$$

Since $\cos\theta_2/\sin^3\theta_2 > 0$ from $\theta_2 > 0$, the sign of (6.19) is determined by $f(\varepsilon,\theta_2)$. In order to analyze (6.20), Eq. (6.20) is transformed to

$$f(\varepsilon,\theta_2) = \varepsilon^2\left[\frac{\sin\varepsilon}{\varepsilon}\left\{\Theta_1 - \left(\frac{\tan\frac{\varepsilon}{2}}{\frac{\varepsilon}{2}}\right)\Theta_2\right\} - 1\right], \tag{6.22}$$

where the following transformation given by the formulas for the double and half angle is utilized:

$$2\frac{1-\cos\varepsilon}{\varepsilon\sin\varepsilon} = 2\frac{2\sin^2\frac{\varepsilon}{2}}{\varepsilon\times 2\sin\frac{\varepsilon}{2}\cos\frac{\varepsilon}{2}} = \frac{\tan\frac{\varepsilon}{2}}{\frac{\varepsilon}{2}}.$$

Partial differentiation of (6.22) with respect to θ_2 is given by

$$\frac{\partial}{\partial\theta_2}f(\varepsilon,\theta_2) = \varepsilon\sin\varepsilon\left\{\Theta_1' - \left(\frac{\tan\frac{\varepsilon}{2}}{\frac{\varepsilon}{2}}\right)\Theta_2'\right\} = \varepsilon\sin\varepsilon\Theta_1'\left\{1 - \left(\frac{\tan\frac{\varepsilon}{2}}{\frac{\varepsilon}{2}}\right)\frac{\Theta_2'}{\Theta_1'}\right\}. \tag{6.23}$$

In the following, in order to investigate the sign of (6.23), the terms in the right hands of (6.23) and (6.22) are investigated.

(i) $\frac{\sin\varepsilon}{\varepsilon}$:

The differential of $\frac{\sin\varepsilon}{\varepsilon}$ is given by

$$\left(\frac{\sin\varepsilon}{\varepsilon}\right)' = \frac{\varepsilon\cos\varepsilon - \sin\varepsilon}{\varepsilon^2}.$$

The above equation is evidently negative in the case $\frac{\pi}{2} \le \varepsilon < \pi$. In the case $0 < \varepsilon < \frac{\pi}{2}$, since the differentials of ε and $\tan\varepsilon$ at $\theta_2 = 0, \frac{\pi}{2}$ are

$$\varepsilon'|_{\varepsilon=0,\frac{\pi}{2}} = 1, \quad \begin{cases}\lim\limits_{\varepsilon\downarrow 0}(\tan\varepsilon)' = 1 \\ \lim\limits_{\varepsilon\uparrow\frac{\pi}{2}}(\tan\varepsilon)' = \infty\end{cases},$$

the following inequality is holds:

$$\left(\frac{\sin\varepsilon}{\varepsilon}\right)' = \frac{\varepsilon\cos\varepsilon - \sin\varepsilon}{\varepsilon^2} = \frac{\cos\varepsilon}{\varepsilon^2}(\varepsilon - \tan\varepsilon) < 0.$$

Therefore, $\frac{\sin\varepsilon}{\varepsilon}$ is a monotone decreasing function. From $\lim_{\varepsilon\downarrow 0}\frac{\sin\varepsilon}{\varepsilon} = 1$, it follows that the following equation holds:

$$0 < \frac{\sin\varepsilon}{\varepsilon} < 1. \tag{6.24}$$

(ii) $\frac{\tan\frac{\varepsilon}{2}}{\frac{\varepsilon}{2}}$:

From (6.24), since the differential of $\frac{\tan\frac{\varepsilon}{2}}{\frac{\varepsilon}{2}}$ is given by

$$\left(\frac{\tan\frac{\varepsilon}{2}}{\frac{\varepsilon}{2}}\right)' = \frac{\frac{1}{2}\frac{1}{\cos^2\frac{\varepsilon}{2}}\frac{\varepsilon}{2} - \frac{1}{2}\tan\frac{\varepsilon}{2}}{\frac{\varepsilon^2}{4}} = \frac{\varepsilon - 2\sin\frac{\varepsilon}{2}\cos\frac{\varepsilon}{2}}{\varepsilon^2\cos^2\frac{\varepsilon}{2}} = \frac{1-\frac{\sin\varepsilon}{\varepsilon}}{\varepsilon\cos^2\frac{\varepsilon}{2}} > 0,$$

the term $\frac{\tan\frac{\varepsilon}{2}}{\frac{\varepsilon}{2}}$ is a monotone increasing function. On the other hand, the infimum of $\frac{\tan\frac{\varepsilon}{2}}{\frac{\varepsilon}{2}}$ is given by

$$\lim_{\varepsilon\downarrow 0}\frac{\tan\frac{\varepsilon}{2}}{\frac{\varepsilon}{2}} = \lim_{\varepsilon\downarrow 0}\frac{\frac{1}{2}\frac{1}{\cos^2\frac{\varepsilon}{2}}}{\frac{1}{2}} = 1.$$

Therefore, the following equation holds:

$$\frac{\tan\frac{\varepsilon}{2}}{\frac{\varepsilon}{2}} > 1. \tag{6.25}$$

(iii) Θ_1', Θ_2' :

From (6.21), the differentials of Θ_1 and Θ_2 are given by

$$\Theta_1' = \theta_2\cos\theta_2 - \sin\theta_2, \tag{6.26}$$

$$\begin{aligned}\Theta_2' &= -\sin\theta_2(\cos\theta_2 + \theta_2\sin\theta_2) + \theta_2\cos^2\theta_2 \\ &= -\sin\theta_2\cos\theta_2 + \theta_2(\cos^2\theta_2 - \sin^2\theta_2) \\ &= \frac{1}{2}(2\theta_2\cos 2\theta_2 - \sin 2\theta_2).\end{aligned} \tag{6.27}$$

By using the following equation

$$g(x) := x\cos x - \sin x, \quad 0 < x < \pi, \tag{6.28}$$

Eqs. (6.26) and (6.27) are represented by

$$\Theta_1' = g(\theta_2), \quad \Theta_2' = \frac{1}{2}g(2\theta_2). \tag{6.29}$$

Since the property of $g(x)$ is

$$g'(x) = -x\sin x < 0, \quad \lim_{x\downarrow 0} g(x) = 0, \tag{6.30}$$

the inequality $g(x) < 0$ holds. Therefore, the following inequalities hold:

$$\Theta_1' < 0, \quad \Theta_2' < 0. \tag{6.31}$$

(iv) $\frac{\Theta_2'}{\Theta_1'}$:

From (6.29) and (6.30), the differential of $\frac{\Theta_2'}{\Theta_1'}$ is given by

$$\left(\frac{\Theta_2'}{\Theta_1'}\right)' = \frac{1}{2}\left\{\frac{g(2\theta_2)}{g(\theta_2)}\right\}' = \frac{2\{g(2\theta_2)\}'g(\theta_2) - g(2\theta_2)g'(\theta_2)}{2\{g(\theta_2)\}^2}$$
$$= \frac{-8\theta_2 \sin\theta_2 \cos\theta_2 g(\theta_2) + g(2\theta_2)\theta_2 \sin\theta_2}{2\{g(\theta_2)\}^2}$$
$$= \frac{\theta_2 \sin\theta_2}{2\{g(\theta_2)\}^2} h(\theta_2), \tag{6.32}$$

where

$$h(\theta_2) := -8\cos\theta_2 g(\theta_2) + g(2\theta_2). \tag{6.33}$$

From (6.30), the differential of $h(\theta_2)$ is given by

$$\begin{aligned} h'(\theta_2) &= 8\sin\theta_2 g(\theta_2) - 8\cos\theta_2 g'(\theta_2) + \{g(2\theta_2)\}' \\ &= 8\sin\theta_2 g(\theta_2) + 8\theta_2 \sin\theta_2 \cos\theta_2 - 4\theta_2 \sin 2\theta_2 \\ &= 8\sin\theta_2 g(\theta_2) < 0. \end{aligned}$$

Therefore, since $\lim_{\theta_2 \downarrow 0} h(\theta_2) = 0$ from (6.33), the inequality $h(\theta_2) < 0$ holds. From (6.32), since the differential $\left(\frac{\Theta_2'}{\Theta_1'}\right)'$ is negative, the term $\frac{\Theta_2'}{\Theta_1'}$ is a monotone decreasing function. Therefore, from (6.28) and (6.29), since the infimum of $\frac{\Theta_2'}{\Theta_1'}$ is given by

$$\lim_{\theta_2 \downarrow \frac{\pi}{2}} \frac{\Theta_2'}{\Theta_1'} = \frac{1}{2} \lim_{\theta_2 \downarrow \frac{\pi}{2}} \frac{g(2\theta_2)}{g(\theta_2)} = \frac{\pi}{2},$$

the following equation holds:

$$\frac{\Theta_2'}{\Theta_1'} > \frac{\pi}{2}. \tag{6.34}$$

From the analyses **(i)–(iv)**, since the infimums and supremum of the terms in the left hand of (6.23) are given by

$$\frac{\sin\varepsilon}{\varepsilon} < 1, \quad \frac{\tan\frac{\varepsilon}{2}}{\frac{\varepsilon}{2}} > 1, \quad \Theta_1' < 0, \quad \Theta_2' < 0, \quad \frac{\Theta_2'}{\Theta_1'} > \frac{\pi}{2}, \tag{6.35}$$

the following inequality holds:

$$\frac{\partial}{\partial\theta_2} f(\varepsilon, \theta_2) = \underbrace{\varepsilon \sin\varepsilon}_{>0} \underbrace{\Theta_1'}_{<0} \underbrace{\left\{1 - \underbrace{\left(\frac{\tan\frac{\varepsilon}{2}}{\frac{\varepsilon}{2}}\right)}_{>1} \underbrace{\frac{\Theta_2'}{\Theta_1'}}_{>\frac{\pi}{2}}\right\}}_{<0} > 0. \tag{6.36}$$

Therefore, $f(\varepsilon, \theta_2)$ of (6.22) is a monotone increasing function of θ_2 irrespective of ε.

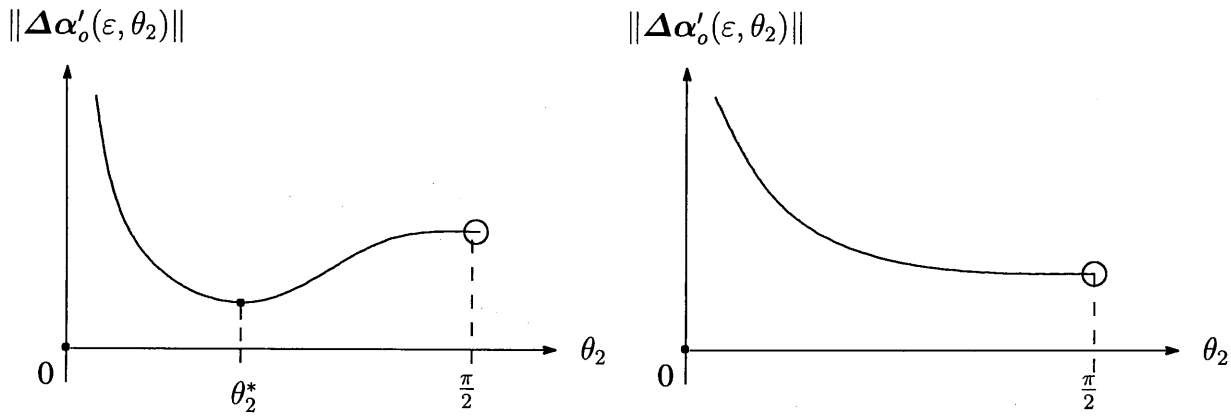

Figure 6.5 Sckech of $\|\Delta\alpha'_o(\varepsilon,\theta_2)\|$ as a function of θ_2.

Next, from (6.22), (6.21), (6.24) and (6.25), the limit values of $f(\varepsilon,\theta_2)$ with respect to $\theta_2 \to 0$ and $\theta_2 \to \frac{\pi}{2}$ are given by

$$\lim_{\theta_2 \downarrow 0} f(\varepsilon,\theta_2) = \varepsilon^2 \left[\frac{\sin\varepsilon}{\varepsilon}\left\{2 - \left(\frac{\tan\frac{\varepsilon}{2}}{\frac{\varepsilon}{2}}\right)\right\} - 1\right] < 0, \tag{6.37}$$

$$\lim_{\theta_2 \uparrow \frac{\pi}{2}} f(\varepsilon,\theta_2) = \varepsilon^2 \left[\frac{\pi}{2}\left(\frac{\sin\varepsilon}{\varepsilon}\right) - 1\right] \begin{cases} > 0 & (0 < \varepsilon < \frac{\pi}{2}) \\ \leq 0 & (\frac{\pi}{2} \leq \varepsilon < \pi) \end{cases}. \tag{6.38}$$

First, consider the case $0 < \varepsilon < \frac{\pi}{2}$. From (6.37) and (6.38), there exists θ_2 in the neighborhood of $\theta_2 = 0$ such that the value of $f(\varepsilon,\theta_2)$ is negative and there exists θ_2 in the neighborhood of $\theta_2 = \frac{\pi}{2}$ such that the value of $f(\varepsilon,\theta_2)$ is positive. Therefore, since $f(\varepsilon,\theta_2)$ is a monotone increasing function, the equation $f(\varepsilon,\theta_2) = 0$ has only a solution. Define the solution of $f(\varepsilon,\theta_2) = 0$ by θ_2^*. From (6.19), $\|\Delta\alpha'_o(\varepsilon,\theta_2)\|^2$ has a minimum value at $\theta_2 = \theta_2^*$. This proves the claim **(i)**. Second, consider the case $\frac{\pi}{2} \leq \varepsilon < \pi$. From (6.37) and (6.38), the function $f(\varepsilon,\theta_2)$ is always negative. Therefore, from (6.19), the function $\|\Delta\alpha'_o(\varepsilon,\theta_2)\|^2$ is a monotone decreasing function. This proves the claim **(ii)**. □

Figure 6.5 shows the shapes of the function $\|\Delta\alpha'_o(\varepsilon,\theta_2)\|$ described in Theorem 6.1. The case $\varepsilon < \frac{\pi}{2}$ is depicted in the left figure, where the value of $\|\Delta\alpha'_o(\varepsilon,\theta_2)\|$ is a minimal value at $\theta_2 = \theta_2^*$. On the other hand, the case $\varepsilon \leq \frac{\pi}{2}$ is depicted in the right figure, where $\|\Delta\alpha'_o(\varepsilon,\theta_2)\|$ is a monotone decreasing function.

Since the behavior of $\|\Delta\alpha'_o(\varepsilon,\theta_2)\|$ is evident from Theorem 6.1, it is possible to estimate the boundaries of the reachable area Ω. To be more precise, for each ε in the range (6.14), it is possible to obtain the values of θ_2 to give the minimum and maximum values of $\|\Delta\alpha'_o(\varepsilon,\theta_2)\|$ in the domain of θ_2 (6.16) (See Figure 6.4). Furthermore, the values of θ_1 are given by substituting the obtained values of θ_2 and ε into (6.15).

In the following, we show the calculation method of the values of θ_2 to give the minimum and maximum values of $\|\Delta\alpha'_o(\varepsilon,\theta_2)\|$ in the condition that the parameters θ_1 and θ_2 are constrained

such that (6.9). The values of θ_2 to give the minimum and maximum values are described by $\theta_{2\min}$ and $\theta_{2\max}$. Note that the range of θ_2 is

$$\sin^{-1}\left(\frac{\varepsilon}{\bar{\theta}_1}\right) \leq \theta_2 \leq \bar{\theta}_2 \tag{6.39}$$

since the case such that $\theta_2 > 0$ is considered.

Calculation Method of the Reachable Area Ω

(i) $\boxed{\varepsilon < \frac{\pi}{2}}$ (The case shown in the left hand of Figure 6.5)

1) $\underline{\bar{\theta}_2 < \theta_2^*}$ (There exists the domain in the left side of θ_2^*.)

In the domain, the function $\|\Delta\boldsymbol{\alpha}_o'(\varepsilon, \theta_2)\|$ is a monotone decreasing function. Therefore, $\theta_{2\min}$ and $\theta_{2\max}$ are the right end and the left end of the domain respectively:

$$\theta_{2\min} = \bar{\theta}_2, \quad \theta_{2\max} = \sin^{-1}\left(\frac{\varepsilon}{\bar{\theta}_1}\right). \tag{6.40}$$

2) $\underline{\sin^{-1}(\frac{\varepsilon}{\bar{\theta}_1}) \leq \theta_2^* \leq \bar{\theta}_2}$ (The domain involves θ_2^*.)

Since the function $\|\Delta\boldsymbol{\alpha}_o'(\varepsilon, \theta_2)\|$ takes a minimal value at $\theta_2 = \theta_2^*$, the value $\theta_{2\min}$ is θ_2^*. On the other hand, Since the value of $\|\Delta\boldsymbol{\alpha}_o'(\varepsilon, \theta_2)\|$ can be maximum at the left or right end of the domain, both cases are considered:

a) $\|\Delta\boldsymbol{\alpha}_o'(\varepsilon, \sin^{-1}(\frac{\varepsilon}{\bar{\theta}_1}))\| \geq \|\Delta\boldsymbol{\alpha}_o'(\varepsilon, \bar{\theta}_2)\|$

$$\theta_{2\min} = \theta_2^*, \quad \theta_{2\max} = \sin^{-1}\left(\frac{\varepsilon}{\bar{\theta}_1}\right). \tag{6.41}$$

b) $\|\Delta\boldsymbol{\alpha}_o'(\varepsilon, \sin^{-1}(\frac{\varepsilon}{\bar{\theta}_1}))\| < \|\Delta\boldsymbol{\alpha}_o'(\varepsilon, \bar{\theta}_2)\|$

$$\theta_{2\min} = \theta_2^*, \quad \theta_{2\max} = \bar{\theta}_2. \tag{6.42}$$

3) $\underline{\theta_2^* < \sin^{-1}(\frac{\varepsilon}{\bar{\theta}_1})}$ (There exists the domain in the right side of θ_2^*.)

In the domain, the function $\|\Delta\boldsymbol{\alpha}_o'(\varepsilon, \theta_2)\|$ is a monotone increasing function. Therefore, $\theta_{2\min}$ and $\theta_{2\max}$ are the left end and the right end of the domain respectively:

$$\theta_{2\min} = \sin^{-1}\left(\frac{\varepsilon}{\bar{\theta}_1}\right), \quad \theta_{2\max} = \bar{\theta}_2. \tag{6.43}$$

(ii) $\boxed{\varepsilon \geq \frac{\pi}{2}}$ (The case shown in the right hand of Figure 6.5)

Since the function $\|\Delta\boldsymbol{\alpha}_o'(\varepsilon, \theta_2)\|$ is a monotone decreasing function, $\theta_{2\min}$ and $\theta_{2\max}$ are the right end and the left end of the domain respectively:

$$\theta_{2\min} = \bar{\theta}_2, \quad \theta_{2\max} = \sin^{-1}\left(\frac{\varepsilon}{\bar{\theta}_1}\right). \tag{6.44}$$

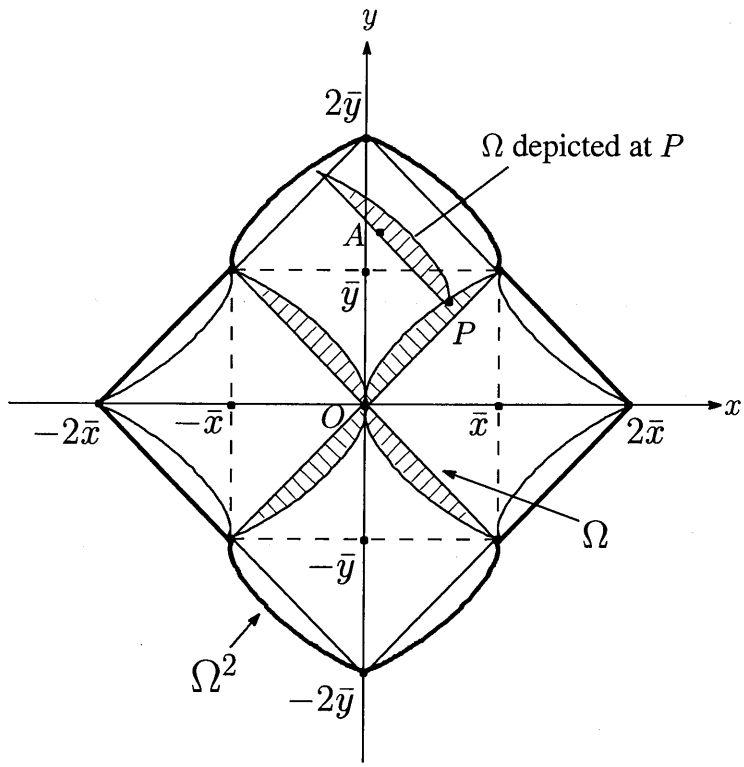

Figure 6.6 Reachable area by the iteration of two closed paths.

Remark 6.2. In the case **(i)** $\varepsilon < \frac{\pi}{2}$, since θ_2^* is the solution of $f(\varepsilon, \theta_2) = 0$ as mentioned in the proof of Theorem 6.1, it is necessary to obtain the solution by the numerical calculation. This value can be easily calculated by the bisection method since $f(\varepsilon, \theta_2)$ is a monotone increasing function in the range $[0, \frac{\pi}{2}]$ and the signs of $f(\varepsilon, \theta_2)$ are different each other at $\theta_2 = 0$ and $\theta_2 = \frac{\pi}{2}$ from (6.37) and (6.38).

6.3 Algorithm for Determination of Parameters

In this section, we propose the regulation algorithm for the control variable $(\|\boldsymbol{\alpha}_o\|, \psi)$ to converge to the origin (target point) by the finite iterative shifts along the boundaries on the reachable area Ω on the plane $(\|\Delta\boldsymbol{\alpha}'_o\|, \Delta\psi)$. The parameter φ is determined by (5.13) as mentioned in Chapter 5. It follows that the target point is involved in the first or fourth quadrant of the plane $(\|\Delta\boldsymbol{\alpha}'_o\|, \Delta\psi)$.

First, the reachable area by two interation of the closed path is characterized as in Figure 6.6. In Figure 6.6, the negative range with respect to the $\|\Delta\boldsymbol{\alpha}'_o\|$-axis is depicted for simplicity of explanation. This negative range can be given by transforming φ of (5.13) into $\varphi + \pi$. The shaded areas represent the reachable areas by one iteration Ω. Furthermore, The area surrounded by the heavy line represents the reachable area by two iteration, which is obtained by depicting Ω at points on the boundaries of Ω. We call this area Ω^2 in this chapter. The origin O represents the initial point of $(\|\boldsymbol{\alpha}_o\|, \psi)$ and the point A is the target point. Then, since the reachable area Ω

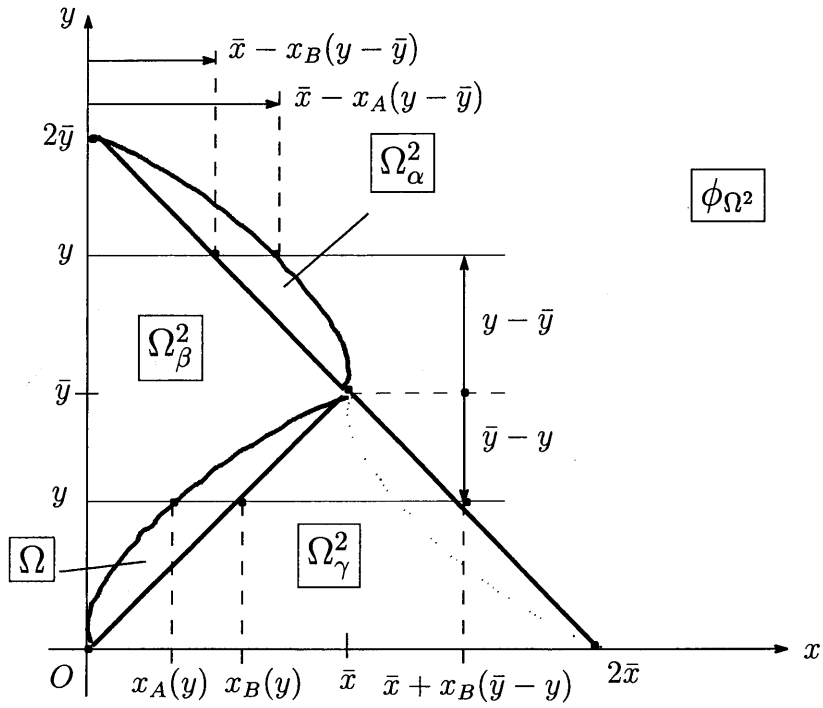

Figure 6.7 Decomposition of (x, y) plane.

with the origin P includes the target point A, by two iteration composed of the shift toward P at first iteration and the shift toward A at second iteration, it is realized for $(\|\boldsymbol{\alpha}_o\|, \psi)$ to converge to A. In the following, for simplicity of description, the coordinates $\|\Delta\boldsymbol{\alpha}'_o\|$ and $\Delta\psi$ is represented by

$$x := \|\Delta\boldsymbol{\alpha}'_o(\theta_1, \theta_2)\|, \quad y := \Delta\psi(\theta_1, \theta_2) \tag{6.45}$$

and the plane $(\|\Delta\boldsymbol{\alpha}'_o\|, \Delta\psi)$ is called the plane (x, y). The values $\bar{x}$ and $\bar{y}$ represent the coordinate of the end point $(\bar{x}, \bar{y})$ of Ω and they are the maximum values of x and y respectively. The value $\bar{y}$ is given by the maximum value of ε, which is $\bar{\varepsilon} = \bar{\theta}_1 \sin\bar{\theta}_2$ from (6.13), (6.14) and (6.45). On the other hand, the value $\bar{x}$ is given by the value maximum value of $\|\Delta\boldsymbol{\alpha}'_o(\varepsilon, \theta_2)\|$, which is $\|\Delta\boldsymbol{\alpha}'_o(\bar{\varepsilon}, \theta_{2\max})\|$. Since $\theta_{2\max}$ is given by $\bar{\theta}_2$ from (6.40)–(6.44) in the case such that $\varepsilon = \bar{\varepsilon} = \bar{\theta}_1 \sin\bar{\theta}_2$, the values $\bar{x}$ and $\bar{y}$ are defined by

$$\bar{x} := \|\Delta\boldsymbol{\alpha}'_o(\bar{\varepsilon}, \bar{\theta}_2)\|, \quad \bar{y} := \bar{\varepsilon} = \bar{\theta}_1 \sin\bar{\theta}_2. \tag{6.46}$$

Furthermore, for the explanation, since the minimum and maximum values of $\|\Delta\boldsymbol{\alpha}'_o(\varepsilon, \theta_2)\|$ are the coordinate of x on the boundaries **(A)** and **(B)** of Ω in the case $y = \varepsilon$ respectively (See Figure 6.4), they are represented by

$$x_A(\varepsilon) := \|\Delta\boldsymbol{\alpha}'_o(\varepsilon, \theta_{2\min})\|, \; x_B(\varepsilon) := \|\Delta\boldsymbol{\alpha}'_o(\varepsilon, \theta_{2\max})\|. \tag{6.47}$$

Second, for the determination of the parameters, the plane (x, y) of Figure 6.6 is decomposed by the heavy lines as shown in Figure 6.7. As mentioned previously, note that there exists the target point in the first or fourth quadrant since the parameter φ is determined by (5.13) as mentioned in Chapter 5. Furthermore, since the reachable area Ω^2 is symmetry with respect to x-

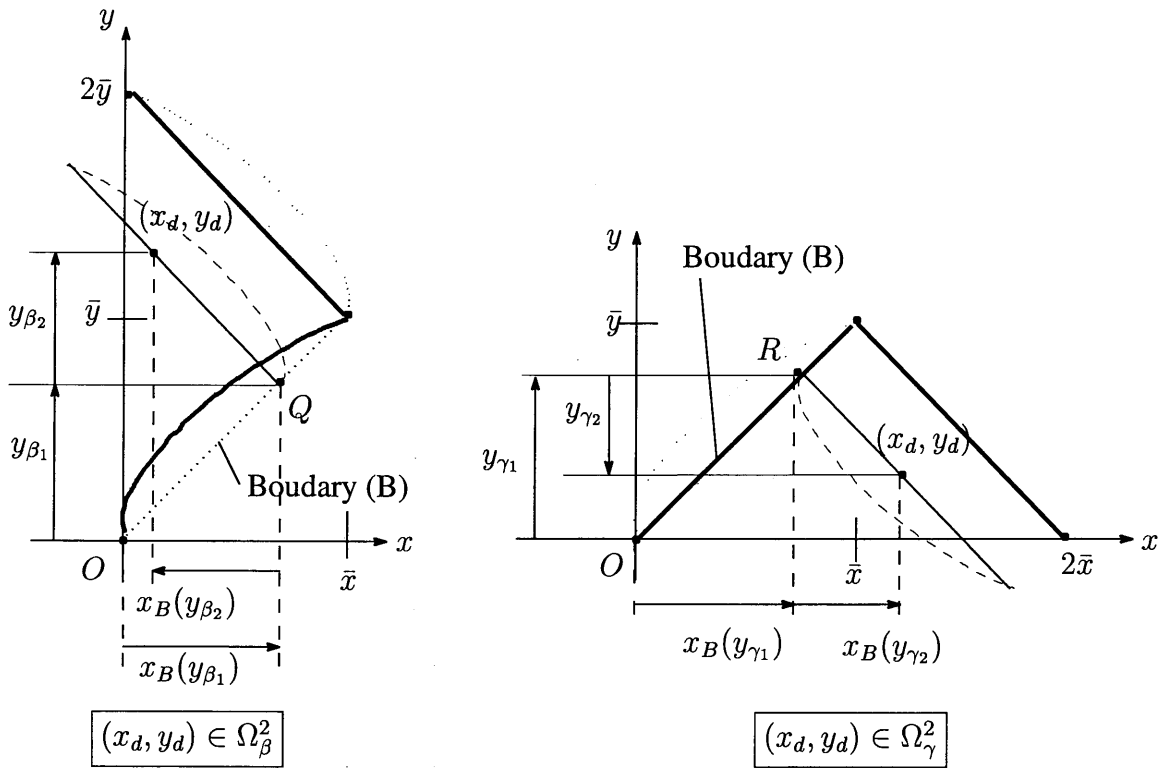

Figure 6.8 Scheme of the algorithm for decision of parameters

axis, it can be discussed as the similar way of the target point in the first quadrant that the target point exists in the fourth quadrant. These are the reason why the first quadrant is only shown in Figure 6.7. Figure 6.7 shows that the first quadrant of the reachable area Ω^2 is decomposed into the five areas Ω, Ω^2_α, Ω^2_β, Ω^2_γ and ϕ_{Ω^2}. The definitions of these areas are given by the followings:

$$\Omega := \{\, (x,y) \mid x_A(y) \le x \le x_B(y),\ y \le \bar{y} \,\}, \tag{6.48}$$

$$\Omega^2_\alpha := \{\, (x,y) \mid \bar{x} - x_B(y-\bar{y}) \le x \le \bar{x} - x_A(y-\bar{y}),\ \bar{y} < y \le 2\bar{y} \,\}, \tag{6.49}$$

$$\Omega^2_\beta := \{\, (x,y) \mid x < x_A(y),\ y \le \bar{y} \text{ or } x < \bar{x} - x_B(y-\bar{y}),\ \bar{y} < y < 2\bar{y} \,\}, \tag{6.50}$$

$$\Omega^2_\gamma := \{\, (x,y) \mid x_B(y) < x \le \bar{x} + x_B(\bar{y}-y),\ y < \bar{y} \,\}, \tag{6.51}$$

$$\phi_{\Omega^2} := \{\, (x,y) \mid x,y \notin \Omega^2,\ \Omega^2 = \Omega \cup \Omega^2_\alpha \cup \Omega^2_\beta \cup \Omega^2_\gamma \,\}, \tag{6.52}$$

where Ω is the reachable area by one iteration, Ω^2_α, Ω^2_β and Ω^2_γ are the reachable area by two iteration and ϕ_{Ω^2} is the reachable area by the more iteration, the number of which is greater than or equal to three.

Third, in the cases that the target point exists in the above decomposed areas, the method of the shift along the boundaries **(A)** and **(B)** is proposed. The origin O is the initial point and the point (x_d, y_d) represents the target point. The fundamental concept of the proposed method is composed of the followings:

(1) In the case where the target point (x_d, y_d) is included in ϕ_{Ω^2}, to iterate the shift to the end point $(\bar{x}, \bar{y})$ of the reachable area Ω at each iteration until the target point is involved in Ω^2. Since

the distances of the shifts have finite values, the target point can be involved in the reachable area Ω^2 by finite iteration.

(2) In the case that there exists the target point in Ω^2, to determine the first shift of the two iteration as following ways for the target point to be involved in Ω:

(2)-(i) The target point is involved in Ω^2_α:
The target point is involved in the reachable area Ω by the shift to the end point $(\bar{x}, \bar{y})$ of Ω^2 (See Figure 6.7).

(2)-(ii) The target point is involved in Ω^2_β:
The details of the determination are shown later.

(2)-(iii) The target point is involved in Ω^2_γ:
The details of the determination are shown later.

(3) In the case that there exists the target point (x_d, y_d) in the reachable area $\Omega \subset \Omega^2$, to shift to the target point.

The details of the above terms **(2)-(ii)** and **(2)-(iii)** are shown in the followings:

(2)-(ii) The target point is involved in Ω^2_β:

In this case as in the left hand of Figure 6.8, to shift to the point Q along the boundary **(B)** of Ω at first iteration. Note that Q is the point such that the target point (x_d, y_d) is involved in the boundary **(B)** of Ω depicted at Q. The first and second distances of the shifts of y direction are defined by $y_{\beta_1} > 0$ and $y_{\beta_2} > 0$ respectively. Then, the distances of the shifts of x direction by each iteration are given by $x_B(y_{\beta_1})$ and $x_B(y_{\beta_2})$ from (6.47). Therefore, the condition such that the point Q must satisfy is as follows:

$$\begin{cases} x_B(y_{\beta_1}) - x_B(y_{\beta_2}) &= x_d \\ y_{\beta_1} + y_{\beta_2} &= y_d \end{cases}. \tag{6.53}$$

Combining two equations of (6.53) leads to the following equation:

$$x_B(y_{\beta_1}) - x_B(y_d - y_{\beta_2}) = x_d, \tag{6.54}$$

where the range of y_{β_1} is $0 < y_{\beta_1} < y_d$ in the case $y_d < \bar{y}$ or $0 < y_{\beta_1} < \bar{y}$ in the case $y_d \geq \bar{y}$ since $y_{\beta_1} < y_d$ from $y_{\beta_2} = y_d - y_{\beta_1} > 0$ and $y_{\beta_1} < \bar{y}$. Therefore, since the value of y_{β_1} is given by solving (6.54) on this range, $x_B(y_{\beta_1})$ is given by (6.47) from the obtained value of y_{β_1}, i.e. the coordinate of Q is obtained. By shifting to the obtained point Q, the target point is involved in Ω at second iteration.

(2)-(iii) The target point is involved in Ω^2_γ:

In this case as in the right hand of Figure 6.8, to shift to the point R along the boundary **(B)** of Ω at first iteration. Note that R is the point such that the target point (x_d, y_d) is involved in the boundary **(B)** of Ω depicted at R. The first and second distances of the shifts of y direction are defined by $y_{\gamma_1} > 0$ and $y_{\gamma_2} < 0$ respectively. Then, the distances of the shifts of x direction by

each iteration are given by $x_B(y_{\gamma_1})$ and $x_B(y_{\gamma_2})$ from (6.47). Therefore, the condition such that the point R must satisfy is as follows:

$$\begin{cases} x_B(y_{\gamma_1}) + x_B(y_{\gamma_2}) &= x_d \\ y_{\gamma_1} + y_{\gamma_2} &= y_d \end{cases}. \tag{6.55}$$

Combining two equations of (6.55) leads to the following equation:

$$x_B(y_{\gamma_1}) + x_B(y_d - y_{\gamma_2}) = x_d, \tag{6.56}$$

where the range of y_{γ_1} is $y_d < y_{\gamma_1} \leq \bar{y}$ since $y_d < y_{\gamma_1}$ from $y_{\gamma_2} = y_d - y_{\gamma_1} < 0$ and $y_{\gamma_1} \leq \bar{y}$. Therefore, since the value of y_{γ_1} is given by solving (6.56) on this range, $x_B(y_{\gamma_1})$ is given by (6.47) from the obtained value of y_{γ_1}, i.e. the coordinate of R is obtained. By shifting to the obtained point R, the target point is involved in Ω at second iteration.

Summarizing the previous discussion, we show the algorithm to determine the parameters (θ_1, θ_2) in the following. In the algorithm, k is the number of the iterations of the closed paths $(x[k], y[k])$ is the target point represented in the orthogonal coordinate system (x, y) at kth interation. As mentioned previously, note that the target point $(x_d[k], y_d[k])$ exists in the first quadrant, i.e. $x_d[k] > 0$ and $y_d[k] > 0$.

Algorithm for Determination of the Parameters of the Closed Path

1) $\boxed{(x_d[k], y_d[k]) \in \phi_{\Omega^2}}$

To iterate the shift to the end point $(\bar{x}, \bar{y})$ of the reachable area Ω at each iteration until the target point $(x_d[k], y_d[k])$ is involved in Ω^2. Then, from (6.15) and (6.46), the values $\theta_1[k]$ and $\theta_2[k]$ are given by

$$\theta_2[k] = \bar{\theta}_2, \quad \theta_1[k] = -\frac{\bar{\theta}_1 \sin \bar{\theta}_2}{\sin \theta_2[k]}. \tag{6.57}$$

2) $\boxed{(x_d[k], y_d[k]) \in \Omega^2}$

To determine the first shift of the two iteration as following ways:

(i) $\underline{(x_d[k], y_d[k]) \in \Omega^2_\alpha}$

To shift to the end point $(\bar{x}, \bar{y})$ of Ω^2 (See Figure 6.7). Then, from (6.15) and (6.46), the values $\theta_1[k]$ and $\theta_2[k]$ are given by

$$\theta_2[k] = \bar{\theta}_2, \quad \theta_1[k] = -\frac{\bar{\theta}_1 \sin \bar{\theta}_2}{\sin \theta_2[k]}. \tag{6.58}$$

(ii) $\underline{(x_d[k], y_d[k]) \in \Omega^2_\beta}$

First, to obtain y_{β_1} by solving the following equation:

$$\{x_B(y_{\beta_1}) - x_B(y_d[k] - y_{\beta_1})\} - x_d[k] = 0, \quad \begin{cases} 0 < y_{\beta_1} < y_d & (y_d \leq \bar{y}) \\ 0 < y_{\beta_1} < \bar{y} & (y_d > \bar{y}) \end{cases}. \tag{6.59}$$

Second, to obtain $\theta_2[k]$ to give the point on the boundary **(B)** by the estimation method shown in Sec. 6.2 by using $\varepsilon = y_{\beta_1}$. Furthermore, the value $\theta_1[k]$ is given by (6.15).

$$\theta_2[k] = \theta_{2\max}, \quad \theta_1[k] = -\frac{y_{\beta_1}}{\sin\theta_2[k]}. \tag{6.60}$$

(iii) $\underline{(x_d[k], y_d[k]) \in \Omega_\gamma^2}$

First, to obtain y_{γ_1} by solving the following equation:

$$\{x_B(y_{\gamma_1}) + x_B(y_d[k] - y_{\gamma_1})\} - x_d[k] = 0, \quad y_d < y_{\gamma_1} < \bar{y}. \tag{6.61}$$

Second, to obtain $\theta_2[k]$ to give the point on the boundary **(B)** by the estimation method shown in Sec. 6.2 by using $\varepsilon = y_{\gamma_1}$. Furthermore, the value $\theta_1[k]$ is given by (6.15).

$$\theta_2[k] = \theta_{2\max}, \quad \theta_1[k] = -\frac{y_{\gamma_1}}{\sin\theta_2[k]}. \tag{6.62}$$

3) $\boxed{(x_d[k], y_d[k]) \in \Omega}$

First, to obtain $\theta_{2\min}$ and $\theta_{2\max}$ to give the boundaries **(A)** and **(B)** by the estimation method shown in Sec. 6.2 by using $\varepsilon = y_d[k]$. Second, to obtain $\theta_2[k]$ by solving the following equation:

$$\|\Delta\boldsymbol{\alpha}_o'(y_d[k], \theta_2[k])\| - x_d[k] = 0, \quad \begin{cases} \theta_{2\min} \le \theta_2[k] \le \theta_{2\max} & (\theta_{2\min} \le \theta_{2\max}) \\ \theta_{2\max} \le \theta_2[k] \le \theta_{2\min} & (\theta_{2\min} > \theta_{2\max}) \end{cases}. \tag{6.63}$$

Furthermore, the value $\theta_1[k]$ is given by (6.15).

Remark 6.3. In the algorithm, the solutions of (6.57) and (6.58) are directly given by the left and right ends of the domain. On the other hand, it is necessary to solve (6.59), (6.61) and (6.63) by the numerical calculation. However, the left functions of these equations are one value nonlinear equation with the fixed domains and the signs of the function at the left and right ends of the domains are different each other. This fact easily follows from the definitions of the areas Ω, Ω_β^2 and Ω_γ^2 of (6.48), (6.50) and (6.51). Therefore, these equations can be easily solved by the bisection method.

Remark 6.4. Since the parameters $\theta_1[k]$, $\theta_2[k]$ and $\varphi[k]$ can be obtained only from $\widetilde{\boldsymbol{\eta}}[k]$ which is the sates at the start time of kth number of iterations, the method can be interpreted as a discrete-time feedback by regarding the start time of the iteration as the sampling instant. Therefore, the method is expected to have robustness against disturbances.

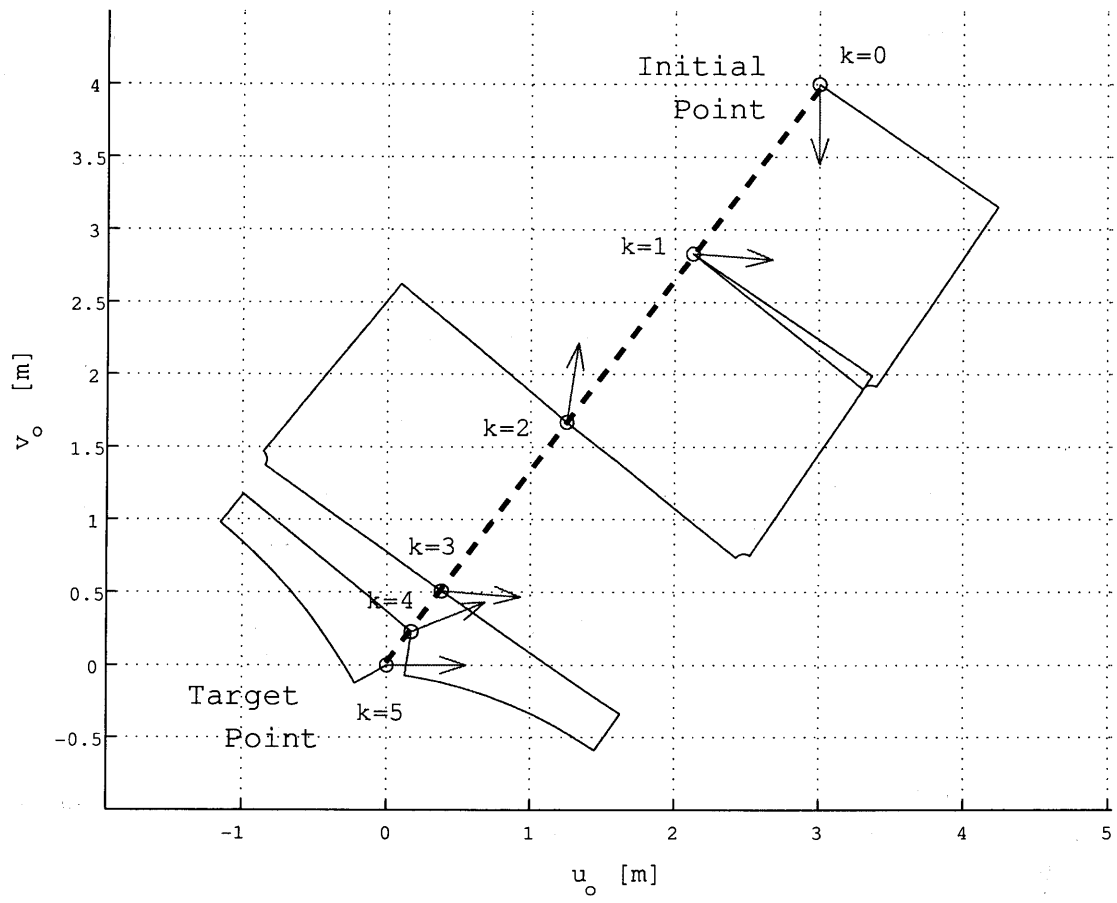

Figure 6.9 Trajectory of $\boldsymbol{\alpha}_o$ and ψ on $\boldsymbol{\alpha}_o$ plane

6.4 Numerical Example

In this section, the effectiveness of the algorithm proposed in the previous section is shown by a numerical example. The radius of the sphere is $\rho = 1$[m]. The initial states are $\boldsymbol{\alpha}_f = [\ 0\ \ 0\ ]^{\mathrm{T}}$[rad], $\boldsymbol{\alpha}_o = [\ 3\ \ 4\ ]^{\mathrm{T}}$[m] and $\psi = \frac{\pi}{2}$[rad]. Furthermore, the value of the boundary of the rolling motion θ_r is set to $\theta_r \approx 1.56 < \frac{\pi}{2}$, which means the case that the contact point on the sphere $\boldsymbol{\alpha}_f = [\ u_f\ \ v_f\ ]^T$ is restricted to the area on the semisphere. This value is given by (6.12) with $\bar{\theta}_1 = \bar{\theta}_2 = 1.5 < \frac{\pi}{2}$.

Figures 6.9–6.11 show the simulation result. Figure 6.9 shows the shifts of $\boldsymbol{\alpha}_o$ on the plane $\boldsymbol{\alpha}_o$, where the kth circle represents the position of $\boldsymbol{\alpha}_o[k]$ by the kth closed path and the kth arrow represent the angle of $\psi[k]$ by the kth closed path. Figure 6.10 shows the shifts on the plane (x, y), i.e. $(\|\Delta\boldsymbol{\alpha}'_o\|, \Delta\psi)$. In Figure 6.10, the kth circle represents the position $(\|\Delta\boldsymbol{\alpha}'_o[k]\|, \Delta\psi[k])$ by the kth closed path, the oblique lines represent the oblique coordinate system (X, Y) and the areas shaped as the lunes are the reachable areas Ω. Figure 6.11 shows the trajectory of $\boldsymbol{\alpha}_f$, where the closed paths are generated with time interval 2[sec] and the heavy lines show the values of the boundaries of the rolling motion θ_r. In Figure 6.9, $\boldsymbol{\alpha}_o$ and ψ have converged on the target point simultaneously by five number of the iterations. Furthermore, there exist the

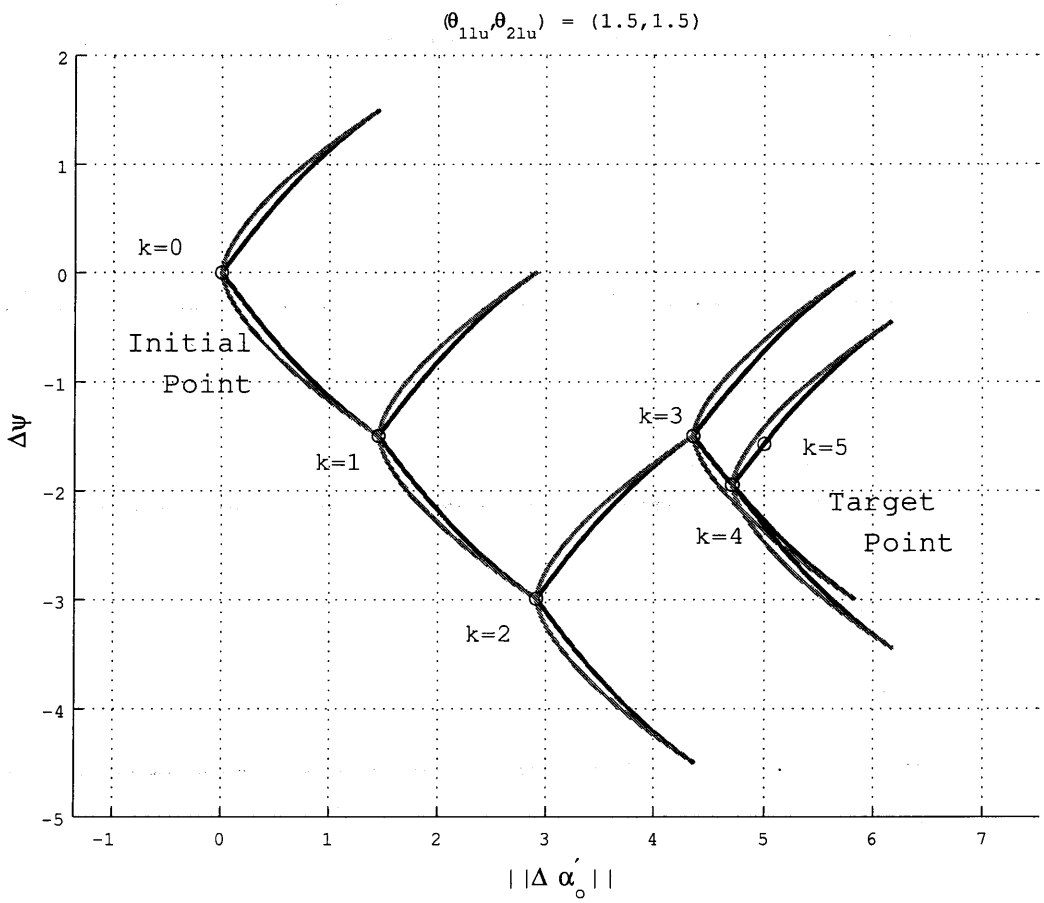

Figure 6.10 Shift of $(\|\boldsymbol{\alpha}_o\|, \psi)$ on $(\|\boldsymbol{\Delta\alpha}'_o\|, \Delta\psi)$ plane

circles ○ on the dashed line from the initial point to the target point. This corresponds to the fact that the direction of the shift of $\boldsymbol{\alpha}_o$ is determined by φ such that (5.13) (See Figure 5.3). In Figure 6.10, the points of $k = 1, 2, 3$ to which the control variable shifts are the end points of the reachable areas Ω at each iteration. Next, those of $k = 4, 5$ are adjusted such that the control variable converges to the target point. These transitions show the effectiveness of the algorithm. In Figure 6.11, it is evident for u_f and v_f of $\boldsymbol{\alpha}_f = [\ u_f \ \ v_f\ ]^{\mathrm{T}}$ to involve in the range between $-\theta_r$ and θ_r, where $\theta_r \approx 1.56$.

6.5 Summary

In this chapter, we discussed the control of the contact coordinates by iterative closed paths on the sphere with constrained rolling motion. The type of the closed path was the same used in Chapters 3 and 5. First, in order to utilize the reachable area of the closed path at the maximum, we precisely analyzed the boundary of the reachable area of the closed path with constrained rolling motion. Second, we proposed the method for the contact coordinates to converge to a target point by the finite iterative shifts along the boundary as mentioned earlier. Since the

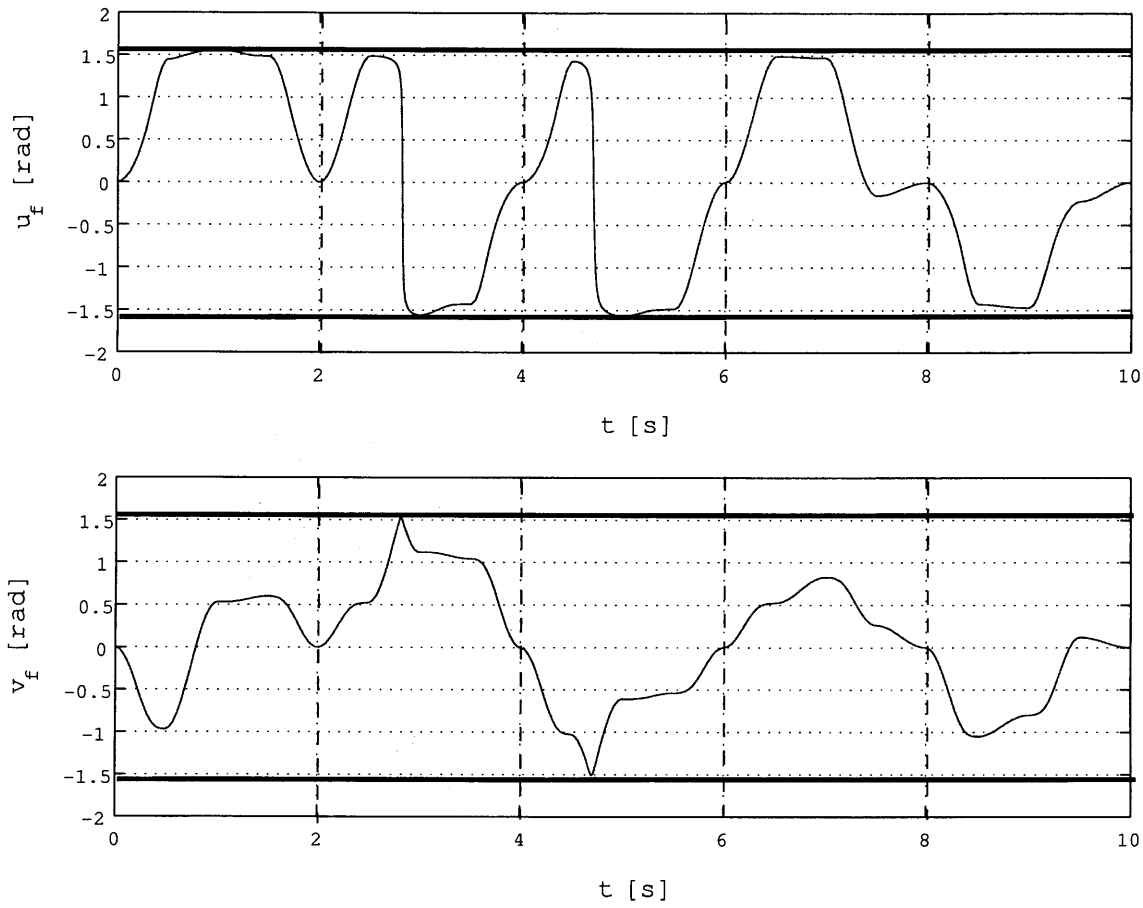

Figure 6.11 Trajectory of α_f.

proposed method can impose the limitation of the rolling motion, the method has the beneficial effect on the application to multi-fingered robot hands. Since the reachable area of the closed path is utilized at the maximum, the required number of the contact coordinates to converge can be less than the method in Chapter 5. Furthermore, similar to the method in Chapter 5, the parameters at each iteration can be easily calculated by the bisection method.

Chapter 7

Conclusions

In this chapter, the conclusions of this thesis are summarized and some topics of the further research are suggested.

7.1 Summary

In the literature, the dexterity in the dexterous manipulation is mainly discussed from the viewpoints of the force-closure and the manipulability. In this thesis, to enrich the dexterity, we discussed the manipulation by rolling since the reachable configuration of the manipulation by rolling can be as extensive as that of the manipulation at large due to the nonholonomy of rolling. The purpose of this thesis was to establish control methods to realize the simultaneous control of grasp/manipulation and contact points of an object by a multi-fingered robot hand with the nonholonomy of rolling. The key topics to realize the purpose were the followings:

(A) For a dynamical model composed of fingers and a grasped object, to establish control methods which can utilize the nonholonomy of rolling for control of contact points simultaneously with grasp and manipulation of the object. In this thesis, the number of the fingers would be restricted to two which is the minimum number.

(B) For a nonholonomic system of two rolling rigid bodies with pure rolling contact, to establish methods such that all of the contact coordinates can be regulated simultaneously by using a single specified closed path. In this thesis, the surfaces of the bodies would be restricted to a sphere and a plane.

The details of these topics were as follows:

In Chapter 3, to be devoted to the topics (A) and (B), we discussed the simultaneous control by a two-fingered robot hand, each finger of which had six degrees of freedom. The contact motion between each finger and the object was assumed to be the pure rolling contact, and the surfaces of each finger and the object were assumed to be the regular surfaces. As for the control method to utilize the nonholonomy of rolling for control of contact points, we first clarified the degree of freedom of the whole system by investigating the property of the motion constraint on the generalized coordinates, which could be associated with the constraint of the contact

coordinates. Second, we proposed the general formulation of the linearizing compensator for the internal force, the object motion and the rolling motion. Due to the linearization, the contact motion conforms to the kinematic model of two rolling bodies whose input is the rolling motion. As for the regulation algorithm, for the kinematic model of a sphere and a plane which correspond to a spherical finger and a cuboid object, we proposed the method to regulate all the contact coordinates by iterative closed paths on the contact point of the sphere. The closed path was shaped as a trapezoid on the sphere parameterized by three variables. This closed path was called the *trapezoidal closed path.* The parameters was determined with respect to each interation. Furthermore, the convergence to arbitrary target points of the regulation method was guaranteed by proving that there always existed the parameters to reduce the euclidean norm of the distance to the target point. Since the method can be interpreted as a discrete-time feedback by regarding the start time of the iteration as the sampling instant, the method is expected to have robustness against disturbances. The numerical example was presented to show the effectiveness of the method.

In Chapter 4, to be devoted to the topic (A), for the simultaneous control, we proposed the control method which could utilize the nonholonomy of rolling for control of contact points by a two-fingered robot hand with constrained DOF. The contact motion between each finger and the object was assumed to be the pure rolling contact, and the surfaces of each finger and the object were assumed to be the regular surfaces. We first clarified the condition such that the position of the DOF of the whole system was maximum. This represented that arbitrary rolling motion could be generated by using finger and object motion. This was characterized by the number and the direction of the DOF of the fingers. Second, we proposed the general formulation of the linearizing compensator for the internal force, the motion of a certain coordinates of the fingers and the object, and the rolling motion. For the construction of the linearizing compensator, the finger and object motion were decomposed into a component which caused the rolling motion and a component which did not cause the rolling motion. The second component correspond to a certain coordinates of the fingers and the object. The numerical example showed the effectiveness of the method.

In Chapter 5, to be devoted to the topic (B), for the kinematic model of a sphere and a plane with pure rolling contact, we proposed the regulation algorithm for the contact coordinates to converge to a target point by the finite iterative trapezoidal closed paths of the contact point on the sphere. First, we showed that, from the viewpoint of the norm minimization, one of the parameters could be determined independent of the other two parameters. Due to this determination, the control problem was discussed on the two-dimensional space (plane) which characterizes the contact coordinates. Second, we proved that the reachable area of the closed path had two finite lines crossing at the origin which represents the contact coordinates at each iteration. Third, we proposed the method for the contact coordinates to converge to a target point by the finite iterative shifts along the lines as mentioned earlier. At each iteration, since the proposed method requires solving only one variable equation, the solutions can be easily obtained by the bisection method. Finally, The numerical example was shown to prove the effectiveness of the proposed method.

In Chapter 6, to be devoted to the topic (B), for the kinematic model of a sphere and a plane with pure rolling contact, we discussed control of the contact coordinates by iteration of the trapezoidal closed path on the sphere with constrained rolling motion. It was assumed that the parameter of the direction of the closed path was determined from the viewpoint of the norm minimization shown in Chapter 5. Due to this determination, the control problem was discussed on the two-dimensional space (plane) which characterized the contact coordinates. First, in order to utilize the reachable area of the closed path at the maximum, we precisely analyzed the boundary of the reachable area of the closed path with constrained rolling motion. Second, we proposed the method for the contact coordinates to converge to a target point by the finite iterative shifts along the boundary as mentioned earlier. Since the proposed method can impose the limitation of the rolling motion, the method has the beneficial effect on the application to multi-fingered robot hands. Since the reachable area of the closed path is utilized at the maximum, the required number of the contact coordinates to converge can be less than the method in Chapter 5. Furthermore, similar to the method in Chapter 5, the parameters at each iteration can be easily calculated by the bisection method. The numerical example where the rolling motion is restricted to the area on the semisphere showed the effectiveness of the proposed method.

7.2 Further Research

Some topics are suggested for the further research.

Closely related to the topics of this thesis, the following problems are interesting. As for the topic related to the purpose (A), to loosen the restriction of the number of the fingers is a issue. In this issue, the analysis of the condition to realize the rolling motion can be easily investigated. Rather, it is a key topics to introduce appropriate expressions of the internal force. The expressions of the internal force have redundancy if the number of the contact points is more than five in the case where the contact type is a so-called hard finger contact, which causes translational forces at a contact point. An expression which reduces the redundancy is given by [60]. However, as in this thesis, in the case where the contact type is a soft-finger contact which causes translational forces and a moment about the contact normal, the appropriate expressions have been not derived. Since the soft-finger contact is also more reasonable than the hard finger contact, to establish appropriate expressions of the internal force in the case of the soft-finger contact is a significant issue.

As for the topic related to the purpose (B), to loosen the restriction of the surfaces of two rolling rigid bodies is a issue. There exist studies for a object with arbitrary surface and a plane by multiple closed paths [40, 41] and the study for a polyhedra object and a plane by multiple closed paths [42]. However, since for the problem of two rigid bodies having arbitrary surfaces there have not existed methods by iterating a single specified close path, to establish such methods is a significant issue.

On the other hand, the following topics are also stimulating. As mentioned in Chapter 1, the elemental technologies which are important to improve and develop dexterity of multi-fingered robot hands are the followings [1]: 1. *Mechanical designs of hands*, 2. *Sensor technology and information processing*, 3. *Control schemes*. Some topics associated with these terms are described in the following.

1. *To introduce soft-finger tips with deformations.*
2. *To establish methods of contact sensing and sensor fusions.*
3. *To establish control methods based on the passivity.*

The first topic aims to the versatility due to deformations of soft materials. The soft-fingers with the deformations have some advantages [61]: the friction coefficient is large, the deformations reduce impact strengths by contacts, there is compatibility for shapes of grasped objects. The key issues are the modeling of the deformations and the control design. There have been some studies associated with soft-fingers [62, 63]. In these studies, the deformation of each soft-finger tip is expressed as one-dimensional compressive force and the control method is designed based on the passivity with the grasp stability. On the other hand, in our studies [64, 65], the deformations is expressed as the pair of the compressive and shearing forces and the control method is designed based on the passivity with the internal force. This research area is interesting and has many issues.

The second topic aims to the more practical application of multi-fingered robot hands. It is evident that the sensor technologies are absolutely imperative for the practical application. As the topics associated with this thesis, the sensing of contact points is an important research area, which is decomposed to the contact detection using the information of force sensor (e.g., see Ref. [66]) and the tactile sensing (e.g., see Ref. [67]). On the other hand, the detection of a grasped object by the sensor fusion [68] is also important. The sensor fusion means complementary information processing of some physical values. This research area is also interesting and has many issues.

The third topic aims to enhance the robustness of the control method. The passivity is a fundamental property of many physical systems which may be roughly defined in terms of energy dissipation and transformation. Since the controller based on the passivity needs less quantitative information than linearizing compensators, the controller may be more simple and robust [69]. The studies associated with robot fingers are a few, e.g. Refs. [62, 63, 64, 65]. This research area is also interesting and has many issues.

Appendix A

Rigid Body Motion

A rigid motion of an object is a motion which preserves distance between points. At its heart, the study of robot kinematics, dynamics and control is the study of the motion of rigid bodies. Therefore, in this section, the fundamental theories of the rigid body motion are summarized briefly.

A.1 Configuration Space

To represent the *configuration* of a rigid body, we attach a Cartesian coordinate frame to some point on the rigid body relative to a fixed frame. Consider a rigid body on which a coordinate frame Σ_B is attached and an inertial frame Σ_A in Figure A.1. ${}^A\boldsymbol{p}_B \in \mathbb{R}^3$ is the position vector of the origin of Σ_B from the origin of Σ_A expressed in Σ_A and $\boldsymbol{R}_{AB} \in \mathbb{R}^{3\times3}$ is the rotation matrix of Σ_B relative to Σ_A. A configuration of the system consists of the pair

$$g_{AB} = ({}^A\boldsymbol{p}_B, \boldsymbol{R}_{AB}) \in SE(3), \tag{A.1}$$

where ${}^A\boldsymbol{p}_B$ and $\boldsymbol{R}_{AB}$ correspond to the position and the orientation of Σ_B respectively. $SE(3)$ is the *configuration space* of the system and the notation SE abbreviates *special Euclidean*. The

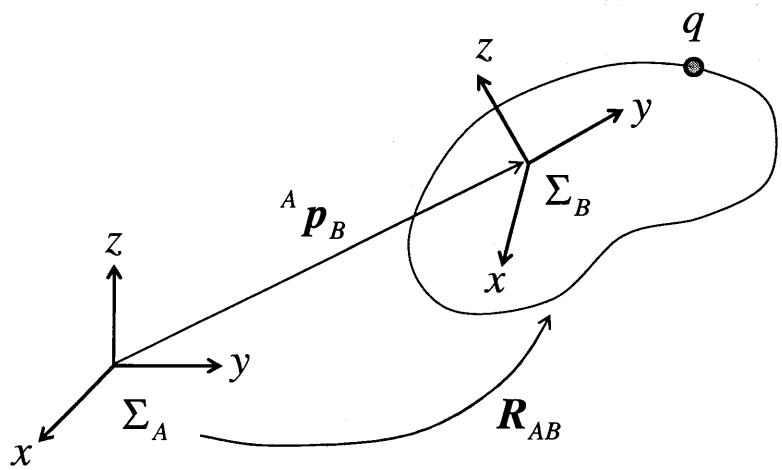

Figure A.1 Coordinate frames for specifying rigid motions.

definition of $SE(3)$ is given by

$$SE(3) := \{(\boldsymbol{p}, \boldsymbol{R}) : \boldsymbol{p} \in \mathbb{R}^3, \boldsymbol{R} \in SO(3)\} = \mathbb{R}^3 \times SO(3). \tag{A.2}$$

In (A.2), $SO(3)$ is the space of rotation matrices in $\mathbb{R}^{3\times3}$ which is defined by

$$SO(3) := \{\boldsymbol{R} \in \mathbb{R}^{3\times3} : \boldsymbol{R}\boldsymbol{R}^{\mathrm{T}} = \boldsymbol{I}_3, \det(\boldsymbol{R}) = +1\}, \tag{A.3}$$

where $\boldsymbol{R}\boldsymbol{R}^{\mathrm{T}} = \boldsymbol{I}_3$ represents that the columns of $\boldsymbol{R}$ are mutually orthonormal and $\det(\boldsymbol{R}) = +1$ represents that the coordinate frame is right-handed. The notation SO abbreviates *special orthogonal* and special refers to $\det(\boldsymbol{R}) = +1$.

A.2 Rigid Body Transformation

A.2.1 Rigid body transformation

An element $g = (\boldsymbol{p}, \boldsymbol{R}) \in SE(3)$ serves as both a specification of the configuration of a rigid body and a transformation taking the coordinates of a point from one frame to another. Given ${}^A\boldsymbol{p}_q, {}^B\boldsymbol{q}_q \in \mathbb{R}^3$ which are the coordinates of a point q relative to Σ_A and Σ_B, a transformation of coordinates is given by

$${}^A\boldsymbol{p}_q = {}^A\boldsymbol{p}_A + \boldsymbol{R}_{AB}{}^B\boldsymbol{p}_q. \tag{A.4}$$

The element $g = (\boldsymbol{p}, \boldsymbol{R}) \in SE(3)$ may be viewed as a mapping $g : \mathbb{R}^3 \mapsto \mathbb{R}^3$ which preserves distances and angles between points:

$$g \circ \boldsymbol{p} = \boldsymbol{p} + \boldsymbol{R}\boldsymbol{p}. \tag{A.5}$$

In general, mappings which preserves distances and angles between points is called the *rigid body transformations* and is used to describe the instantaneous position and orientation of a body coordinate frame relative to an inertial frame.

A.2.2 Homogeneous representation

In *homogeneous coordinates* of $\boldsymbol{p} \in \mathbb{R}^3$, i.e.,

$$\overline{\boldsymbol{p}} = \begin{bmatrix} \boldsymbol{p} \\ 1 \end{bmatrix} \in \mathbb{R}^4,$$

the relation between ${}^A\boldsymbol{p}_q$ and ${}^B\boldsymbol{q}_q$ is given by

$${}^A\overline{\boldsymbol{p}}_q = \overline{\boldsymbol{g}}_{AB}{}^B\overline{\boldsymbol{p}}_q, \tag{A.6}$$

where

$$\overline{\boldsymbol{g}} := \begin{bmatrix} \boldsymbol{R} & \boldsymbol{p} \\ 0_{1\times3} & 1 \end{bmatrix} \in \mathbb{R}^{4\times4} \tag{A.7}$$

is the *homogeneous representation* of $g = (\boldsymbol{p}, \boldsymbol{R}) \in SE(3)$.

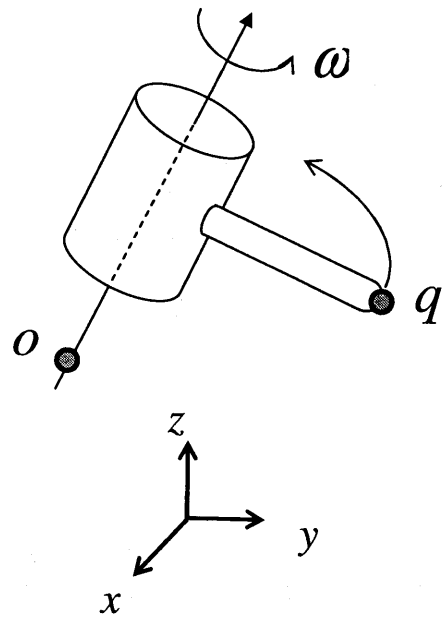

Figure A.2 A revolute joint.

A.3 Velocity of a Rigid Body

A.3.1 Twists and twist coordinates

Consider the simple case of a one-link robot as shown in Figure A.2, where the axis of rotation is $\boldsymbol{\omega} := [\,\omega_1 \;\; \omega_2 \;\; \omega_3\,]^{\mathrm{T}} \in \mathbb{R}^3$ and $\boldsymbol{p}_o \in \mathbb{R}^3$ is a point on the axis. The velocity of a point q attached to the rigid body is given by

$$\dot{\boldsymbol{p}}_q(t) = \boldsymbol{\omega} \times (\boldsymbol{p}_q(t) - \boldsymbol{p}_o) = \boldsymbol{\omega}^{\wedge}(\boldsymbol{p}_q(t) - \boldsymbol{p}_o), \tag{A.8}$$

where $\boldsymbol{\omega}^{\wedge} \in \mathbb{R}^{3\times 3}$ is the matrix equivalent to the vector product $\boldsymbol{\omega}\times$ and is defined by

$$\boldsymbol{\omega}^{\wedge} := \begin{bmatrix} 0 & -\omega_3 & \omega_2 \\ \omega_3 & 0 & -\omega_1 \\ -\omega_2 & \omega_1 & 0 \end{bmatrix}. \tag{A.9}$$

We will often use the notation $\widehat{\boldsymbol{\omega}}$ as a replacement for $\boldsymbol{\omega}^{\wedge}$. Note that $\boldsymbol{\omega}^{\wedge}$ is a skew-symmetric matrix, i.e., $(\boldsymbol{\omega}^{\wedge})^{\mathrm{T}} = -\boldsymbol{\omega}^{\wedge}$. We also define the operator $\vee$ such that

$$(\boldsymbol{\omega}^{\wedge})^{\vee} := \boldsymbol{\omega}. \tag{A.10}$$

In homogeneous coordinates of $\boldsymbol{v} = \dot{\boldsymbol{p}} \in \mathbb{R}^3$, i.e.,

$$\overline{\boldsymbol{v}} = \begin{bmatrix} \boldsymbol{v} \\ 0 \end{bmatrix} \in \mathbb{R}^4,$$

analogous to the homogeneous representation of g of (A.7), i.e., $\overline{\boldsymbol{g}} \in \mathbb{R}^{4\times 4}$, Eq. (A.8) can be represented by using $\widehat{\boldsymbol{\xi}} \in \mathbb{R}^{4\times 4}$ as

$$\overline{\boldsymbol{v}}_q = \widehat{\boldsymbol{\xi}}\overline{\boldsymbol{p}}_q, \tag{A.11}$$

where

$$\widehat{\boldsymbol{\xi}} := \begin{bmatrix} \boldsymbol{\omega}^\wedge & \boldsymbol{v} \\ \mathbf{0}_{1\times 3} & 0 \end{bmatrix} \in \mathbb{R}^{4\times 4}, \quad \boldsymbol{v} := -\boldsymbol{\omega} \times \boldsymbol{p}_q. \tag{A.12}$$

$\widehat{\boldsymbol{\xi}}$ is referred to as a *twist*, or a (infinitesimal) generator of the Euclidean group and is the *generalization* of the skew-symmetric matrix $\boldsymbol{\omega}^\wedge$. Analogous to (A.10), we define the operator $\vee$ to extract the 6-dimensional vector which parameterizes a twist,

$$(\widehat{\boldsymbol{\xi}})^\vee = \left(\begin{bmatrix} \boldsymbol{\omega}^\wedge & \boldsymbol{v} \\ \mathbf{0}_{1\times 3} & 0 \end{bmatrix} \right)^\vee := \begin{bmatrix} \boldsymbol{v} \\ \boldsymbol{\omega} \end{bmatrix} \in \mathbb{R}^6, \tag{A.13}$$

and call

$$\boldsymbol{\xi} := \begin{bmatrix} \boldsymbol{v} \\ \boldsymbol{\omega} \end{bmatrix} \in \mathbb{R}^6 \tag{A.14}$$

the *twist coordinates* of $\widehat{\boldsymbol{\xi}}$. The twist coordinates are the generalized velocity which can be represented by two expressions, i.e., the spatial velocity and the body velocity described in the latter subsection.

A.3.2 Rotational velocity

Here, we call Σ_A the *spatial* coordinate frame and Σ_B the *body* coordinate frame. The word "spatial" means "relative to a fixed (inertial) coordinate frame."

Let $\boldsymbol{R}_{AB}(t) \in SO(3)$ be a curve representing a trajectory of an object frame Σ_B, with origin at the origin of the frame Σ_A, rotating relative to the fixed frame Σ_A. An point q attached to the rigid body follows a path in spatial coordinates given by

$${}^A\boldsymbol{p}_q(t) = \boldsymbol{R}_{AB}(t)\,{}^B\boldsymbol{p}_q,$$

where the coordinates ${}^B\boldsymbol{p}_q$ are fixed in the body frame. The velocity of the point in Σ_A is

$$\begin{aligned} {}^A\boldsymbol{v}_q(t) := \frac{d}{dt}{}^A\boldsymbol{p}_q(t) &= \dot{\boldsymbol{R}}_{AB}(t)\,{}^B\boldsymbol{p}_q \\ &= \{\dot{\boldsymbol{R}}_{AB}(t)\boldsymbol{R}_{AB}^{\mathrm{T}}(t)\}\boldsymbol{R}_{AB}(t)\,{}^B\boldsymbol{p}_q \qquad \text{(A.15)} \\ &= \boldsymbol{R}_{AB}(t)\{\boldsymbol{R}_{AB}^{\mathrm{T}}(t)\dot{\boldsymbol{R}}_{AB}(t)\}\,{}^B\boldsymbol{p}_q. \qquad \text{(A.16)} \end{aligned}$$

Noting the structure of (A.8) and the fact such that the matrices $\dot{\boldsymbol{R}}_{AB}\boldsymbol{R}_{AB}^{\mathrm{T}}$ and $\boldsymbol{R}_{AB}^{\mathrm{T}}\dot{\boldsymbol{R}}_{AB}$ are skew-symmetric [6], we can rewrite (A.15) and (A.16) as

$$\begin{aligned} {}^A\boldsymbol{v}_q(t) &= (\boldsymbol{\omega}_{AB}^s)^\wedge \boldsymbol{R}_{AB}(t)\,{}^B\boldsymbol{p}_q = \boldsymbol{\omega}_{AB}^s \times {}^A\boldsymbol{p}_q(t) \qquad \text{(A.17)} \\ {}^B\boldsymbol{v}_q(t) &:= \boldsymbol{R}_{AB}^{\mathrm{T}}(t)\,{}^A\boldsymbol{v}_q(t) = (\boldsymbol{\omega}_{AB}^b)^\wedge\,{}^B\boldsymbol{p}_q = \boldsymbol{\omega}_{AB}^b \times {}^B\boldsymbol{p}_q, \qquad \text{(A.18)} \end{aligned}$$

where

$$\begin{aligned} (\boldsymbol{\omega}_{AB}^s)^\wedge &:= \dot{\boldsymbol{R}}_{AB}(t)\boldsymbol{R}_{AB}^{\mathrm{T}}(t) \qquad \text{(A.19)} \\ (\boldsymbol{\omega}_{AB}^b)^\wedge &:= \boldsymbol{R}_{AB}^{\mathrm{T}}(t)\dot{\boldsymbol{R}}_{AB}(t). \qquad \text{(A.20)} \end{aligned}$$

The vector $\boldsymbol{\omega}^s_{AB} \in \mathbb{R}^3$ is called the *instantaneous spatial angular velocity* which corresponds to the instantaneous angular velocity of the object as seen from the spatial coordinate frame. Similarly, the vector $\boldsymbol{\omega}^b_{AB} \in \mathbb{R}^3$ is called the *instantaneous body angular velocity* which corresponds to corresponds to the instantaneous angular velocity of the object as seen from the body coordinate frame.

For any rotation matrix $\boldsymbol{R} \in \mathbb{R}^{3\times3}$, and any vectors $\boldsymbol{v}, \boldsymbol{w} \in \mathbb{R}^3$, the following properties hold:

$$\boldsymbol{R}(\boldsymbol{v} \times \boldsymbol{w}) = (\boldsymbol{R}\boldsymbol{v}) \times (\boldsymbol{R}\boldsymbol{w}) \tag{A.21}$$

$$\boldsymbol{R}(\boldsymbol{w})^\wedge \boldsymbol{R}^{\mathrm{T}} = (\boldsymbol{R}\boldsymbol{w})^\wedge. \tag{A.22}$$

A.3.3 Rigid body velocity

Consider a rigid body whose motion is given by $g_{AB}(t)$, a curve parameterized by time t in $SE(3)$:

$$\overline{\boldsymbol{g}}_{AB}(t) = \begin{bmatrix} \boldsymbol{R}_{AB}(t) & {}^A\boldsymbol{p}_B(t) \\ \boldsymbol{0}_{1\times3} & 1 \end{bmatrix}.$$

Analogous to (A.19) and (A.20), the following twists is obtained:

$$\widehat{\boldsymbol{V}}^s_{AB} := \dot{\overline{\boldsymbol{g}}}_{AB}\overline{\boldsymbol{g}}^{-1}_{AB} = \begin{bmatrix} (\boldsymbol{\omega}^s_{AB})^\wedge & -(\boldsymbol{\omega}^s_{AB})^\wedge {}^A\boldsymbol{p}_B + {}^A\dot{\boldsymbol{p}}_B \\ \boldsymbol{0}_{1\times3} & 0 \end{bmatrix} \tag{A.23}$$

$$\widehat{\boldsymbol{V}}^b_{AB} := \overline{\boldsymbol{g}}^{-1}_{AB}\dot{\overline{\boldsymbol{g}}}_{AB} = \begin{bmatrix} (\boldsymbol{\omega}^b_{AB})^\wedge & \boldsymbol{R}^{\mathrm{T}}_{AB}{}^A\dot{\boldsymbol{p}}_B \\ \boldsymbol{0}_{1\times3} & 0 \end{bmatrix}. \tag{A.24}$$

From these twists, we define the *spatial velocity* $\boldsymbol{V}^s_{AB} \in \mathbb{R}^6$ and the *body velocity* $\boldsymbol{V}^b_{AB} \in \mathbb{R}^6$ given by

$$\boldsymbol{V}^s_{AB} = \begin{bmatrix} \boldsymbol{v}^s_{AB} \\ \boldsymbol{\omega}^s_{AB} \end{bmatrix} := (\widehat{\boldsymbol{V}}^s_{AB})^\vee = \begin{bmatrix} -(\boldsymbol{\omega}^s_{AB})^\wedge {}^A\boldsymbol{p}_B + {}^A\dot{\boldsymbol{p}}_B \\ \boldsymbol{\omega}^s_{AB} \end{bmatrix} \tag{A.25}$$

$$\boldsymbol{V}^b_{AB} = \begin{bmatrix} \boldsymbol{v}^b_{AB} \\ \boldsymbol{\omega}^b_{AB} \end{bmatrix} := (\widehat{\boldsymbol{V}}^b_{AB})^\vee = \begin{bmatrix} \boldsymbol{R}^{\mathrm{T}}_{AB}{}^A\dot{\boldsymbol{p}}_B \\ \boldsymbol{\omega}^b_{AB} \end{bmatrix}. \tag{A.26}$$

The interpretation of the spatial velocity is that $\boldsymbol{v}^s_{AB}$ and $\boldsymbol{\omega}^s_{AB}$ are the translational velocity and angular velocity of the point q attached to the rigid body, expressed in Σ_A. On the other hand, the interpretation of the body velocity is that $\boldsymbol{v}^b_{AB}$ is the velocity of the origin of the body coordinate frame Σ_B relative to the spatial frame Σ_A as viewed in the current body frame and $\boldsymbol{\omega}^b_{AB}$ is the angular velocity of the body coordinate frame Σ_B relative to the spatial frame Σ_A as viewed in the current body frame. The relation between the spatial velocity and the body velocity is given by

$$\boldsymbol{V}^s_{AB} = \boldsymbol{Ad}_{g_{AB}}\boldsymbol{V}^b_{AB}, \tag{A.27}$$

where

$$\boldsymbol{Ad}_{g_{AB}} := \begin{bmatrix} \boldsymbol{R}_{AB} & {}^A\boldsymbol{p}^\wedge_B\boldsymbol{R}_{AB} \\ \boldsymbol{0}_{3\times3} & \boldsymbol{R}_{AB} \end{bmatrix} \in \mathbb{R}^{6\times6} \tag{A.28}$$

is referred to as the *adjoint transformation* associated with g. The adjoint transformation has the following properties:

$$\boldsymbol{Ad}^{-1}_g = \begin{bmatrix} \boldsymbol{R}^{\mathrm{T}} & -(\boldsymbol{R}^{\mathrm{T}}\boldsymbol{p})^\wedge\boldsymbol{R}^{\mathrm{T}} \\ \boldsymbol{0}_{3\times3} & \boldsymbol{R}^{\mathrm{T}} \end{bmatrix} = \begin{bmatrix} \boldsymbol{R}^{\mathrm{T}} & -\boldsymbol{R}^{\mathrm{T}}\boldsymbol{p}^\wedge \\ \boldsymbol{0}_{3\times3} & \boldsymbol{R}^{\mathrm{T}} \end{bmatrix} = \boldsymbol{Ad}_{g^{-1}} \tag{A.29}$$

$$\boldsymbol{Ad}_{g_{AB}}\boldsymbol{Ad}_{g_{BC}} = \boldsymbol{Ad}_{g_{AC}}. \tag{A.30}$$

A seemingly natural way of representing the velocity of the rigid body is to use ${}^{A}\dot{\boldsymbol{p}}_{AB}$ to represent the linear velocity and $\boldsymbol{\omega}^{s}_{AB}$ to represent the angular velocity. The pair

$$\boldsymbol{V}^{h}_{AB} := \begin{bmatrix} {}^{A}\dot{\boldsymbol{p}}_{B} \\ \boldsymbol{\omega}^{s}_{AB} \end{bmatrix} \in \mathbb{R}^6 \tag{A.31}$$

is called the *hybrid velocity* of the rigid body. The hybrid velocity is related to the body velocity by the relationship:

$$\boldsymbol{V}^{h}_{AB} = \begin{bmatrix} \boldsymbol{R}_{AB} & \boldsymbol{0}_{3\times3} \\ \boldsymbol{0}_{3\times3} & \boldsymbol{R}_{AB} \end{bmatrix} \boldsymbol{V}^{b}_{AB}. \tag{A.32}$$

A.3.4 Coordinate transformations

Consider the motion of three coordinate frames Σ_A, Σ_B and Σ_C. Then, for the spatial velocities, the body velocities and the hybrid velocities the following relations exists:

$$\boldsymbol{V}^{s}_{AC} = \boldsymbol{V}^{s}_{AB} + \boldsymbol{Ad}_{g_{AB}}\boldsymbol{V}^{s}_{BC} \tag{A.33}$$

$$\boldsymbol{V}^{b}_{AC} = \boldsymbol{Ad}_{g^{-1}_{BC}}\boldsymbol{V}^{b}_{AB} + \boldsymbol{V}^{b}_{BC} \tag{A.34}$$

$$\boldsymbol{V}^{h}_{AC} = \boldsymbol{Ad}_{(-R_{AB}{}^{B}p_{BC})}\boldsymbol{V}^{h}_{AB} + \boldsymbol{Ad}_{R_{AB}}\boldsymbol{V}^{h}_{BC}, \tag{A.35}$$

where

$$\boldsymbol{Ad}_{p} := \begin{bmatrix} \boldsymbol{I}_3 & -\boldsymbol{p}^{\wedge} \\ \boldsymbol{0}_{3\times3} & \boldsymbol{I}_3 \end{bmatrix} \tag{A.36}$$

$$\boldsymbol{Ad}_{R} := \begin{bmatrix} \boldsymbol{R} & \boldsymbol{0}_{3\times3} \\ \boldsymbol{0}_{3\times3} & \boldsymbol{R} \end{bmatrix}. \tag{A.37}$$

The transformation $\boldsymbol{Ad}_{p}$ denotes the adjoint map corresponding to a pure translation by $\boldsymbol{p}$ and $\boldsymbol{Ad}_{p}$ denotes the adjoint map corresponding to a pure rotation.

A.4 Wrenches and Transformations

A.4.1 Wrenches

A generalized force acting on a rigid body consists of a linear component (pure force) and an angular component (pure moment) acting at a point. We can represent this generalized force as a vector in $\mathbb{R}^6$:

$$\boldsymbol{F} = \begin{bmatrix} \boldsymbol{f} \\ \boldsymbol{\tau} \end{bmatrix} \in \mathbb{R}^6, \tag{A.38}$$

where $\boldsymbol{f} \in \mathbb{R}^3$ is a linear component and $\boldsymbol{\tau} \in \mathbb{R}^3$ is a rotational component. We will refer to a force/moment pair as a *wrench*.

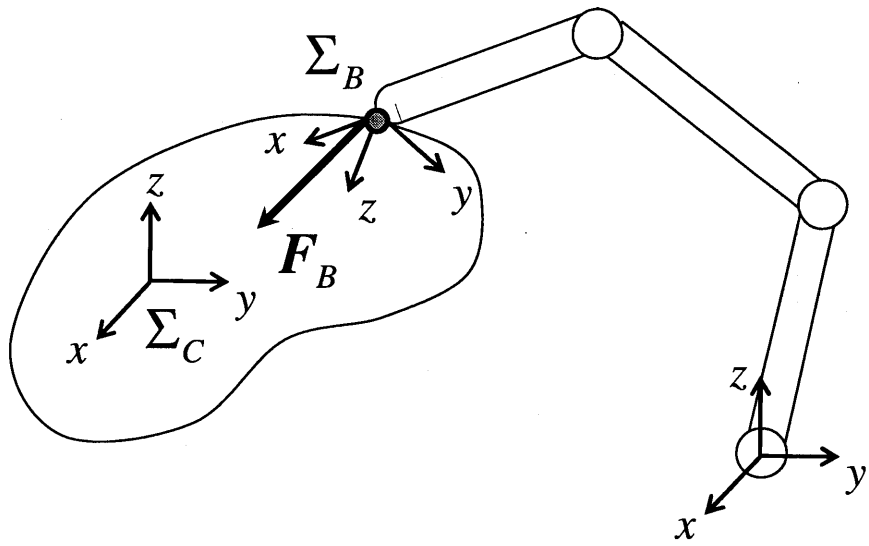

Figure A.3 Transformation of wrenches between coordinate frames.

A.4.2 Transformations

Consider the motion of a rigid body parameterized by $g_{AB}(t)$, where Σ_A is an inertial frame and Σ_B is a frame attached to the rigid body. Let $\boldsymbol{F}_B$ represent a wrench applied at the origin of Σ_B expressed in Σ_B and let $\boldsymbol{V}^b_{AB}$ represent the instantaneous body velocity of the rigid body. Both of these quantities are represented relative to Σ_B and their dot product is the infinitesimal work:

$$\delta W = \boldsymbol{V}^b_{AB} \cdot \boldsymbol{F}_B. \tag{A.39}$$

Two wrenches are said to be *equivalent* if they generate the same work for every possible rigid body motion. *Equivalent wrenches* can be used to rewrite a given wrench in terms of a wrench applied at a different point and with respect to a different coordinate frame. Figure A.3 shows that a manipulator pushes at a point on a rigid body. Σ_A and Σ_C are the fixed frames to the manipulator and the rigid body respectively and Σ_B is attached to the contact point. Let $g_{BC} = ({}^B\boldsymbol{p}_{BC}, \boldsymbol{R}_{BC})$ be the configuration of Σ_C relative to Σ_B. By equating the instantaneous work done by the wrenches $\boldsymbol{F}_B$ and $\boldsymbol{F}_C$, we have that

$$\boldsymbol{V}^b_{AC} \cdot \boldsymbol{F}_C = \boldsymbol{V}^b_{AB} \cdot \boldsymbol{F}_B = \left(\boldsymbol{Ad}_{g_{BC}} \boldsymbol{V}^b_{AC}\right)^{\mathrm{T}} \cdot \boldsymbol{F}_B = \boldsymbol{V}^b_{AC} \cdot \boldsymbol{Ad}^{\mathrm{T}}_{g_{BC}} \boldsymbol{F}_B, \tag{A.40}$$

where $\boldsymbol{V}^b_{AB} = \boldsymbol{Ad}_{g_{BC}} \boldsymbol{V}^b_{AC}$ from (A.34) and $\boldsymbol{V}^b_{CB} = 0$. Since $\boldsymbol{V}^b_{AC}$ is free, the following transformation is obtained:

$$\boldsymbol{F}_C = \boldsymbol{Ad}^{\mathrm{T}}_{g_{BC}} \boldsymbol{F}_B. \tag{A.41}$$

Eq. (A.41) transforms a wrench applied at the origin of Σ_B into an equivalent wrench applied at the origin of Σ_C. Expanding (A.41) leads to

$$\begin{bmatrix} \boldsymbol{f}_C \\ \boldsymbol{\tau}_C \end{bmatrix} = \begin{bmatrix} \boldsymbol{R}^{\mathrm{T}}_{BC} & 0_{3\times 3} \\ -\boldsymbol{R}^{\mathrm{T}}_{BC} {}^B\boldsymbol{p}^{\wedge}_C & \boldsymbol{R}^{\mathrm{T}}_{BC} \end{bmatrix} \begin{bmatrix} \boldsymbol{f}_B \\ \boldsymbol{\tau}_B \end{bmatrix} = \begin{bmatrix} \boldsymbol{R}^{\mathrm{T}}_{BC} \boldsymbol{f}_B \\ -\boldsymbol{R}^{\mathrm{T}}_{BC} {}^B\boldsymbol{p}^{\wedge}_C \boldsymbol{f}_B + \boldsymbol{R}^{\mathrm{T}}_{BC} \boldsymbol{\tau}_B \end{bmatrix}. \tag{A.42}$$

We see that the adjoint transformation rotates the force and torque vectors from Σ_B into Σ_C and includes an additional torque of the form $-{}^B\boldsymbol{p}_{BC} \times \boldsymbol{f}_B$, which is the torque generated by applying a fore $\boldsymbol{f}_B$ at a distance $-{}^B\boldsymbol{p}_{BC}$.

A.4.3 Wrench representations

A net wrench $\boldsymbol{F}_B$ acting on the rigid body has three natural representations. The *body* representation of the wrench is written as $\boldsymbol{F}_B^b$ and represents the equivalent force and moment applied at the origin of the Σ_B, which is expressed in Σ_B. The *spatial* representation of the wrench is written as $\boldsymbol{F}_B^s$ and is the equivalent wrench expressed in Σ_A. The *hybrid* representation of the wrench is written as $\boldsymbol{F}_B^h$ and represents the equivalent force and moment applied at the origin of the Σ_B, which is expressed in Σ_A. Analogous to (A.40) and by using the relations (A.27) and (A.32), the relations between these wrenches are given by

$$\boldsymbol{F}^b = \boldsymbol{Ad}_g^{\mathrm{T}} \boldsymbol{F}^s = \boldsymbol{Ad}_R^{\mathrm{T}} \boldsymbol{F}^h. \tag{A.43}$$

Appendix B

Contact Kinematics

In this appendix, we show the surface parametrizations and the kinematic equations for one object rolling and/or sliding along another.

B.1 Surface Models

We begin with a brief description of the *surface parametrizations*. Given an object in $\mathbb{R}^3$, the surface of the object is described by using a *local coordinate chart*,

$$\boldsymbol{c} : U \subset \mathbb{R}^2 \mapsto \mathbb{R}^3, \tag{B.1}$$

as shown in Figure B.1. The map $\boldsymbol{c}$ takes a point $\boldsymbol{\alpha} = [\ u\ \ v\ ]^{\mathrm{T}} \in U \subset \mathbb{R}^2$ to a point $\boldsymbol{p} \in \mathbb{R}^3$ on the surface of the object expressed in the object frame, as in the following:

$$\boldsymbol{p} = \boldsymbol{c}(\boldsymbol{\alpha}). \tag{B.2}$$

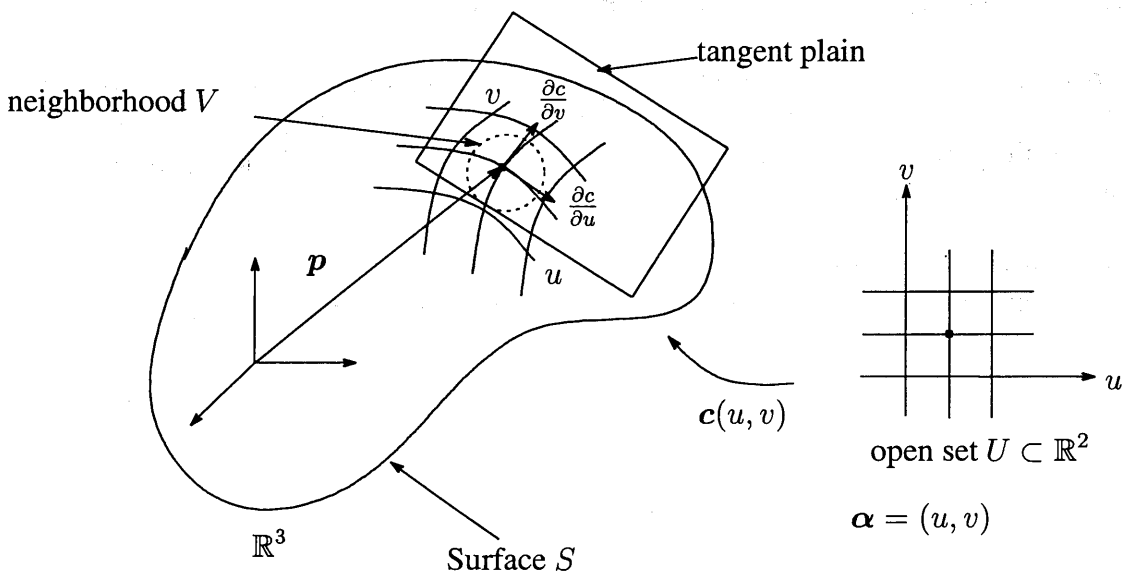

Figure B.1 Surface chart for a two-dimensional object in $\mathbb{R}^3$.

In general, it may take several coordinate charts to completely describe the surface of the object. A property of a surface is *regular* described by the following definition:

Definition B.1 (Regular surfaces).
A surface S is *regular* if for each point $\boldsymbol{p} \in S$ there exists a neighborhood $V \subset \mathbb{R}^3$, an open set $U \subset \mathbb{R}^2$, and a map $\boldsymbol{c} : U \mapsto V \cap S$ such that

1. $\boldsymbol{c}$ is differentiable.
2. $\boldsymbol{c}$ is a homeomorphism from U to $V \cap S$. That is, $\boldsymbol{c}$ is continuous, bijective (one-to-one and onto), has a continuous inverse.
3. For every $\boldsymbol{\alpha} = [\, u \;\; v \,]^{\mathrm{T}} \in U$, the map $\dfrac{\partial \boldsymbol{c}}{\partial \boldsymbol{\alpha}}(\boldsymbol{\alpha}) : \mathbb{R}^2 \mapsto \mathbb{R}^3$ is injective (one-to-one).

At any point on the object, we can define the *tangent plane* which consists of the space of all vectors which are tangent to the surface of the object at that point.

Definition B.2 (Tangent planes).
The *tangent plane* at a point $\boldsymbol{c}(\boldsymbol{\alpha})$ on a surface of an object is spanned by the vectors $\boldsymbol{c}_u := \dfrac{\partial \boldsymbol{c}}{\partial u}(\boldsymbol{\alpha})$ and $\boldsymbol{c}_v := \dfrac{\partial \boldsymbol{c}}{\partial v}(\boldsymbol{\alpha})$.

A coordinate chart is an *orthogonal coordinate chart* if $\boldsymbol{c}_u$ and $\boldsymbol{c}_v$ are orthogonal.

Theorem B.1 (Orthogonal coordinate charts).
Locally, there exists an orthogonal chart for all regular surfaces.

In the following, local coordinate charts are assumed to be orthogonal.

B.2 Evolution of Contact Frames

Let $\boldsymbol{p}(t) \in S$ be a curve on a surface of a object and $\boldsymbol{p}$ is parametrized by a local coordinate chart $\boldsymbol{c} : U \subset \mathbb{R}^2 \mapsto \mathbb{R}^3$ and local coordinates $\boldsymbol{\alpha} = [\, u \;\; v \,]^{\mathrm{T}} \in U \subset \mathbb{R}^2$, i.e., $\boldsymbol{p} = \boldsymbol{c}(\boldsymbol{\alpha})$. For the orthogonal coordinate chart $\boldsymbol{c}$, the *normalized Gauss frame* is described by the following definition.

Definition B.3 (Normalized Gauss frames).
For an orthogonal coordinate chart $\boldsymbol{c}$, the *normalized Gauss frame* is defined by

$$[\boldsymbol{x} \;\; \boldsymbol{y} \;\; \boldsymbol{z}] := \left[\frac{\boldsymbol{c}_u}{\|\boldsymbol{c}_u\|} \;\; \frac{\boldsymbol{c}_v}{\|\boldsymbol{c}_v\|} \;\; \boldsymbol{n} \right], \tag{B.3}$$

where

$$\boldsymbol{c}_u := \frac{\partial \boldsymbol{c}}{\partial \boldsymbol{u}}, \;\; \boldsymbol{c}_v := \frac{\partial \boldsymbol{c}}{\partial \boldsymbol{v}}, \;\; \boldsymbol{n} := \boldsymbol{N}(u, v) = \frac{\boldsymbol{c}_u \times \boldsymbol{c}_v}{\|\boldsymbol{c}_u \times \boldsymbol{c}_v\|}. \tag{B.4}$$

The map $\boldsymbol{N} : S \mapsto \mathbb{S}^2$ is *Gauss map*, which gives the unit normal at each point on the surface S.

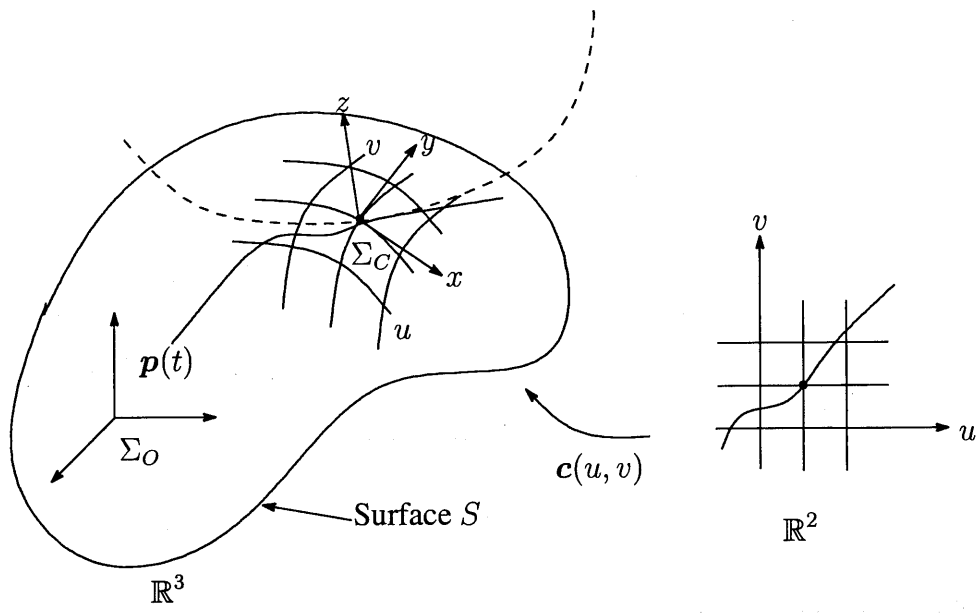

Figure B.2 The contact frame is a moving frame along a curve $p(t)$.

The normal Gauss frame provides an orthogonal frame at each point on the surface. By using the normalized Gauss frame, for a curve $\boldsymbol{p}(t)$, the *contact frame* is described by the following definition as shown in Figure B.2.

Definition B.4 (Contact frames).
For a curve $\boldsymbol{p}(t)$, the *contact frame* along the curve is defined by the frame Σ_C which coincides with the normalized Gauss frame at time t.

To determine the motion of the contact frame, we will use the following *geometric parameters* of the surface:

$$\boldsymbol{M}_g := \begin{bmatrix} \|\boldsymbol{c}_u\| & 0 \\ 0 & \|\boldsymbol{c}_v\| \end{bmatrix} \in \mathbb{R}^{2\times 2} \tag{B.5}$$

$$\boldsymbol{K}_g := \begin{bmatrix} \boldsymbol{x}^{\mathrm{T}} \\ \boldsymbol{y}^{\mathrm{T}} \end{bmatrix} \begin{bmatrix} \dfrac{\boldsymbol{n}_u}{\|\boldsymbol{c}_u\|} & \dfrac{\boldsymbol{n}_v}{\|\boldsymbol{c}_v\|} \end{bmatrix} = \begin{bmatrix} \dfrac{\boldsymbol{c}_u^{\mathrm{T}}\boldsymbol{n}_u}{\|\boldsymbol{c}_u\|^2} & \dfrac{\boldsymbol{c}_u^{\mathrm{T}}\boldsymbol{n}_v}{\|\boldsymbol{c}_u\|\|\boldsymbol{c}_v\|} \\ \dfrac{\boldsymbol{c}_v^{\mathrm{T}}\boldsymbol{n}_u}{\|\boldsymbol{c}_u\|\|\boldsymbol{c}_v\|} & \dfrac{\boldsymbol{c}_v^{\mathrm{T}}\boldsymbol{n}_v}{\|\boldsymbol{c}_v\|^2} \end{bmatrix} \in \mathbb{R}^{2\times 2} \tag{B.6}$$

$$\boldsymbol{T}_g := \boldsymbol{y}^{\mathrm{T}} \begin{bmatrix} \dfrac{\boldsymbol{x}_u}{\|\boldsymbol{c}_u\|} & \dfrac{\boldsymbol{x}_v}{\|\boldsymbol{c}_v\|} \end{bmatrix} = \begin{bmatrix} \dfrac{\boldsymbol{c}_v^{\mathrm{T}}\boldsymbol{c}_{uu}}{\|\boldsymbol{c}_u\|^2\|\boldsymbol{c}_v\|} & \dfrac{\boldsymbol{c}_v^{\mathrm{T}}\boldsymbol{c}_{uv}}{\|\boldsymbol{c}_u\|\|\boldsymbol{c}_v\|^2} \end{bmatrix} \in \mathbb{R}^{1\times 2}, \tag{B.7}$$

which are the *metric tensor*, the *curvature tensor* and the *torsion form* respectively. The metric tensor is used to normalize tangent vectors. The curvature tensor is a measure of how the unit normal varies across the surface, as projected on the tangent plane. The torsion form is a measure of how the Gauss frame twists as we move across the surface, again projected onto the tangent plane. These parameters describe the local geometry of the surface and play an important role in the kinematics of the contact frame.

The motion of the contact frame is determined as a function of the geometric parameters and

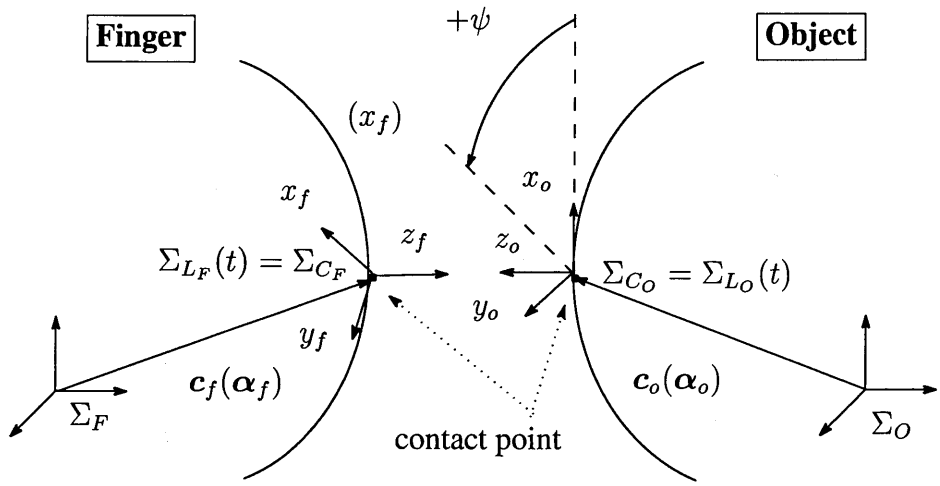

Figure B.3 Contact coordinates.

the velocity of the curve. The motion of the contact frame Σ_C relative to the object frame Σ_O is given by the following lemma.

Lemma B.1 (Induced velocity of the contact frame).
The body velocity of the contact frame Σ_C relative to the reference frame Σ_O of the object is given by $\boldsymbol{V}_{OC}^b = (\boldsymbol{v}_{OC}^b, \boldsymbol{\omega}_{OC}^b)$ where

$$\boldsymbol{v}_{OC}^b = \begin{bmatrix} \boldsymbol{M}_g \dot{\boldsymbol{\alpha}} \\ 0 \end{bmatrix} \tag{B.8}$$

$$\boldsymbol{\omega}_{OC}^b = \begin{bmatrix} \boldsymbol{E}\boldsymbol{K}_g\boldsymbol{M}_g\dot{\boldsymbol{\alpha}} \\ \boldsymbol{T}_g\boldsymbol{M}_g\dot{\boldsymbol{\alpha}} \end{bmatrix}, \quad \boldsymbol{E} := \begin{bmatrix} 0 & -1 \\ 1 & 0 \end{bmatrix}, \tag{B.9}$$

and $\boldsymbol{M}_g$, $\boldsymbol{K}_g$ and $\boldsymbol{T}_g$ are the geometric parameters of the surface relative to the coordinate chart $(\boldsymbol{c}, U)$.

B.3 Contact Kinematics

Consider a finger with a surface S_F and an object with a surface S_O which are touching at a point as shown in Figure B.3, where the finger and the object are depicted separately. Σ_F and Σ_O are the reference frames fixed to the finger and the object respectively. Let $\boldsymbol{p}_f(t) \in S_f$ and $\boldsymbol{p}_o(t) \in S_o$ be the positions at time t of the point of contact relative to Σ_F and Σ_O respectively. Σ_{C_F} and Σ_{C_O} are the contact frames for the curves $\boldsymbol{p}_f(t)$ and $\boldsymbol{p}_o(t)$. Let $(\boldsymbol{c}_f, U_f)$ and $(\boldsymbol{c}_o, U_o)$ be charts for the two surfaces, and $\boldsymbol{\alpha}_f = \boldsymbol{c}_f^{-1}(\boldsymbol{p}_f) \in U_f$ and $\boldsymbol{\alpha}_o = \boldsymbol{c}_o^{-1}(\boldsymbol{p}_o) \in U_o$ be local coordinates. Let ψ be the angle between the x-axes of Σ_{C_F} and Σ_{C_O} as shown in Figure B.3, then the configuration of the contact points is described by

$$\boldsymbol{\eta} := \begin{bmatrix} \boldsymbol{\alpha}_f \\ \boldsymbol{\alpha}_o \\ \psi \end{bmatrix} \in \mathbb{R}^5, \tag{B.10}$$

which is called the *contact coordinates* for the contact point. From the definition of ψ, the rotation matrix of the x- and y-axes of Σ_{C_F} relative to the x- and y-axes of Σ_{C_O} is given by

$$\boldsymbol{R}_\psi := \begin{bmatrix} \cos\psi & -\sin\psi \\ -\sin\psi & -\cos\psi \end{bmatrix}. \tag{B.11}$$

Furthermore, let $(\boldsymbol{M}_{gf}, \boldsymbol{K}_{gf}, \boldsymbol{T}_{gf})$ and $(\boldsymbol{M}_{go}, \boldsymbol{K}_{go}, \boldsymbol{T}_{go})$ to be the geometric parameters of the finger and the object respectively.

Here, we derive the relationship between the relative configuration $g_{OF} \in SE(3)$ and the contact coordinates $\boldsymbol{\eta} \in \mathbb{R}^5$. To do so, we assume that $g_{OF} \in W \subset SE(3)$, where W is the set of all relative configurations for which the finger and the object are in contact (in the latter paragraph, this is described by $v_{Cz} = 0$). For $g_{OF} \in W$ and $\boldsymbol{\eta}$, the following proposition holds.

Proposition B.1.
There is a smooth local bijection between $\boldsymbol{\eta} \in \mathbb{R}^5$ and $g_{OF} \in W \subset SE(3)$ if and only if

$$\boldsymbol{K}_R := \boldsymbol{K}_{gf} + \boldsymbol{R}_\psi \boldsymbol{K}_{go} \boldsymbol{R}_\psi^{\mathrm{T}} \tag{B.12}$$

is full rank.

$\boldsymbol{K}_R \in \mathbb{R}^{2\times 2}$ is called the *relative curvature form.*

To describe the motion of Σ_O and Σ_F at time t, we use a *continuous family of coordinate frames* defined as follows:

Definition B.5 (Continuous family of coordinate frames).
The *local coordinate frames* $\Sigma_{L_F}(\tau)$ and $\Sigma_{L_O}(\tau)$ are defined by the coordinate frames fixed relative to Σ_F and Σ_O, respectively, which coincide at time $t = \tau$ with normalized Gauss frame at $\boldsymbol{p}_f$ and $\boldsymbol{p}_o$.

Note that the local coordinate frames $\Sigma_{L_F}(\tau)$ and $\Sigma_{L_O}(\tau)$ which coincide at time $t = \tau$ with Σ_{C_F} and Σ_{C_O}.

To represent the contact motion, we use the body velocity $\boldsymbol{V}_C \in \mathbb{R}^6$ defined by

$$\boldsymbol{V}_C = \begin{bmatrix} v_{Cx} \\ v_{Cy} \\ \hline v_{Cz} \\ \omega_{Cx} \\ \omega_{Cy} \\ \omega_{Cz} \end{bmatrix} := \boldsymbol{V}^b_{L_O L_F}. \tag{B.13}$$

$(\omega_{Cx}, \omega_{Cy})$ are the *rolling velocities* along the tangent plane at the point of contact, and ω_{Cz} is the rotational velocity about the contact normal. Likewise, (v_{Cx}, v_{Cy}) are linear velocities along the tangent plane, i.e., the *sliding velocities*, and v_{Cz} is the linear velocity in the direction of the contact normal. As long as the two bodies remain in contact, $v_{Cz} = 0$. It is called the *pure rolling contact* that $v_{Cx} = v_{Cy} = v_{Cz} = 0$ and $\omega_{Cz} = 0$. On the other hand, it is called the *pure sliding contact* that $v_{Cz} = 0$ and $\omega_{Cx} = \omega_{Cy} = \omega_{Cz} = 0$.

The relationship between $\boldsymbol{V}_C$ and $\boldsymbol{\eta}$ is given by the following theorem [17]:

Theorem B.2 (Kinematic equations of contact).
The motion of the contact coordinates, $\dot{\eta}$, as a function of the relative motion is given by

$$\begin{aligned}
\dot{\alpha}_f &= M_{gf}^{-1} K_R^{-1} \left(\begin{bmatrix} -\omega_{Cy} \\ \omega_{Cx} \end{bmatrix} - R_\psi K_{go} R_\psi^{\mathrm{T}} \begin{bmatrix} v_{Cx} \\ v_{Cy} \end{bmatrix} \right) \\
\dot{\alpha}_o &= M_{go}^{-1} R_\psi K_R^{-1} \left(\begin{bmatrix} -\omega_{Cy} \\ \omega_{Cx} \end{bmatrix} + K_{gf} \begin{bmatrix} v_{Cx} \\ v_{Cy} \end{bmatrix} \right) \\
\dot{\psi} &= \omega_{Cz} + T_{gf} M_{gf} \dot{\alpha}_f + T_{go} M_{go} \dot{\alpha}_o \\
0 &= v_{Cz}.
\end{aligned} \tag{B.14}$$

B.4 Another Derivation of Contact Kinematics

In this section, we derive the contact kinematics by differentiating (2.18) and (2.19) with respect to time t.

Firstly, by using the relationships with respect to the velocities of (A.34), (A.30), (A.22), (A.32), (2.15) and (2.17), we calculate the relation between V_C and $(\dot{\theta}_F, \dot{x}_O)$ as follows:

$$\begin{aligned}
V_C = V_{L_O L_F}^b &= Ad_{g_{FL_F}^{-1}} V_{OF}^b \\
&= Ad_{g_{FL_F}^{-1}} (Ad_{g_{BF}^{-1}} V_{OB}^b + V_{BF}^b) \quad (\because V_{AB}^b = Ad_{g_{BC}^{-1}} V_{AB}^b + V_{BC}^b) \\
&= Ad_{g_{FL_F}^{-1}} (-Ad_{g_{BF}^{-1}} Ad_{g_{BO}} V_{BO}^b + V_{BF}^b) \quad (\because V_{AB}^b = -Ad_{g_{BA}} V_{BA}^b) \\
&= Ad_{g_{FL_F}^{-1}} V_{BF}^b - Ad_{g_{FL_F}^{-1}} Ad_{g_{BF}^{-1}} Ad_{g_{BO}} V_{BO}^b \\
&= Ad_{g_{FL_F}^{-1}} V_{BF}^b - Ad_{g_{L_O L_F}^{-1}} \underbrace{Ad_{g_{L_O L_F}} Ad_{g_{FL_F}^{-1}} Ad_{g_{BF}^{-1}} Ad_{g_{BO}}}_{Ad_{g_{L_O O}}} V_{BO}^b \\
&= Ad_{g_{FL_F}^{-1}} V_{BF}^b - Ad_{g_{L_O L_F}^{-1}} Ad_{g_{L_O O}} V_{BO}^b \\
&= Ad_{g_{FC_F}^{-1}} V_{BF}^b - Ad_{g_{C_O C_F}^{-1}} Ad_{g_{C_O O}} V_{BO}^b \\
&\quad (\because \Sigma_{C_F} = \Sigma_{L_F} \text{ and } \Sigma_{C_O} = \Sigma_{L_O} \text{ at time } t = \tau) \\
&= \begin{bmatrix} R_{FC_F}^{\mathrm{T}} & -R_{FC_F}^{\mathrm{T}} {}^F p_{C_F}^\wedge \\ 0_{3\times 3} & R_{FC_F}^{\mathrm{T}} \end{bmatrix} \begin{bmatrix} R_{BF}^{\mathrm{T}} & 0_{3\times 3} \\ 0_{3\times 3} & R_{BF}^{\mathrm{T}} \end{bmatrix} V_{BF}^h \\
&\quad - \begin{bmatrix} R_{C_O C_F}^{\mathrm{T}} & 0_{3\times 3} \\ 0_{3\times 3} & R_{C_O C_F}^{\mathrm{T}} \end{bmatrix} \begin{bmatrix} R_{OC_O}^{\mathrm{T}} & -R_{OC_O}^{\mathrm{T}} {}^O p_{C_O}^\wedge \\ 0_{3\times 3} & R_{OC_O}^{\mathrm{T}} \end{bmatrix} \begin{bmatrix} R_{BO}^{\mathrm{T}} & 0_{3\times 3} \\ 0_{3\times 3} & R_{BO}^{\mathrm{T}} \end{bmatrix} V_{BO}^h \\
&= \begin{bmatrix} R_{BC_F}^{\mathrm{T}} & -R_{BC_F}^{\mathrm{T}} R_{BF} {}^F p_{C_F}^\wedge R_{BF}^{\mathrm{T}} \\ 0_{3\times 3} & R_{BC_F}^{\mathrm{T}} \end{bmatrix} V_{BF}^h \\
&\quad - \begin{bmatrix} R_{BC_F}^{\mathrm{T}} & -R_{BC_F}^{\mathrm{T}} R_{BO} {}^F p_{C_O}^\wedge R_{BO}^{\mathrm{T}} \\ 0_{3\times 3} & R_{BC_F}^{\mathrm{T}} \end{bmatrix} V_{BO}^h \\
&= \begin{bmatrix} R_{BC_F}^{\mathrm{T}} & -R_{BC_F}^{\mathrm{T}} (R_{BF} {}^F p_{C_F})^\wedge \\ 0_{3\times 3} & R_{BC_F}^{\mathrm{T}} \end{bmatrix} J_F \dot{\theta}_F \\
&\quad - \begin{bmatrix} R_{BC_F}^{\mathrm{T}} & -R_{BC_F}^{\mathrm{T}} (R_{BO} {}^O p_{C_O})^\wedge \\ 0_{3\times 3} & R_{BC_F}^{\mathrm{T}} \end{bmatrix} T_O \dot{x}_O.
\end{aligned}$$

Therefore, we get the following relationship:

$$\boldsymbol{V}_{C_i} = \boldsymbol{D}_{J_{F_i}}(\boldsymbol{\theta}_{F_i}, \boldsymbol{\eta}_i)\dot{\boldsymbol{\theta}}_{F_i} - \boldsymbol{D}_{T_{O_i}}(\boldsymbol{x}_O, \boldsymbol{\eta}_i)\dot{\boldsymbol{x}}_O. \tag{B.15}$$

Secondly, differentiating (2.18) with respect to time t and using relation $\dot{\boldsymbol{R}} = (\boldsymbol{\omega}^s)^\wedge \boldsymbol{R}$ from (A.19) lead to

$${}^B\dot{\boldsymbol{p}}_F - (\boldsymbol{R}_{BF}{}^F\boldsymbol{p}_{C_F})^\wedge {}^B\boldsymbol{\omega}_F + \boldsymbol{R}_{BF}{}^F\dot{\boldsymbol{p}}_{C_F} = {}^B\dot{\boldsymbol{p}}_O - (\boldsymbol{R}_{BO}{}^F\boldsymbol{p}_{C_O})^\wedge {}^B\boldsymbol{\omega}_O + \boldsymbol{R}_{BO}{}^O\dot{\boldsymbol{p}}_{C_O}.$$

Premultiplying this equation by $\boldsymbol{R}_{BC_F}^{\mathrm{T}}$ and using (2.15) and (2.17) lead to

$$\begin{aligned}&\left[\, \boldsymbol{R}_{BC_F}^{\mathrm{T}} \quad -\boldsymbol{R}_{BC_F}^{\mathrm{T}}(\boldsymbol{R}_{BF}{}^F\boldsymbol{p}_{C_F})^\wedge \,\right] \boldsymbol{J}_F\dot{\boldsymbol{\theta}}_F - \left[\, \boldsymbol{R}_{BC_F}^{\mathrm{T}} \quad -\boldsymbol{R}_{BC_F}^{\mathrm{T}}(\boldsymbol{R}_{BO}{}^O\boldsymbol{p}_{C_O})^\wedge \,\right] \boldsymbol{T}_O\dot{\boldsymbol{x}}_O \\ &= \boldsymbol{R}_{C_OC_F}^{\mathrm{T}}\boldsymbol{R}_{OC_O}^{\mathrm{T}}{}^O\dot{\boldsymbol{p}}_{C_O} - \boldsymbol{R}_{FC_F}^{\mathrm{T}}{}^F\dot{\boldsymbol{p}}_{C_F}.\end{aligned}$$

From the definition of the body velocity (A.26) and the structure of (B.15), we get

$$\boldsymbol{v}_C = \boldsymbol{R}_{C_OC_F}^{\mathrm{T}}\boldsymbol{v}_{OC_O}^b - \boldsymbol{v}_{FC_F}^b, \tag{B.16}$$

where $\boldsymbol{v}_C \in \mathbb{R}^3$ is the linear component of $\boldsymbol{V}_C$. Furthermore, differentiating (2.19) with respect to time t and using relations $\dot{\boldsymbol{R}} = (\boldsymbol{\omega}^s)^\wedge \boldsymbol{R}$ from (A.19) and $\dot{\boldsymbol{R}} = \boldsymbol{R}(\boldsymbol{\omega}^b)^\wedge$ from (A.20) lead to

$$\begin{aligned}&({}^B\boldsymbol{\omega}_F)^\wedge \boldsymbol{R}_{BC_F} + \boldsymbol{R}_{BC_F}(\boldsymbol{\omega}_{FC_F}^b)^\wedge \\ &= ({}^B\boldsymbol{\omega}_O)^\wedge \boldsymbol{R}_{BC_F} + \boldsymbol{R}_{BC_F}\boldsymbol{R}_{C_OC_F}^{\mathrm{T}}(\boldsymbol{\omega}_{OC_O}^b)^\wedge \boldsymbol{R}_{C_OC_F} + \boldsymbol{R}_{BC_F}(\boldsymbol{\omega}_{C_OC_F}^b)^\wedge.\end{aligned}$$

Premultiplying this equation by $\boldsymbol{R}_{BC_F}^{\mathrm{T}}$ and using the relation $\boldsymbol{R}\boldsymbol{p}^\wedge\boldsymbol{R}^{\mathrm{T}} = (\boldsymbol{R}\boldsymbol{p})^\wedge$ from (A.22) lead to

$$(\boldsymbol{R}_{BC_F}{}^B\boldsymbol{\omega}_F)^\wedge + (\boldsymbol{\omega}_{FC_F}^b)^\wedge = (\boldsymbol{R}_{BC_F}{}^B\boldsymbol{\omega}_O)^\wedge + (\boldsymbol{R}_{C_OC_F}^{\mathrm{T}}\boldsymbol{\omega}_{OC_O}^b)^\wedge + (\boldsymbol{\omega}_{C_OC_F}^b)^\wedge.$$

From the definition of the body velocity (A.26) and the structure of (B.15), we get

$$\boldsymbol{\omega}_C = \boldsymbol{R}_{C_OC_F}^{\mathrm{T}}\boldsymbol{\omega}_{OC_O}^b - \boldsymbol{\omega}_{FC_F}^b + \boldsymbol{\omega}_{C_OC_F}^b, \tag{B.17}$$

where $\boldsymbol{\omega}_C \in \mathbb{R}^3$ is the rotational component of $\boldsymbol{V}_C$.

Finally, substituting (B.8) and (B.9) into (B.16) and (B.17), we get the motion of the contact coordinates $\dot{\boldsymbol{\eta}}$ as a function of the relative motion $\boldsymbol{V}_C$:

$$\dot{\boldsymbol{\eta}}_i = \boldsymbol{H}_i(\boldsymbol{\eta}_i)\boldsymbol{V}_{C_i} \tag{B.18}$$

$$0 = v_{Cz_i}, \tag{B.19}$$

where

$$\boldsymbol{H}_i := \left[\begin{array}{cc|cc} -\boldsymbol{M}_{gf_i}^{-1}\boldsymbol{K}_{R_i}^{-1}\tilde{\boldsymbol{K}}_{go_i} & \boldsymbol{0}_{2\times 1} & \boldsymbol{M}_{gf_i}^{-1}\boldsymbol{K}_{R_i}^{-1}\boldsymbol{E} & \boldsymbol{0}_{2\times 1} \\ \hline \boldsymbol{M}_{go_i}^{-1}\boldsymbol{R}_{\psi_i}\boldsymbol{K}_{R_i}^{-1}\boldsymbol{K}_{gf_i} & \boldsymbol{0}_{2\times 1} & \boldsymbol{M}_{go_i}^{-1}\boldsymbol{R}_{\psi_i}\boldsymbol{K}_{R_i}^{-1}\boldsymbol{E} & \boldsymbol{0}_{2\times 1} \\ \hline -\boldsymbol{T}_{gf_i}\boldsymbol{K}_{R_i}^{-1}\tilde{\boldsymbol{K}}_{go_i} & 0 & \boldsymbol{T}_{gf_i}\boldsymbol{K}_{R_i}^{-1}\boldsymbol{E} & 1 \\ +\boldsymbol{T}_{go_i}\boldsymbol{R}_{\psi_i}\boldsymbol{K}_{R_i}^{-1}\boldsymbol{K}_{gf_i} & & +\boldsymbol{T}_{go_i}\boldsymbol{R}_{\psi_i}\boldsymbol{K}_{R_i}^{-1}\boldsymbol{E} & \end{array}\right] \tag{B.20}$$

where

$$\tilde{\boldsymbol{K}}_{go_i} := \boldsymbol{R}_{\psi_i}\boldsymbol{K}_{go_i}\boldsymbol{R}_{\psi_i}. \tag{B.21}$$

Combining (B.15) and (B.18) leads to

$$\dot{\boldsymbol{\eta}}_i = \boldsymbol{H}_i(\boldsymbol{D}_{J_{F_i}}\dot{\boldsymbol{\theta}}_{F_i} - \boldsymbol{D}_{T_{O_i}}\dot{\boldsymbol{x}}_O). \tag{B.22}$$

B.5 Definition of Specular Images

Here, we show the definition of the specular image defined in Ref. [40]. See Ref. [40] for more precise definition of the specular image.

Consider a finger with a surface S_F and an object with a surface S_O which are touching at a point as shown in Figure B.3. Σ_F and Σ_O are the reference frames fixed to the finger and the object respectively. Let $\boldsymbol{p}_f(t) \in S_f$ and $\boldsymbol{p}_o(t) \in S_o$ be the positions at time t of the point of contact relative to Σ_F and Σ_O respectively. Σ_{C_F} and Σ_{C_O} are the contact frames for the curves $\boldsymbol{p}_f(t)$ and $\boldsymbol{p}_o(t)$. Let $(\boldsymbol{c}_f, U_f)$ and $(\boldsymbol{c}_o, U_o)$ be charts for the two surfaces, and $\boldsymbol{\alpha}_f = \boldsymbol{c}_f^{-1}(\boldsymbol{p}_f) \in U_f$ and $\boldsymbol{\alpha}_o = \boldsymbol{c}_o^{-1}(\boldsymbol{p}_o) \in U_o$ be local coordinates. Let $\overline{\boldsymbol{\alpha}}_f$ and $\overline{\boldsymbol{\alpha}}_o$ be the coordinates which correspond to the contact point.

For a local coordinate chart $\boldsymbol{c}$ with local coordinates $\boldsymbol{\alpha}$, we define the *symmetry* map $s : \mathbb{R}^3 \mapsto \mathbb{R}^3$

$$s \circ \boldsymbol{c}(\boldsymbol{\alpha}) = \hat{\Sigma}\boldsymbol{c}(\boldsymbol{\alpha}) + \hat{\boldsymbol{t}}, \tag{B.23}$$

where

$$\hat{\Sigma} := \hat{\boldsymbol{R}}\Sigma\hat{\boldsymbol{R}}^{\mathrm{T}} \in \mathbb{R}^{3\times 3} \tag{B.24}$$

$$\hat{\boldsymbol{t}} := -\hat{\boldsymbol{R}}(\Sigma - \boldsymbol{I}_3)\hat{\boldsymbol{R}}^{\mathrm{T}}\boldsymbol{c}(\boldsymbol{\alpha}) \in \mathbb{R}^3 \tag{B.25}$$

$$\Sigma := \begin{bmatrix} 1 & 0 & 0 \\ 0 & 1 & 0 \\ 0 & 0 & -1 \end{bmatrix} \tag{B.26}$$

$$\hat{\boldsymbol{R}} := \left[\frac{\boldsymbol{c}_u}{\|\boldsymbol{c}_u\|} \quad \frac{\boldsymbol{c}_v}{\|\boldsymbol{c}_v\|} \quad \boldsymbol{n} \right]_{\alpha=\overline{\alpha}}. \tag{B.27}$$

Note that $\hat{\Sigma}$ satisfies $\hat{\Sigma}\hat{\Sigma}^{\mathrm{T}} = \boldsymbol{I}_3$ and $\det(\hat{\Sigma}) = -1$.

Definition B.6 (Specular images).
A surface $\boldsymbol{c}_f(\boldsymbol{\alpha}_f)$ is said to be *specular image* of a surface $\boldsymbol{c}_o(\boldsymbol{\alpha}_o)$ at a point $\boldsymbol{c}_o(\overline{\boldsymbol{\alpha}}_o)$ if there exist a rigid motion $g = (\boldsymbol{R}, \boldsymbol{z})$, a symmetry $s = (\hat{\Sigma}, \hat{\boldsymbol{t}})$, and a diffeomorphism $\Phi : (x, y) \mapsto (u, v)$ such that

$$g \circ \boldsymbol{c}_f(\boldsymbol{\alpha}_f) = s \circ \boldsymbol{c}_o \circ \Phi(\boldsymbol{\alpha}_f). \tag{B.28}$$

Appendix C

Determination of Desired Internal Force

In this appendix, a method of the determination of the desired internal force is shown.

The condition such that the contact force at the ith contact point lie in the friction cone is the followings:

$$\frac{{}^C\boldsymbol{f}_{C_i}^{\mathrm{T}}\boldsymbol{n}_{C_i}}{\|{}^C\boldsymbol{f}_{C_i}\|} \geq \frac{1}{\sqrt{1+\mu^2}} \tag{C.1}$$

$${}^C\tau_{C_i} \leq \left({}^C\boldsymbol{f}_{C_i}^{\mathrm{T}}\boldsymbol{n}_{C_i}\right)\gamma, \tag{C.2}$$

where

$${}^C\boldsymbol{F}_{C_i} := \begin{bmatrix} {}^C\boldsymbol{f}_{C_i} \\ {}^C\tau_{C_i} \end{bmatrix} \in \mathbb{R}^4$$

and $\boldsymbol{n}_{C_i} := [\ 0\ \ 0\ \ 1\ ]^{\mathrm{T}}$ in the contact normal. The parameters μ and γ are the coefficient of friction and the coefficient of the torsional friction. From the expression of the internal force (3.29), the components of the contact force ${}^C\boldsymbol{f}_{C_i}$ and ${}^C\tau_{C_i}$ are rewritten as follows:

$${}^C\boldsymbol{f}_{C_i} = \boldsymbol{f}_{C_{O_i}} + f_{N_1}\boldsymbol{k}_{1f_i} + f_{N_2}\boldsymbol{k}_{2f_i}, \tag{C.3}$$

$${}^C\tau_{C_i} = \tau_{C_{O_i}} \qquad\qquad + f_{N_2}k_{2\tau_i}, \tag{C.4}$$

where

$$\begin{bmatrix} \boldsymbol{f}_{C_{O_1}} \\ \tau_{C_{O_1}} \\ \boldsymbol{f}_{C_{O_2}} \\ \tau_{C_{O_2}} \end{bmatrix} := (\boldsymbol{A}_O^{\mathrm{T}})^{+B}\boldsymbol{F}_O, \quad \begin{cases} \boldsymbol{k}_{1f_1} := \boldsymbol{R}_{BC_{F_1}}^{\mathrm{T}}\boldsymbol{e}_{12} \\ \boldsymbol{k}_{1f_2} := \boldsymbol{R}_{BC_{F_2}}^{\mathrm{T}}\boldsymbol{e}_{21} \end{cases}, \quad \begin{bmatrix} \boldsymbol{k}_{2f_1} \\ k_{2\tau_1} \\ \boldsymbol{k}_{2f_2} \\ k_{2\tau_2} \end{bmatrix} := \begin{bmatrix} \boldsymbol{R}_{BC_{F_1}}^{\mathrm{T}}({}^B\boldsymbol{p}_{C_{O_{12}}}^{\wedge})^{+}\boldsymbol{\tau}_N \\ \dfrac{1}{({}^B\boldsymbol{p}_{C_{O_{12}}})^{\mathrm{T}B}\boldsymbol{e}_{1z}} \\ -\boldsymbol{R}_{BC_{F_2}}^{\mathrm{T}}({}^B\boldsymbol{p}_{C_{O_{12}}}^{\wedge})^{+}\boldsymbol{\tau}_N \\ \dfrac{-1}{({}^B\boldsymbol{p}_{C_{O_{12}}})^{\mathrm{T}B}\boldsymbol{e}_{2z}} \end{bmatrix}.$$

Consider the desired magnitudes f_{N_1} and f_{N_2} of the internal force to satisfy (C.1) and (C.2). For the simplicity of the determination of f_{N_1} and f_{N_2}, we set the desired value of f_{N_2} to $f_{N_2} = 0$. Substituting (C.3) and (C.4) into (C.1) and (C.2) leads to

$$A_{2i}f_{N_1}^2 + 2A_{1i}f_{N_1} + A_{0i} \geq 0 \tag{C.5}$$

$$B_{1i}f_{N_1} + B_{0i} \geq 0, \tag{C.6}$$

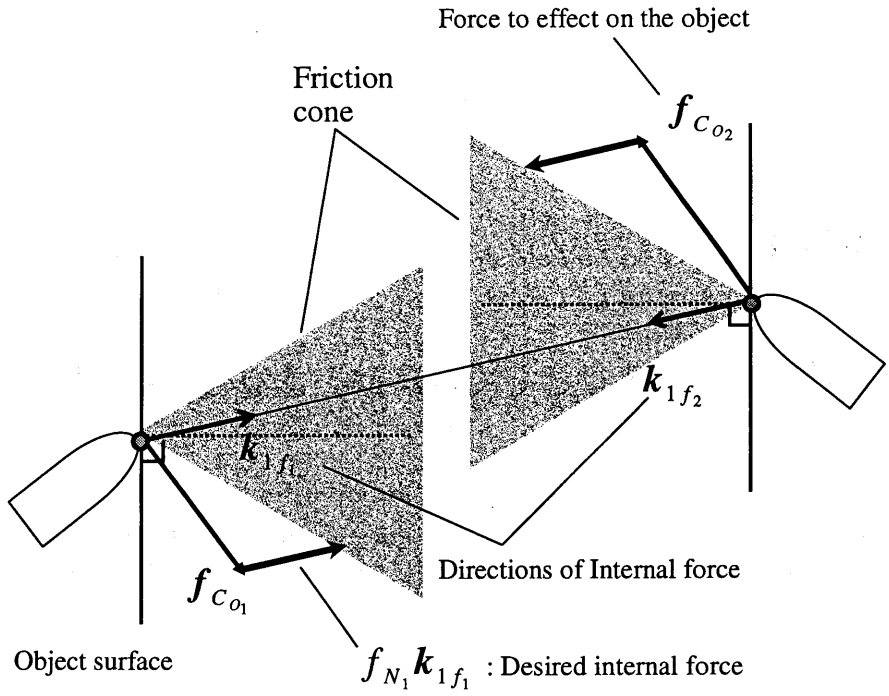

Figure C.1 Determination of a desired internal force.

where

$$\begin{cases} A_{2i} &= (1+\mu^2)(\boldsymbol{k}_{1f_i}^{\mathrm{T}}\boldsymbol{n}_{C_i})^2 - \boldsymbol{k}_{1f_i}^{\mathrm{T}}\boldsymbol{k}_{1f_i} \\ A_{1i} &= (1+\mu^2)(\boldsymbol{f}_{C_{O_i}}^{\mathrm{T}}\boldsymbol{n}_{C_i})(\boldsymbol{k}_{1f_i}^{\mathrm{T}}\boldsymbol{n}_{C_i}) - \boldsymbol{f}_{C_{O_i}}^{\mathrm{T}}\boldsymbol{k}_{1f_i} \\ A_{0i} &= (1+\mu^2)(\boldsymbol{f}_{C_{O_i}}^{\mathrm{T}}\boldsymbol{n}_{C_i})^2 - \boldsymbol{f}_{C_{O_i}}^{\mathrm{T}}\boldsymbol{f}_{C_{O_i}} \\ B_{1i} &= (\boldsymbol{k}_{1f_i}^{\mathrm{T}}\boldsymbol{n}_{C_i})\gamma \\ B_{0i} &= (\boldsymbol{f}_{C_{O_i}}^{\mathrm{T}}\boldsymbol{n}_{C_i})\gamma - \tau_{C_{O_i}}. \end{cases} \tag{C.7}$$

Since $\boldsymbol{f}_{C_{O_i}}^{\mathrm{T}}\boldsymbol{n}_{C_i} > 0$ from the fact such that the contact force is the pushing force, the solution of (C.6) is

$$f_{N_1} \geq -\frac{B_{0i}}{B_{1i}}. \tag{C.8}$$

On the other hand, the solution of (C.5) is

$$\begin{cases} f_{N_1} \leq \dfrac{-A_{1i} - \sqrt{A_{1i}^2 - A_{2i}A_{0i}}}{A_{2i}} \quad \text{or} \quad \dfrac{-A_{1i} + \sqrt{A_{1i}^2 - A_{2i}A_{0i}}}{A_{2i}} \leq f_{N_1} & (A_{2i} > 0) \\ \dfrac{-A_{1i} - \sqrt{A_{1i}^2 - A_{2i}A_{0i}}}{A_{2i}} \leq f_{N_1} \leq \dfrac{-A_{1i} + \sqrt{A_{1i}^2 - A_{2i}A_{0i}}}{A_{2i}} & (A_{2i} < 0) \end{cases}. \tag{C.9}$$

To satisfy the conditions (C.8) and (C.9), we determine f_{N_1} as a following method:

$$f_{N_1} = \max\left\{f_{N_1\mu}^{(1)}, f_{N_1\gamma}^{(1)}, f_{N_1\mu}^{(2)}, f_{N_1\gamma}^{(2)}\right\}, \tag{C.10}$$

where

$$f_{N_1\mu}^{(i)} := \frac{-A_{1i} + \sqrt{A_{1i}^2 - A_{2i}A_{0i}}}{A_{2i}}, \quad f_{N_1\gamma}^{(i)} := -\frac{B_{0i}}{B_{1i}}. \tag{C.11}$$

This determination is illustrated in Figure C.1. Note that $\boldsymbol{f}_{C_{O_i}} \in \mathbb{R}^3$ is the force which effects on the object motion, and $f_{N_1}\boldsymbol{k}_{1f_i} \in \mathbb{R}^3$ is a desired internal force. Since the summation of $\boldsymbol{f}_{C_{O_i}}$ and $f_{N_1}\boldsymbol{k}_{1f_i}$ is the net contact translational force at the i contact point, the magnitude f_{N_1} is determined such that the net translational forces ($i = 1, 2$) lie in the boundaries of the friction cone. In addition, f_{N_1} is determined such that the torques about the contact normals lie in the torsional friction cone, i.e., (C.8) is satisfied. Among all of the determinations, the maximum value is adopted.

Acknowledgements

This thesis is submitted for Doctor degree in Electric and Mechanical Engineering at Nagoya University, Japan. Dr. Yoshikazu HAYAKAWA, Professor of Nagoya University, was my supervisor. I would not have made this thesis without the help and support of a number of individuals. Here, I hope to give some recognition for their efforts on my behalf.

Firstly, I would like to express my deepest gratitude to Dr. Yoshikazu HAYAKAWA, for the supervision, his valuable discussions and technical advice throughout this work. He has shown great to tolerance and patience while guiding me into several interesting areas of research.

Secondly, I wish to express my acknowledge greatly to Dr. Shigeyuki HOSOE, Professor of Nagoya University, Dr. Sampei MITSUJI, Professor of Tokyo Institute of Technology, and Dr. Kenji FUJIMOTO, Associate Professor of Nagoya University. Their critical reading of the manuscript provides me with many valuable suggestions.

Thirdly, I would like to express my deepest gratitude to Dr. Kenji NAGASE, assistant professor of Nagoya University, for his enthusiastic and patient guidance throughout this work. His stimulating discussions, good advice, and valuable comment have enabled me to complete this thesis. Without his valuable advice and encouragement, this thesis would never be completed.

Fourthly, I would like to thank all the staff and students for Intelligent Mechatronics Laboratory of Nagoya University. Especially, I am grateful to Dr. Kazuya OGATA, my senior Shigenori SANO, my junior Masaki MITA, my junior Kousuke YOSHINAGA and my junior Kohnosuke SOBAJIMA.

Lastly, I am grateful to my parents Yasushi and Yoshiko NAKASHIMA and my big brother Tsuyoshi NAKASHIMA for their patient and warm encouragement.

December 2004,

Akira NAKASHIMA.

Bibliography

[1] T. Yoshikawa, "Dexterous mechanical hand," *Trans. RSJ*, vol. 18, no. 6, pp. 763–766, 2000. (in japanease).

[2] A. Bicchi, "Hands for dexterous manipulation and robust grasping: A difficult road toward simplicity," *IEEE Trans. Robot. Automat*, vol. 16, no. 6, pp. 652–662, 2000.

[3] A. M. Okamura, N. Smaby, and M. R. Cutkosky, "An overview of dexterous manipulation," in *Proc. IEEE Int. Conf. on Robot. Automat.*, pp. 255–262, 2000.

[4] A. Bicchi and V. Kumar, "Robotic grasping and contact: A review," in *Proc. IEEE Int. Conf. on Robot. Automat.*, pp. 348–353, 2000.

[5] T. Yoshikawa, "Foundations of grasp and manipulation (part: 1–3)," *Trans. RSJ*, vol. 13, no. 7–9, pp. 763–766, 1995. (in japanease).

[6] R. M. Murray, Z. Li, and S. S. Sastry, *A Mathematical Introduction to ROBOTIC MANIPULATION*. CRC Press, 1994.

[7] K. Mirza and D. E. Orin, "Control of force distribution for power grasp in the digits system," in *Proc. IEEE 29th CDC*, pp. 1960–1965, 1990.

[8] J. C. Trinkle, J. M. Abel, and R. P. Paul, "An investigation of frictionless enveloping grasping in the plane," *Int. J. Robot. Res.*, vol. 7, no. 3, pp. 33–51, 1987.

[9] J. K. Salisbury, "Whole-arm manipulation," in *Proc. IEEE Int. Symp. Robot. Res.*, MIT Press, 1987.

[10] H. Hanafusa and H. Asada, "Stable prehension by a robot hand with elastic fingers," in *Robot Motion Planning and Control* (M. Brady, ed.), pp. 323–336, MIT Press, 1982.

[11] K. Nagai and T. Yoshikawa, "Dynamic manipulation/grasping control of multifingered robot hands," in *Proc. IEEE Int. Conf. Robot. Automat.*, pp. 1027–1032, 1993.

[12] M. T. Manson and J. K. Salisbury, *Robot Hands and the Mechanics of Manipulation*. Cambridge, Mass: MIT Press, 1985.

[13] P. Tournassoud, T. Lozano-Perez, and E. Mazer, "Regrasping," in *Proc. IEEE Int. Conf. Robot. Automat.*, pp. 1924–1928, 1987.

[14] A. B. A. Cole, O. Hsu, and S. S. Sastry, "Dynamic control of sliding by robot hands for regrasping," *IEEE Trans. Robot. Automat.*, vol. 8, pp. 42–52, Feb. 1992.

[15] R. Fearing, "Simplified grasping and manipulation with dexterous robot hands," *IEEE J. Robot. Automat.*, vol. RA-2, pp. 188–195, Aug. 1986.

[16] L. Han and J. C. Trinkle, "Dexterous manipulation by rolling and finger gaiting," in *Proc. IEEE Int. Conf. Robot. Automat.*, pp. 730–735, 1998.

[17] D. J. Montana, "The kinematics of contact and grasp," *Int. J. Robot. Res.*, vol. 7, no. 3, pp. 17–32, 1988.

[18] C. Cai and B. Roth, "On the spatial motion of a rigid body with point contact," in *Proc. IEEE Int. Conf. Robot. Automat.*, pp. 686–695, 1987.

[19] K. Honda, T. Hasegawa, and T. Matsuoka, "Detection and measurement of fingertip slip in multi-fingered manipulation with rolling contact," *Trans. RSJ*, vol. 19, no. 7, pp. 913–919, 2001. (in japanease).

[20] X.-Z. Zheng, R. Nakashima, and T. Yoshikawa, "On dynamic control of finger sliding and object motion in manipulation with multifingered hands," *IEEE Trans. Robot. Automat.*, vol. 16, no. 5, pp. 469–481, 2000.

[21] A. B. A. Cole, J. E. Hauser, and S. S. Sastry, "Kinematics and control of multifingered hands with rolling contact," *IEEE Trans. Automat. Contr.*, vol. 34, no. 4, pp. 398–404, 1989.

[22] N. Sarkar, X. Yun, and V. Kumar, "Dynamic control of 3-d rolling contacts in two-arm manipulation," *IEEE Trans. Robot. Automat.*, vol. 13, no. 3, pp. 364–376, 1997.

[23] T. Schlegl, M. Buss, and G. Schmidt, "A hybrid systems approach toward modeling and dynamical simulation of dextrous manipulation," *IEEE Trans. Mechatronics*, vol. 8, no. 3, pp. 352–361, 2003.

[24] Y. Nakamura, "Nonholonomic robot system (part: 1–5)," *Trans. RSJ*, vol. 11–12, no. 4–7, 2, pp. 798–806, 1993–1994. (in japanease).

[25] M. Sampei, "Feedback control of nonholonomic systems," *J. SICE*, vol. 36, no. 6, pp. 396–403, 1997. (in japanease).

[26] M. Ishikawa, "Topology of symmetric affine nonholonomic systems," *SYSTEMS, CONTROL AND INFORMATION*, vol. 45, no. 9, pp. 536–543, 2001. (in japanease).

[27] I. Kolmanovsky and N. H. McClamrosh, "Developments in nonholonomic control problems," *IEEE Control Systems Magazine*, vol. 15, no. 6, pp. 20–36, 1995.

[28] R. W. Brockett, "Asymptotic stability and feedback stabilization," in *Differential Geometric Control Theory: Progress in Mathematics* (R. W. Brocket, R. Millman, and H. Sussman, eds.), vol. 27, pp. 181–208, Springer-Verlag, 1983.

[29] J. B. Pomet, "Explicit design of time-varying stabilizing control laws for a class of controllable systems without drift," *System & Control Letters*, vol. 18, pp. 147–158, 1992.

[30] A. Astolfi, "Discontinuous control of nonholonomic systems," *System & Control Letters*, vol. 27, pp. 37–45, 1996.

[31] M. Sampei, "A control strategy for a class of nonholonomic systems —time-state control form and its application—," in *Proc. IEEE 33rd CDC*, pp. 1120–1121, 1994.

[32] H. Kiyota and M. Sampei, "Stabilization of a class of nonholonomic systems without drift using time-state control form," *Trans. ISICE*, vol. 12, no. 11, pp. 647–654, 1999. (in japanease).

[33] G. A. Lafferriere and H. Sussmann, "A differential geometric approach to motion planning," in *Nonholonomic Motion Planning* (Z. Li and J. J. Canny, eds.), pp. 235–270, Kluwer, 1993.

[34] R. M. Murray and S. S. Sastry, "Nonholonomic motion planning: Steering using sinusoids," *IEEE Trans. Automat. Contr.*, vol. 38, no. 5, pp. 700–716, 1993.

[35] J. E. Marsden, "Lectures on mechanics," in *London Mathematical Society Lecture Notes Series*, vol. 174, Cambridge University Press, 1992.

[36] T. Urakubo, K. Tsuchiya, and K. Tsujita, "Lyapunov control of a class of non-holonomic systems," *Trans. SICE*, vol. 37, no. 11, pp. 1020–1025, 2001. (in japanease).

[37] H. Date, M. Sampei, M. Ishikawa, and M. Koga, "Simultaneous control of position and orientation for ball-plate manipulation problem based on time-state control form," *IEEE Trans. Robot. Automat.*, vol. 20, no. 3, pp. 465–479, 2004.

[38] A. Bicchi and R. Sorrentino, "Dextrous manipulation through rolling," in *Proc. IEEE Int. Conf. Robot. Automat.*, pp. 452–257, 1995.

[39] Z. Li and J. Canny, "Motion of two rigid bodies with rolling constraint," *IEEE Trans. Robot. Automat.*, vol. 6, no. 1, pp. 62–72, 1990.

[40] A. Marigo and A. Bicchi, "Rolling bodies with regular surface: Controllability theory and applications," *IEEE Trans. Automat. Contr.*, vol. 45, no. 9, pp. 1586–1599, 2000.

[41] A. Bicchi and A. Marigo, "Dextrous grippers: Putting nonholonomy to work for fine manipulation," *Int. J. Robot. Res.*, vol. 21, no. 5–6, pp. 427–442, 2002.

[42] A. Bicchi, Y. Chitour, and A. Marigo, "Reachability and steering of rolling polyhedra: A case study in discrete nonholonomy," *IEEE Trans. Automat. Contr.*, vol. 49, no. 5, pp. 710–726, 2004.

[43] K. Harada, T. Kawashima, and M. Kaneko, "Rolling based manipulation under neighborhood equilibrium," *Int. J. Robot. Res.*, vol. 21, no. 5–6, pp. 463–474, 2002.

[44] R. M. Murray and S. S. Sastry, "Grasping and manipulation using multifingered robot hands," in *Robotics: Proceedings of Symposia in Applied Mathematics* (R. W. Brockett, ed.), vol. 41, pp. 91–128, American Mathematical Society, 1990.

[45] A. Isidori, *Nonlinear Control Systems*. Springer-Verlag, 3 ed., 1995.

[46] T. Mita, *Introduction to Nonlinear Control Theory —Skill Control of Underactuated Robots—*. SOKODO, 2000. (in japanese).

[47] B. Kiss, J. Lévine, and B. Jantos, "On motion planning for robotic manipulation with permanent rolling contacts," *Int. J. Robot. Res.*, vol. 21, no. 5-6, pp. 443–461, 2002.

[48] A. Nakashima, K. Nagase, and Y. Hayakawa, "Control of grasping/manipulation of an object and contact points with rolling contact by two-fingered robot hand," *Trans. SICE*, vol. 40, no. 1, pp. 70–79, 2004. (in japanese).

[49] A. Nakashima, K. Nagase, and Y. Hayakawa, "Control of contact points by multi-fingered robot hand with manipulating an object," in *Proc. ICASE/SICE Joint Workshop*, (Muju Resort, Korea), pp. 120–125, 2002.

[50] A. Nakashima, K. Nagase, and Y. Hayakawa, "Grasping and manipulation of an object by two-fingered robot hand with rolling contact at the fingertip —control of the object and contact points by using the nonholonomy of the constraints—," in *Proc. SICE 2nd Annual Conference on Control Systems*, pp. 513–518, 2002. (in japanese).

[51] A. Nakashima, K. Nagase, Y. Hayakawa, and M. Mita, "Simultaneous control of grasp/manipulation and contact points of an object with rolling contact by two-fingered robot hand with constraint of degrees of freedom," *Trans. SICE*. Submitted. (in japanese).

[52] A. Nakashima, K. Nagase, and Y. Hayakawa, "Control of grasp/manipulation of an object with rolling contact by two-fingered robot hand with four joints," in *Int. Symp. on Micro-NanoMechatronics and Human Science*, (Nagoya Municipal Industrial Research Institute, Japan), 2004.

[53] A. Nakashima, K. Nagase, Y. Hayakawa, and M. Mita, "Simultaneous control of grasp/manipulation and contact points by finger-tips with constraint of degrees of freedom," in *Proc. SICE 33rd Control Theory Symposium*, pp. 39–44, 2004. (in japanese).

[54] A. Nakashima, K. Nagase, and Y. Hayakawa, "Simultaneous control of grasp/manipulation and contact points with rolling contact," in *16th IFAC World Congress*, (Praha, Czech Republic), 2005. Accepted.

[55] S. MacLane and G. Birkoff, *ALGEBRA*. London: Collier Macmillan, 1967.

[56] A. Nakashima, K. Nagase, and Y. Hayakawa, "Control of contact coordinates between a sphere and a plane with pure rolling contact by using iterative closed paths," *Trans. SICE*, vol. 40, no. 4, pp. 434–441, 2004. (in japanese).

[57] A. Nakashima, K. Nagase, and Y. Hayakawa, "Control of a contact point between a sphere and a plane with rolling contact by using finite iterations of a closed path," in *Proc. SICE 31st Control Theory Symposium*, pp. 25–30, 2002. (in japanease).

[58] A. Nakashima, K. Nagase, and Y. Hayakawa, "Control of contact coordinates of a sphere rolling on a plane with constraint on range of rolling motion," *Trans. SICE*, vol. 40, no. 1, pp. 1088–1097, 2004. (in japanease).

[59] A. Nakashima, K. Nagase, and Y. Hayakawa, "Control of contact coordinates of a sphere rolling on a plane with constraint on range of rolling motion," in *Proc. SICE 4th Annual Conference on Control Systems*, pp. 311–318, 2004. (in japanease).

[60] T. Yoshikawa, "Virtual truss model for characterization of internal forces for multiple finger grasps," in *Proc. IEEE Int. Conf. Robot. Automat.*, pp. 941–947, 1999.

[61] K. B. Shimoga and A. A. Goldenberg, "Soft robotic fingertips part i: A comparison of construction materials," *Int. J. Robot. Res.*, vol. 15, no. 4, pp. 320–334, 1996.

[62] S. Arimoto, P. T. A. Nguyen, H.-Y. Han, and Z. Doulgeri, "Dynamics and control of a set of dual fingers with soft tips," *Robotica*, vol. 18, pp. 71–80, 2000.

[63] S. Arimoto, Z. Doulgeri, P. T. A. Nguyen, and J. Fasoulas, "Stable pinching by a pair of robot fingers with soft tips under the effect of gravity," *Robotica*, vol. 20, pp. 241–249, 2002.

[64] K. Nagase, A. Nakashima, Y. Hayakawa, and K. Sobajima, "Control of grasping and manipulation of an object with soft finger-tips," *Trans. SICE*, vol. 40, no. 5, pp. 518–527, 2004. (in japanease).

[65] K. S. A. Nakashima, K. Nagase, and Y. Hayakawa, "Control of grasping and manipulation of an unknown object with soft finger-tips," in *Proc. SICE 3rd Annual Conference on Control Systems*, pp. 693–698, 2003. (in japanease).

[66] A. Bicchi, J. K. Salisbury, and D. L. Brock, "Contact sensing from force measurements," *Int. J. Robot. Res.*, vol. 12, pp. 249–262, 1993.

[67] M. H. Lee and H. R. Nicholls, "Tactile sensing for mechatronics— a state of the art survey," *Mechatronics*, vol. 9, pp. 1–31, 1999.

[68] B. K. Ghosh, N. Xi, and T. J. Tarn, *Control in Robotics and Automation Sensor-Based Integration*. ACADEMIC PRESS, 1999.

[69] K. Osuka, "Control system design theory for mechanical systems," *J. SICE*, vol. 40, no. 6, pp. 403–410, 2001. (in japanease).

Published Papers

Most parts of this research have been either published as journal or conference papers, or submitted as journal. A list is given below.

Chapter 3

[48] A. Nakashima, K. Nagase, and Y. Hayakawa, "Control of grasping/manipulation of an object and contact points with rolling contact by two-fingered robot hand," *Trans. SICE*, vol. 40, no. 1, pp. 70–79, 2004. (in japanease).

[49] A. Nakashima, K. Nagase, and Y. Hayakawa, "Control of contact points by multi-fingered robot hand with manipulating an object," in *Proc. ICASE/SICE Joint Workshop*, Muju Resort, Korea, pp. 120–125, 2002.

[50] A. Nakashima, K. Nagase, and Y. Hayakawa, "Grasping and manipulation of an object by two-fingered robot hand with rolling contact at the fingertip —control of the object and contact points by using the nonholonomy of the constraints—," in *Proc. SICE 2nd Annual Conference on Control Systems*, pp. 513–518, 2002. (in japanease).

Chapter 4

[51] A. Nakashima, K. Nagase, Y. Hayakawa, and M. Mita, "Simultaneous control of grasp/ manipulation and contact points of an object with rolling contact by two-fingered robot hand with constraint of degrees of freedom," *Trans. SICE*. Submitted. (in japanease).

[52] A. Nakashima, K. Nagase, and Y. Hayakawa, "Control of grasp/ manipulation of an object with rolling contact by two-fingered robot hand with four joints," in *Int. Symp. on Micro-NanoMechatronics and Human Science*, Nagoya Municipal Industrial Research Institute, Japan, 2004.

[53] A. Nakashima, K. Nagase, Y. Hayakawa, and M. Mita, "Simultaneous control of grasp/ manipulation and contact points by finger-tips with constraint of degrees of freedom," in *Proc. SICE 33rd Control Theory Symposium*, pp. 39–44, 2004. (in japanease).

[54] A. Nakashima, K. Nagase, and Y. Hayakawa, "Simultaneous control of grasp/manipulation and contact points with rolling contact," in *16th IFAC World Congress*, Praha, Czech Republic, 2005. Accepted.

Chapter 5

[56] A. Nakashima, K. Nagase, and Y. Hayakawa, "Control of contact coordinates between a sphere and a plane with pure rolling contact by using iterative closed paths," *Trans. SICE*, vol. 40, no. 4, pp. 434–441, 2004. (in japanese).

[57] A. Nakashima, K. Nagase, and Y. Hayakawa, "Control of a contact point between a sphere and a plane with rolling contact by using finite iterations of a closed path," in *Proc. SICE 31st Control Theory Symposium*, pp. 25–30, 2002. (in japanese).

Chapter 6

[58] A. Nakashima, K. Nagase, and Y. Hayakawa, "Control of contact coordinates of a sphere rolling on a plane with constraint on range of rolling motion," *Trans. SICE*, vol. 40, no. 1, pp. 1088–1097, 2004. (in japanese).

[59] A. Nakashima, K. Nagase, and Y. Hayakawa, "Control of contact coordinates of a sphere rolling on a plane with constraint on range of rolling motion," in *Proc. SICE 4th Annual Conference on Control Systems*, pp. 311–318, 2004. (in japanese).